Analytic Approaches to Stochastic Many-Particle Systems

Scaling and Renormalization in Microbial Communities and in Chemical Kinetics

Anton Winkler

München 2012

Analytic Approaches to Stochastic Many-Particle Systems

Scaling and Renormalization in Microbial Communities and in Chemical Kinetics

Anton Winkler

Dissertation
an der Fakultät für Physik
der Ludwig–Maximilians–Universität
München

vorgelegt von
Anton Winkler
aus Landau an der Isar

München, den 16. März 2012

Erstgutachter: Prof. E. Frey
Zweitgutachter: Prof. K. Wiese
Tag der mündlichen Prüfung: 3. Mai 2012

Zusammenfassung

Die Grundkräfte der Physik wirken immer nur zwischen zwei Teilchen und werden bei der Wechselwirkung von drei oder mehr Teilchen lediglich überlagert. Dennoch gilt auch für die Physik, dass das Ganze mehr ist als die Summe seiner Teile. Oft führt nämlich das Zusammenspiel von Abermillionen Teilchen in sogenannten „Vielteilchensystemen“ sogar zu grundlegend neuen Phänomenen. Ein allgemein bekanntes Beispiel hierfür sind die drei Phasen der Materie, fest, flüssig und gasförmig, denn sie werden durch die komplexe Wechselwirkung von quasi unendlich vielen Atomen oder Molekülen erklärt. Darüber hinaus wurden in den letzten hundert Jahren weitere, überraschende Vielteilchen-Phänomene entdeckt, zum Beispiel Bose-Einstein Kondensation, Supraleitung oder eine metallische Phase von Wasserstoff. Bereits eine Materieprobe, die so klein ist, dass sie in unsere Hand passen würde, stellt aufgrund ihrer etwa 10^{23} miteinander wechselwirkenden Teilchen ein Studienobjekt dar, das die Komplexität des ganzen Universums widerspiegelt. So haben neueste Untersuchungen gezeigt, dass die quantenmechanisch verschränkten Elektronen in bestimmen Festkörpern im Rahmen der Stringtheorie beschrieben werden können und aufgrund ihrer Korrelationen eine Art Schwarzes Loch ausbilden – hier tauchen also Begriffe auf, die sonst eher im Zusammenhang mit den riesigen Größen- und Energieskalen der Kosmologie und Hochenergiephysik stehen [1].

Diese Arbeit befasst sich mit dem breiten Themenbereich der stochastischen Vielteilchensysteme, in deren Rahmen die Interaktion einer großen Anzahl an Teilchen untersucht werden kann. Im Gegensatz zur Gleichgewichtsphysik wird dabei auch die zeitliche Entwicklung des Systems berücksichtigt, welche stochastischen Gesetzmäßigkeiten folgt. Zur Veranschaulichung betrachten wir die Bewegung eines Brownschen Teilchens in Wasser. Nach Albert Einstein liegt die Ursache der Bewegung in den zufälligen Stößen mit H_2O Molekülen [2]. Es wäre wohl unmöglich die Bewegung jedes einzelnen der Wassermoleküle genau zu beschreiben. Das ist glücklicherweise auch gar nicht nötig. Zwar weiß man, aufgrund der komplizierten Wechselwirkung der Wassermoleküle untereinander, sehr wenig über diese Stöße, außer dass sie zufällig verteilt sind. Dies ist aber nicht gleichbedeutend damit, dass man gar nichts über die Teilchenbewegung aussagen kann, denn es greifen hier die Gesetze der Wahrscheinlichkeitstheorie. Danach gehorcht die Bewegung des Brownschen Teilchens in guter Näherung der Diffusionsgleichung, mit einer Diffusionskonstanten, die nur von seiner Masse und der Temperatur bestimmt ist. Indem man sich also bei stochastischen Vielteilchensystemen auf die wesentlichen Eigenschaften der Dynamik beschränkt und unwichtige Details zugunsten einer effektiven Beschreibung ausspart, kann man seine Aufmerksamkeit dem genauen Studium der vielfältigen Phänomene widmen, die aus den komplizierten Korrelationen und der Wechselwirkung der Unmengen an Teilchen folgen können.

Im ersten Modell, das wir in dieser Arbeit studieren, stehen drei Spezies in zyklischer, nichthierarchischer Wechselwirkung. Derartige Interaktionen dienen beispielsweise der vereinfachten Beschreibung von Nahrungsketten, werden im Paarungsverhalten einer bestimmten kalifornischen Echsenart beobachtet, oder bestimmen das Wachstum in Kolonien von speziell

gezüchteten Stämmen des Bakteriums Escherichia Coli. Zumeist beobachtet man in diesen Modellen, dass sich zwar im Kleinen Domänen ausbilden, wo sich eine der drei Spezies durchgesetzt hat, aber im Großen die zyklische Dynamik für den Erhalt der Koexsistenz sorgt. Aus diesem Grund werden zyklische, nicht-hierarchische Wechselwirkungen oft (neben anderen Mechanismen) genannt, wenn es um die Erklärung der erstaunlichen Vielfalt der Natur geht, deren Reichtum an Arten scheinbar Darwin's These des „Survival of the Fittest" widerspricht. In dieser Arbeit untersuchen wir eine eindimensionale Version des Modells. Im Gegensatz zu höheren Dimensionen ist hier das Wachstum der Domänen, in denen nur eine Spezies übrig ist, unbegrenzt und wird in unserem Fall erst durch spontane Mutationen aufgehalten, die wir als weiteren natürlicher Mechanismus, der die Artenvielfalt begünstigt, einführen. Wir studieren den Einfluss dieser Mutationen auf die Größe dieser Domänen (als Maß für die Artenvielfalt) mit analytischen und numerischen Methoden. Erstaunlicherweise befindet sich das System für den besonders interessanten Fall von sehr niedrigen Mutationsraten im Gleichgewicht, obwohl ähnliche Systeme mit zyklischen Wechselwirkungen gerade wichtige Repräsentanten für Systeme fernab vom Gleichgewicht darstellen. Die üblichen Methoden der Statistischen Mechanik erlauben so für unser Modell exakte Lösungen.

In dem größeren Teil dieser Arbeit setzen wir uns damit auseinander, welche Rolle Vielteilcheneffekte bei der Geschwindigkeit von chemischen Reaktionen spielen. Standardmäßig wird angenommen, dass hier das allgemein bekannte Massenwirkungsgesetz gilt. Es besagt, dass die Geschwindigkeit einer elementaren Reaktion proportional dem Produkt der Konzentrationen der Reaktanten ist. Wir haben diese klassische Problematik der Reaktionsgeschwindigkeit und die Gültigkeit des Massenwirkungsgesetzes anhand von bimolekularen, irreversiblen Reaktionen studiert, in denen sich zwei Teilchen zu einem Komplex verbinden, der dann weiter reagieren kann. Ursprünglich wurde dieses Reaktionsschema vor über 100 Jahren eingeführt, um den Mechanismen, die zur Koagulation von Goldsolen führen, auf den Grund zu gehen. Es spielt heute in verschiedensten Bereichen der Naturwissenschaft eine Rolle, um etwa die Dynamik von Aerosolen, die Bindung von Proteinen, oder den Zerfall von Defekten in Festkörpern zu beschreiben. Unsere Analysen zeigen, dass das Massenwirkungsgesetz in diesem System verletzt wird. Die Abweichungen sind umso gewichtiger, je höher die Teilchenkonzentration ist. Sie sind auf Vielteilchenwechselwirkung und damit verbundene starke Fluktuationen in der Konzentration zurückzuführen. Interessanterweise ist die berechnete Korrektur zum Massenwirkungsgesetz eine einfache und universelle Funktion der „klassischen" Reaktionsrate (dem Proportionalitätsfaktor im Massenwirkungsgesetz). Im Gegensatz dazu ist diese klassische Reaktionsrate selbst nicht-universell. Sie wird also von der spezifischen mikroskopischen Realisierung des Systems bestimmt, etwa der Form und Größe der Teilchen. Wir haben diese Abhängigkeit genau studiert, indem wir mit modernen Methoden der Statistischen Physik eine mathematische Beziehung zwischen der Physik auf den mikroskopischen Skalen der Teilchen und der beobachtbaren Physik auf makroskopischen Skalen herstellen. Unseres Wissens handelt es sich hier um eines der ausgesprochen seltenen Beispiele, bei denen die Idee der Renormierungsgruppen, die Physik von den mikroskopischen Skalen auf die makroskopischen Skalen zu übertragen, exakt durchgeführt werden kann. Aus einem eher theoretischen Blickwinkel betrachtet, zeigen wir, wie sich die nichtperturbative Renormierungsgruppe zur Analyse von Vielteilchensystemen oberhalb der kritischen Dimension eignet, während ähnliche Methoden grundsätzlich auf niedrig dimensionale Systeme beschränkt sind.

Abstract

The fundamental forces of nature act between only two particles, while they are simply superposed for the interaction of three and more particles. However, also in physics the whole is more than the sum of its parts, and completely novel phenomena can emerge in systems of large numbers of particles. Among the well known there are the three phases of matter, solid, liquid and gas, which are attributed to the complex interaction of quasi infinitely many atoms. In the last 100 years or so, science has also revealed more exotic phases, such as superconductivity, superfluidity or a metallic phase of hydrogen. Due to the interaction of the $\sim 10^{23}$ particles, a sample of condensed matter that could fit in our hands, provides the physicist an object of study which reflects the complexity of the universe itself. Recent studies even reveal that the correlations of entangled electrons in certain solids imply physics that is effectively described by string theory, and display phenomena related to black holes; terms which are normally associated to the huge energy and length scales of cosmology and high energy physics [1].

This work revolves around the broad context of stochastic many-particle systems, which provide a framework to study the implications of the interaction of a large number of agents distributed in space. As compared to equilibrium statistical physics there is an emphasis on the time evolution of the system, governed on intermediate timescales by stochastic laws. To illustrate this, consider the erratic motion of a Brownian particle in water. As was first explained by Albert Einstein, it is caused by random collisions with the surrounding H_2O molecules [2]. Gaining a complete knowledge of the motion of every single molecule is futile, and in fact not necessary, because approximating the collisions as random is not tantamount to the absence of a law for the motion. On the contrary, probability theory provides an adequate description of the Brownian particle as diffusing with a diffusion constant D that depends on the mass of the particle and the temperature. Thus, simplifying the dynamics by subsuming its details to an effective description on intermediate timescales, stochastic many-particle systems allow to focus on the rich and complex phenomena which can arise from the interplay and correlations between the particles.

In the first model studied in this work, three species are subject to cyclic, non-hierarchical interaction. This scheme serves as a simplified model for food chains, is observed in mating strategies of a certain species of lizards, and obeyed by cultured strains of Escherichia coli bacteria, whose colonies can be examined in the lab. Typically the interaction leads to domains of one species, where the other two species have gone extinct, but the coexistence of the three species is conserved on the large scale. Therefore the cyclic interaction has been put forward as a candidate for maintaining the rich biodiversity observed in nature, which still puzzle scientists, as it seemingly defies Darwin's law of the "survival of the fittest". A part of the thesis is devoted to the treatment of the model in one-dimensional space, where, as opposed to two and higher dimensional systems, the growth of the domains of one

species is not halted by the cyclic interaction and coexistence is jeopardized. We study the impact of spontaneous mutations, a further mechanism which supports biodiversity, on the dynamics of the system. We derive accurate formulas explaining the size of the domains found in the stochastic simulations on the computer. Curiously, although the three species cyclic interaction models are often taken as important representatives of processes far from equilibrium, in certain regimes our model behaves as an equilibrium system, fulfilling detailed balance, and it thus allows for a complete and exact solution of the stationary state.

In the largest part of this work, we revisit the classical problem of bimolecular chemical reactions, employing a non-perturbative renormalization group scheme. This model has been introduced more than one hundred years ago to help understand the physics behind the coagulation of gold particles suspended in an electrolyte. It is of interest for a large variety of fields of natural science with applications to the dynamics of aerosols, the binding of proteins, the decay of defects in solids or the kinetics of chemical reactions. The "gold standard" in these reaction diffusion systems is the fundamental law of mass action, which state that the rate of an elementary reaction is proportional to the product of concentration of its participants. We show that for three-dimensional systems the law of mass action is violated. The effects become more pronounced as the particle density increases and can be attributed to long range fluctuations and many-particle correlations. Although the system is not critical, the corresponding additional term is a universal function of the macroscopic decay rate. To calculate the latter, we construct a relation from the physics at the microscopic scale, influenced by the shape and size of the particles or the structure of the lattice, to an effective macroscopic description. To the best of our knowledge this is one of the very few instances where the renormalization group idea of mapping physics from the micro- to the macro-scale can be accomplished exactly. From a more theoretical perspective, we demonstrate how the non-perturbative renormalization group can be employed to analyze the effects of long range and many-particle interactions above the critical dimension, whereas previous approaches are conceptually limited to low-dimensional systems.

Contents

1 Introduction

The complexity of the world seems infinite. Richard Feynman compares it to a large game of chess which we are allowed to watch but not to play [3]. Curiosity and careful inspection might allow us to derive the elementary rules of the game, although now and then we are still confronted with castlings we fail to understand. Yet even with a complete knowledge of these rules, most situations would be far too complicated for our predicting the next move. As an example in physics, consider the motion of a pendulum which can be solved analytically, after some simplifying assumptions (neglecting friction, allowing only for small angles). Already the seemingly not much more complicated double pendulum, where a pendulum is attached to the end of another pendulum, is hardly amenable to analytic treatment, and even the validity of numerical solutions is restrained by its chaotic motion: slight deviations in the initial conditions, or tiny errors in the calculations, say due to rounding, will increase exponentially and soon lead to completely different outcome.

The subjects of study in Statistical Physics usually bear much more degrees of freedom than the double pendulum. A key to treating these systems is to reduce the depth of the description. For instance, calculating the motion of every single particle in a gas would be futile, yet one can access macroscopic quantities such as its volume and temperature by averaging over ensembles of configurations. It may seem paradoxical that Statistical Physics provides unified descriptions for system which at first sight have little in common. A striking example is the critical behavior of gases and magnets. Not only do they share the qualitative phenomenon of a phase transition, characterized by the singular behavior of macroscopic quantities. The critical exponents describing these singularities often also agree quantitatively. This is known as "universality", and underscores the significance of specific models as benchmarks for more general systems. Therefore, rather than trying to recover every detail, the models studied in Statistical Physics are usually based on a simplified microscopic description boiled down to the main ingredients, whereby they capture the macroscopic behavior and, notwithstanding, are amenable to analytic treatment.

A prominent and widely studied example is the Ising model for ferromagnets. It reduces the complex interaction between the atoms to coupling of discrete spins. Successful as this model is in unveiling the nature of phase transitions, it is restricted to the equilibrium distribution of the system. To study the time evolution and the relaxation to the equilibrium state, it is necessary to introduce dynamics to the model. Again it should be noted that the goal of these approaches is not to describe the microscopic dynamics correctly in every detail, but they should rather be understood as mesoscopic descriptions. Thus, even if the dynamics of the spin flips were deterministic, a quite satisfactory description is already provided in the framework of stochastic many-particle systems with Markovian rules for the time evolution (viz. the Glauber and the Kawasaki dynamics [4]), such that the future probability distribution of the system depends only on the current state.

The study of these time dependent magnetic systems gave the field of stochastic many-particle system strong impetus. Today they provide a fruitful testing ground for more complicated systems in fields as diverse as ecology, spread of infection, behavioral systems, tumor growth and chemistry [5–7]. In this thesis we discuss two representatives of stochastic many-particle systems in detail. Firstly, a paradigmatic model for biodiversity is considered, where three agents are subject to cyclic competition. The model itself exists in many variations and an immense body of work has been developed in recent years. In this introduction we give the reader a resumé of some of the most intriguing findings, and relate our specific model to previous work. Secondly, we present a fundamental model for the coagulation of colloids, where two particles clot upon contact. Seminal works date back almost one hundred years, and there has been ongoing interest as the rise of more sophisticated mathematical tools allowed to gain new insights. To put our work into perspective, we give the reader a short overview of the most relevant results in this introduction.

1.1 Three-Species Cyclic Dominance

The world's ecosystems display a fascinating richness and abundance in coexisting species. As a striking example of this biodiversity, it has been estimated that a 30 gram sample of soil from a Norwegian forest contains half a million different species of bacteria [8, 9]. Such phenomena pose a great challenge to science: On the one hand biodiversity is beneficial to the ecological systems itself, enhances its viability and supports its productivity [10]. On the other hand, each species will hardly look for the well-being of the whole community, so that their coevolving seemingly defies Darwin's postulate of the "survival of the fittest" [11–13] (and also alternative theories of neutral evolution [14]). In a naive interpretation one might expect the stronger of the species to outcompete the weaker, and if they fight for the same, limited resources this will eventually lead to the extinction of the weaker species. The counterintuitive biodiversity in ecological systems is epitomized in the so called paradox of the plankton [13]. A large number of different species of plankton coexist, despite the fact that most of them rely on and share the same limited resources, constituted mainly by solar energy and minerals which are dissolved in the surrounding water. Here, the concept of ecological niches, one of the mechanisms which can maintain biodiversity, evidently fails; the species of plankton all seem to follow the same strategy. Rather, a possible solution of this apparent paradox is the spatial segregation of the different species of plankton [15].

Theoretical advances to explain the behavior of multispecies systems have been achieved in the framework of evolutionary game theory and population dynamics [7, 16–18]. A model which has attracted a lot of attention in recent years, and whose remarkably rich and complex behavior promises to shed light on at least some of the mechanism that maintain biodiversity, is the three-species cyclic population model [19–42]. Often it is metaphorically described by the children's game of Rock-Paper-Scissors (RPS), where rock crushes scissors, paper covers rock, and scissors cuts paper. This model is characterized by a cyclic, non-hierarchical structure. Three is the minimum number of agents to achieve this type of interactions. Typically the model develops a dynamics, where the system or a part of it is subsequently dominated by rock before paper before scissors... in an endlessly spinning wheel of species chasing species. Incidentally, this transition from one species to the next is connected to

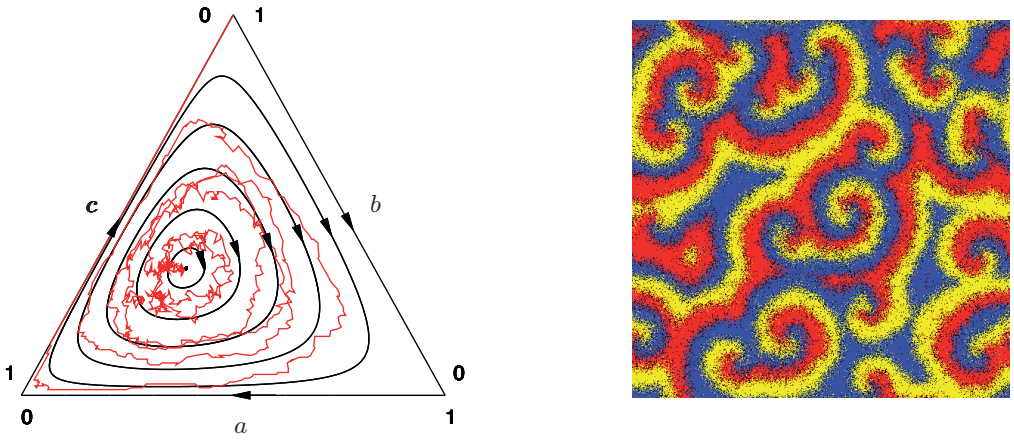

Figure 1.1: Solution of the RPS model, illustrated in the three-species simplex (left, the picture is reproduced from [25]). The deterministic rate equations imply neutrally stable cycles around the reactive fixed point. Yet after introducing stochasticity, by considering an urn model with a finite number of particles, one observes a spiraling out to the edges of the simplex. The system finally reaches one of the three absorbing states, where only one species has survived. On the right we depict a snapshot of a two-dimensional cyclic dominance model (reproduced from [26]). It is characterized by a dynamic pattern of entangled spirals. The arms of the spirals are domains where one species prevails; on one edge the domains intrude the neighboring domain of their "prey" only to give way to their "predator" on the opposite edge.

the non-equilibrium nature of the RPS dynamics, and the processes consumes entropy [34], similar as, for instance, plants harness solar energy.

The RPS lends itself as a paradigm for more complex species interaction. It is hoped to reveal generic features for realistic ecological systems, and serves as a lead for the analysis of more complicated models [43, 44]. Nevertheless, there is a host of examples in nature, where the cyclic dominance interaction of three species is observed directly. For instance, the interaction pattern was found to characterize the interaction between the agents of many marine communities which consist of three species [45]. Another, well documented, example is provided by lizard populations in the inner Coast Range of California [46]. Curiously, the mating strategy of the males are visually coded on their throats, allowing for a simple and reliable identification. Males with orange throats are very aggressive and reign over large territories. They thus outperform the less aggressive blue throated males, which restrict to smaller territories. However, the latter do this rather thoroughly, so as to defend their territory successfully against yet another type of males, the "sneakers", with yellow stripes on the throats, which resemble females and do not guard territories. The cycle closes since in the competition with the "sneakers" the aggressive orange throated males overstrain the size of their territory, which is thus invaded. A further example of RPS interactions is provided by certain strains of Escherichia coli bacteria, which can be studied on the Petri dish [23]. One strain produces toxin that is fatal to a another sensitive strain. Furthermore, there is a resistant strain that is not affected by the toxin and grows faster than the toxic strain, since it does not incur the cost of producing the poison. Finally, the sensitive strain outgrows the resistant one because also resistance bears some cost in fitness.

In a first approach one often ignores the spatial structure and considers a set of rate equations which describe the time evolution of the number of each species. These equations can then be analyzed by the usual means of non-linear dynamics. Famously, such an approach has been rather successful, for the related Lotka-Volterra predator-prey model, whose non-linear rate equations give rise to a limit cycle in the plane of the densities of predator and prey. Theses limit cycles were posited to describe the fluctuations in fish catches in the Adriatic [16, 47, 48]. Corresponding deterministic Lotka-Volterra equations can be set up for the RPS model, based on the reactions $AB \to AA$, $BC \to BB$, and $CA \to CC$, where A, B and C stand for rock, paper, and scissors, respectively. However, they have been argued to provide only an unrealistic description for ecological systems [25]. It was found that, in addition to the three trivial solutions of the rate equations, where only one of the three species remains and the other two are extinct, there is a stable fixed point, where all three species coexist. Around this reactive fixed point the system evolves along neutrally stable cycles in the three-species simplex, c.f. Figure 1.1. Thus, the deterministic solution predicts infinitely many solutions where the species coexist. Yet, if one introduces stochasticity into the model, by considering an urn model with a finite particle number of agents, fluctuations cause an erratic motion on the phase plane, characterized by random hopping between the deterministic cycles. The radial motion away from the reactive fixed point is aptly described by a random walk with an absorbing boundary, which, up to a constant factor, is attained on average after the rescaled time t/N, where N is the number of agents in the urn. Thus, stochasticity, which should be an integral part of any realistic model destabilizes the system and leads to extinction of two of the three species. (It is remarked in passing that even in a deterministic description of the three-species cyclic interaction, coexistence is not a robust feature. Seemingly irrelevant changes can destabilize the cyclic orbits and give rise to directed motion towards the edges and absorbing corners of the simplex. This is the case for the May-Leonard model, where instead of an immediate invasion, an empty spot is created, $AB \to A\varnothing$, $BC \to B\varnothing$, and $CA \to C\varnothing$, on which an offspring can then be produced, $A\varnothing \to AA$, $B\varnothing \to BB$, and $C\varnothing \to CC$ [49].)

The crucial ingredient which lacks the above urn model is spatial expansion in combination with short range interaction. This stabilizes the coexistence of the three species and makes it more robust to small changes in the model, as was most cogently demonstrated in the work of Kerr et al. on the Escherichia coli strains described above [23]. Their numerical simulations and experimental observations suggest that, as long as the bacteria are locally dispersed on the Petri dish, they form a mosaic of patches dominated by one strain. The gains of first species are at the cost of the second, and are soon enjoyed by the third strain, and so on. In an alternative scenario, the bacteria were put in a flask that was stirred to obtain a well-mixed environment, where the bacteria are delocalized and the spatial extension is immaterial. In stark contrast to the outcome on the Petri dish, for the stirred flask Kerr et al. observed the extinction of two of the three strains, in an almost deterministic development: First the sensitive strain is killed, since it cannot form defensive patches against the toxin. This settles the fate of the toxin producing strain, since the resistant strain, having lost its only enemy, outgrows the toxin producing strain and finally prevails.

The importance of explicit space for maintaining the coexistence of the species has also been underscored in a number of further, theoretical works [7, 26, 50–52]. We highlight the results of Reichenbach et.al. [26], who studied the implications of mobility on the cyclic dominance interactions on a square lattice. As long as the hopping rate between the sites is below a

certain threshold, one observes stable coexistence with an intriguing pattern of entangled spirals, c.f. Figure 1.1. As the mobility is raised and the interacting agents are more and more delocalized, the size of the spiral structures increases continuously, until the mobility exceeds a critical value where they outgrow the system size and two of the three species go extinct.

The cyclic dynamics can not only maintain coexistence in two-dimensional lattices, but also for higher dimensions and for complex networks [7]. However, the scenario differs markedly when one goes to one-dimensional systems, where the cyclic dynamics imply a transition to one of the three absorbing states. (A similar phenomenon is observed for the "voter model", where two voters which may have either of two political positions, are distributed on a lattice and adapt the opinion of one of their neighbors after some time. This may be perceived as the two-species cyclic dominance process. In one and two dimensions, the system is characterized by an infinite coarsening of domains of voters with the same position. In three and higher dimensions, the coarsening eventually stops and there is coexistence of the two political positions.) To understand the behavior in one dimension, it is important to notice that, while the number of domains of one species can decrease, the creation of new domains is impossible. To illustrate this, let us assume that part of the lattice is in the configuration ABA and another part in ABC, with the species B squeezed between domains of A and C. For both configurations, in the next instant, the domain of B (here consisting of only one site) can be conquered by its predator A and thus vanishes. Thus the number of domains decreases, their average size grows and the system undergoes coarsening. (Strictly speaking, our arguments are only true for a "fermionic" system, where each lattice site is occupied by exactly one agent. But the general conclusion of the coarsening of domains is preserved also for "bosonic" systems, where each site can be occupied by several particles, even if there appear additional mechanisms for the coarsening [35]).

There has been some dispute over the law that governs this growth of the domains in one dimension. A generalized mean-field approach suggests that their average size diverges as $l \sim t^{\alpha}$, with an exponent $\alpha = 1$. This has been challenged by simulation results, which indicate that $\alpha \approx 0.8$ [53], while theoretical work on a similar model, with deterministic dynamics, points to $\alpha = 1/2$. The dispute could be settled by the work of Frachebourg et al. [19, 20]. The authors remarked that the dynamics leads to a building up of superdomains, with sequences of domain walls (the border between two domains) that either all move to the right or to the left. For example, suppose a part of the lattice is in the configuration $AABBCCCABCC$, which is a superdomain of the right-moving domain walls, AB, BC, and CA. Since the domain walls avoid each other by moving in the same direction, the coarsening of the domains is decelerated as compared to the mean-field result. On the other hand, in contrast to the deterministic model, the domain walls display diffusive motion. Therefore it can occur that two right-moving domain walls meet, say $CAB \to CCB$. This stochastic effect implies accelerated growth of the domain size as compared to the deterministic model. Indeed, the true exponent $\alpha = 3/4$ lies between the mean-field result and the result for the deterministic model.

The model treated in the next chapter is motivated by the work on these one-dimensional systems. By introducing spontaneous mutations, a natural mechanism is provided which puts a stop to the eternal growth of domains. Thus, the system tends to a stationary state with coexistence, characterized by the competition between coarsening and mutation.

1.2 Reaction-Diffusion Processes and Rate Equations

The second stochastic many-particle system studied in this work is a simple decay process, where two particles clot to form one particle, $A+A \to A$, and explore space by diffusion due to Brownian motion. In the spirit of studying idealized and simplified models for gaining insight into microscopically much more complex processes, this reaction scheme was introduced by Smoluchowski to help reveal the mechanisms behind the coagulation in a colloid suspension of gold, supported by experimental work of Zsigmondy [54, 55]. Smoluchowski's work marks a cornerstone in the development of a theory for reaction-diffusion processes. His approach of solving the problem, which we will briefly describe below, and his results are until today an important reference point in the theoretical and experimental study not only of colloid suspensions but also in fields as diverse as meteorology, micro-biology, chemistry, solid state physics, and astronomy, with various applications such as the growth of aerosol particles [56], protein binding [57], chemical kinetics [58, 59], exciton fusion [60], the evolution of excitations in spin ice [61], or the evolution of superheavy monopoles produced in the early universe [62].

Generally, in such reaction-diffusion processes one distinguishes two regimes, the *diffusion-controlled* regime and the *reaction-controlled* regime. To elucidate these terms, suppose that the two particles coagulate with rate λ once they meet within a distance R. If this microscopic reaction rate λ is very low, or alternatively fast diffusion ensures a well-mixed system, it will be the bottleneck of the reaction. Let ρ denote the particle density at time t. The probability for a particle to be in reach of another particle will simply be $\frac{4}{3}\pi R^3\rho$ and thus in the reaction-controlled regime

$$\partial_t \rho = -\lambda \frac{2}{3}\pi R^3 \rho^2 \,. \tag{1.1}$$

This reasoning breaks down when the reaction rate becomes large, $\lambda \to \infty$, i.e. when two particles meet they coagulate with certainty and immediately. In contradiction to Eq. (1.1) the speed of the reaction will not become infinite: If initially the particles are randomly distributed, then in the next instant all "pairs" are taken out of the system and one relies on a mechanism to redistribute the particles, in our case by diffusive mixing, in order to have new pairs which can react. Thus, the mean-field dynamics of Eq. (1.1) is slowed down due to anti-correlations, which build up in the system, because a configuration of nearby particles is unstable.

Smoluchowski found a way to tackle this interesting case of diffusion-controlled reaction kinetics, where, because of a separation in time scales, the bottleneck of the kinetics is the ineffective diffusional mixing. His approach to solving the reaction kinetics lends intuitive insight into the nature of the anti-correlations [54] (also see [63, 64]): We put ourselves in the inertial system of a test particle which is fixed at the origin. The surrounding particles, with density ρ, are effectively treated as a non-interacting diffusive field. Whenever one of the surrounding particles is within a distance R of the test particle at the origin, it is annihilated with rate λ, whereas our test particle is supposed to survive. In the limiting case of infinite reaction rate, $\lambda \to \infty$, which was considered by Smoluchowski, the problem reduces to a diffusion equation with absorbing boundaries at a distance $|x| = R$ from the test particle, and can be solved easily with the full time dependence, by constructing the Green's function. For three dimensions, the solution converges to a stationary state which is depleted at the origin, see Figure 1.2. The particle flux into the reach of the test particle is found to be $J = 8\pi D\rho$.

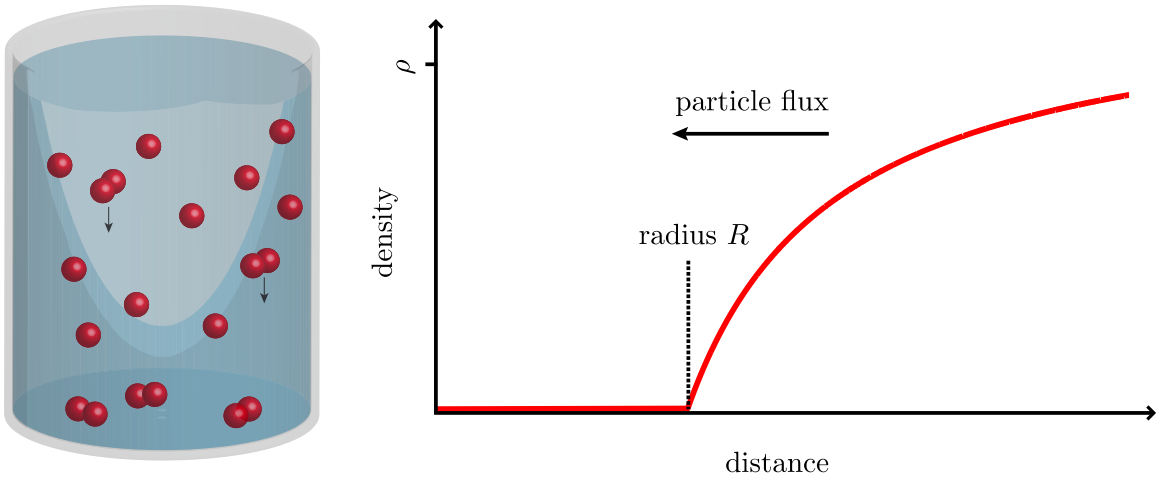

Figure 1.2: Illustration of the annihilation process, where two particles form an inert complex $A+A \to A_2$, which is taken out of the system (left). Mathematically this process is equivalent to the coagulation $A + A \to A$, as will be demonstrated in Chapter 4. On right side we present the Smoluchowski's argument, for which a test particle is placed at the origin, surrounded by a density field of noninteracting particles subject to diffusion. When one of the particles approaches the test particle it is taken out of the system. The density of the particle field is therefore determined by a diffusion equation with absorbing boundaries. Shown here is the stationary solution in three dimensions. For large distances it approaches the absolute density ρ and displays a minimum in the vicinity of the test particle. These anti-correlations decelerate the kinetics, as compared to a well mixed system and ensure a finite particle flux into the test particle, even for infinitely large microscopic reaction rates λ. In the Smoluchowski approach, one assumes that the particle flux into the test particle determines the kinetics such that $\partial_t \rho = \frac{1}{2} J\rho$. Due to the linearity of the diffusion equation, the particle flux J is proportional to the density ρ. Therefore, the kinetic equation $\partial_t \rho = \frac{1}{2} J\rho = -4\pi D\rho$ (where D is the diffusion constant) is quadratic on the density ρ, in accordance with the law of mass action.

Smoluchowski's crucial assumption is that the number of reactions taking place per unit time and unit volume is the density of test particles ρ times the particle flux $8\pi D\rho$, divided by two (in the coagulation reaction $A + A \to A$ only one of the two reactants disappears, whence a factor 1/2). Thus,

$$\partial_t \rho = -\mu\rho^2 \,, \tag{1.2}$$

with the effective decay rate $\mu = 4\pi DR$. As for Eq. (1.1), because of the linearity of the diffusion equation, the kinetics is described by an equation that is quadratic in the density ρ. This is in accordance with the famous law of mass action, stating that the rate of an elementary reaction is proportional to the product of the concentrations of its participants. In the diffusion-controlled limit, however, the rate of the decay μ is an effective, macroscopic rate. As compared to the mean-field result $\lambda \frac{2}{3}\pi R$ (see Eq. (1.1)) it is restricted by heterogeneities in the particle density, which are a consequence of the interaction of the particles, their discrete nature and the ineffective diffusive mixing.

In the appendix we also give the stationary solution to the ensuing diffusion equation for finite microscopic reaction rates λ. Because of a sink of the particle density around the test

particle, the kinetics is always decelerated, as compared to the reaction-controlled regime, c.f. Eq. (1.1). The effective decay rate μ now depends on the microscopic rate λ and is not only limited by the diffusion constant D. The result reads

$$\mu(\lambda) = 4\pi D \left[R - \sqrt{\frac{2D}{\lambda}} \tanh\left(R\sqrt{\frac{\lambda}{2D}} \right) \right] . \tag{1.3}$$

As one should expect, the macroscopic rate $\mu(\lambda)$ is monotonously increasing with the microscopic rate λ, but nevertheless tends to a finite value, when the latter diverges. It bridges the gap between the reaction-controlled regime (where one indeed recovers the mean-field equation, Eq. (1.1)) and the diffusion-controlled regime for large λ, where $\mu = 4\pi DR$.

Smoluchowski's heuristic approach captures the contributions of the fluctuations very well. Indeed, it is established that above the critical dimension two, the law of mass action describes the kinetics of the system accurately, such that the density becomes $\rho \sim \mu^{-1} t^{-1}$ at long times t. It has even been confirmed rigorously, by field theoretic means, that the Smoluchowski approach delivers the correct decay rate μ [64]. It is well known, however, that in low dimensions the law of mass action is no longer valid and there are marked deviations from the classical scaling t^{-1} of the density. This can be understood most vividly by first noting that in the diffusion-controlled limit, dimensional analysis and the law of mass action imply a decay

$$\rho \sim cR^{2-d}(Dt)^{-1} , \tag{1.4}$$

with a dimensionless constant c [62]. Below two dimensions this formula cannot possibly hold, since an increase in the interaction radius R would certainly speed up the reaction and not slow it down. The reason for this failure is that the random walk is recurrent below two dimensions, i.e. every point in the system is passed with certainty if one waits sufficiently long. Thus, in one dimension, within time t, a particles sweeps out a stretch of the lattice of length $\sqrt{Dt}$. If we take this as the effective size of the particles, this suggests a decay of the density,

$$\rho \sim \mathcal{A}(Dt)^{-\frac{1}{2}} , \tag{1.5}$$

(where $\mathcal{A}$ is some dimensionless amplitude) much slower than predicted by the classical theory.

This anomalous kinetics of the coagulation process in low-dimensional (two and below) systems, with its violation of the law of mass action, has fascinated scientists and sparked a great body of work. Specialized to one dimensional systems, a whole host of different methods has been devised, which allow to extract exact solutions. In particular, the decay amplitude $\mathcal{A}$ has been calculated exactly for the coagulation model [65–68] and a number of variations of it (for instance with synchronous dynamics [69], where all the particles are updated at once, or with asymmetric diffusion [70]). These theoretical predictions are probed by experimental studies on effectively one-dimensional exciton dynamics [71–75]. In the two dimensional realization of the model, there are logarithmic corrections to the classical scaling,

$$\rho \sim \mathcal{A}\frac{\ln(Dt)}{Dt} . \tag{1.6}$$

Here rigorous theoretical results have been obtained by means of the perturbative renormalization group [76, 77] which are of experimental interest for instance in the study of reactions in biological membranes [78]. Finally, studying fractal systems, also the regime between one

and two dimensions has been explored [60, 79]. It is found that $\rho = c(Dt)^{-d_s/2}$, when d_s is the so called spectral dimension, defined by the recurrence property of the random walk (the probability for a random walker to return to the origin at time t behaves as $t^{-d_s/2}$).

In contrast to these new insights and methods for low dimensional system, fundamental progress in higher dimensions has remained largely elusive. One reason for this might be that Smoluchowski's approximation of only considering two particle correlations already delivers exact results. Indeed, whereas in low dimensional systems, long range and many-particle interactions strongly impact the long time kinetics, it is established that in three and higher dimensions the effect of these fluctuations can be neglected and that Smoluchowski's approach becomes exact in the long time and low density limit [58, 64, 80]. The underlying reason is that the random walk is not recurrent above two dimensions, which implies that it is unlikely that a particle returns to a small volume around, say, the origin, after it has traveled a distance away from it to another small volume. Thus, the correlations building up between these two, separated volumes will be relatively small, and therefore also the correlations between different particles (placed in such volumes) should be small.

However, Smoluchowski's classical theory and the law of mass action do not hold for all decay processes in three dimensions. A counterexample is the annihilation reaction of two species of particles, $A + B \to \varnothing$. Here, it is well known that Smoluchwski's arguments fail, due to long range density fluctuations in the initial conditions [62, 81]. Toussaint and Wilczek begin their analysis of the process with an intuitive argument: If initially the particles are randomly distributed, with equal densities ρ_0 for both species, the excess in the number of one species in a volume V is of the order $\sqrt{\rho_0 V}$. On diffusional length scales $l_D = \sqrt{Dt}$ there will be domains where only one species prevails. This mechanism is the bottleneck of the reaction kinetics (for one dimension it even implies a slower decay than Eq. (1.5)), namely

$$\rho(t) \sim c\rho_0^{1/2}(Dt)^{-\frac{d}{4}}\,, \tag{1.7}$$

on condition that $d < 4$. Incidentally, when the initial long range correlations are suppressed due to the pairwise productions of particle A and particle B, the above arguments are invalidated and in the three dimensional model the law of mass action is recovered [58, 62]. This is the case, for example, for certain solids where point defects are created in pairs [58], since, due to radiation damage, atoms loose their ground state position in the lattice structure and leave nearby vacancies, with which they can recombine. This is particularly interesting for us since a field theoretic analysis displays an intimate relation to the coagulation model $A + A \to A$ on which we put the focus in this work [82]. Thus, our results have direct and quantitative implications also for the two particle annihilation process.

Despite this counterexample, in three dimensions the validity of the law of mass action is usually taken for granted [57, 73, 83, 84]. The focus is rather on the correct value for the macroscopic decay rate μ than on possible deviations from it. Of course, determining μ is a very important point too, especially since, as criticized in [57], the classical result $\mu = 4\pi DR$ for interacting spheres often serves as an upper bound for the reaction rate in protein-protein and protein-ligand binding, although it grossly overestimates it by several order of magnitude, due to orientational constraints for the binding. Nevertheless, we think it essential to also explore possible violations of the law of mass action for finite densities. Indeed, as we show in this work employing field theoretic methods and the non-perturbative renormalization group,

instead of the rate Eq. (1.2), the kinetic equation should be written in the more general form

$$\partial_t \rho = -F(\rho)\,, \tag{1.8}$$

with the non-equilibrium force $F(\rho)$. For very low densities we recover the law of mass action $F(\rho) \approx \mu\rho^2$. However, long range fluctuations and many-particle interactions give rise to a relatively strong, non-analytic term $c(\mu)\rho^{5/2}$, which is only the first term in the infinite series $F(\rho) = \mu\rho^2 + c(\mu)\rho^{5/2} + c_{3,\ln}\rho^3 \ln(\rho) + c_3\rho^3 + c_4\rho^{7/2} + \ldots$. Intriguingly, the first correction $c(\mu)\rho^{5/2}$ is a universal function of the macroscopic decay rate μ, but otherwise does not depend on the microscopic realization of the model, such as the shape and size of the reactants.

2 Three-Species Cyclic Dominance with Mutations

Stochastic many-particle systems are a fruitful testing ground for understanding generic principles in non-equilibrium dynamics. Unfortunately, the treatment of such processes is marred by the absence of detailed balance, so that the insight one has gained by analytical means is not yet satisfactory and only few systems have been solved exactly [5, 6, 85]. Some of them serve as a paradigm for very complex biological and sociological systems. An example is the contact process, which describes the outbreak of an epidemic, displaying a phase transition from an absorbing to an active state as the rate of infection is increased [86]. Another famous example is the voter model, caricaturing opinion making. It is proven rigorously that on a regular lattice there is a stationary state where the two "opinions" coexist, so long as the dimension is larger than two, such that the random walk is not recurrent [6, 87]. Extensive studies have also been conducted on the coarsening dynamics of coalescing or annihilating particles, both for diffusional motion and ballistic motion of the particles [19, 20, 88, 89]. In this context, much work was devoted to the long time behavior of the average domain size, which as a function of time typically displays scaling.

Frachebourg et al. [19, 20] have investigated the coarsening dynamics of a model known as the Rock-Paper-Scissors game (RPS), a widely studied prototype model for biodiversity [23, 25–27, 30], displaying cyclic dominance between its three agents. Here, we study the influence of mutations on this model, a work which originates in the author's diploma thesis [90]. An integral part of evolution, mutations have been posited to promote biodiversity in microbial communities [52]. We will argue that the RPS is a natural framework for a non-equilibrium version of the Ising-Glauber model, which at zero temperature amounts to an annihilating random walk. While previous studies have addressed coarsening and the transition to an absorbing state, we focus on the description of the stationary reactive state at finite "temperature", i.e. interfaces between domains are created at finite mutation rate. In the Ising-Glauber model the interfaces perform a random walk, whereas for the RPS they drift left or right. Since the coarsening dynamics is counteracted by the creation of interfaces, the system evolves into a non-trivial stationary state. For very large and very low mutation rates, equilibrium turns out to be only slightly broken. Discriminating between two types of mutations, we can thus obtain asymptotically exact descriptions for the average size of the domains in the stationary state. As the final arbiter of the validity of our arguments we employ stochastic lattice simulations. In an shorter version than is presented here, this first part of the chapter has been published in our article "Coexistence in a one-dimensional cyclic dominance process" which appeared in Physical Review E [39].

The RPS is often named as an important representative of non-equilibrium processes [7, 27, 34]. The non-equilibrium nature manifests itself in the cyclic dominance of the species, implying a net probability flow from a state where rock is predominant, to a state where

paper is predominant, to a state where scissors is predominant, and so on. In contrast, for equilibrium systems one expects the probability flow to obey the detailed balance principle, such that the net probability flow from rock to paper and back should cancel [91]. The reactive stationary state that RPS displays in two (and higher) dimensional systems, is truly far from equilibrium, because there are three absorbing stationary states (with only one species left), and the flow into these absorbing states cannot (by definition of absorbing) be equilibrated. Also for a zero-dimensional RPS model equipped with spontaneous mutations (as they are also introduced in this work) the process is far from equilibrium, as shown in [34], where the non-equilibrium aspects of this process have been studied and quantified by measuring the entropy production. It reaches its peak at a critical mutation rate which becomes small as the system size increases. Thus, it came as a surprise to us to find that for our realization of the model, in the regime of very low mutation rates, the system reaches a stationary state which displays detailed balance. This is the starting point of the second part of this chapter. The fact that detailed balance is fulfilled allows us to apply the tools of equilibrium statistical mechanics and to obtain rigorous analytic solutions for the equilibrium state of the model. The existence of such an equilibrium stationary state, however, turns out not to be robust to the breaking of the symmetry between the species, because here there are additional transitions which are not balanced by a reverse transition.

Asymmetries between the species are of course the norm; in particular they are observed in the laboratory experiments on Escherichia coli [23]. As described in Section 1.1, one strain produces toxin that is fatal to another sensitive strain, which outgrows a strain that is resistant to the toxin. Here the asymmetry is rather strong, since the toxic environment relatively quickly causes the death of the sensitive strain, so that the toxic strain invades the domain of the sensitive strain much faster than the sensitive strain invades the resistant strain. Curiously, in the limit of infinitely fast reproduction of one species, motivated by these experiments on Escherichia coli, we find that the process again attains an equilibrium state which is exactly solvable.

2.1 Definition of the Model and the Dual Picture

On a one-dimensional integer lattice $\{1, \ldots, S\}$ of size S, the RPS game can be defined by the following cyclic dominance reaction equations for nearest neighbors.

$$AB \xrightarrow{r_A} AA\,, \quad BC \xrightarrow{r_B} BB\,, \quad CA \xrightarrow{r_C} CC\,, \tag{2.1}$$

i.e. paper (A) covers rock (B), rock crushes scissors (C) and scissors cuts paper. Here we presuppose left-right symmetry such that, for instance, A can invade a neighboring B to its left or right, and we consider a Markov process in continuous time with sequential updating. Unless otherwise stated, we consider the symmetric case, with equal cyclic dominance rates

$$r_A = r_B = r_C = 1\,, \tag{2.2}$$

which are set to one to define the timescale. These equations have been studied in detail in [19, 20]. In particular it was shown that, starting from some random distribution, the species organize in domains that undergo coarsening until finally—providing the system size is finite—one species takes over the whole lattice.

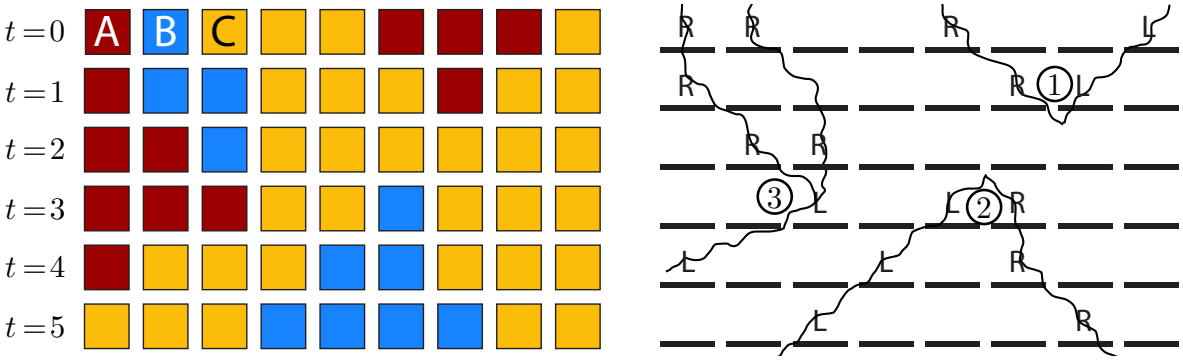

Figure 2.1: Illustration of the one-dimensional Rock-Paper-Scissors game with mutations and the passing to its dual description. The configuration of the lattice is given at subsequent points in time, resulting in a two-dimensional space-time plot. A mutation $C \to B$ occurs somewhere between $t = 2$ and $t = 3$. In the particle picture, for each lattice site the species are explicitly given (left part of the figure). In the dual picture, or interface picture, one keeps track of the domain walls, also called interfaces, instead (right part of the figure). The dual picture is characterized by interfaces moving left (L) or right (R). Notice that the annihilation of two interfaces, reaction (1), is simply the time reversal of reaction (2). Reaction (3) breaks the time reversal symmetry. However, as the mutation rates becomes smaller, and the average domain size grows, from a coarse grained point of view the motion of the interfaces becomes effectively ballistic (moving at constant speed). Therefore, one can neglect reaction (3), which is dominated by the diffusional motion of the two Rs relative to each other. We will show that, because of the ensuing time reversal symmetry, in the limit of low mutation rates the process attains an equilibrium stationary state (i.e. obeys detailed balance), which allows for an exact solution.

In addition to the above reaction scheme for cyclic dominance we allow for spontaneous mutations to the respective "prey" with rate μ_r,

$$A \xrightarrow{\mu_r} B \xrightarrow{\mu_r} C \xrightarrow{\mu_r} A\,, \tag{2.3}$$

and to the respective "predator" with rate μ_l,

$$A \xrightarrow{\mu_l} C \xrightarrow{\mu_l} B \xrightarrow{\mu_l} A\,. \tag{2.4}$$

Notice that both types of mutations conserve the cyclic symmetry. The mutations counteract the coarsening of the system and ensure a reactive stationary state. However, for low mutation rates, which we shall focus upon, one still expects the system to organize in large domains of one species separated by interfaces. Thus, it is adequate to utilize the so-called dual picture (or interface picture), obtained by representing the interfaces, i.e. the walls between the domains of one species, by particles and two consecutive spots occupied by the same species by empty sites $\varnothing$. This mapping is illustrated in Figure 2.1. There are left and right moving interfaces, denoted R and L, respectively. The interfaces reflect the one-dimensional structure of the lattice, which critically affects the dynamics since in higher dimensions the coexistence is maintained even without mutations.

The density of the interfaces is simply the reciprocal of the average size of the domains and is thus a measure for the coarse graining. For zero mutation rates the number of interfaces is bound to decrease when they interact: Either an R and an L collide and there is pair

annihilation $RL \xrightarrow{2} \varnothing\varnothing$ (see reaction (1) in Figure 2.1), or two interfaces moving in the same direction interact and turn into one interface that moves in the converse direction, $LL \xrightarrow{1} R\varnothing$, and analogous for left and right interchanged, $RR \xrightarrow{1} \varnothing L$ (see reaction (3) in Figure 2.1). The situation is more complicated when mutations are involved, because a number of cases need to be distinguished, and we will discuss the relevant reactions as we go along. Here we only highlight one mechanism that mutations provide for creation of interfaces, namely $\varnothing\varnothing \xrightarrow{\mu_l} LR$, labeled by (2) in Figure 2.1. This pair creation is just the time reversed pair annihilation and, as we will explain further below, this fact permits an equilibrium stationary state for very low mutation rates and interface densities.

2.2 The Mean-Field Equation and Large Mutation Rates

As a starting point for our analysis we derive the mean-field rate equation for the interface density. Let $P(R), P(L)$, and $P(\varnothing)$ be the probabilities of finding a right moving interface R, a left moving interface L or a vacancy $\varnothing$, respectively, at some lattice site. To obtain the rate equation, one assumes the system to be well mixed, i.e. the occupancy of different sites is approximately uncorrelated. In particular, the probability for a configuration XY on two neighboring sites simply factors, $P(XY) = P(X)P(Y)$. Let us calculate the time evolution $\dot{P}(R)$ of the probability that a site is occupied with an R. The reactions for zero mutation rates, discussed above, $RL \xrightarrow{2} \varnothing\varnothing$, $LL \xrightarrow{1} R\varnothing$, and $RR \xrightarrow{1} \varnothing L$, contribute a term $-2P(R)^2 - 2P(R)P(L) + P(L)^2$. As for reactions involving mutations, they always affect two adjacent sites on the dual lattice. When there is a μ_l (μ_r) mutation, the left (right) one of the two sites turns from $\varnothing$ to L, L turns to R, and R turns again to $\varnothing$, and the right (left) site turns from $\varnothing$ to R to L and again to $\varnothing$. Since in the mean-field approximation the sites are taken as uncorrelated, there is no distinction between the left and the right site and the two types of mutations, μ_r and μ_l, are treated on equal footing. This is in contrast to our results below. Let us define the overall mutation rate $\mu := \mu_l + \mu_r$. An R is destroyed when there is a mutation on its left or on its right, providing a term $-2\mu P(R)$ to the rate equation. An R can be created if a site is empty or occupied with a left moving interface L, which gives the contributions $\mu P(\varnothing)$ and $\mu P(L)$, respectively. In summary, we obtain the mean-field rate equation

$$\dot{P}(R) = -2P(R)^2 - 2P(R)P(L) + P(L)^2 + \mu\left(P(\varnothing) + P(L) - 2P(R)\right) . \tag{2.5}$$

Solving for the stationary state, where $P(R) = P(L)$, the interface density becomes

$$n := P(R) + P(L) = \sqrt{\frac{4\mu}{3} + \mu^2} - \mu . \tag{2.6}$$

It increases sharply, $\sim \sqrt{\mu}$, for small mutation rates. When the mutation rate is large, all three outcomes, $\varnothing$, L, and R, should be equally likely, and indeed, Eq. (2.6), indicates that the interface density saturates to $2/3$ in this regime.

For sufficiently large mutation rates, the mean-field result, Eq. (2.6), is in excellent agreement with the stochastic simulations, see Figure 2.2. To better understand the reason why this is the case, we point out an analogy to the Ising model. It can be easily verified that the two-particle version of our process (i.e. $AB \xrightarrow{1} AA$, $BA \xrightarrow{1} BB$, and $A \xrightarrow{\mu} B \xrightarrow{\mu} A$; the two

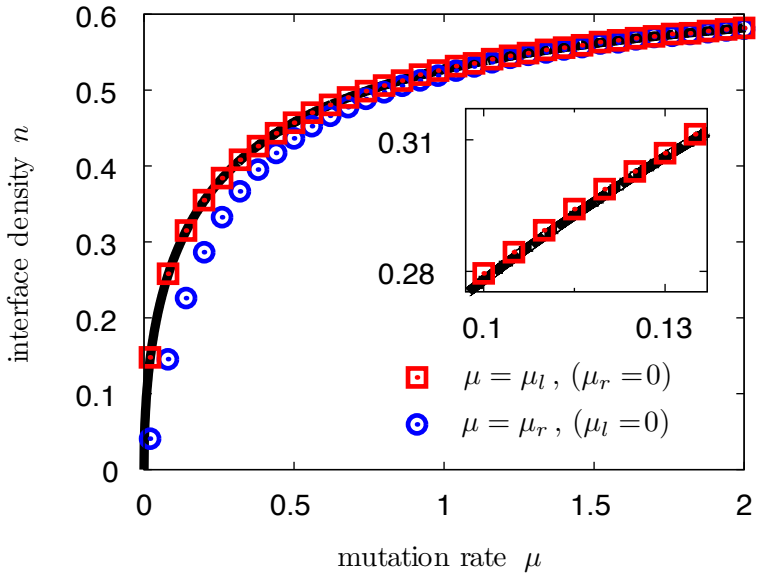

Figure 2.2: Comparison of the stationary density of the interfaces obtained by stochastic simulations with the mean-field result, Eq. (2.6) (solid black line), for relatively large mutation rates $\mu = \mu_r + \mu_l$. When there are only mutations to the respective prey ($\mu = \mu_r$, blue circles), there are distinct deviations from the theoretical curve, and they become more and more pronounced as the mutation rate is lowered. This disagreement is due to the fact that long range correlations build up in the form of large domains of one species. In the dual picture, this corresponds to long stretches of empty sites $\varnothing$. For such a systems which is almost void of interfaces, the most likely μ_r mutation is $\varnothing\varnothing \to RL$. This is very ineffective in increasing the interface density, since in most cases the pair will be subject to annihilation $RL \to \varnothing\varnothing$ shortly afterwards. However, the mean-field calculation does not capture the impact of the short survival time of the pairs RL on the interface density, since it does not distinguish between the left and right site and is only valid when the system is well mixed. Therefore, in the case of μ_r mutations, the interface density is overestimated by mean-field. When there are only mutations to the predator ($\mu = \mu_l$, red squares), the agreement with Eq. (2.6) is so close that only in the inset one can see that the data points indicate slightly larger values. However the deviations do become more pronounced, when one goes to very small mutation rates, as discussed in Section 2.3.

types of mutations, μ_l and μ_r, obviously cannot be distinguished here) is equivalent to a process that has been proposed by Glauber as a way to study the dynamic effects of the one-dimensional Ising model, with, say, A corresponding to "spin up" and B corresponding to "spin down" [92, 93]. After expressing the energy in terms of the nearest neighbor sum $E(\{s\}) = -J\sum_{<k,l>} s_k s_l$, where s_k is 1 for "spin up" and -1 for "spin down" and J is a coupling constant, the temperature T is related to the mutation rate μ by

$$\frac{\mu}{1+\mu} = 1 - \tanh\left(\frac{2J}{k_B T}\right) , \tag{2.7}$$

with the Boltzmann constant k_B. μ is small in the low temperature regime and large in the high temperature regime. Thus, we may think of the mutation rates μ_l and μ_r for the RPS as temperature-like parameters. For fast mutation rates, or high temperature, the system becomes rather uncorrelated, and therefore mean-field (2.6) makes for a good approximation.

2.3 The Limit of Low Mutation Rates

When the mutation rate becomes smaller, the correlation length becomes larger. There arise large domains where one of the three species has completely taken over. When the correlation length is finite, the dynamics can still be treated well by a generalized mean-field approach, known as cluster approximation [7, 94, 95], as long as one chooses clusters that are larger than the typical domains. Here however we shall discuss the limit of infinitely low mutation rates $\mu = \mu_l + \mu_r$, where the typical size of the domains becomes infinitely large. The above comparison with the one-dimensional Ising model suggests that at $\mu = 0$, corresponding to zero temperature, the system displays critical behavior with the correlation length going to infinity. In the following we show that this is indeed corroborated by scaling arguments as well as stochastic simulations.

2.3.1 Mutations to the Predator

First, let us restrict ourselves to the regime of a vanishing mutation rate to the prey, $\mu_r = 0$, and small mutation rates to the predator, $\mu_l \ll 1$. The analysis of the limit of small mutation rates for the opposite case (only mutation to the prey) and for the general case (both types of mutations allowed) is quite similar, yet slightly more complicated, and for this reason it is postponed to the end of this section. Since the interface density is low, the single most probable mutation event occurs on two adjacent vacant sites

$$\varnothing\varnothing \xrightarrow{\mu_l} LR\,. \tag{2.8}$$

In the particle picture this is achieved by, e.g., $AAA \xrightarrow{\mu_l} ACA$. Notice that the mutation induces a predator in a—typically large—domain of prey, where it can spread subsequently. Hence the incidence has strong impact on the system. In the dual picture this is expressed in the fact that the pair LR, unlike RL, can separate, e.g.

$$\varnothing\varnothing\varnothing\varnothing \xrightarrow{\mu_l} \varnothing LR\varnothing \xrightarrow{1} L\varnothing R\varnothing \xrightarrow{1} L\varnothing\varnothing R \to \ldots \tag{2.9}$$

Consider what happens next to the, say, R interface. It moves to the right from site to site with rate 1, until it meets and reacts with some other interface. For example, from the right a left moving interface L could approach and they collide,

$$R\varnothing\varnothing L \xrightarrow{1} \varnothing R\varnothing L \xrightarrow{1} \varnothing RL\varnothing \xrightarrow{2} \varnothing\varnothing\varnothing\varnothing\,. \tag{2.10}$$

It is crucial to note that diffusion becomes negligible when the particles are far apart, since their directional motion is described by a Poisson process, whose mean square displacement $\sigma(t) = \sqrt{t}$ becomes small relative to the average distance $\langle x(t)\rangle = t$ it has traveled. Therefore, in our regime one should think of the particles as moving *ballistically*.

For our scaling argument, we partition the lattice in cells of size b and consider the dynamics from this coarse grained point of view. The size of the cells defines the new unit of space, which corresponds to rescaling space as

$$x' = b^{-1}x\,. \tag{2.11}$$

Empty cells become the new vacancies $\varnothing$, cells that contain exactly one interface the new Rs or Ls, respectively. Since the lattice is supposed to be sparsely populated, we disregard the unlikely case of cells containing more than one interface. A μ_l mutation now occurs with b-fold rate, since the whole cell is at disposal. We rescale time t by a factor of b,

$$t' = b^{-1}t\,, \tag{2.12}$$

so that the velocity of the (ballistic) interfaces is unchanged. This implies a rescaled rate

$$\mu_l' = b^2\mu_l\,, \tag{2.13}$$

one factor b for rescaling space and another one for rescaling time. The density evidently becomes b-fold,

$$n(\mu_l') = bn(\mu_l)\,, \tag{2.14}$$

and thus, the interface density will behave as

$$n = \mathscr{A}\sqrt{\mu_l}\,, \tag{2.15}$$

for some factor $\mathscr{A}$, in the limit of an infinitely large lattice. This result is indeed validated by our numerical simulations (Figure 2.3).

At this point, we remark that for the symmetric case with equal cyclic dominance rates $r_A = r_B = r_C = 1$ (defined in Eq. (2.1)), the stationary state can be solved exactly, leading to $\mathscr{A} = \sqrt{2}$. The calculation is deferred to the next section. Here we only illustrate the underlying physics by the following heuristic argument. For symmetric rates, reactions of the type $RR \to \varnothing L$ are negligible, because it takes much longer for an interface to catch up with an interface of the same kind than to collide with a different kind of interface, which it can meet halfway, as it were. Hence $P(RR) = 0$, where $P(RR)$ stands for the probability of finding two interfaces next to each other. We suppose that otherwise the system is uncorrelated, in particular $P(RL) = P(R)P(L)$. Then, up to terms of the order μ_l and due to the symmetry between R and L one has the master equation,

$$\dot{P}(R) \approx \mu_l P(\varnothing\varnothing) - 2P(RL) \approx \mu_l - 2\left[P(R)\right]^2\,. \tag{2.16}$$

Solving for the stationary value indeed yields

$$\mathscr{A} = \sqrt{2}\,. \tag{2.17}$$

2.3.2 First Correction for Mutations to the Predator

To motivate the first correction to the result $n = \sqrt{2\mu_l}$, notice that two interfaces of the same kind move diffusively relative to each other, with diffusion constant 1. The diffusional length scale associated to the average survival time $1/n$ is $1/\sqrt{n} \ll 1/n$ (for small mutation rates). Suppose an R is created x sites to the left of another R, with no other interface (R or L) between them. The probability $P_{\text{pair}}(x,t)$ that the pair of R interfaces is intact after a time t will just be the probability $\int_0^{\frac{x}{2\sqrt{t}}} \mathrm{d}s\; e^{-s^2}$ (see, e.g., [96]) that they have not yet interacted "diffusively" (by the reaction $RR \to \varnothing L$), times the probability that the right R has not

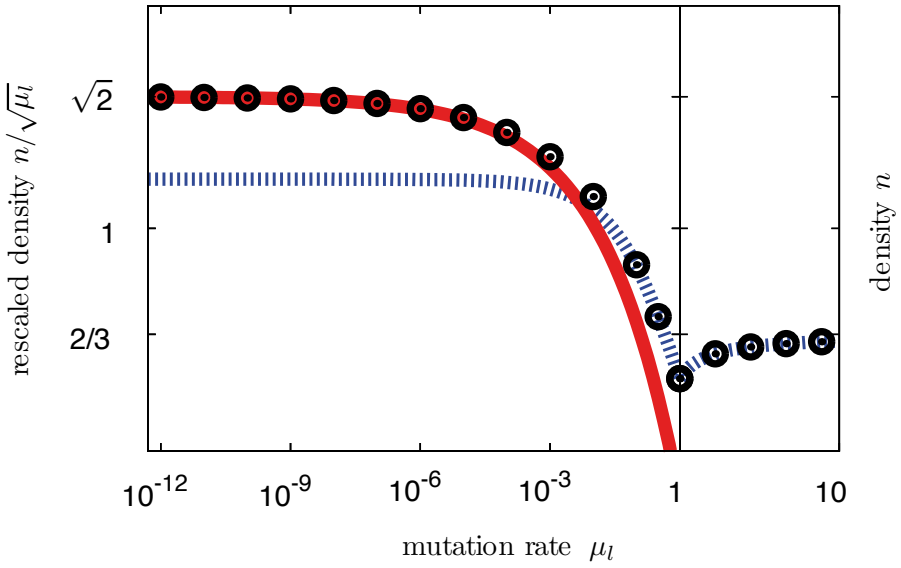

Figure 2.3: Theoretical and empirical (by stochastic simulations) result for the interface density when there are mutations to the respective predator only ($\mu_r = 0$). For low mutation rates we found it convenient to plot the rescaled interface density $n/\sqrt{\mu_l}$, whereas for larger mutation rates ($\mu_l > 1$) we preferred to plot the actual interface density. These two parts of the plot are separated by a line. The results presented here are for the symmetric case with equal cyclic dominance rates $r_A = r_B = r_C = 1$, where the rescaled interface density $n(\mu_l, \mu_r = 0)/\sqrt{\mu_l}$ approaches the law $\sqrt{2} - (3/4)2^{3/4}\mu_l^{1/4}$ (solid red line) as μ_l becomes small. For low mutation rates this formula is indeed in excellent agreement with the numerical data (black circles, the estimated standard deviation is smaller than the size of the circles). As the mutation rate increases, this approximation becomes worse and the curve is described best by the mean-field result, Eq. (2.6) (dotted blue line).

yet collided with an L ($RL \to \varnothing\varnothing$), which is given by an exponential distribution $\exp(-nt)$. For the latter factor we assume that the system is uncorrelated, so that in every time step the right R collides with an L with probability n. The probability that an R is created at a distance x to the left of another R is $n/2$ when $x \ll 1/n$. Upon integrating over space x and time t one finds that the probability of an R interacting diffusively with an R on its right is $\sqrt{n}/2$. If we simply subtract these "failed attempts" of creating it from the mutation rate $\mu_l \to \mu_l(1 - \sqrt{n}/2)$, and multiply it with the average time of survival $1/n$ of an interface, we obtain the density $n/2$ of the R interfaces,

$$\mu_l \left(1 - \frac{\sqrt{n}}{2}\right) \cdot \frac{1}{n} = \frac{n}{2}\,, \tag{2.18}$$

or, solving this for the interface density n up to order μ_l,

$$n \approx \sqrt{2\mu_l}\left(1 - \frac{\sqrt{n}}{4}\right) \approx \sqrt{2\mu_l} - \frac{2^{3/4}}{4}\mu_l^{3/4}\,. \tag{2.19}$$

More careful analysis, as presented in Appendix B, yields an even larger correction

$$n = \sqrt{2\mu_l} - \frac{3}{4}2^{3/4}\mu_l^{3/4}\,, \tag{2.20}$$

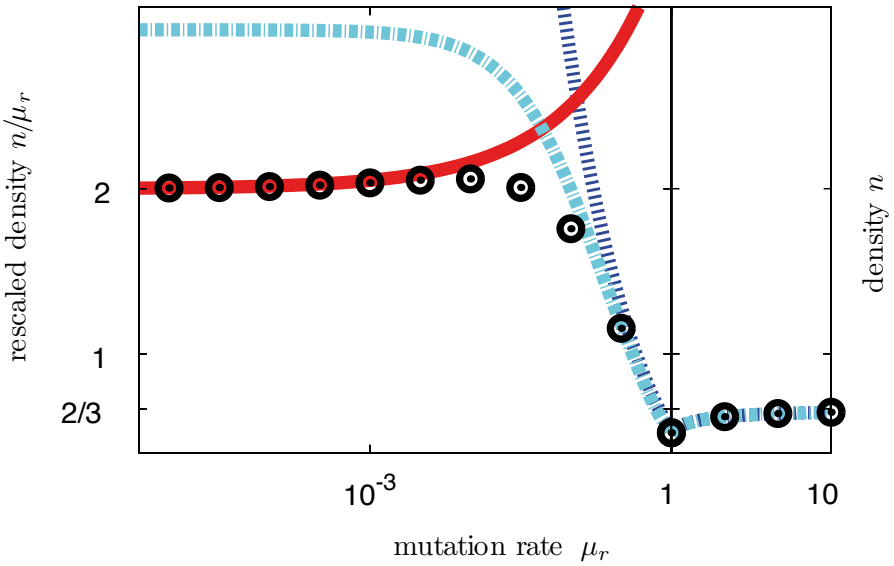

Figure 2.4: Theoretical and empirical (by stochastic simulations) result for the interface density when there are mutations to the respective prey only ($\mu_l = 0$). For low mutation rates μ_r, the rescaled interface density n/μ_r is plotted, whereas for larger rates we show the absolute density n. We consider symmetric cyclic dominance rates $r_A = r_B = r_C = 1$, where our analysis shows that the rescaled density converges to $n(\mu_l = 0, \mu_r)/\mu_r = 2 + 3\sqrt{\mu_r}/2$ (solid red line). This is confirmed by the numerical data (black circles, the estimated standard deviation is smaller than the size of the circles). The mean-field result (dotted dark blue line) and the generalized mean-field result for pairs of two adjacent sites (dotted turquoise line) is also shown. Notice that this pair approximation already predicts the correct scaling $n \sim \mu_r$ for small μ_r, in contrast to the original mean-field result, which wrongly gives $n \sim \sqrt{\mu_r}$. The reason for this is that for an almost vacant lattice the mutations usually create a pair RL which is unstable. To capture this effect one needs to consider pairs of sites or larger clusters, while in the mean-field calculation one considers single, uncorrelated sites. There is only a small regime where none of the approximations describes the results of the simulations well.

up to terms of order 1 and higher in μ_l. The increased amplitude may appear counterintuitive. One should think that the analytic result for the interface density would become larger when one adds the contribution of the interfaces that are undergoing the diffusional interaction. After all, they do not collide immediately and react $RR \to \varnothing L$ (or $LL \to R\varnothing$), but they do so only after some time, which should give a positive contribution to the interface density. However, for truly ballistic interfaces, where diffusional interaction is ruled out, the Rs which are created within a short distance x to the left of another R have a life span of about $2/n$, twice as long as the life span of an arbitrary interface, because they are shielded by the R to their right. Therefore, they are particularly "valuable". If diffusion is turned on, many of them (with an initial distance x smaller or comparable to the diffusional length scale $1/\sqrt{n}$) are taken out of the system by diffusive interaction, $RR \to \varnothing L$. Their destruction implies a relatively strong negative contribution to the interface density n, which is not taken into account in Eq. (2.19). Our improved result, Eq. (2.20), derived in Appendix B, is in agreement with the numerics (Figure 2.3).

2.3.3 Mutations to the Prey

Let us proceed to discuss the case $\mu_l = 0$ and $\mu_r \ll 1$. Since the system is coarse grained, the major part of the mutations will result in one prey in the middle of large domains of predators, for instance $AAA \xrightarrow{\mu_r} ABA$. Evidently, this configuration is rather unstable and one expects that in most cases the cyclic dominance reactions reestablish the original state, that is B turns again to A. In the dual picture, this translates into the creation of a pair RL, which in most cases annihilates quickly,

$$\varnothing\varnothing \xrightarrow{\mu_r} RL \xrightarrow{2} \varnothing\varnothing\,. \tag{2.21}$$

Owing to the longevity of its products, one also needs to take into account that a second mutation may occur,

$$\varnothing\varnothing \xrightarrow{\mu_r} RL \xrightarrow{\mu_r} LR\,, \tag{2.22}$$

effectively leading to

$$\varnothing\varnothing \xrightarrow{\mu_r^2/2} LR\,. \tag{2.23}$$

Just as for mutations to the predator, a pair LR is produced, but this time the reaction is mediated by two μ_r mutations instead of one μ_l mutation. In the particle picture this means that the prey B in a domain of A may be turned into the predator C by a second mutation. The former, reaction (2.21), implies a contribution of μ_r to the interface density. The latter, reaction (2.22), leads to the same dynamics as in the μ_l case and to another term of magnitude $\sqrt{2\,(\mu_r^2/2)} = \mu_r$ to the interface density n. Therefore, to lowest order $n = 2\mu_r$.

For the leading correction, in addition to reactions of the type $RR \to \varnothing L$, one needs to treat instances of mutations when there is exactly one interface around,

$$R\varnothing \xrightarrow{\mu_r} LL\,, \quad \varnothing L \xrightarrow{\mu_r} RR\,. \tag{2.24}$$

In the particle picture, this corresponds to, e.g., $ABB \xrightarrow{\mu_r} ACB$, and $AAC \xrightarrow{\mu_r} ABC$, respectively. Similar reactions can occur, when there is a mutation nearby an interface, for instance,

$$R\varnothing\varnothing\varnothing \xrightarrow{\mu_r} R\varnothing RL \xrightarrow{1} \varnothing RRL \xrightarrow{1} \varnothing\varnothing LL\,. \tag{2.25}$$

An analysis analogous to the pure μ_l case yields an overall positive contribution (see Appendix B)

$$n = 2\mu_r + \frac{3}{2}\mu_r^{3/2}\,, \tag{2.26}$$

up to order 2 and higher in μ_r. Figure 2.4 confirms this behavior. Again mean-field is an excellent approximation for large mutation rates. But as mutations become less frequent, Eq. (2.6) provides a gross over-estimate of the interface density, because the approach cannot keep track of the large amount of pairs of RL that annihilate quickly. This can be amended by a generalized mean-field approach [7, 94, 95], where the master equation for clusters of N adjacent sites is considered. A truncation in the hierarchy of probability distributions yields a closed set of differential equations, which can be solved numerically. For clusters of size 2 we already retrieve the right scaling law $n \sim \mu_r$ ($\mu_r \ll 1$).

Again, we explain how a scaling analysis helps us understand the behavior of the density $n(\mu_r, \mu_l = 0)$. This will also extend our results to the more general processes of the next

subsection. We partition the lattice in cells of size b. Then the probability for a cell to contain a pair RL, which are created and destroyed according to reaction (2.21), becomes $\mu_r' = b\mu_r$, while the rate of creating a pair LR out of RL (2.22) evidently remains μ_r. Again, we rescale time, $t' = b^{-1}t$, in order that the velocity of R and L, measured in the average number of cells they traverse in unit time, stays one. Now the right-hand side of reaction (2.22) occurs at a rate $b\mu_r$, while the probability of finding a pair LR remains $b\mu_r$. This implies

$$\mu_r' = b\mu_r\,, \quad n(\mu_r') = bn(\mu_r)\,, \tag{2.27}$$

whereby we conclude

$$n = \mathscr{B}\mu_r\,, \tag{2.28}$$

for some factor $\mathscr{B}$. Of course, from Eq. (2.26) we already know that for mutations to the prey $\mathscr{B} = 2$.

2.3.4 The General Case

We have seen in the previous subsection that the mutations to the prey effectively create a pair LR with rate $\mu_r^2/2$, whereas for mutations to the predator this rate is simply μ_l. It poses no additional difficulties to introduces both mutations at the same time. The effective rate of the creation of LR then becomes

$$\mu_{\text{eff}} = \mu_l + \frac{\mu_r^2}{2}\,, \tag{2.29}$$

and to lowest order

$$n = \sqrt{2\mu_{\text{eff}}} + \mu_r\,. \tag{2.30}$$

The additional term μ_r stems from the unstable pairs RL, see reactions (2.21).

Up to now we have restricted to symmetric cyclic dominance rates $r_A = r_B = r_C = 1$ (defined in Eq. (2.1)), where reactions governed by diffusion, $RR \to \varnothing L$ and $LL \to R\varnothing$, give rise to the correction terms in Eqs. (2.20,2.26) which do not agree with our scaling arguments. Now consider what happens if r_A, r_B, r_C are not identical, for instance suppose that $r_A > r_B = r_C$. The dual picture then only gives a complete description if one distinguishes different types of right moving and of left moving interfaces. For the right moving interfaces we have the three cases R_{AB}, R_{BC} and R_{CA}, where the index stands for the corresponding sequence in the particle picture. Compared to R_{BC} and R_{CA} the interface R_{AB} moves faster. When the interface density is low, the stochastic effects in the motion are negligible and their relative motion does not have a diffusive character but is best described as ballistic. Thus, an R_{AB} escapes an R_{CA} to its left with velocity $r_A - r_B$ and is on collision course with an R_{BC} to its right with velocity $r_A - r_C$. Of course the relative motion of the right moving and the left moving interfaces is also approximately ballistic.

After rescaling space by a factor b^{-1}, by subsuming b adjacent sites to one cell, and likewise rescaling time by b^{-1}, the relative velocities remain the same. By the same arguments as for the symmetric case, the rates which cause the creation of a pair LR rescale as $\mu_l' = b^2\mu_l$ and $\mu_r' = b\mu_r$. For the asymmetric case, however, we need to take into account two

additional mechanisms which increase the number of interfaces. Firstly, reactions where a pair of interfaces moving in the same direction are created from one interface, for instance,

$$\varnothing L_{CB} \xrightarrow{\hat{\mu}_r} R_{CA}R_{AB}\,, \tag{2.31}$$

with rate $\hat{\mu}_r = \mu_r$. When $r_A > r_B = r_C$, there is a finite probability that the R_{AB} escapes the left R_{CA}. For a cell of size b, with probability b^{-1} the mutation takes place at the right spot in order to create the two right moving interfaces. On the other hand there is a factor b for the increase in the density of the L_{CB} interfaces and another factor b for the rescaling of time. Thus, we have the rescaling

$$\hat{\mu}'_r = b\hat{\mu}_r\,, \tag{2.32}$$

in agreement with a b-fold mutation rate $\mu'_r = b\mu_r$ to the prey. (In contrast, for mutations to the predator, reactions of the form $L_{CB}\varnothing \to R_{CA}R_{AB}$ with rate μ_l are negligible since they only scale as $b\mu_l$, whereas the rate for the creation of LR pairs scales as $b^2\mu_l$.)

The second mechanism which gives a relevant contribution to the production of interfaces is related to the unstable pairs RL, which are created by the μ_r mutation and in most cases are subject to pair annihilation $RL \to \varnothing\varnothing$ shortly after their creation. In every step an L_{CB} moves to the left, with the small probability $\mu_r/(2r_C) =: \tilde{\mu}_r$ it collides with a pair $R_{CA}L_{AC}$, triggering the reaction $R_{CA}L_{AC}L_{CB} \to \varnothing R_{CA}R_{AB}$. Since R_{AB} moves faster to the right than R_{BA}, with a finite probability it escapes. Thus, effectively this mechanism gives rise to the production of a pair $R_{CA}R_{AB}$ from an L_{CB} interface (and correspondingly for left and right interchanged). Under our coarse graining, because of the rescaling of time, $t' = b^{-1}t$, the rate with which a pair $R_{CA}R_{AB}$ is effectively produced from an L_{AB} becomes b-fold,

$$\tilde{\mu}'_r = b\tilde{\mu}_r\,. \tag{2.33}$$

Since $\tilde{\mu}_r = \frac{\mu_r}{2r_C}$ and $r'_C = r_C$ (the velocities of the interfaces remain the same) this is again in agreement to a b-fold rate $\mu'_r = b\mu_r$ to the prey.

In summary, under the coarse graining, mutations leading to the pairs LR, LL and RR all effectively obey the scaling $\mu'_l = b^2\mu_l$, and $\mu'_r = b\mu_r$, and the interface density behaves as $n' = bn$. We thus conclude that for the general model, the interface density in the low density regime must behave as

$$n(\mu_l, \mu_r) = \sqrt{\mu_l}\,\phi\!\left(\frac{\mu_r}{\sqrt{\mu_l}}\right)\,, \tag{2.34}$$

for some scaling function ϕ, which depends on the rates r_A, r_B and r_C. This is corroborated by the results of the stochastic simulations, c.f. Figure 2.5. For symmetric rates $r_A = r_B = r_C = 1$ the scaling function is simply given by $\phi(x) = \sqrt{2 + x^2} + x$. As we will discuss in the following section, the reason why we can obtain this exact analytic expression is that the system relaxes to an equilibrium state. Moreover, we will argue that, in contrast, for asymmetric rates, the stationary state is far from equilibrium, and we therefore cannot apply the tools from equilibrium physics to solve it and to obtain an analytic expression for the scaling function ϕ. There is one exception to this, however: In the limit of $r_A \to \infty$, with fixed $r_B = r_C = 1$, one obtains again an equilibrium stationary state. The exact calculations for this limiting case, presented in Subsection 2.4.3, yield the scaling function $\phi(0) \to 1$. Figure 2.5 indicates that even for $r_A = 5$ this is a good approximation.

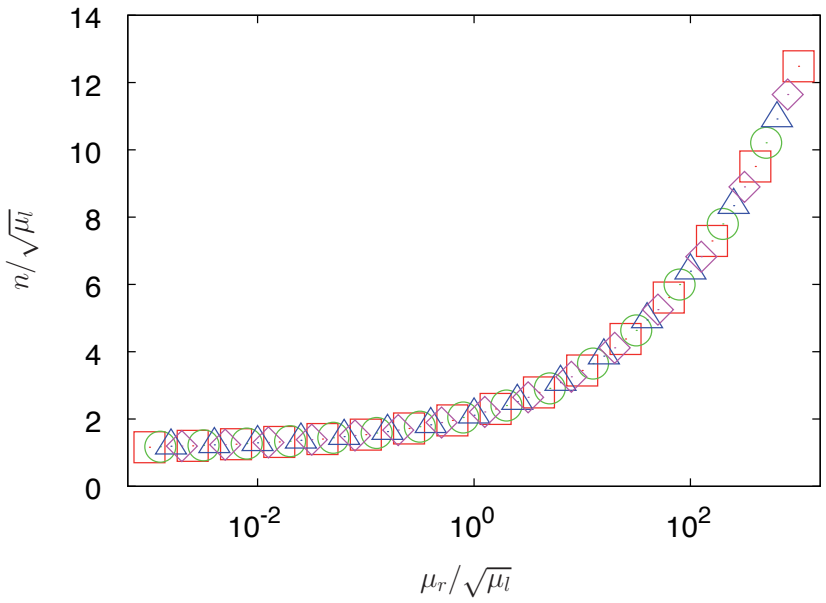

Figure 2.5: Collapse of the data for the rescaled interface density $n/\sqrt{\mu_l}$ onto a scaling function $\phi(\mu_r/\sqrt{\mu_l})$. In certain limiting cases, in particular for symmetric rates, $r_A = r_B = r_C$, one can find an analytic expression for the scaling function. However, our scaling arguments should also hold for asymmetric rates r_A, r_B, r_C. This is indeed corroborated by our simulation results. The data plotted here is for the cyclic dominance rates $r_A = 5$, $r_B = r_C = 1$. The data points are $\mu_l = 2^{-10}(\square), 2^{-11}(\bigcirc), 2^{-12}(\triangle), 2^{-13}(\diamond)$.

2.4 The Low Density Limit and Detailed Balance

As shown in the previous section, when both mutation rates are comparably small, $\mu_l \approx \mu_r \ll 1$, then the effect of the mutations to the prey with rate μ_r is negligible. Let us therefore restrict to mutations to the predator $\mu_l \ll 1$, $\mu_r = 0$ in the following. By a heuristic approach we have argued that when the mutation rate μ_l becomes very small, the interface density behaves as $n = \sqrt{2\mu_l}$. In this section we provide a rigorous derivation of the probability distribution of the number of interfaces in a system of finite size, and we indeed recover $n = \sqrt{2\mu_l}$ for large systems. For the time being, we assume perfect symmetry between the species, i.e. the cyclic dominance rates, defined in (2.1), are equal, $r_A = r_B = r_C = v$. We will relax this condition later in this section.

Since the mutation rate is assumed to be very low, most lattice sites are vacant and the interfaces, on average, travel long distances before they collide with another interface. Therefore we may neglect the diffusional motion (whose standard deviation compared to the distance traveled becomes small) and regard the interfaces as ballistic, i.e. traveling at constant velocity in continuous (one-dimensional) space. Thus the interfaces L, R move along a line of length M (which denotes the system size) at speed $-v$, $+v$ respectively. As usual we consider toroid boundary conditions.

The only reactions which are relevant for very low mutation rates are R and L annihilating on impact (reaction (1) in Figure 2.1) and pairs LR of interfaces being created with rate μ_l on

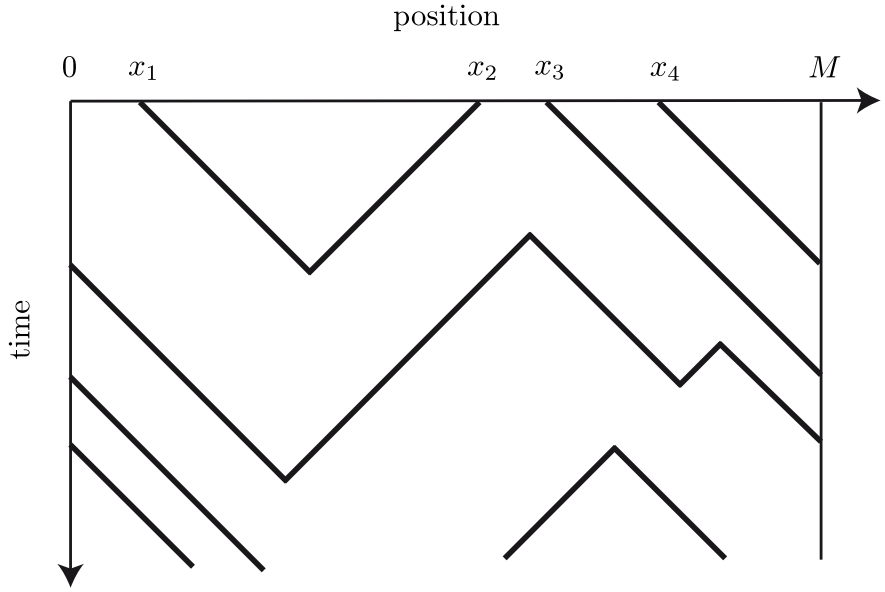

Figure 2.6: Illustration of the dynamics for very low mutation rates μ_l and low interface densities n, when the rates $r_A = r_B = r_C$ are equal, so that there is symmetry between the three species, rock, paper, and scissors. Initially, distributed on the line $]0, M]$, there are three right moving interfaces at x_1, x_3 and x_4, with velocity v, and one left moving interface at x_2, with velocity $-v$. Compared to the long distances $\sim 1/n$ which the interfaces travel on average until they collide with another interfaces, their deviation from the linear path by diffusional motion can be neglected, since this deviation is only of the order $\sqrt{1/n}$. We can therefore describe the interfaces as ballistic particles which annihilate when they meet and are created in pairs on a random position $x \in]0, M]$ with mutation rate μ_l. Notice the time reversal symmetry: If we let time run backwards the creation of pairs of interfaces simply turns to pair annihilation and vice versa. Reactions which would breach the time reversal symmetry, such as $RR \to \varnothing L$ ($LL \to R\varnothing$), can be ruled out, because for ballistic motion a right (left) moving interface cannot catch up with another right (left) moving interface.

a random point in the interval $]0, M]$ (reaction (2) in Figure 2.1). Of course, under suitable rescaling (e.g. time $t \to c_1 t$ and space $x \to c_2 x$, with $c_1 = \frac{v}{M}$ and $c_2 = \frac{1}{M}$) one can eliminate all but one of the three parameters v, M, μ_l. However, they can help us keep track of the dimensions. $[v] = \frac{m}{s}$, $[M] = m$, $[\mu_l] = \frac{1}{ms}$, where "meter" m and second "s" stand for units of space and time, respectively. Notice the dimensionless product

$$\frac{\mu_l M^2}{v} \,. \tag{2.35}$$

For a unique stationary state, dimensionless quantities, such as the probability distribution of the number of interfaces in the system, can only depend on this product. As an application, we employ dimensional analysis to recover the scaling law of the interface density n for large M: The dimension of the density is $[n] = \frac{1}{m}$. In the limit of infinitely large system size, $M \to \infty$, we only dispose of v and μ_l to fix the dimension. Therefore, the only possible solution is that $n \sim \sqrt{\frac{\mu_l}{v}}$. (Alternatively we can argue that the dimensionless quantity $n/\sqrt{\frac{\mu_l}{v}}$ depends

only on the ratio (2.35), $n/\sqrt{\frac{\mu_l}{v}} = f\left(\frac{\mu_l M^2}{v}\right)$, some function f which attains a finite value as $M \to \infty$.)

Now, the crucial observation is that the two reactions, illustrated in Figure 2.1, of pair annihilation (1) and pair creation (2) are just the time reversals of each. Thus, we expect that, as is the case for most physical systems, the process is invariant under time reversal, once it has reached its stationary state and it fulfills the detailed balance principle. This principle roughly states that every transition is balanced by its reversed transition [91, 97], in which case one also speaks of equilibrium. Indeed, as we will rigorously prove below, there is stationary state that obeys these equilibrium conditions, despite the fact that RPS is often given as a paradigmatic example of a non-equilibrium process. Moreover, we will see that the system obeys a Boltzmann statistics with an energy that is a function of the number of interfaces (for large systems sizes M this energy becomes approximately proportional to the number of interfaces).

2.4.1 Exact Solution to the Stationary State

Since the interfaces are created and destroyed in pairs, the difference d in the number $m+d$ of left moving interfaces L and the number m of right moving interfaces R is conserved. Without restriction of generality, let us assume that there are more Ls than Rs, i.e. $d \geq 0$. We can write the configuration as the $2m+d$-tuple

$$(z_1, \ldots, z_{2m+d}) = \mathbf{z}\,, \tag{2.36}$$

with elements that can be expressed in terms of complex numbers

$$z_k = x_k + iy_k = (x_k, y_k)\,, \quad x_k \in]0, M], \quad y_k \in \{v, -v\}\,. \tag{2.37}$$

Here the coordinate $x_k \in]0, M]$ specifies the position on the line, and $y_k \in \{v, -v\}$ specifies the velocity of the interface ($+v$ for R and $-v$ for L). (Complex numbers are convenient, because under time reversal z_k turns to its complex conjugate $z_k^\star = x_k - iy_k = (x_k, -y_k)$). We demand that the positions x_k be ordered,

$$x_1 \leq x_2 \leq \ldots \leq x_{n-1} \leq x_n\,. \tag{2.38}$$

An equal sign, $x_k = x_{k+1}$, either means that there is a pair LR, which has just been created by a mutation and which then will move apart, in which case $y_k = -v$ and $y_{k+1} = v$; or it means that we have a pair RL which will be annihilated in the next instant, in which case $y_k = v$ and $y_{k+1} = -v$. Let us provisionally rule out configurations with LR pairs. Then the probability density evolves as,

$$\begin{aligned}\partial_t \rho_{m,m+d}(\mathbf{z}) = &-\sum_{k=1}^{2m+d} \partial_{x_k} \rho_{m,m+d}(\mathbf{z}) y_k - \mu_l M \rho_{m,m+d}(\mathbf{z}) + \\ &+ 2v \int \mathrm{d}x\, \rho_{m+1,m+d+1}(\mathbf{z} \cup \{x+iv, x-iv\})\,.\end{aligned} \tag{2.39}$$

Here $\rho_{m,m+d}(\mathbf{z})$ denotes the probability density of a configuration $\mathbf{z}$ that has m right moving and $m+d$ left moving interfaces, and the union $\mathbf{z} \cup \{x+iv, x-iv\}$ stands for the $2m+d+2$-tupel which contains the elements of $\mathbf{z}$ together with the two elements $x+iv$, and $x-iv$,

for the pair RL. These elements must be reordered in accord with the relation (2.38). The first term on the right hand side of Eq. (2.39) causes the ballistic motion of the interfaces. The second term describes a flow away from the configuration $\mathbf{z}$ due to mutations. The third, positive term accounts for the annihilation of a pair RL for configurations $\mathbf{z} \cup x + iv \cup x - iv$ which are, up to this pair, identical to $\mathbf{z}$.

Because of the relation (2.38), there arises a subtlety concerning the spatial derivative ∂_{x_k}, in the case that we have a pair LR. It is essential to keep in mind that the derivative is defined as the limiting process

$$\partial_{x_k} \rho_{m,m+d}(\mathbf{z})\big|_{z_k = x_k + iy_k} = \lim_{\epsilon \to 0} \frac{\rho_{m,m+d}(\mathbf{z})\big|_{z_k = x_k + iy_k} - \rho_{m,m+d}(\mathbf{z})\big|_{z_k = x_k - y_k \epsilon + iy_k}}{|\tilde{y}|\epsilon}\,, \tag{2.40}$$

i.e. the derivative is in the opposite direction of the motion of the particles. Thus it is well-defined if we have a RL pair, $x_k = x_{k+1}$, with $y_k = v$, $y_{k+1} = -v$, since the ordering $x_k \leq x_{k+1}$ is conserved. Below, we will also have to deal with LR pairs, $x_k = x_{k+1}$, with $y_k = -v$, $y_{k+1} = v$. In this case, due to the ordering (2.38), the probability density for a configuration with $x_k > x_{k+1}$ vanishes by definition. Thus, the derivative in space typically gives rise to a delta function.

For the solution of Eq. (2.39), our ansatz is that the probability density only depends on the numbers m and $m + d$ of R and L interfaces, respectively, i.e.

$$\rho_{m,m+d}(\mathbf{z}) \equiv \rho_{m,m+d}\,. \tag{2.41}$$

The ballistic term (involving the spatial derivatives ∂_{x_k}) then trivially cancels, while the third term gives $2vM\rho_{2m+d+2}$. If this is to cancel with the second term we must have

$$\rho_{m+1,m+d+1} = \frac{\mu_l}{2v}\rho_{m,m+d} \quad \Longrightarrow \quad \rho_{m,m+d} = \left(\frac{\mu_l}{2v}\right)^m \rho_{0,d}\,. \tag{2.42}$$

Therefore, if we attribute to the creation of a pair LR an energy difference of $\Delta E = \ln(2v/\mu_l)$, we obtain the Boltzmann distribution $\rho_{m,m+d} = e^{-m\,\Delta E}\rho_{0,d}$.

To obtain the probability, $p_{m,m+d}$ that there are m right moving interfaces and $m + d$ left moving interfaces, we integrate over all configurations,

$$p_{m,m+d} = \frac{1}{m!(m+d)!}\left(\frac{\mu_l M^2}{2v}\right)^m p_{0,d}\,, \tag{2.43}$$

with the "partition function"

$$p_{0,d}^{-1} = \sum_{m=0}^{\infty} \frac{1}{m!(m+d)!}\left(\frac{\mu_l M^2}{2v}\right)^m\,. \tag{2.44}$$

As one should expect, the dimensionless probabilities $p_{m,m+d}$ are functions of the aforementioned dimensionless quantity $\frac{\mu_l M^2}{v}$. In these equations the factorials $m!$ and $(m+d)!$ account for the fact that the m right moving interfaces R are indistinguishable and so are $m + d$ left moving interfaces L. Eq. (2.44) guarantees the normalization of the probability distribution $p_{m,m+d}$ for a fixed difference d. Incidentally, the right hand side of Eq. (2.44) may be expressed as a Bessel function of the first kind, with an imaginary argument, $p_{0,d}^{-1} = J_\alpha\left(i\frac{\mu_l M^2}{v}\right)$.

From the probability distribution $p_{m,m+d}$, c.f. Eqs. (2.43,2.44), we can now calculate the expectation value of the interface density n. Without loss of generality, let us set the velocity of the interfaces equal to one, $v = 1$, in the following calculations. We then find that the interface density is given by

$$n = \frac{1}{M}\sum_{k=1}^{\infty}\frac{2m+d}{m!(m+d)!}\left(\frac{\mu_l M^2}{2}\right)^m p_{0,d}^{-1} = \frac{2}{M}\mu_l\partial_{\mu_l}\left[\sum_{k=1}^{\infty}\frac{1}{m!(m+d)!}\left(\frac{\mu_l M^2}{2}\right)^m\right]p_{0,d}^{-1} + \frac{d}{M} =$$

$$= \frac{2\mu_l}{M}\partial_{\mu_l}\ln\left(p_{0,d}^{-1}\right) + \frac{d}{M}\,. \tag{2.45}$$

In the limit of large system size M, only large numbers m of R interfaces need to be considered and we can employ the Stirling formula $m! \approx \left(\frac{m}{e}\right)^m \approx (m+d)!$ Thus,

$$p_{0,d}^{-1} = \sum_{m=0}^{\infty}\frac{1}{m!(m+d)!}\left(\frac{\mu_l M^2}{2}\right)^m \approx \sum_{m=0}^{\infty}\frac{1}{(m/e)^m\cdot(m/e)^m}\left(\frac{\mu_l M^2}{2}\right)^m \approx$$

$$\approx \sum_{m=0}^{\infty}\frac{1}{(2m)!}\left(\sqrt{2\mu_l M^2}\right)^m \approx \sum_{m'=0}^{\infty}\frac{1}{m'!}\left(\sqrt{2\mu_l M^2}\right)^{m'} = \exp\left(2\mu_l M^2\right)\,. \tag{2.46}$$

For large system sizes M, this yields

$$n = \frac{2\mu_l}{M}\partial_{\mu_l}\sqrt{2\mu_l M^2} = \sqrt{2\mu_l}\,. \tag{2.47}$$

We thus rigorously recover a central result of the previous section, which before was only derived by heuristic means.

To complete the proof that in Section 2.3 we have actually guessed the correct stationary probability distribution, we need to consider also the case when there is a pair LR. Suppose that $z_k = x_k - iv$ and $z_{k+1} = x_{k+1} + iv$, then we now allow the two interfaces to share the same position $x_k = x_{k+1}$. These configurations were ruled out in the derivation of Eq. (2.39). The general differential equation determining the time evolution of the probability density reads

$$\partial_t\rho_{m,m+d}(\mathbf{z}) = -\sum_{k=1}^{2m+d}\partial_{x_k}\rho_{m,m+d}(\mathbf{z})y_k - \mu_l M\rho_{m,m+d}(\mathbf{z}) + \tag{2.48}$$

$$+ 2v\int \mathrm{d}x\,\rho_{m+1,m+d+1}(\mathbf{z}\cup\{x+iv, x-iv\}) -$$

$$+ \sum_{k=1}^{2m+d-1}\mu_l\delta(x_k - x_{k+1})\delta_{y_k,-v}\delta_{y_{k+1},v}\,\rho_{m-1,m-1+d}(\mathbf{z}\backslash\{z_k, z_{k+1}\})\,, \tag{2.49}$$

which is identical to Eq. (2.39) up to the additional last term that describes the pair creation. Some readers may find it more intuitive to express this term as

$$\sum_{k=1}^{2m+d-1}\mu_l\sum_{\tilde{\mathbf{y}}\in\{-v,v\}^{2m+d}}\int \mathrm{d}^{2m+d}\tilde{x}\,\delta(z_k - z_k^\star)\delta(\mathbf{z} - \tilde{\mathbf{z}}\cup\{z_k, z_{k+1}\})\,\rho_{m-1,m-1+d}(\tilde{\mathbf{z}})\,. \tag{2.50}$$

Now, x_{k+1} cannot be smaller than x_k because these coordinates are ordered (see relation (2.38)), i.e. the probability density $\rho_{m,m+d}(\mathbf{z})$ vanishes when $x_k > x_{k+1}$. Therefore, according to our definition of the derivatives ∂_{x_k}, Eq. (2.40), the first term in Eq. (2.49) gives rise to a delta function. Explicitly, if $z_k = x - iv$ and $z_{k+1} = x + iv$, then

$$-\partial_{x_k}\rho_{m,m+d}(\mathbf{z})y_k - \partial_{x_{k+1}}\rho_{m,m+d}(\mathbf{z})y_{k+1} = -2v\,\delta(x_k - x_{k+1})\delta_{y_k,-v}\,\delta_{y_k,+v}\,\rho_{m,m+d}(\mathbf{z})\,. \quad (2.51)$$

For our guess for the stationary distribution, with constant $\rho_{m,m+d}(\mathbf{z}) \equiv \rho_{m,m+d}$ and $\rho_{m,m+d} = \frac{\mu_l}{2v}\rho_{m-1,m-1+d}$ (see Eq. (2.42)), this evidently cancels with the last term in Eq. (2.49). Furthermore, the second and third term of Eq. (2.49) cancel each other for the same reason as before, which completes the proof that Eq. (2.42) is a stationary solution of our process.

2.4.2 Proof of Detailed Balance

We have not yet exploited the principle of detailed balance, apart from arguing that it should hold because of the time reversal symmetry between pair annihilation and pair creation (reactions (1) and (2) in Figure 2.1), and claiming that it indicates a relatively simple stationary state. Let us look more carefully at this principle, show that it is actually fulfilled and thus again prove that Eq. (2.42) gives a stationary solution.

Detailed balance concerns transitions between two configurations. Consider, for instance, a gas whose configuration at time t is specified by the coordinates $\mathbf{x} = (x_1, \ldots, x_n)$ of its particles and their velocities $(y_1, \ldots, y_n)$. If at a later instance in time $t + \Delta t$ the system is in the configuration $\mathbf{x}'$ and $\mathbf{y}'$ (for the position and velocity coordinates, respectively) one speaks of a transition

$$(\mathbf{x}, \mathbf{y}, t) \to (\mathbf{x}', \mathbf{y}', t + \Delta t)\,, \quad (2.52)$$

between these two configurations. Its reversed transition is defined as

$$(\mathbf{x}', -\mathbf{y}', t) \to (\mathbf{x}, -\mathbf{y}, t + \Delta t)\,, \quad (2.53)$$

where in addition to interchanging the primed and unprimed coordinates, one changes the signs of the velocities. One speaks of detailed balance when, in the stationary state, the joint probabilities of these transitions are equal,

$$\rho(\mathbf{x}', \mathbf{y}', t + \Delta t; \mathbf{x}, \mathbf{y}, t) = \rho(\mathbf{x}, -\mathbf{y}, t + \Delta t; \mathbf{x}', -\mathbf{y}', t)\,. \quad (2.54)$$

For a Markov process, which has no memory and whose time evolution therefore only depends on the current state of the system but not on the past (as is the case for our model), this can be expressed as

$$p(\mathbf{x}', \mathbf{y}', t + \Delta t|\mathbf{x}, \mathbf{y}, t)\rho(\mathbf{x}, \mathbf{y}, t) = p(\mathbf{x}, -\mathbf{y}, t + \Delta t|\mathbf{x}', -\mathbf{y}', t)\rho(\mathbf{x}', -\mathbf{y}', t)\,, \quad (2.55)$$

where $p(\ldots|\ldots)$ denotes the conditional probability for the transition. (Of course, in the stationary state, these quantities are independent of the time t.) It readily follows that for two subsequent transitions

$$p(\mathbf{x}'', \mathbf{y}'', t + 2\Delta t|\mathbf{x}', \mathbf{y}', t + \Delta t)p(\mathbf{x}', \mathbf{y}', \Delta t|\mathbf{x}, \mathbf{y}, t)\rho(\mathbf{x}, \mathbf{y}, t) =$$

$$= p(\mathbf{x}, -\mathbf{y}, t + 2\Delta t|\mathbf{x}', -\mathbf{y}', t + \Delta t)p(\mathbf{x}', -\mathbf{y}', t + \Delta t|\mathbf{x}'', -\mathbf{y}'', t)\rho(\mathbf{x}'', -\mathbf{y}'', t)\,, \tag{2.56}$$

and so on for longer chains of transitions. Therefore, it is enough to verify detailed balance for infinitesimally small time intervals Δt.

Let us return to the treatment of our RPS model. The ballistic part of the time evolution is almost trivial. Consider the configurations $\mathbf{z} = (\mathbf{x}, \mathbf{y})$ and $\mathbf{z}^* = (\mathbf{x}, -\mathbf{y})$. The probability flow due to the ballistic motion in the direction $\mathbf{y}/v$ and $-\mathbf{y}/v$ for $\mathbf{z}$ and $\mathbf{z}^\star$, respectively, is evidently equal to $2v\rho_{m,m+d}$ and $2v\rho_{m+d,m}$, for constant $\rho_{m,m+d}(\mathbf{z}) \equiv \rho_{m,m+d}$ and $\rho_{m+d,m}(\mathbf{z}^\star) = \rho_{m,m+d}$. Thus, in order that the probability flow in both directions is balanced we have to demand that

$$\rho_{m,m+d} = \rho_{m+d,m}\,, \tag{2.57}$$

i.e. there is a symmetry between the configurations with m Rs and $m+d$ Ls and the configurations with $m+d$ Rs and m Ls. In particular, this is automatically fulfilled if the difference d between the number of right and left moving interfaces vanishes, $d = 0$. Furthermore, since the annihilation of two interfaces is governed by ballistic motion as well, we need to attribute a probability flow of $2v\rho_{m,m+d}(\mathbf{z})$ to the transition from the configuration $\mathbf{z} \cup x + iv \cup x - iv$ (with a pair RL that is about to annihilate) to the configuration $\mathbf{z}$. This must be balanced with the reversed transition, where due to a mutation a pair LR is added at position x to the configuration $\mathbf{z}^\star$. This gives a probability flow of $\mu_l\rho_{m-1,m-1+d}$ from $\mathbf{z}^\star$ to $\mathbf{z}^\star \cup x - iv \cup x + iv$. Thus, detailed balance is fulfilled if $2v\rho_{m,m+d}(\mathbf{z}) = \mu_l\rho_{m-1,m-1+d}$ and we recover Eq. (2.42).

In Figure 2.7 the detailed balance principle is illustrated for a discretized version of our process, so that we can work with probabilities p of configuration $\mathbf{z}$, rather than probability densities ρ. We consider a model where the interfaces are again on a lattice, defined as follows: With a rate v/a the R interfaces collectively move the right, and with the same rate v/a the L interfaces collectively move to the left, by one lattice site. Here a denotes the lattice spacing. This dynamics rules out reactions of the form $RR \to \varnothing L$ or $LL \to R\varnothing$, where two interfaces of the same type react, and which would breach detailed balance for lack of a corresponding time reversed transition. When two interfaces, R and L, meet on same site, the motion of all interfaces is halted until this pair RL has annihilated, which occurs with rate $2v/a$. We remark that we are particularly interested in the limit of small lattice spacings, $a \to 0$, where this stop of the motion is very rare and therefore has little effect on the average velocity of the interfaces. In the—for small lattice spacing a unlikely—case of several pairs RL, each is subject to pair annihilation independently with rate $2v/a$. By a mutation a pair LR is created at a certain site with rate $a\mu_l$. (Of course, as opposed to pairs RL, they do not annihilate each other.)

Let us denote by $p_{m,m+d}(\mathbf{z}) = p^s_{m,m+d}$ the stationary probability of a particular configuration in this lattice model. The collective motion of, say, the right moving interfaces R implies a probability flow of $\frac{v}{a}\,p^s_{m,m+d}$ from the configuration $\mathbf{z} = (\mathbf{x}, \mathbf{y})$ to the configuration $\mathbf{z}' = (\mathbf{x} + \Delta\mathbf{x}, \mathbf{y})$, where $\Delta\mathbf{x} = a\mathbf{y}/v$ if $y_k = v$ (i.e. if the kth interface is right moving) and $\Delta\mathbf{x} = 0$ if $y_k = -v$ (i.e. if the kth interface is left moving). For pair annihilation, we have a probability flow of $\frac{2v}{a}p^s_{m+1,m+1+d}$ from the configuration $\mathbf{z} \cup x + iv \cup x - iv$ to the configuration $\mathbf{z}$ without the annihilated pair. Furthermore, there is a flow of $a\mu_l p^s_{m,m+d}$ from some configuration $\tilde{\mathbf{z}}$ to a configuration $\tilde{\mathbf{z}} \cup x - iv \cup x + iv$ with an additional pair LR at a particular position x. These two transitions for pair annihilation and pair creation balance on condition that

$2vp^s_{m+1,m+1+d} = a^2\mu_l p^s_{m,m+d}$. When we let the lattice spacing go to zero, $a \to 0$, we recover Eq. (2.42) for the stationary probability density of the continuum model.

2.4.3 Violation of Detailed Balance for Asymmetric Cyclic Dominance Rates

Up to now we have restricted to perfect symmetry between the three species, with identical reaction rates $r_A = r_B = r_C$, c.f (2.1), such that the velocities of the different interfaces were all equal. In the limit of very low interface densities, we found that the system displays a stationary state that is in equilibrium, by explicitly verifying that the detailed balance principle is fulfilled. Let us also consider this limit of low interface densities and low mutation rates, where the motion of the interfaces can be approximated as ballistic, for general reaction rates r_A, r_B, and r_C. We find for this asymmetric case that, in contrast to the identical rates $r_A = r_B = r_C$, detailed balance cannot hold. To see this, suppose that $r_A > r_B$, so that the right moving interface between an A and a B domain, denoted R_{AB}, moves with higher velocity than the interface R_{BC} between the B and C domain. Then the reaction of the two interfaces, $R_{AB} + R_{BC} = L_{AC}$ (where L is the left moving interface R_{BC} between an A and a C domain), is not governed by diffusion as for the symmetric case but by ballistic motion. Therefore, it must not be neglected in our limit of low densities. Since there is no corresponding reverse reaction, where the L_{AB} interface would turn into an R_{AB} and an R_{BC}, this violates detailed balance, and we cannot expect a simple stationary state as in the previous section. There is a notable exception to this, however, when the difference in the speed of the reactions becomes large, as is discussed now.

2.4.4 Time Scale Separation and Recovery of Detailed Balance

In the laboratory experiments by Kerr et al., described in Section 1.1, there is a strain of bacteria which produces a toxin and thus kills a sensitive strain on a relatively short time scale compared to the time scale of the interaction of the resistant strain with the toxic and the sensitive strain. Here, we study the implication of a separation between the time scales of the "toxic" reaction rate and the other two cyclic dominance reaction rates.

Let $r_A = r_B = 1$ and $r_C = \infty$. In Figure 2.8 the ensuing dynamics is illustrated in a two dimensional space-time plot. Strikingly, when a mutation in a domain of A occurs, say

$$BAABBAAAAABBCCB \xrightarrow{5\mu_l} BAABBACAAABBCCB\,, \tag{2.58}$$

with rate μ_l, then the other sites are taken over instantaneously,

$$BAABBACAAABBCCB \xrightarrow{\infty} BAABBCCCCCBBCCB\,, \tag{2.59}$$

with infinite rate. Thus, the combined, effective reaction is

$$BAABBAAAAABBCCB \xrightarrow{5\mu_l} BAABBCCCCCBBCCB\,. \tag{2.60}$$

Since we want to study the detailed balance principle for this process, it is necessary to define reversed transitions. In order to uniquely describe a configuration, we must distinguish

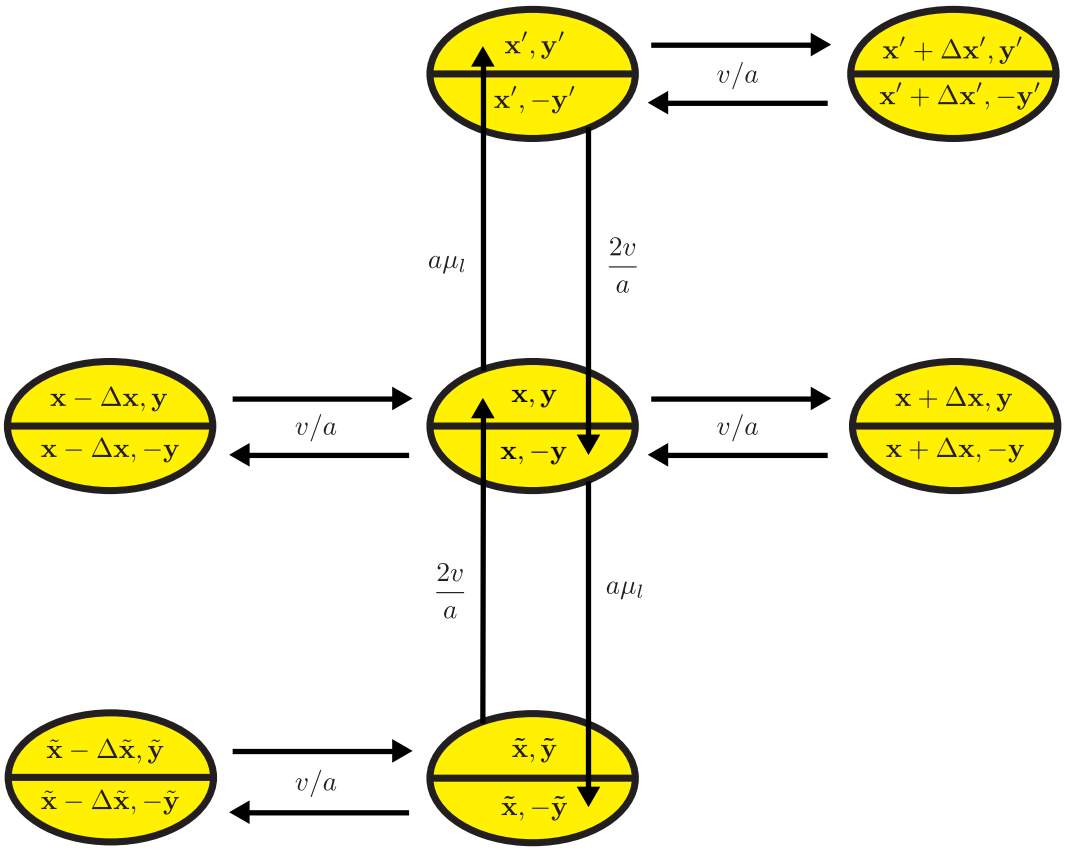

Figure 2.7: Illustration of the detailed balance principle for a discretized version of the RPS model with mutations. Exemplarily, the picture is centered around a configuration $\mathbf{z} = (\mathbf{x}, \mathbf{y})$ with no pairs, LR or RL, which occupy one site. $\mathbf{x} = (x_1, x_n, \ldots)$, where x_k are multiples of the lattice spacing a, denotes the positions of the interfaces and $\mathbf{y} = (y_1, y_2, \ldots)$, with $y_k \in \{-v, v\}$ and velocity v, determines whether they are left (L) of right (R) moving. Of course, not all possible transitions are shown, for instance, by a further mutation with rate $a\mu_l$, the configuration $\mathbf{z}' = (\mathbf{x}', \mathbf{y}')$ with one pair LR would go to a $\mathbf{z}'' = (\mathbf{x}'', \mathbf{y}'')$ with two pairs LR. As described in the text, the R interfaces can move collectively to the right, with rate v/a, while the L interfaces remain at rest. Thus, there is a transition from $\mathbf{z} = (\mathbf{x}, \mathbf{y})$ to $\mathbf{z}_\Delta = (\mathbf{x} + \Delta\mathbf{x}, \mathbf{y})$, with $\Delta\mathbf{x} = a\mathbf{y}/v$ if $y_k = v$, and $\Delta\mathbf{x} = 0$ if $y_k = -v$. If instead the L interfaces move collectively, then there is a transition from $\mathbf{z} = (\mathbf{x}, \mathbf{y})$ to $\mathbf{z}_{\tilde{\Delta}} = (\mathbf{x} + \tilde{\Delta}\mathbf{x}, \mathbf{y})$, where $\tilde{\Delta}\mathbf{x} = 0$ if $y_k = v$, and $\tilde{\Delta}\mathbf{x} = a\mathbf{y}/v$ if $y_k = -v$. For the sake of a neat illustration, we only show transitions by $\pm\Delta\mathbf{x}$, and neglect those by $\pm\tilde{\Delta}\mathbf{x}$. When one or several pairs RL meet, the collective motion to the right and to the left is halted until the pairs are annihilated. The pair annihilation occurs with rate $2v/a$. On the other hand a pair RL is created on some site with rate $a\mu_l$, effecting for instance the transition between $\mathbf{z} = (\mathbf{x}, \mathbf{y})$ and $\mathbf{z}' = (\mathbf{x}', \mathbf{y}')$. It is therefore easily seen that every transition is balanced by a reversed transition when $p^s_{m+d,m} = p^s_{m,m+d}$ and $2vp^s_{m+1,m+1+d} = a^2\mu_l p^s_{m,m+d}$, where $p^s_{m,m+d}$ denotes the probability for a configuration with m Rs and $m+d$ Ls in the stationary state. In the limit $a \to 0$, we recover the condition $\rho_{m+1,m+d+1} = \frac{\mu_l}{2v}\rho_{m,m+d}$, c.f. Eq. (2.42) for the probability density ρ. Moreover, it is readily verified that the net flow for each state evidently vanishes, as it should be for a stationary distribution. Thus, we expect that after an initial transition time the system relaxes to this equilibrium state.

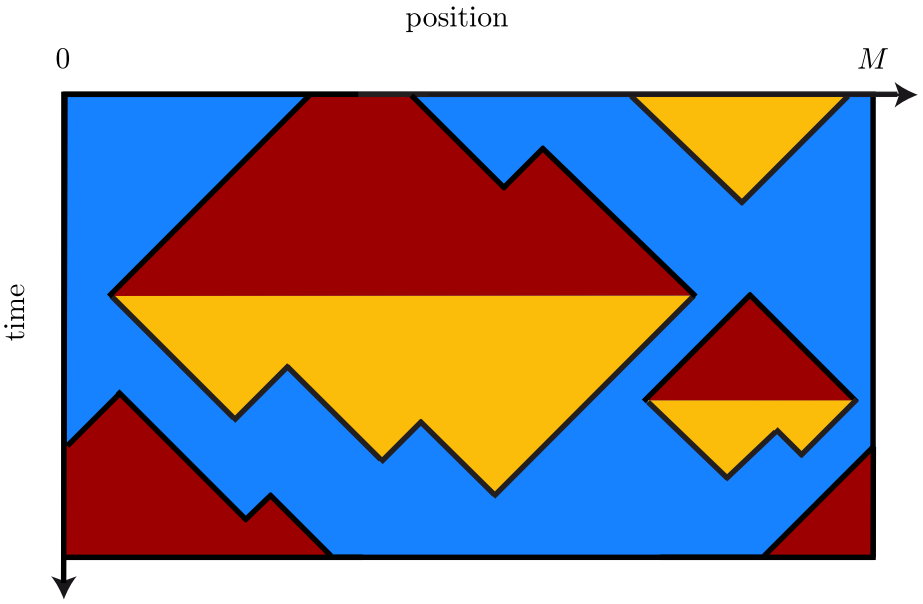

Figure 2.8: Illustration of the dynamics for time scale separation, $1 = r_A = r_B \ll r_C = \infty$, where species C kills and takes over an adjacent site of A at once. It is characterized by "islands" of A and C in one large, simply connected "sea" of species B. Due to the instantaneous invasion of an A domain by C, there cannot be a common boundary in space between the two species. An A domain grows and merges with other A domains until there occurs a spontaneous mutation such that C claims the whole domain from one moment to the next. From then on the domain shrinks, accelerated by mutations $C \to B$. The symmetry under reversal of time and interchanging A and C is evident. This is the underlying reason why, after a transient time, the system reaches an equilibrium state, which obeys a Boltzmann statistics and can be solved analytically. It is striking that the beneficiary of the large rates r_C is not species C but its predator B. Our analysis shows that on average it occupies exactly half of the system.

four kinds of interfaces R_{AB}, L_{BA}, R_{BC} and L_{CB}. (Interfaces between domains of A and C can be ruled out because of the infinitely fast cyclic dominance rate r_C.) Letting time run backwards corresponds to multiplying the velocities of the interfaces by -1. This is achieved by interchanging A and C, which in the interface picture amounts to $R_{AB} \rightleftarrows L_{CB}$ and $L_{BA} \rightleftarrows R_{BC}$. Then the reverse to transition (2.60) is

$$BCCBBAAAAABBAAB \xrightarrow{5\mu_l} BCCBBCCCCCBBAAB\,, \tag{2.61}$$

which is balanced with transition (2.60) on condition that the initial configurations have equal probability. The simplest way to achieve this is a probability distribution which depends only on the overall number of interfaces, but not on their type. We will demonstrate below that this is really the case for the stationary distribution.

We express a configuration by a vector $\mathbf{z} = (\mathbf{x}, \mathbf{y})$, where again the vectors

$$\mathbf{x} = (x_1, \ldots, x_{2m})\,, \quad x_k \in]0, M]\,, \tag{2.62}$$

give the positions of the interfaces in ascending order $x_1 \leq \ldots \leq x_{2m}$, and the type of the interfaces is specified by

$$\mathbf{y} = (y_1, \ldots, y_{2m}), \quad y_k \in \{R_{AB}, L_{BA}, R_{BC}, L_{CB}\}. \tag{2.63}$$

Because of the infinitely fast reaction $AC \to CC$, $CA \to CC$ there are some restrictions on the vector $\mathbf{y}$: If $y_k = L_{BA}$ then $y_{k+1} = R_{AB}$, and if $y_k = R_{BC}$ then $y_{k+1} = L_{CB}$ (here we take $k+1$ to be modulo $2m$). As for the symmetric case of Subsection 2.4.1, our ansatz is that the probability density only depends on the number $2m$ of interfaces in the system. Then detailed balance trivially holds for transition (2.60) and its reversed transition (2.61). As for the ballistic motion and for the creation or annihilation of pairs of interfaces, we evidently obtain the same condition as in the previous section under which detailed balance is fulfilled. Just as above, c.f. Eq. (2.42), the probability distribution must obey

$$2v\rho_{2m+2} = \mu_l \rho_{2m} \quad \Longrightarrow \quad \rho_{2m} = \left(\frac{\mu_l}{2v}\right)^m \rho_0 \,. \tag{2.64}$$

We have thus reduced the calculation of the probability distribution to a combinatorial problem. There are $2m$ domains in the system, which we label $1, \ldots, 2m$ (where domain 1 contains the origin). If the domain 1 is a B domain, then all the odd-numbered domains are B domains, and the even-numbered domains are occupied by either A or C. Otherwise all even-numbered domains are occupied by B and the odd-numbered domains are occupied either by A and C. Therefore, for every position vector $\mathbf{x}$ there are 2^{m+1} possibilities for $\mathbf{y}$. Since the sizes of the domains do not enter the probability distribution, a direct and remarkable consequence is that not only are the concentrations of A and C equal (due to the time reversal symmetry), but A and C each occupy one fourth of the lattice, while the species B has a share of one half of the lattice. This is indeed observed in the simulations, c.f. Figure (2.9).

To obtain the density of the interfaces we integrate over the ordered position vector $\mathbf{x} = (x_1, \ldots, x_{2m})$, giving a factor $M^{2m}/(2m)!$. Thus, the probability to have $2m$ interfaces in the system is

$$p_{2m} = 2^{m+1} \frac{M^{2m}}{(2m)!} \left(\frac{\mu_l}{2v}\right)^m p_0 = \frac{2}{(2m)!} \left(\frac{\mu_l M^2}{v}\right)^m p_0 \,, \tag{2.65}$$

with

$$p_0^{-1} = 2 \sum_{m=0}^{\infty} \frac{1}{(2m)!} \left(\frac{\mu_l M^2}{v}\right)^m . \tag{2.66}$$

For large system sizes the normalization factor becomes approximately

$$p_0^{-1} \approx \exp\left(\sqrt{\frac{\mu_l M^2}{v}}\right) . \tag{2.67}$$

When the velocity $v = 1$ the interface density becomes

$$n = \frac{2\mu_l}{M} \partial_{\mu_l} \ln\left(p_0^{-1}\right) = \sqrt{\mu_l} \,. \tag{2.68}$$

This result is verified by the stochastic lattice simulations, c.f. Figure 2.9.

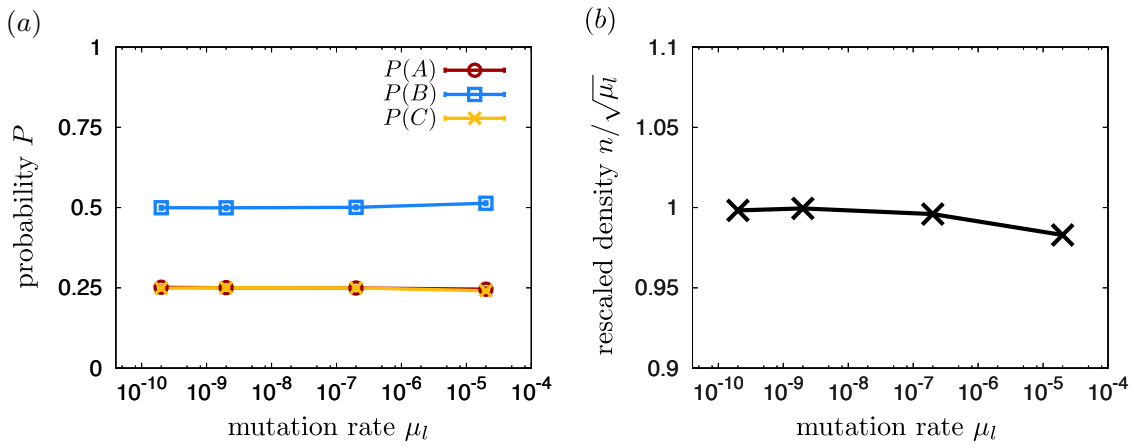

Figure 2.9: Data from of the stochastic lattice simulations for the RPS with mutations to the predator with rate μ_l and instantaneous reactions $AC \to CC$, $CA \to CC$, i.e. with the cyclic dominance rates $r_A = r_B = 1$, and $r_C = \infty$. (The lines between the data points are merely guides to the eye.) In the text it is argued that this particular model obeys detailed balance (under interchanging A and C) in the limit of small mutation rates. In (a) it is not only confirmed that in this limit the densities for A and C are equal, as they should be because of the symmetry between them, but also that they each occupy a quarter of the lattice. In (b) it is shown that the interface density approaches the value $\sqrt{\mu_l}$, c.f. Eq. (2.68), as μ_l becomes small. In both plots the error bars are smaller than the size of the data points. We remark that the deviations from the theoretical values are due to the lattice structure, which was not considered in the calculations. For instance, as the interface density increases, diffusion becomes more important and reactions such as $R_{AB}R_{BC} \to L_{AC}$ (followed by instantaneous invasion of the A domain by C) become more likely. Thus the symmetry between A and C is broken and our analysis is invalidated. Curiously, it is not the gluttonous species C which has the largest share of the lattice, but its predator B. Similar, seemingly paradoxical phenomena have been observed in systems without mutation [31, 95, 98].

Our model was originally motivated by the Drossel-Schwabl Forest Fire Model [99–103], where on a d-dimensional regular lattice each site can either be empty, occupied by a tree, or by a tree on fire. A tree can spontaneously be set on fire by a lightning strike, which occurs with probability f. The fire spreads with rate 1 to a neighboring tree and also with rate 1 a burning tree turns into an empty site, where with probability p a tree regrows. In [99] it was conjectured by scaling arguments that in the limit of double time scale separation, $(f/p)^{-1/d} \ll p^{-1} \ll f^{-1}$ (the average time it takes for a forest cluster to burn down, once the first tree is on fire, is much shorter than the time it takes for a tree to grow, which, again is much shorter than the time between two strikes of lightning), the system is self-organized critical. The time scale separation is motivated as being more frequent in nature than the accidental tuning of a parameter to a specific value where the system is critical. Despite good agreement with the Monte Carlo simulation it later emerged that in $d \geq 2$ dimensions the system is not critical, yet in one dimension self-organized criticality has been proven rigorously [102]. In particular, it was shown that there is a non-trivial distribution of the cluster size $s \sim 1/((s+1)(s+2))$.

The analogy to our process is as follows: We identify trees that are not on fire with A,

empty sites with B, and burning trees with C. The mutation $A \to C$ with rate μ_l may then be regarded as a strike of lightning. Our time scale separation in the cyclic dominance rates, $r_A/\sqrt{\mu_l} = r_B/\sqrt{\mu_l} \ll r_C \to \infty$, guarantees that clusters of As will "burn down" instantaneously, because the average size of the domain should scale as $\sqrt{\mu_l}$ according to our analytical results. In the simulations this was achieved by truly instantaneous updates, where a domain of A is turned to a domain of C immediately if there occurs a $A \to C$ on some site of this domain. Instead of constant input of trees with rate p, the B clusters can recover by invading C clusters at rate r_B, supported by mutations $C \to B$ with rate μ_l. Thus p may be identified with r_B. However, our system becomes rather simple, in particular the distribution of the domain size s of, say, A becomes exponential $n \exp(-ns)$ for large system sizes (where the interfaces approximately obey a Poisson distribution, which implies an exponential distribution for their size).

2.5 Conclusion

The competition between coarsening dynamics and mutations in our model leads to a reactive stationary state which is characterized, on the one hand, by a competition between coarsening and diversifying dynamics, and, on the other hand, by an interplay between equilibrium and non-equilibrium processes. Indeed one can pinpoint exactly which type of reactions (labeled (3) in Figure 2.1) take the system away from equilibrium. It was crucial to discriminate between two types of mutations, namely mutations to predator with rate μ_l and mutations to the prey with rate μ_r. We have demonstrated that the effect of the latter becomes negligible, when the two rates are comparable and small, as one would perhaps intuitively expect. Both for the high and for the low mutation rate regime, we have retrieved asymptotically exact results which we expect to be quite robust to a wide rage of variations, e.g. relaxing the constraints of symmetry between A, B and C. For very low mutation rates, diffusional motion can be neglected and the interfaces are best described as ballistic, i.e. moving at constant velocity to the right or left. To our surprise we found that certain realizations of the model, in particular when there is a perfect symmetry between the three species, display a stationary state which obeys detailed balance. Therefore they can be studied with the tools of equilibrium statistical mechanics. The probability distribution of the stationary state was calculated exactly and shown to obey a Boltzmann statistics, with an energy which is proportional to the number of interfaces.

3 The Non-Perturbative Renormalization Group and Reaction-Diffusion Processes

We now move on from the rock-paper-scissors model to the treatment of the coagulation process, where diffusing particles clot, $A + A \to A$, upon contact. The goal of this chapter is to set the theoretical foundations for the calculations in the next chapters, employing a non-perturbative renormalization group (NPRG) approach. In this formalism one calculates the Gibbs free energy functional Γ, which in principle fully describes the dynamics, by successively integrating out degrees of freedom, going from high energy scales to low ones. As for all renormalization group approaches, one expects that there is an approximate decoupling between the different energy scales, so that, in spite of the necessary truncations, one obtains good results. In this formalism, developed in a series of pioneering works [104–110] (for an authoritative review the reader is referred to [111] and for a concise introduction to [112]), the renormalization group flow is described by the so called Wetterich equation. It connects the microscopic energy functional with the Gibbs free energy functional Γ. Preceding this "average action" approach, there was a similar NPRG approach, the Wilson-Polchinski approach, where instead of Γ the generating functional $W = \ln Z$ was studied, with the partition function Z [113–117]. The Gibbs free energy functional Γ is just the Legendre transformation of W.

The NPRG approach based on the Wetterich equation proved very successful in the treatment of the $O(N)$ models for magnets. It allows to develop a unified framework for an arbitrary number N of spin components and arbitrary dimension [118, 119], and it has helped overcome difficulties of the original Wilson-Polchinski formulation with these $O(N)$ models: At a rather low order of the approximation one could calculate the anomalous dimension (which had been problematic before) [120, 121], one managed to reproduce perturbative one-loop results [111], and the approach naturally captured the Kosterlitz-Thouless phase transition of the XY model in two dimensions [111, 122–124].

In contrast to perturbative renormalization group methods, the NPRG approach allows to study non-universal features, for instance phase diagrams, and since it does not rely on a small parameter, such as the difference ϵ to the critical dimension, the approach lends itself to the study of critical exponents in every dimension. Recently, the formalism has been adapted by Canet to study non-equilibrium systems and, in particular, reaction-diffusion processes [125–127]. A range of paradigmatic processes have been studied by now, for example the contact process [125], branching and annihilating random walks [125, 128, 129] (where it was shown that the phase diagrams behaves differently than predicted by perturbative methods) or the Kardar-Parisi-Zhang equation [130, 131].

The outline of this chapter is as follows. We start by introducing Doi's path integral formalism, where from a second-quantized representation one obtains a field theoretic action, by similar

techniques as are employed for quantum many-particle systems [132]. We then derive the Wetterich equation which connects this action with the Gibbs free energy functional. This functional fully describes the process, and we will show how, in particular, it determines the time evolution of the density. We further discuss approximation methods, which become necessary for most concrete calculation, and derive "dimensionless" formulas which allow to study fixed points of critical systems within these approximations.

3.1 The Fourier Transform and Integration Conventions

Our process will most of the time be embedded on a hypercubic lattice with lattice spacing a. We will often encounter functions $f(\mathbf{x},t)$, depending on time t and position $\mathbf{x} = a\sum_{\nu=1}^{d} n_\nu \mathbf{e}_\nu$, where the $\mathbf{e}_\nu$ are orthogonal unit vectors spanning the d-dimensional vector space and n_ν are integral numbers. To obtain a system of finite size we introduce periodic boundary conditions $f(\mathbf{x},t) = f(\mathbf{x}+N\mathbf{e}_\nu,t)$, where N is a natural number. We are interested in the limit of an infinitely large system, $N\to\infty$.

The Fourier transform is defined, as usual, by

$$f(\mathbf{q},\omega) = \sum_{\mathbf{x}} \int \mathrm{d}t\, \exp(i\omega t - i\mathbf{q}\mathbf{x}) f(\mathbf{x},t)\,, \tag{3.1}$$

where the sum is over the lattice sites with $n_i \in \{0,\dots,N-1\}$ and the momenta $\mathbf{q} = \frac{2\pi}{aN}\sum_\nu \tilde{n}_\nu \mathbf{e}_\nu$ obey $-N/2 < \tilde{n}_\nu \le N/2$. The reverse transform given is

$$f(\mathbf{x},t) = \frac{1}{N^d}\sum_{\mathbf{q}} \int \frac{\mathrm{d}\omega}{2\pi}\, \exp(-i\omega t + i\mathbf{q}\mathbf{x}) f(\mathbf{q},\omega)\,. \tag{3.2}$$

In the limit of infinite system size, $N\to\infty$, the sum over the momenta is replaced by an integral

$$\frac{1}{N^d}\sum_{\mathbf{q}} \to \int_{\mathbf{q}\in]-\frac{\pi}{a},\frac{\pi}{a}]} \frac{\mathrm{d}^d q}{(2\pi/a)^d}\,. \tag{3.3}$$

For concise notation we introduce

$$\int_{\mathbf{q}} := \int_{\mathbf{q}\in]-\frac{\pi}{a},\frac{\pi}{a}]} \frac{\mathrm{d}^d q}{(2\pi/a)^d}\,, \quad \int_{\omega} := \int \frac{\mathrm{d}\omega}{(2\pi)}\,. \tag{3.4}$$

We remark that this notation also covers general Bravais lattices with $\mathbf{x} = \sum_{\nu=1}^{d} n_\nu \mathbf{a}_\nu$, where $\mathbf{a}_\nu$ are the primitive cell vectors. In this case, we simply need to redefine

$$\int_{\mathbf{q}} := \int_{\mathbf{q}\in 1\text{st B.Z.}} \frac{\mathrm{d}^d q}{V_{1\text{st B.Z.}}}\,, \tag{3.5}$$

i.e. the momentum $\mathbf{q}$ is integrated over the first Brillouin zone and the integral is divided by the volume $V_{1\text{st B.Z.}}$ of the first Brillouin zone.

It is important to keep in mind that the volume of the system is not infinite, although of course we want to consider the limit of an infinitely large system. In particular therefore, the Dirac delta $\delta(\mathbf{q})$ has a well-defined value at $\mathbf{q} = 0$, namely

$$\delta(\mathbf{q} = 0) = \left(\frac{Na}{2\pi}\right)^d = \left(\frac{V}{2\pi}\right)^d . \tag{3.6}$$

Sometimes it is adequate to let the lattice spacing a become small and to go to continuous variables also in position space,

$$\sum_{\mathbf{x}} \to \int \mathrm{d}^d x \, a^{-d} , \quad f(\mathbf{x}) \to f(\mathbf{x}) a^d . \tag{3.7}$$

The Fourier transform then reads $f(\mathbf{q}, \omega) = \int \mathrm{d}\mathbf{x} \, \mathrm{d}t \, \exp(i\omega t - i\mathbf{q}\mathbf{x}) f(\mathbf{x}, t)$ and the reverse transform $f(\mathbf{x}, t) = \int_\omega \frac{\mathrm{d}^d q}{(2\pi)^d} \exp(-i\omega t + i\mathbf{q}\mathbf{x}) f(\mathbf{q}, \omega)$. ($\mathbf{q}$ is integrated over the whole space $\mathbb{R}^d$.) In this case, we redefine

$$\int_{\mathbf{q}} := \int \frac{\mathrm{d}^d q}{2\pi^d} . \tag{3.8}$$

3.2 Second Quantized Representation of Reaction-Diffusion Systems

In order to give flesh to our discussion, we consider the process $A + A \to A$ (coagulation) with rate λ and $A + A \to \varnothing$ (annihilation) with rate λ' on a regular d-dimensional lattice. In addition the particles diffuse with diffusion constant D. To render this process amenable to the non-perturbative renormalization group approach, we map it on a field theory by the well-established Doi formalism, an approach developed by several authors [64, 133–136], for a review see [137]. Here we provide a description of this mapping, which was originally applied in a similar fashion to quantum systems as described in standard textbooks (see e.g. [132]).

Since the particles are indistinguishable, one does not need to keep track of every single one of them. Instead, it is sufficient to specify the configuration of the system by the occupation numbers of the sites of the lattice

$$\vec{n} = (n(\mathbf{x}), n(\mathbf{y}), \ldots) , \tag{3.9}$$

where $\mathbf{x}, \mathbf{y}, \ldots$ denote the positions of the lattice sites. The stochastic dynamics describing the time evolution of the probability distribution $P(\vec{n}, t)$ is then given by the master equation (with $< \mathbf{x}, \mathbf{y} >$ indicating that the sum is over nearest neighbors),

$$\partial_t P(\vec{n}, t) = -D \sum_{<\mathbf{x},\mathbf{y}>} \{[n(\mathbf{x}) P(\vec{n}, t) - (n(\mathbf{x}) + 1) P(n(\mathbf{x}) + 1, n(\mathbf{y}) - 1, \ldots, t)] +$$

$$+ [n(\mathbf{y}) P(\vec{n}, t) - (n(\mathbf{y}) + 1) P(n(\mathbf{x}) - 1, n(\mathbf{y}) + 1, \ldots, t)]\} -$$

$$- \lambda \sum_{\mathbf{x}} [n(\mathbf{x})(n(\mathbf{x})-1)P(\vec{n},t) - (n(\mathbf{x})+1)n(\mathbf{x})P(n(\mathbf{x})+1,\ldots,t)] -$$
$$- \lambda' \sum_{\mathbf{x}} [n(\mathbf{x})(n(\mathbf{x})-1)P(\vec{n},t) - (n(\mathbf{x})+2)(n(\mathbf{x})+1)P(n(\mathbf{x})+2,\ldots,t)] \,. \tag{3.10}$$

We may regard the configurations $\vec{n}$ of the system as vectors $|\vec{n}\rangle = |n(\mathbf{x})\rangle \otimes |n(\mathbf{y})\rangle \otimes \cdots$ of a Hilbert space $\mathcal{H}$ which is the tensor product $h \otimes h \otimes \cdots$ of a Hilbertspace h for each site. h is equipped with the scalar product

$$\langle m|n\rangle = n!\, \delta_{m,n} \,. \tag{3.11}$$

We introduce creation and destruction operators $\hat{a}^\dagger, \hat{a}$ acting on h and defined by

$$\hat{a}^\dagger|n\rangle = |n+1\rangle \,, \quad \hat{a}|n\rangle = n|n-1\rangle \,. \tag{3.12}$$

Notice that these definitions differ from the standard conventions in quantum mechanics. By $\hat{a}^\dagger(\mathbf{x}), \hat{a}(\mathbf{x})$ we denote the corresponding creation and destruction operators which only affect the site $\mathbf{x}$ and are the identity on all other sites. They are subject to the "bosonic" commutation relations,

$$[\hat{a}(\mathbf{x}), \hat{a}^\dagger(\mathbf{y})] = \delta_{\mathbf{x},\mathbf{y}} \,, \quad [\hat{a}(\mathbf{x}), \hat{a}(\mathbf{y})] = [\hat{a}^\dagger(\mathbf{x}), \hat{a}^\dagger(\mathbf{y})] = 0 \,. \tag{3.13}$$

It is easily verified that $a^\dagger(\mathbf{x})$ is the adjoint operator of $a(\mathbf{x})$, with respect to the scalar product defined by Eq. (3.11), i.e.

$$\langle \vec{m}|a(\mathbf{x})|\vec{n}\rangle = \langle \vec{n}|\hat{a}^\dagger(\mathbf{x})|\vec{m}\rangle \,. \tag{3.14}$$

Let us denote with $|0\rangle$ the "vacuum state", which stands for a completely empty lattice. We can express the state vector of the entire system at time t by

$$|\phi\rangle = \sum_{\vec{n}} P(\vec{n},t)|\vec{n}\rangle = \sum_{\vec{n}} P(\vec{n},t) \prod_{\mathbf{x}} \left(\hat{a}^\dagger(\mathbf{x})\right)^{n(\mathbf{x})} |0\rangle \,, \tag{3.15}$$

thus

$$P(\vec{n},t) = \prod_{\mathbf{x}} \frac{1}{n(\mathbf{x})!} \langle \vec{n}|\phi\rangle \,. \tag{3.16}$$

This allows us to cast the master equation into an "imaginary-time Schrödinger equation"

$$\partial_t |\phi(t)\rangle = -\hat{H}|\phi(t)\rangle \,. \tag{3.17}$$

The stochastic (and, in general, non-hermitian) Hamiltonian $\hat{H}$ is given by

$$\hat{H} = \hat{H}_\epsilon + \hat{H}_{\lambda,\lambda'} \,, \tag{3.18}$$

with the diffusion part

$$\hat{H}_\epsilon = D \sum_{<\mathbf{x},\mathbf{y}>} \left(\hat{a}^\dagger(\mathbf{x}) - \hat{a}^\dagger(\mathbf{y})\right)\left(\hat{a}(\mathbf{x}) - \hat{a}(\mathbf{y})\right) , \tag{3.19}$$

(ϵ stands for the dispersion relation, see below) and the reaction part of the Hamiltonian

$$\hat{H}_{\lambda,\lambda'} = \lambda \sum_{\mathbf{x}} \left[(\hat{a}^\dagger(\mathbf{x}))^2 - \hat{a}^\dagger(\mathbf{x})\right] \hat{a}(\mathbf{x})^2 + \lambda' \sum_{\mathbf{x}} \left[(\hat{a}^\dagger(\mathbf{x}))^2 - 1\right] \hat{a}(\mathbf{x})^2 \,. \tag{3.20}$$

The Hamiltonian looks rather neat, since the annihilation and creation operators naturally take care of the factors $n(\mathbf{x}), n(\mathbf{y}), \ldots$ which somewhat complicate the original representation of the master equation, Eq. (3.10). The different terms of the Hamiltonian have a simple interpretation. Consider for example the first term of $\hat{H}_{\lambda,\lambda'}$ which goes with λ: By applying $(\hat{a}^\dagger(\mathbf{x}))^2\hat{a}(\mathbf{x})^2$ one obtains the number of (ordered) pairs at site $\mathbf{x}$ without changing the state of the system. By applying $\hat{a}^\dagger(\mathbf{x})\hat{a}(\mathbf{x})^2$, which first destroys a pair of particles at site $\mathbf{x}$ and then creates one particle at the same site $\mathbf{x}$, the coagulation reaction $A + A \to A$ is effected.

The stochasticity of the Hamiltonian is fulfilled, because the diagonal part is positive with respect to the basis of state vectors $|\vec{n}\rangle$ and the sum over the rows vanishes [93, 138],

$$\sum_{\vec{m}} \frac{1}{\prod_{\mathbf{x}} m(\mathbf{x})!} \langle \vec{m}|\hat{H}|\vec{n}\rangle = 0\,. \tag{3.21}$$

This relation can most conveniently be seen by noting that the sum

$$\langle S| := \sum_{\vec{m}} \frac{1}{\prod_{\mathbf{x}} m(\mathbf{x})!} \langle \vec{m}| = \langle 0| \exp\left(\sum_{\mathbf{x}} \hat{a}(\mathbf{x})\right)\,, \tag{3.22}$$

and therefore by applying $\langle S|$ from the left to $\hat{H}$ the creation operators of the (normal ordered) Hamiltonian $\hat{H}$ can be set to one. Thus, according to Eqs. (3.19,3.20), $\langle S|\hat{H} = 0$. This relation guarantees probability conservation: The formal solution to the evolution equation, Eq. (3.17), is

$$|\phi(t)\rangle = \exp(-\hat{H}t)|\phi(t=0)\rangle\,. \tag{3.23}$$

The sum over the probabilities at time t is

$$\langle S|\phi(t)\rangle = \langle S|\exp(-\hat{H}t)|\phi(t=0)\rangle = \langle S|\phi(t=0)\rangle\,, \tag{3.24}$$

which is equal to one if the initial state $|\phi(t=0)\rangle$ corresponds to a real probability distribution.

Expectation values of an observable $\hat{\mathcal{O}}$, defined by the quantities $\mathcal{O}(\vec{n})$ which are assigned when the system is found to be in the configuration $|\vec{n}\rangle$, are calculated by,

$$\langle \mathcal{O}(t)\rangle = \langle S|\mathcal{O}(\hat{a}^\dagger, \hat{a})|\phi(t)\rangle\,, \tag{3.25}$$

where we express $\hat{\mathcal{O}} = \mathcal{O}(\hat{a}^\dagger, \hat{a})$ in terms of the creation and destruction operators. For instance, the operator for the average number of particle is $\sum_{\mathbf{x}} \hat{n}(\mathbf{x}) \equiv \sum_{\mathbf{x}} \hat{a}^\dagger(\mathbf{x})\hat{a}(\mathbf{x})$ and for the average square of the number of particles it is $\sum_{\mathbf{x},\mathbf{y}} a^\dagger(\mathbf{x})\hat{a}(\mathbf{x})\hat{a}^\dagger(\mathbf{y})\hat{a}(\mathbf{y})$. It is often favorable to represent these observables in "normal" form, such that the creation operators $\hat{a}(\mathbf{x})^\dagger$ are arranged to the left of the destruction operators $\hat{a}(\mathbf{x})$, which is easily realized by use of the commutation relation, Eq. (3.13). In this case that the creation operators can be replaced by 1, $\hat{a}(\mathbf{x})^\dagger \to 1$ in Eq. (3.25), and $\mathcal{O}(\hat{a}^\dagger, \hat{a}) \to \mathcal{O}(\hat{a})$. Thus, the above operators for the average number of particles and the average square of the number of particles are rewritten as $\sum_{\mathbf{x}} \hat{a}(\mathbf{x})$ and $\sum_{\mathbf{x},\mathbf{y}} \hat{a}(\mathbf{x})\hat{a}(\mathbf{y}) - \sum_{\mathbf{x}} \hat{a}(\mathbf{x})$, respectively.

Let us choose the initial state to obey a Poisson distribution with density ρ,

$$|\phi(t=0)\rangle = e^{\rho \sum_{\mathbf{x}} (\hat{a}^\dagger(\mathbf{x})-1)}|0\rangle\,. \tag{3.26}$$

(A general state can be represented as a sum or an integral of these states, if we allow ρ to be a complex number, see below.) Clearly, the average of an observable may then be rewritten as an infinite sum over expectation values of products of destruction and creation operators, by expanding the observable $\hat{\mathcal{O}} = \mathcal{O}(\hat{a})$, the Hamiltonian $\hat{H} = H(\hat{a}^\dagger, \hat{a})$ and the exponential functions in

$$\langle \mathcal{O}(t) \rangle = \langle 0 | e^{\sum_{\mathbf{x}} \hat{a}(\mathbf{x})} \mathcal{O}(\hat{a}) e^{-H(\hat{a}^\dagger, \hat{a})t} e^{\rho \sum_{\mathbf{x}} (\hat{a}^\dagger(\mathbf{x}) - 1)} | 0 \rangle \,. \tag{3.27}$$

This can be exploited to set up a diagrammatic formalism. For this purpose, let us provisionally give the operators a trivial time dependence, $\hat{a}^\dagger(\mathbf{x}, t) \equiv \hat{a}^\dagger(\mathbf{x})$ and $\hat{a}(\mathbf{x}, t) \equiv \hat{a}(\mathbf{x})$, such that we can write

$$\langle \mathcal{O}(t) \rangle = \langle 0 | T e^{\sum_{\mathbf{x}} \hat{a}(\mathbf{x},t)} \mathcal{O}(\hat{a}(t)) e^{-\int_0^t \mathrm{d}t' \, H(\hat{a}(t')^\dagger, \hat{a}(t'))} e^{\rho \sum_{\mathbf{x}} (\hat{a}(\mathbf{x},0)^\dagger - 1)} | 0 \rangle \,, \tag{3.28}$$

with the chronological operator T, which arranges the destruction and creation operators from right to left with increasing time. Wick's theorem [132, 139] tells us that destruction and creation operators need to be paired up, i.e.

$$\begin{aligned} &\langle 0 | T \hat{a}(\mathbf{x}_m, t_m) \dots \hat{a}(\mathbf{x}_1, t_1) \hat{a}^\dagger(\mathbf{x}'_n, t'_n) \dots \hat{a}^\dagger(\mathbf{x}'_1, t'_1) | 0 \rangle = \\ &= \delta_{m,n} \sum_{\text{pairs } p} \prod_{i=1}^{n} \langle 0 | T \hat{a}(x_{p(i,1)}, t_{p(i,1)}) \hat{a}^\dagger(x'_{p(i,2)}, t'_{p(i,2)}) | 0 \rangle \,. \end{aligned} \tag{3.29}$$

Thus the terms in Eq. (3.28) are readily translated to Feynman graphs by representing the factor for the paired up propagators $\langle 0 | T \hat{a}(\mathbf{x}, t_2) \hat{a}^\dagger(\mathbf{x}, t_1) | 0 \rangle$ (which is 1 if $t_2 > t_1$ and zero otherwise) by lines, and the couplings by nodes with a certain number of incoming lines (for the creation operator) and outgoing lines (for the destruction operator). For instance, the term $\lambda \sum_{\mathbf{x}} \hat{a}^\dagger(\mathbf{x}) \hat{a}(\mathbf{x})^2$ in Eq. (3.20) corresponds to a node with two incoming lines and one outgoing line.

As we have written it, there are nodes with one incoming and one outgoing line. Therefore, on a line between creation at time t and destruction at time t' we can place $1, 2, 3, \dots$ of these "harmonic nodes". One can sum over this set of diagrams analytically. Due to translational symmetry, the diffusion part, c.f. Eq. (3.19), becomes diagonal in Fourier space, i.e. it can be expressed as $\hat{H}_\epsilon = -\int \frac{\mathrm{d}\mathbf{q}}{(2\pi)^d} \hat{a}^\dagger(\mathbf{q}) \hat{a}(-\mathbf{q}) \epsilon(\mathbf{q})$, where d denotes the dimension (see Section 5.1 and Eq. (5.7) for an explicit calculation of the dispersion relation $\epsilon(\mathbf{q})$). We thus obtain the propagator

$$\begin{aligned} G_0(t_2 - t_1) &:= \langle 0 | \hat{a}(\mathbf{q}_1, t_2) \hat{a}^\dagger(\mathbf{q}_2, t_1) | 0 \rangle_0 := \\ &= 1 - \int_{t_1 < t' < t_2} \mathrm{d}t' \, \epsilon(\mathbf{q}) + \int_{t_1 < t'_1 < t'_2 < t_2} \mathrm{d}t'_1 \, \mathrm{d}t'_2 \epsilon(\mathbf{q})^2 \mp \dots = \\ &= \exp(-\epsilon(\mathbf{q})(t_2 - t_1)) \,. \end{aligned} \tag{3.30}$$

Often it is convenient to shift the creation operator by one,

$$\hat{a}^\dagger(\mathbf{x}) \to \hat{a}^\dagger(\mathbf{x}) - 1 =: \hat{\tilde{a}}^\dagger(\mathbf{x}) \,. \tag{3.31}$$

It is readily verified that $\hat{\tilde{a}}^\dagger_{\mathbf{x}}$ is the adjoint operator to the creation operator $\hat{a}(\mathbf{x})$ with respect to the scalar product [135, 136]

$$'\langle \phi | \psi \rangle' := \langle \phi | e^{\sum_{\mathbf{x}} \hat{a}^\dagger(\mathbf{x})} e^{\sum_{\mathbf{x}} \hat{a}(\mathbf{x})} | \psi \rangle \,.$$

Indeed,

$$\begin{aligned}{}'\langle\phi|\hat{a}(\mathbf{y})|\psi\rangle' &= \langle\phi|e^{\sum_{\mathbf{x}}\hat{a}^\dagger(\mathbf{x})}e^{\sum_{\mathbf{x}}\hat{a}(\mathbf{x})}\hat{a}(\mathbf{y})|\psi\rangle = \langle\psi|\hat{a}^\dagger(\mathbf{y})e^{\sum_{\mathbf{x}}\hat{a}^\dagger(\mathbf{x})}e^{\sum_{\mathbf{x}}\hat{a}(\mathbf{x})}|\phi\rangle = \\ &= \langle\psi|e^{\sum_{\mathbf{x}}\hat{a}^\dagger(\mathbf{x})}e^{\sum_{\mathbf{x}}\hat{a}(\mathbf{x})}(\hat{a}^\dagger(\mathbf{y})-1)|\phi\rangle = {}'\langle\psi|\hat{\tilde{a}}^\dagger(\mathbf{y})|\phi\rangle' \,. \end{aligned} \tag{3.32}$$

The commutation relation, Eq. (3.13), and Wick's theorem still hold after replacing $\hat{a}^\dagger(\mathbf{x})$ with $\hat{\tilde{a}}^\dagger(\mathbf{x})$. Therefore, our above analysis is also valid for the new operators. The average of an operator is now expressed as

$$\langle\mathcal{O}(t)\rangle = {}'\langle 0|\hat{\mathcal{O}}(\hat{a})e^{-H(\hat{\tilde{a}}^\dagger,\hat{a})t}e^{\rho\sum_{\mathbf{x}}\hat{\tilde{a}}^\dagger(\mathbf{x})}|0\rangle' \,, \tag{3.33}$$

where we exploit that $\langle S| = \langle 0|e^{\sum_{\mathbf{x}}\hat{a}(\mathbf{x})} = \langle 0|e^{\sum_{\mathbf{x}}\hat{a}^\dagger(\mathbf{x})}e^{\sum_{\mathbf{x}}\hat{a}(\mathbf{x})} = {}'\langle 0|$. Again this can be translated to a sum over Feynman graphs. The propagator $G_0(t)$ even remains the same as above, c.f. Eq. (3.30)) since the form of the diffusion part of the Hamiltonian, as given in Eq. (3.19), is not altered.

An important advantage of the shifted operator is that for the expectation value of the observables $\hat{\mathcal{O}}(\hat{a}) = \hat{a}(\mathbf{x})$, $\hat{\mathcal{O}}(\hat{a}) = (\hat{a}(\mathbf{x}))^2$, ..., it is sufficient to sum over Feynman diagrams with $1, 2, \ldots$ outgoing legs (finally connected with the destruction operators of $\hat{\mathcal{O}}(\hat{a})$). This is because of the fact that the projection state $\langle S| = \langle 0|e^{\sum_{\mathbf{x}}\hat{a}(\mathbf{x})}$ equals the adjoint ${}'\langle 0|$ of the vacuum state with respect to our new scalar product, and ${}'\langle 0|\hat{\tilde{a}}^\dagger(\mathbf{x}) = 0$. It can also be seen directly within the original scalar product upon replacing the projection state $\langle S|$ by $\langle\alpha| = \langle 0|e^{\alpha\sum_{\mathbf{x}}\hat{a}(\mathbf{x})}$. Feynman diagrams with n outgoing legs then pick up the factor $(\alpha-1)^n$, since $\langle\alpha|\hat{\tilde{a}}^\dagger(\mathbf{x}) = (\alpha-1)\langle\alpha|$. Upon writing $\langle S|\mathcal{O}(\hat{a}) = \langle S|\hat{a}(\mathbf{x})^n = \partial_\alpha^n\langle\alpha|$ at $\alpha = 1$, we see that indeed all diagrams cancel expect for those with n outgoing lines. Notice that these diagrams need not be connected. However, all the terms of stochastic Hamiltonians for reaction diffusion processes go with $\hat{\tilde{a}}^\dagger(\mathbf{x})$ (as shown, for instance, in [140]), i.e. every node has at least one outgoing line. Therefore, all Feynman diagrams must be connected to the "final" destruction operators stemming from $\mathcal{O}(\hat{a})$. In particular, for the mean density, obtained by applying $\hat{\mathcal{O}}(\hat{a}) = \hat{a}(\mathbf{x})$, one only needs to sum up connected Feynman diagrams.

3.3 Mapping to a Field Theory

For the NPRG approach it is necessary to derive a field theory. To do this, we introduce coherent states

$$|\phi\rangle := e^{\phi\hat{a}^\dagger}|0\rangle \,, \tag{3.34}$$

for a system that contains only a single site (we generalize to larger systems below). Here, ϕ is a complex number. Coherent states are the eigenstates of the destruction operator, $\hat{a}|\phi\rangle = \phi|\phi\rangle$, with the adjoint formula $\langle\phi|\hat{a}^\dagger = \langle\phi|\phi^\star$. In the following, we will often have to calculate the scalar product of two coherent states, which becomes

$$\langle\tilde{\phi}|\phi\rangle = \sum_{n=0}^{\infty}\langle 0|\frac{\left(\tilde{\phi}^\star\hat{a}\right)^n\left(\phi\hat{a}^\dagger\right)^n}{(n!)^2}|0\rangle = e^{\tilde{\phi}^\star\phi} \,. \tag{3.35}$$

The coherent states are overcomplete and allow for a number of representations of the identity [132]. Here we employ [136]

$$\mathbb{1} = \int_{\phi\in\mathbb{R},\tilde{\phi}\in i\mathbb{R}} \frac{\mathrm{d}\phi\,\mathrm{d}\tilde{\phi}}{2\pi} e^{\phi\tilde{\phi}} |\phi\rangle\langle\tilde{\phi}|\,, \tag{3.36}$$

where ϕ is to be integrated over the real line and $\tilde{\phi}$ over the imaginary line. This relation is proven using partial integration and

$$n!\delta_{mn} = \int_{\phi\in\mathbb{R}} \mathrm{d}\phi\, \phi^n \left(-\frac{\mathrm{d}}{\mathrm{d}\phi}\right)^m \delta(\phi)\,. \tag{3.37}$$

A cautionary remark is in order at this point. The representation of the identity (3.36) is given by an integral over coherent states. In the calculations below, the unitary operator $\exp(-\hat{H}t)$ implies sums from the expansion of the exponential. Often these integrals and sums do not commute [137]. As an example, consider $\langle 0|\exp(\hat{a}^k)|0\rangle = 1$, with a natural number k. Inserting our expression for the identity, Eq. (3.36),

$$\langle 0|e^{\hat{a}^k} \int_{\phi\in\mathbb{R},\tilde{\phi}\in i\mathbb{R}} \frac{\mathrm{d}\phi\,\mathrm{d}\tilde{\phi}}{2\pi} e^{\phi\tilde{\phi}} |\phi\rangle\langle\tilde{\phi}|0\rangle = \sum_n \frac{1}{n!} \int_{\phi\in\mathbb{R},\tilde{\phi}\in i\mathbb{R}} \frac{\mathrm{d}\phi\,\mathrm{d}\tilde{\phi}}{2\pi} e^{\phi\tilde{\phi}} \phi^{nk}\,, \tag{3.38}$$

which, because of $\int_{\tilde{\phi}\in i\mathbb{R}} \frac{\mathrm{d}\tilde{\phi}}{2\pi} e^{\phi\tilde{\phi}} = \delta(\phi)$ and Eq. (3.37), indeed equals one. If, however, we interchange sum and integral, we obtain instead

$$\int_{\phi\in\mathbb{R},\tilde{\phi}\in i\mathbb{R}} \frac{\mathrm{d}\phi\,\mathrm{d}\tilde{\phi}}{2\pi} e^{\phi\tilde{\phi}+\phi^k}\,. \tag{3.39}$$

For $k \geq 3$ this only gives the correct result when the integration of $\tilde{\phi}$ is carried out before the integration of ϕ. Similarly, by looking at $\langle 0|\exp[(\hat{a}^\dagger)^k]|0\rangle = 1$, we can construct a case, where the integration of ϕ needs to be performed first. Therefore, to be on the safe side such terms must always be understood perturbatively. For our non-perturbative approach, we will see in the next section that we have to rule out such terms, where the order of summation and integration matters.

It is instructive to consider a further example where the order of integration and summation matters. Applying Eq. (3.36) to the coherent state $|\psi\rangle$ without interchanging sum and integral, a coherent state can be written as

$$\begin{aligned}|\psi\rangle =& \int_{\phi\in\mathbb{R},\tilde{\phi}\in i\mathbb{R}} \frac{\mathrm{d}\phi\,\mathrm{d}\tilde{\phi}}{2\pi} e^{\phi\tilde{\phi}} |\phi\rangle\langle\tilde{\phi}|\psi\rangle = \sum_{n=0}^{\infty} \frac{1}{n!} \int_{\phi\in\mathbb{R},\tilde{\phi}\in i\mathbb{R}} \frac{\mathrm{d}\phi\,\mathrm{d}\tilde{\phi}}{2\pi} e^{\tilde{\phi}\phi} \left(-\tilde{\phi}\psi\right)^n |\phi\rangle \\ =& \sum_{n=0}^{\infty} \frac{\psi^n}{n!} \int_{\phi\in\mathbb{R}} \mathrm{d}\phi \left(-\frac{\mathrm{d}}{\mathrm{d}\phi}\right)^n \delta(\phi)|\phi\rangle\,. \end{aligned} \tag{3.40}$$

If we now apply $\langle m| = \langle 0|\hat{a}^m$ from the left, and employ Eq. (3.37) we obtain the correct result $\frac{\psi^n}{n!} = \langle m|\psi\rangle$. This prescription works even if we do not integrate ϕ over the complete real line. Indeed, as also remarked in [136], in the definition of the identity (3.36) it would suffice

to integrate ϕ along any path which $\mathcal{P}$ traverses the origin, e.g. we could restrict the integral to $\mathcal{P} = \phi \in]-1, 1[$. However, if we then do interchange integration and summation, we have

$$|\psi\rangle = \int_{\phi\in\mathcal{P},\tilde{\phi}\in i\mathbb{R}} \frac{\mathrm{d}\phi\,\mathrm{d}\tilde{\phi}}{2\pi} e^{\phi\tilde{\phi}} |\phi\rangle\langle\tilde{\phi}|\psi\rangle = \int_{\phi\in\mathcal{P},\tilde{\phi}\in i\mathbb{R}} \frac{\mathrm{d}\phi\,\mathrm{d}\tilde{\phi}}{2\pi} e^{\tilde{\phi}\phi-\tilde{\phi}\psi} |\psi\rangle = \int_{\phi\in\mathcal{P}} \mathrm{d}\phi\,\delta(\phi-\psi)|\psi\rangle\,. \tag{3.41}$$

As a matter of fact, below we will encounter such expressions and we will interchange integration and summation. We are allowed to do so as long as we integrate ϕ over the complete real line $\mathbb{R}$.

Generalizing from a system with only one site to a lattice with coherent states

$$|\phi\rangle = e^{\sum_{\mathbf{x}} \phi(\mathbf{x})\hat{a}^\dagger(\mathbf{x})}|0\rangle = |\phi(\mathbf{x})\rangle \otimes |\phi(\mathbf{y})\rangle \otimes \dots\,, \tag{3.42}$$

instead of Eq. (3.36) we have the identity

$$\mathbb{1} = \int_{\phi(\mathbf{x})\in\mathbb{R},\tilde{\phi}(\mathbf{x})\in i\mathbb{R}} \prod_{\mathbf{x}} \frac{\mathrm{d}\phi(\mathbf{x})\,\mathrm{d}\tilde{\phi}(\mathbf{x})}{2\pi} e^{\phi(\mathbf{x})\hat{\phi}(\mathbf{x})} |\phi\rangle\langle\tilde{\phi}|\,. \tag{3.43}$$

To obtain a field theoretic description, we slice up the evolution of time, c.f. Eq. (3.23), in small pieces by applying Trotter's formula

$$\exp(-\hat{H}t) = \lim_{N\to\infty} \left(1 - \hat{H}\frac{t}{N}\right)^N\,. \tag{3.44}$$

Between each time slice we insert the identity of Eq. (3.43). Thus, the creation and destruction operators in Eq. (3.28) are replaced by complex numbers, $\hat{a}^\dagger(\mathbf{x}) \to \tilde{\phi}(\mathbf{x})$ and $\hat{a}(\mathbf{x}) \to \phi(\mathbf{x})$. Explicitly,

$$\langle\mathcal{O}(t)\rangle = \lim_{\Delta t\to 0} \int_{\phi(\mathbf{x},t')\in\mathbb{R},\tilde{\phi}(\mathbf{x},t')\in i\mathbb{R}} \left(\prod_{\mathbf{x},t'\in\{0,\Delta t,\dots,t\}} \frac{\mathrm{d}\phi(\mathbf{x},t')\,\mathrm{d}\tilde{\phi}(\mathbf{x},t')}{2\pi} e^{\phi(\mathbf{x},t')\tilde{\phi}(\mathbf{x},t')} \right) \cdot$$

$$\cdot\,\langle S|\mathcal{O}(\phi(t))|\phi(t)\rangle \left(\prod_{t'\in\{\Delta t,2\Delta t,\dots,t\}} \langle\tilde{\phi}(t')|\left(1 - H(\phi(t'),\phi(t'-\Delta t)\right)|\phi(t'-\Delta t)\rangle \right) \langle\tilde{\phi}(t=0)|\rho\rangle\,, \tag{3.45}$$

with an initial state $|\phi(t=0)\rangle = |\rho\rangle = e^{\rho\sum_{\mathbf{x}}(\hat{a}^\dagger(\mathbf{x})-1)}|0\rangle$ which obeys a Poisson distribution with a mean density ρ. After noting, that

$$\langle\tilde{\phi}(t')|\phi(t'-\Delta t)\rangle = \prod_{\mathbf{x}} \langle\tilde{\phi}(\mathbf{x},t')|\phi(\mathbf{x},t'-\Delta t)\rangle = \prod_{\mathbf{x}} e^{-\phi(\mathbf{x},t')\tilde{\phi}(\mathbf{x},t'-\Delta t)}\,, \tag{3.46}$$

and exploiting that $\phi(\mathbf{x},t') - \phi(\mathbf{x},t'-\Delta t) = \partial_t\phi(\mathbf{x},t')\Delta t$ to second order in Δt, we obtain

$$\langle\mathcal{O}(t)\rangle = \int_{\phi(\mathbf{x},t')\in\mathbb{R},\tilde{\phi}(\mathbf{x},t')\in i\mathbb{R}} \left(\prod_{\mathbf{x}} \mathcal{D}\phi(\mathbf{x},t)\mathcal{D}\tilde{\phi}(\mathbf{x},t) \right) \mathcal{O}(\phi(t)) \exp\Big(-\mathcal{S}[\tilde{\phi},\phi]_0^t\Big)\,. \tag{3.47}$$

Here, the functional integral $\mathcal{D}\phi(\mathbf{x})\mathcal{D}\tilde{\phi}(\mathbf{x})$ stands for $\prod_{t'\in\{0,\Delta t,\ldots,t\}}\mathrm{d}\phi_{\mathbf{x},t'}$ in the limit $\Delta t\to 0$ and the action is given by

$$\mathcal{S}[\tilde{\phi},\phi]_0^t=\sum_{\mathbf{x}}\left[-\phi(\mathbf{x},t)-\tilde{\phi}(\mathbf{x},0)(\phi(\mathbf{x},0)-\rho)+\int_0^t\mathrm{d}t'\tilde{\phi}(\mathbf{x},t')\partial_t\phi(\mathbf{x},t')\right]+ \\ +\int_0^t\mathrm{d}t' H(\tilde{\phi}(t'),\phi(t'))\,. \tag{3.48}$$

Notice that integration over $\tilde{\phi}(\mathbf{x},0)$ results in a delta function, $\delta(\phi(\mathbf{x},0)-\rho)$ and thus sets the initial condition $\phi(\mathbf{x},0)=\rho$.

Similar to the above shift of the destruction operator, it is favorable to perform a shift of the integration variable

$$\tilde{\phi}(\mathbf{x},t')\to\bar{\phi}(\mathbf{x},t')=\tilde{\phi}(\mathbf{x},t')-1\,. \tag{3.49}$$

According to Cauchy's integral theorem this does not change the integral since there are no singularities in between the line $i\mathbb{R}$ and $i\mathbb{R}-1$ and contributions to the integral at infinity are negligible. We find the action

$$\mathcal{S}[\bar{\phi},\phi]_0^t=\sum_{\mathbf{x}}\left[-\bar{\phi}(\mathbf{x},0)(\phi(\mathbf{x},0)-\rho)+\int_0^t\mathrm{d}t'\bar{\phi}(\mathbf{x},t)\partial_t\phi(\mathbf{x},t)\right]+\int_0^t\mathrm{d}t'\,H(\bar{\phi}(t'),\phi(t'))\,, \tag{3.50}$$

where $H(\bar{\phi}(t'),\phi(t'))$ is the Hamiltonian of Eq. (3.18) where the operators $\hat{a}^\dagger(\mathbf{x})$ are replaced by $\bar{\phi}(\mathbf{x},t')$ and $\hat{a}(\mathbf{x})$ by $\phi(\mathbf{x},t')$. One advantage of this representation is that the final term $\sum_{\mathbf{x}}-\phi(\mathbf{x},t)$ in Eq. (3.48) cancels, which greatly simplifies perturbative analysis.

We remark in passing that starting from Eq. (3.33) we can also arrive at Eq. (3.50) without having to invoke a shift of the integration variable, by employing the identity [136]

$$\int_{\phi\in\mathbb{R},\bar{\phi}\in i\mathbb{R}}\frac{\mathrm{d}\phi\,\mathrm{d}\bar{\phi}}{2\pi}e^{-\phi\bar{\phi}}|\phi\rangle\!\rangle\langle\bar{\phi}|\,, \tag{3.51}$$

and then proceed in an analogous fashion as we did above.

Instead of demanding that initially the system be Poisson distributed with density ρ, we can introduce particle input $\varnothing\to A$ with a rate $J(\mathbf{x},t)$. This gives rise to a term $-\int\mathrm{d}t\,J(\mathbf{x},t)\bar{\phi}(\mathbf{x},t)$ in the action (3.50). Let us demand that the system is initially empty and prepone the initial time to $-\infty$. If we then set $J(\mathbf{x},t)=\rho\delta(0)$, we recover Eq. (3.50). The final time in the integration of the action is determined by the observable and not by the action itself. Let us therefore drop the integration boundaries and write the general result as

$$\mathcal{S}[\bar{\phi},\phi]=\sum_{\mathbf{x}}\int\mathrm{d}t\left(\bar{\phi}(\mathbf{x},t)\partial_t\phi(\mathbf{x},t)+H(\bar{\phi}(t),\phi(t))-J(\mathbf{x},t)\bar{\phi}(\mathbf{x},t)\right)\,. \tag{3.52}$$

For our process of diffusing particles which coagulate and annihilate, we can therefore split up the action as

$$\mathcal{S}=\mathcal{S}_Z+\mathcal{S}_\epsilon+\mathcal{S}_{\lambda,\lambda'}+\mathcal{S}_J\,, \tag{3.53}$$

with a term of the time evolution

$$\mathcal{S}_Z[\bar{\phi},\phi]=\sum_{\mathbf{x}}\int\mathrm{d}t\,\bar{\phi}(\mathbf{x},t)\partial_t\phi(\mathbf{x},t)\,, \tag{3.54}$$

a diffusion term (a particle can hop from site $\mathbf{x}$ to site $\mathbf{y}$ with rate D, when $\mathbf{x}$ and $\mathbf{y}$ are adjacent sites),

$$\mathcal{S}_\epsilon[\bar{\phi},\phi] = D \sum_{<\mathbf{x},\mathbf{y}>} \int \mathrm{d}t \, \left(\bar{\phi}(\mathbf{x},t) - \bar{\phi}(\mathbf{y},t)\right)\left(\phi(\mathbf{x},t) - \phi(\mathbf{y},t)\right) , \tag{3.55}$$

a reaction term for coagulation $2A \to A$ with rate λ and annihilation $2A \to \varnothing$ with rate λ',

$$\mathcal{S}_{\lambda,\lambda'}[\bar{\phi},\phi] = \sum_{\mathbf{x}} \int \mathrm{d}t \, \left[(\lambda+\lambda')\bar{\phi}(\mathbf{x},t)^2\phi(\mathbf{x},t)^2 + (\lambda+2\lambda')\bar{\phi}(\mathbf{x},t)\phi(\mathbf{x},t)^2\right] , \tag{3.56}$$

and a part for the particle input $\varnothing \to A$

$$\mathcal{S}_J[\bar{\phi},\phi] = -\sum_{\mathbf{x}} \int \mathrm{d}t \, J(\mathbf{x},t)\bar{\phi}(\mathbf{x},t) . \tag{3.57}$$

Often it is adequate to assume that the lattice spacing a is small so that one can perform the continuum limit. In Section 5.1 the diffusion term in Fourier space is explicitly calculated, $\mathcal{S}_\epsilon = \int_{\mathbf{q}} \epsilon(\mathbf{q})\bar{\phi}(-\mathbf{q})\phi(\mathbf{q})$, with the dispersion relation $\epsilon(\mathbf{q}) = \frac{4D}{a^2}\sum_{\nu=1}^{d}\sin(q_\nu a/2)^2$. Dependence on the lattice spacing a guarantees that the diffusion constant D is kept fixed. (D is defined via the relation $\langle x^2\rangle \sim 2Dt$, which at large times holds for the variance of a particle's distance from the initial position, if this particle is only subject to this diffusion but not to further reactions, $\lambda = \lambda' = J = 0$.) When a becomes small we can approximate

$$\epsilon(\mathbf{q}) = Dq^2 . \tag{3.58}$$

This is allowed if large momenta q can be neglected, as will be the case in the next chapter, where we treat universal behavior below the critical dimension, and similarly in Section 5.5 where a finite radius R of the particles suppresses momenta $q \gg 1/R$. Thus, the diffusion term reads $\mathcal{S}_\epsilon[\bar{\phi},\phi] = \int_{\mathbf{q}} Dq^2\bar{\phi}(-\mathbf{q})\phi(\mathbf{q})$ and transforming back to position space, we have

$$\mathcal{S}_\epsilon[\bar{\phi},\phi] = D \sum_{<\mathbf{x},\mathbf{y}>} \left(\bar{\phi}(\mathbf{x},t) - \bar{\phi}(\mathbf{y},t)\right)\left(\phi(\mathbf{x},t) - \phi(\mathbf{y},t)\right) \to -D \int \mathrm{d}\mathbf{x}\,\mathrm{d}t \, \bar{\phi}(\mathbf{x},t)\nabla^2\phi(\mathbf{x},t) . \tag{3.59}$$

For reference let us note down the full action of our process in the continuum limit (for zero particle input)

$$\begin{aligned}\mathcal{S}[\bar{\phi},\phi] = &\int \mathrm{d}\mathbf{x}\,\mathrm{d}t \, \bar{\phi}(\mathbf{x},t)(\partial_t - D\nabla^2)\phi(\mathbf{x},t) + \\ &+ \int \mathrm{d}\mathbf{x}\,\mathrm{d}t \left[(\lambda+\lambda')\bar{\phi}(\mathbf{x},t)^2\phi(\mathbf{x},t)^2 + (\lambda+2\lambda')\bar{\phi}(\mathbf{x},t)\phi(\mathbf{x},t)^2\right] .\end{aligned} \tag{3.60}$$

We will utilize this approximation in the next chapter, where the exact form of the diffusion term has no impact on the long time behavior.

3.4 The Wetterich Equation

The Wetterich equation is the central formula of our NPRG approach and describes the flow of the "effective average action", defined below, under successive integration of the degrees of

freedom of the system. The starting point of its derivation is the partition function, defined for our reaction-diffusion system by

$$Z[J,\bar{J}] = \int \mathcal{D}\bar{\phi}\mathcal{D}\phi \exp\left[-\mathcal{S}[\bar{\phi},\phi] + \sum_{\mathbf{x}} \int \mathrm{d}t \, \left(\bar{J}\phi + J\bar{\phi}\right)\right] . \tag{3.61}$$

Here and in the following, to abbreviate the notation in the sums and integrals over $\mathbf{x}$ and t we often do not explicitly write out the position- and time-dependence of the fields (in this case the fields are $\bar{J}(\mathbf{x},t)$, $\phi(\mathbf{x},t)$, $J(\mathbf{x},t)$ and $\bar{\phi}(\mathbf{x},t)$). As shown in the previous section, J induces particle input $\varnothing \to A$, as long as J is positive. This is why $\bar{\phi}$ is sometimes referred to as "response field". For mathematical reasons, we also allow for negative J. There is no simple physical interpretation for $\bar{J}$. These fields are introduced in order that the associated functional

$$W[J,\bar{J}] = \ln Z[J,\bar{J}] \,, \tag{3.62}$$

which is related to the Helmholtz free energy, creates the "connected Green's functions" by functional derivation in the fields J, $\bar{J}$ at $J = \bar{J} = 0$. In particular the average density at position $\mathbf{x}$ and time t becomes $\langle S|\hat{a}(\mathbf{x})|P(t)\rangle = \langle\phi(\mathbf{x},t)\rangle = \frac{\delta}{\delta\bar{J}(\mathbf{x},t)} W[J,\bar{J}]\Big|_{J=\bar{J}=0}$, where $|P(t)\rangle$ is the state of the system at time t.

Part and parcel of renormalization groups is that one integrates the degrees of freedom systematically, going from high energy at the microscopic scale Λ (related to the lattice spacing a) to low energy (or short wavelengths and fast frequencies to long wavelengths and slow frequencies). One hopes the truncations made for higher energy modes of fluctuations do not influence too much the low energy modes. To implement this procedure, we add a momentum- and frequency-dependent "mass term" $\Delta\mathcal{S}_\kappa$ to the action suppressing fluctuations of these modes,

$$Z_\kappa[\bar{J},J] = \int \mathcal{D}\bar{\phi}\mathcal{D}\phi \exp\left[-\mathcal{S}[\bar{\phi},\phi] - \Delta\mathcal{S}_\kappa[\bar{\phi},\phi] + \sum_{\mathbf{x}} \int \mathrm{d}t \, (\bar{J}\phi + J\bar{\phi})\right] . \tag{3.63}$$

There is some freedom in choosing the mass term. We demand that in Fourier space it can be expressed as

$$\Delta\mathcal{S}_\kappa[\bar{\phi},\phi] = \frac{1}{2}\int_{\mathbf{q},\omega} \left(\bar{\phi}(-\mathbf{q},-\omega), \phi(-\mathbf{q},-\omega)\right) \cdot \hat{R}_\kappa(q^2,\omega) \cdot \begin{pmatrix} \bar{\phi}(\mathbf{q},\omega) \\ \phi(\mathbf{q},\omega) \end{pmatrix} . \tag{3.64}$$

with the cutoff function

$$\hat{R}_\kappa(q^2,\omega) = \begin{pmatrix} 0 & R_\kappa(p^2,\omega) \\ R_\kappa(p^2,-\omega) & 0 \end{pmatrix} . \tag{3.65}$$

It is related to spontaneous decay of particles: The reaction $A \to \varnothing$ with rate one, implies a term

$$\sum_{\mathbf{x}} \int \mathrm{d}t \, \bar{\phi}(\mathbf{x},t)\phi(\mathbf{x},t) = \int_{\mathbf{q},\omega} \bar{\phi}(-\mathbf{q},-\omega)\phi(\mathbf{q},\omega) \,, \tag{3.66}$$

which would correspond to a cutoff function which is independent of momentum and frequency.

Before further specifying the cutoff, let us derive a flow equation for the non-equilibrium Helmholtz free energy W_κ. For notational convenience let us write $\phi_1 := \bar{\phi}$, $\phi_2 := \phi$ and $J_1 := J$, $J_2 := \bar{J}$. In particular then we can express the mass term as

$$\begin{aligned}\Delta\mathcal{S}_\kappa[\bar{\phi},\phi] &= \frac{1}{2}\sum_{i,j}\int_{\mathbf{q},\omega}\phi_i(-\mathbf{q},-\omega)\hat{R}_{\kappa,i,j}(q^2,\omega)\phi_j(\mathbf{q},\omega) = \\ &= \frac{1}{2}\sum_{i,j,\mathbf{x},\mathbf{y}}\int \mathrm{d}t\,\mathrm{d}t'\,\phi_i(\mathbf{x},t)\hat{R}_{\kappa,i,j}(\mathbf{x}-\mathbf{y},t-t')\phi_j(\mathbf{y},t')\,, \end{aligned} \tag{3.67}$$

where the indices i,j run over the set $\{1,2\}$. We obtain

$$\begin{aligned}\partial_\kappa e^{W_\kappa[J,\bar{J}]} &= -\frac{1}{2}\int\mathcal{D}\bar{\phi}\,\mathcal{D}\phi\left(\sum_{i,j,\mathbf{x},\mathbf{y}}\int \mathrm{d}t\,\mathrm{d}t'\,\phi_i(\mathbf{x},t)\partial_\kappa\hat{R}_{\kappa,i,j}(\mathbf{x}-\mathbf{y},t-t')\phi_j(\mathbf{y},t')\right)\cdot \\ &\quad\cdot\exp\left[-\mathcal{S}[\bar{\phi},\phi]-\Delta\mathcal{S}_\kappa[\bar{\phi},\phi]+\sum_{i,\mathbf{x}}\int\mathrm{d}t\,J_i(\mathbf{x},t)\phi_i(\mathbf{x},t)\right] = \\ &= \left(-\frac{1}{2}\sum_{i,j,\mathbf{x},\mathbf{y}}\int\mathrm{d}t\,\mathrm{d}t'\,\partial_\kappa\hat{R}_{\kappa,i,j}(\mathbf{x}-\mathbf{y},t-t')\frac{\delta}{\delta J_i(\mathbf{x},t)}\frac{\delta}{\delta J_j(\mathbf{y},t')}\right)e^{W_\kappa[J,\bar{J}]}. \end{aligned} \tag{3.68}$$

Similar as before, for the sake of a more concise notation let us suppress the position- and time-dependence of the cutoff function $\hat{R}_{\kappa,i,j}(\mathbf{x}-\mathbf{y},t-t')$ and of the functional derivatives $\frac{\delta}{\delta J_i(\mathbf{x},t)}$ in the following. Thus, we have that

$$\partial_\kappa W_\kappa[J,\bar{J}] = -\frac{1}{2}\sum_{i,j,\mathbf{x},\mathbf{y}}\int\mathrm{d}t\,\mathrm{d}t'\,\partial_\kappa\hat{R}_{\kappa,i,j}\left(\frac{\delta^2 W_\kappa[J,\bar{J}]}{\delta J_i\delta J_j}+\frac{\delta W_\kappa[J,\bar{J}]}{\delta J_i}\frac{\delta W_\kappa[J,\bar{J}]}{\delta J_j}\right). \tag{3.69}$$

This flow equation for the Helmholtz free energy functional is related to the Polchinski equation, an earlier formulation of our NPRG approach [113, 115]. In recent years, a formally similar approach has proven more successful, where instead of $W_\kappa[J,\bar{J}]$ one considers its Legendre transform, the so called *effective average action* $\Gamma_\kappa[\bar{\psi},\psi]$. It is related to the Gibbs free energy and a functional of the expectation values

$$\bar{\psi}(\mathbf{x},t) := \langle\bar{\phi}(\mathbf{x},t)\rangle = \left.\frac{\delta W_\kappa[J,\bar{J}]}{\delta J(\mathbf{x},t)}\right|_{J=\bar{J}=0}, \quad \psi(\mathbf{x},t) := \langle\phi(\mathbf{x},t)\rangle = \left.\frac{\delta W_\kappa[J,\bar{J}]}{\delta\bar{J}(\mathbf{x},t)}\right|_{J=\bar{J}=0}. \tag{3.70}$$

Notice that both $\bar{\psi}$ and ψ are real numbers. We thus have direct access to the observable ψ, the average density of the particles, which is one advantage of the approach. The effective average action is defined as the Legendre transform of W_κ with an extra term that is added for later convenience,

$$\Gamma_\kappa[\bar{\psi},\psi]+W_\kappa[J,\bar{J}] = \sum_{\mathbf{x}}\int\mathrm{d}t\,\left(\bar{J}\psi+J\bar{\psi}\right)-\Delta\mathcal{S}_\kappa[\bar{\psi},\psi]\,. \tag{3.71}$$

The cutoff function R_κ is defined in a way that long range interactions (in space and time) with momentum $q^2<\kappa^2$, $|\omega|<\kappa^2$ are suppressed, while not affecting those with $q^2\gg\kappa^2$,

$|\omega| \gg \kappa^2$ (see Figure 3.1 for a typical representative of the cutoff function). Thus, the modes are successively integrated out until at $\kappa = 0$ the effective average potential $\Gamma_\kappa[\bar{\phi}, \phi]$ should be equal to the Gibbs free energy

$$\Gamma_{\kappa=0}[\phi, \phi] \equiv \Gamma[\bar{\phi}, \phi]\,, \tag{3.72}$$

the Legendre transformation of $W[J, \bar{J}]$. Thus, we request that the cutoff function R_κ fulfill the properties

$$\begin{cases} R_\kappa(q^2, \omega) \sim \kappa^2 & \text{when } q^2 \ll \kappa^2 \text{ or } \omega^2 \ll \kappa^2\,, \\ R_\kappa(q^2, \omega) \to 0 & \text{when } q^2 \gg \kappa^2 \text{ or } \omega^2 \gg \kappa^2\,, \\ R_\kappa(q^2, \omega) \to 0 & \text{when } \kappa \to 0 \text{ for fixed } q \text{ and } \omega\,, \\ R_\kappa(q^2, \omega) \to \infty & \text{when } \kappa \to \Lambda \text{ for fixed } q \text{ and } \omega\,. \end{cases} \tag{3.73}$$

The first and second constraint guarantee that a "mass" $\sim \kappa^2$ freezes the slow modes, whereas the fast modes are fully integrated. We thus have an infrared cutoff around the scale κ which ensures that the system stays analytic for any finite κ. This analyticity is essential for our truncation schemes, as we will see below. The functional W_κ may be compared with the free energy of a box of finite edge length $\sim \kappa^{-1}$. Divergencies in the functionals, characterizing a system at criticality, build up as the scale κ approaches zero. Once $\kappa = 0$ all degrees of freedom should be integrated out, i.e. $R_{\kappa=0} = 0$ (constraint three), and we indeed have $W_{\kappa=0} = W$ and $\Gamma_{\kappa=0} = \Gamma$. Finally, the fourth constraint in (3.73) freezes all fluctuations at the microscopic scale Λ and renders the system almost trivial so that, as is demonstrated below, the initial condition becomes

$$\Gamma_{\kappa=\Lambda}[\bar{\psi}, \psi] = \mathcal{S}[\bar{\psi}, \psi]\,. \tag{3.74}$$

Only modes with $q \lesssim \Lambda$ are integrated out. Therefore, if we employ the continuum limit in the action $\mathcal{S}$, a finite Λ sets the ultraviolet cutoff, approximately corresponding to the reciprocal lattice spacing, $\Lambda \approx a^{-1}$. Otherwise, if we keep the discrete lattice structure, the components q_ν only run over the set $]-\pi/a, \pi/a]$ and which intrinsically gives a ultraviolet cutoff. Similarly, we have an intrinsic ultraviolet cutoff for finite size objects, such as balls with radius R, where modes with $q \gg R^{-1}$ are suppressed. In these cases there is no need for an explicit cutoff and we can set $\Lambda = \infty$ (see Chapter 5).

The initial condition, Eq. (3.74), reflects the idea that the mass term $\Delta\mathcal{S}_\kappa$ strongly suppresses deviations from the mean $\bar{\psi} = \langle\bar{\phi}\rangle$, $\psi = \langle\phi\rangle$ such that in the κ-dependent partition function (3.63) we may restrict the functional integration to the regime $\bar{\phi} \approx \bar{\psi}$ and $\psi \approx \phi$, which would immediately lead to the desired result. Whereas such an approach is valid for equilibrium models [111], it turns out that for non-equilibrium processes as considered in this work, this procedure is not allowed in general. A proof of Eq. (3.74) was provided in [140] for an action of the special form

$$\mathcal{S}[\bar{\psi}, \psi] = \sum_{\mathbf{x}} \int \mathrm{d}t \left(\bar{\psi} f(\psi) - \bar{\psi}^2 g(\psi)\right)\,, \tag{3.75}$$

where f, g are analytic functions of $\phi(\mathbf{x}, t)$ and differences and derivatives thereof (such that, in particular, the kinetic term $\mathcal{S}_Z[\bar{\psi}, \psi] + \mathcal{S}_\epsilon[\bar{\psi}, \psi] = \bar{\psi}\partial_t\psi + D(\bar{\psi}(\mathbf{x}, t) - \bar{\psi}(\mathbf{y}, t))(\psi(\mathbf{x}, t) - \psi(\mathbf{y}, t))$ is covered by Eq. (3.75)), and g is positive definite, $g > 0$. Notice, that the action (3.53) for

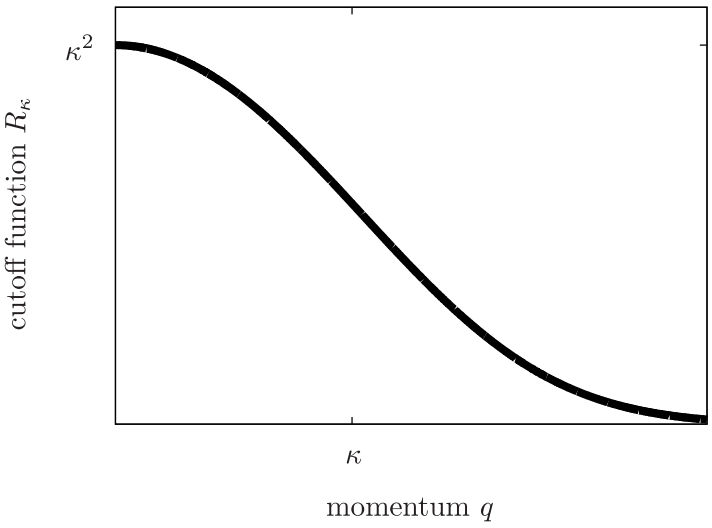

Figure 3.1: A typical form of the cutoff function $R_\kappa(q^2,\omega) \equiv R_\kappa(q^2)$, which gives rise to a momentum dependent mass term suppressing fluctuation. By providing an infrared cutoff it renders the functional W_κ and the average action Γ_κ analytic. This quality is crucial for our approximation scheme. In fact, at finite κ these functionals may be argued to roughly describe a finite size system, with edge length κ^{-1}. Critical behavior is defined by divergencies in the functionals and implies an infinitely long correlation length. This can be described by carefully studying the limit $\kappa \to 0$, as explained in Section 3.7.

the coagulation and annihilation process can be expressed in the form (3.75). Eq. (3.70) together with Eq. (3.71) implies that

$$J(\mathbf{x},t) = \left.\frac{\delta\Gamma_\kappa[\bar\psi,\psi]}{\delta\bar\psi(\mathbf{x},t)}\right|_{\bar\psi=\psi=0} + \sum_{\mathbf{y}}\int \mathrm{d}t'\, R_\kappa(\mathbf{x}-\mathbf{y},t'-t)\psi(\mathbf{y},t')\,, \tag{3.76}$$

$$\bar J(\mathbf{x},t) = \left.\frac{\delta\Gamma_\kappa[\bar\psi,\psi]}{\delta\psi(\mathbf{x},t)}\right|_{\bar\psi=\psi=0} + \sum_{\mathbf{y}}\int \mathrm{d}t'\, R_\kappa(\mathbf{x}-\mathbf{y},t'-t)\bar\psi(\mathbf{y},t')\,. \tag{3.77}$$

Hence, $e^{-\Gamma_\kappa[\bar\psi,\psi]}$ can be expressed as

$$\int \mathcal{D}\bar\phi\mathcal{D}\phi \exp\left[-\mathcal{S}[\bar\psi+\bar\phi,\psi+\phi] - \Delta\mathcal{S}_\kappa[\bar\phi,\phi] + \sum_{\mathbf{x}}\int \mathrm{d}t\, \left(\frac{\delta\Gamma_\kappa[\bar\psi,\psi]}{\delta\bar\psi}\bar\phi + \frac{\delta\Gamma_\kappa[\bar\psi,\psi]}{\delta\psi}\phi\right)\right]. \tag{3.78}$$

Here $\bar\phi$ and ϕ are the deviations from the mean values $\bar\psi$ and ψ, respectively. To see that these deviations are strongly suppressed, we insert the quadratic action, Eq. (3.75), and integrate it with respect to the response field $\bar\phi$ (which is imaginary). Then $e^{-\Gamma_\kappa[\bar\psi,\psi]}$ becomes

$$\int \mathcal{D}\phi\, \exp\left[-\sum_{\mathbf{x}}\int \mathrm{d}t \frac{\left(f(\psi+\phi) - 2\bar\psi g(\psi+\phi) + \sum_{\mathbf{y}} R_\kappa\phi - \frac{\delta\Gamma_\kappa[\bar\psi,\psi]}{\delta\bar\psi}\right)^2}{4g(\psi+\phi)}\right] \cdot$$

$$\cdot \exp\left\{-\sum_{\mathbf{x}}\int \mathrm{d}t\, \left[\left(\bar\psi f(\psi+\phi) + \bar\psi^2\right) + \frac{\delta\Gamma_\kappa[\bar\psi,\psi]}{\delta\psi}\phi - \ln g(\psi+\phi)\right]\right\}, \tag{3.79}$$

up to an irrelevant constant factor. At the ultraviolet cutoff $\kappa = \Lambda$ the cutoff function R_κ diverges. Therefore, we can set

$$f(\psi+\phi) - 2\bar{\psi}g(\psi+\phi) + \sum_{\mathbf{y}} R_\kappa \phi - \frac{\delta\Gamma_\kappa[\bar{\psi},\psi]}{\delta\bar{\psi}} \approx \sum_{\mathbf{y}} R_\kappa \phi\,, \tag{3.80}$$

and we see that all deviations ϕ from the mean-value are strongly suppressed, so that we may set $\phi = 0$ in the second line of Eq. (3.79). The functional integral over ϕ is then trivial and, neglecting an irrelevant constant term, we indeed recover Eq. (3.74).

Finally, we derive the flow equation for the average effective action. Taking the derivative with respect to κ in Eq. (3.71) at constant $\bar{\psi}(\mathbf{x},t) \equiv \bar{\psi}\,, \psi(\mathbf{x},t) \equiv \psi$ while keeping in mind that the fields

$$J(\mathbf{x},t) \equiv J_\kappa(\mathbf{x},t)[\bar{\psi},\psi]\,, \quad \bar{J}(\mathbf{x},t) \equiv \bar{J}_\kappa(\mathbf{x},t)[\bar{\psi},\psi]\,, \tag{3.81}$$

are κ-dependent functionals of $\bar{\psi}$ and ψ, yields

$$\begin{aligned}\partial_\kappa\Gamma[\bar{\psi},\psi] = \sum_{i,\mathbf{x}} \int \mathrm{d}t\, \psi_i \partial_\kappa J_i - \frac{1}{2}\sum_{i,j,\mathbf{x},\mathbf{y}} \int \mathrm{d}t\,\mathrm{d}t'\, \psi_i \partial_\kappa R_{\kappa,i,j}\psi_j - \\ - \partial_\kappa W_\kappa[J,\bar{J}] - \sum_{i,\mathbf{x}} \int \mathrm{d}t \frac{\delta W_\kappa[J,\bar{J}]}{\delta J_i}\partial_\kappa J_i\,.\end{aligned} \tag{3.82}$$

Since $\frac{\delta W_\kappa[J,\bar{J}]}{\delta J_i(\mathbf{x},t)} = \psi_i(\mathbf{x},t)$, the first and the last term of the right hand side cancel. Inserting Eq. (3.69) for the evolution of W_κ also the second term on the right hand side cancels and we obtain

$$\partial_\kappa\Gamma[\bar{\psi},\psi] = \frac{1}{2}\sum_{i,j,\mathbf{x},\mathbf{y}} \int \mathrm{d}t\,\mathrm{d}t'\, \partial_\kappa R_\kappa \frac{\delta^2 W_\kappa[J,\bar{J}]}{\delta J_i \delta J_j}\,. \tag{3.83}$$

Now, $\frac{\delta^2 W_\kappa[J,\bar{J}]}{\delta J_i \delta J_j}$ is just the inverse of the corresponding second derivative $\frac{\delta^2\widetilde{\Gamma}[\bar{\psi},\psi]}{\delta\psi_i\delta\psi_j}$ of $\widetilde{\Gamma}[\bar{\psi},\psi] \equiv \Gamma_\kappa[\bar{\psi},\psi] + \Delta\mathcal{S}_\kappa[\bar{\psi},\psi]$, because

$$\begin{aligned}\sum_{j,\mathbf{y}} \int \mathrm{d}t' \frac{\delta^2 W_\kappa[J,\bar{J}]}{\delta J_i(\mathbf{x},t)\delta J_j(\mathbf{y},t')} \frac{\delta^2\widetilde{\Gamma}_\kappa[\bar{\psi},\psi]}{\delta\psi_j(\mathbf{y},t')\delta\psi_l(\mathbf{z},t'')} = \sum_{j,\mathbf{y}} \int \mathrm{d}t' \frac{\delta\psi_i(\mathbf{x},t)}{\delta J_j(\mathbf{y},t')} \frac{\delta J_j(\mathbf{y},t')}{\delta\psi_l(\mathbf{z},t'')} = \\ = \frac{\delta\psi_i(\mathbf{x},t)}{\delta\psi_l(\mathbf{z},t'')} = \delta_{i,l}\delta(\mathbf{x}-\mathbf{z})\,.\end{aligned} \tag{3.84}$$

We thus arrive at the Wetterich equation

$$\partial_k\Gamma[\bar{\psi},\psi] = \frac{1}{2}\mathrm{Tr}\sum_{\mathbf{x},\mathbf{y}} \int \mathrm{d}t\,\mathrm{d}t'\, \partial_\kappa \hat{R}_\kappa(\mathbf{x}-\mathbf{y},t-t') \left(\hat{\Gamma}^{(2)}_\kappa[\bar{\psi},\psi](\mathbf{x},t,\mathbf{y},t') + \hat{R}_\kappa\right)^{-1}\,, \tag{3.85}$$

with the notation

$$\Gamma^{(2)}_{k,i,j}[\bar{\psi},\psi](\mathbf{x},t,\mathbf{y},t') \equiv \frac{\delta^2\Gamma_k[\bar{\psi},\psi]}{\delta\psi_i(\mathbf{x},t)\psi_j(\mathbf{y},t')}\,, \tag{3.86}$$

and the 2×2-matrices $\hat{R}_\kappa$ and $\hat{\Gamma}^{(2)}_\kappa[\bar{\psi},\psi]$. The trace Tr is over the ensuing 2×2-matrix. If we understand $\hat{R}_k$ and $\hat{\Gamma}^{(2)}_\kappa[\bar{\psi},\psi]$ as operators we may write the Wetterich equation more neatly as

$$\partial_k\Gamma[\bar{\psi},\psi] = \frac{1}{2}\mathrm{Tr}\left[\partial_\kappa\hat{R}_\kappa \left(\hat{\Gamma}^{(2)}_\kappa[\bar{\psi},\psi] + \hat{R}_\kappa\right)^{-1}\right]\,, \tag{3.87}$$

where the trace, in addition to the degrees of freedom of the 2×2-matrix, now is also over the space of position and time.

Of highest relevance for our concrete calculations will be the formulation of the Wetterich equation in momentum and frequency space, where the operators are diagonal, as long as the fields $\bar{\psi}$ and ψ are chosen to be translationally invariant. Then from

$$\hat{\Gamma}_\kappa^{(2)}[\bar{\psi},\psi](\mathbf{x},t,\mathbf{y},t') \equiv \hat{\Gamma}_\kappa^{(2)}[\bar{\psi},\psi](\mathbf{x}-\mathbf{y},t-t')\,, \tag{3.88}$$

it follows that

$$\hat{\Gamma}_\kappa^{(2)}[\bar{\psi},\psi](\mathbf{q},\omega,\mathbf{q}',\omega') \equiv (2\pi)^{d+1}\delta(\mathbf{q}+\mathbf{q}')\delta(\omega+\omega')\hat{\Gamma}_\kappa^{(2)}[\bar{\psi},\psi](\mathbf{q},\omega)\,, \tag{3.89}$$

and the Wetterich equation in Fourier space reads

$$\partial_\kappa \Gamma[\bar{\psi},\psi] = \frac{1}{2}\mathrm{Tr}\int_{\mathbf{q},\omega} \partial_\kappa \hat{R}_\kappa(\mathbf{q},\omega)\left(\hat{\Gamma}_\kappa^{(2)}[\bar{\psi},\psi](\mathbf{q},\omega)+\hat{R}_\kappa(\mathbf{q},\omega)\right)^{-1}\,. \tag{3.90}$$

Here the trace is over the degrees of freedom of the matrix and we only need to calculate the matrix inverse of $\hat{\Gamma}_\kappa^{(2)}[\bar{\psi},\psi](\mathbf{q},\omega)+\hat{R}_\kappa(\mathbf{q},\omega)$, since the inverse over momentum and frequency space is trivial.

3.5 Mean-Field and the Equation of Motion

Let us consider the coagulation process, $A+A\to A$ with rate λ, for particles which perform a random walk with diffusion constant D. We are interested in the time development of the particle density $\rho \equiv \rho(\mathbf{x},t)$ starting from some initial distribution $\rho_0(\mathbf{x}) \equiv \rho(\mathbf{x},t=0)$. A first approximation is the rate equation

$$\partial_t \rho(\mathbf{x},t) = D\nabla^2\rho(\mathbf{x},t) - \lambda\rho(\mathbf{x},t)^2\,, \tag{3.91}$$

which neglects fluctuations in the particle density. Generally, the mean-field rate equation also follows from the "classical field equations" given by the stationarity conditions

$$\frac{\delta\mathcal{S}[\bar{\psi},\psi]}{\delta\psi(\mathbf{x},t)} = 0 = \frac{\delta\mathcal{S}[\bar{\psi},\psi]}{\delta\bar{\psi}(\mathbf{x},t)}\,. \tag{3.92}$$

The first equation is solved by setting the auxiliary field $\bar{\psi}=0$. Inserting the action (3.60) for the coagulation process in the continuum limit (with $\lambda'=0$), and identifying ψ with the density of particles ($\psi\to\rho$) we recover Eq. (3.91).

Mean-field is only a good approximation when the system is well-mixed, i.e. when one is in the reaction-controlled regime with large diffusion constant $D\to\infty$. If instead we consider the limit $\lambda\to\infty$, Eq. (3.91) would suggest and infinitely fast decay. This is of course not the case: Let us consider the process on a cubic lattice with homogeneous initial conditions. For finite times t each site can by occupied by at most one particle. We obtain an upper bound for the effective decay rate by taking into account these finite particle numbers while neglecting the anti-correlations between the sites, which are expected to build up as time

goes on and decelerate the dynamics, see Section 1.2. Thus, the system is approximated by a product state where each site is occupied with probability ρ. A particle can hop with rate D to each of its six neighboring sites, where it is destroyed with probability ρ. Therefore, we obtain the upper bound $6D$ for the decay rate, i.e. the particle decay will not be faster than $\partial_t \rho = -6D\rho^2$. Thus, the kinetics is not infinitely fast but diffusion-limited, by its dependence on the diffusion constant D.

With the formalism developed in the previous section it is possible to account not only for fluctuations in the finite particle numbers but also for spatial and temporal correlations, by considering the non-equilibrium Gibbs free energy functional $\Gamma[\bar{\phi}, \psi] = \Gamma_{k=0}[\bar{\psi}, \psi]$ which by definition (as the Legendre transform of the Helmholtz free energy functional) fulfills the "*extremal principle*"

$$\frac{\delta\Gamma[\bar{\psi}, \psi]}{\delta\psi(\mathbf{x}, t)} = 0\,, \quad \frac{\delta\Gamma[\bar{\psi}, \psi]}{\delta\bar{\psi}(\mathbf{x}, t)} = J(\mathbf{x}, t)\,, \tag{3.93}$$

the macroscopic analog of the classical field equations, Eqs. (3.92). Here we have included the particle input $J(\mathbf{x}, t)$ which quite often is chosen to be $J(\mathbf{x}, t) = \rho(t = 0)\delta(t)$ for Poisson distributed initial conditions. Since normalization implies $\langle S|\hat{\bar{a}}^\dagger(\mathbf{x})|P(t)\rangle = 0$ (for some state $|P(t)\rangle$ of the system) we must have

$$\bar{\psi}(\mathbf{x}, t) = \langle\bar{\phi}(\mathbf{x}, t)\rangle = 0\,. \tag{3.94}$$

Indeed, one can show that $\Gamma[\bar{\psi} = 0, \psi] \equiv 0$ [140], and therefore the first condition of Eq. (3.93) is trivially fulfilled for vanishing auxiliary field $\bar{\psi}$. Again, identifying ψ with the density ρ, the extremal principle yields the macroscopic kinetic equations. We will see in the next chapters that to good approximation it is of the simple form

$$\partial_t \rho = -F(\rho)\,, \tag{3.95}$$

where the "non-equilibrium force" $F(\rho)$ is obtained by a functional derivative of the effective action. The leading term in $F(\rho)$ is the law of mass action term $\mu\rho^2$ where μ is the macroscopic decay rate. But, as we will show explicitly later, there are higher order terms in the density which violate the law of mass action. In particular we will show that the correct value for the decay rate for coagulation on a cubic lattice is not $\mu = 6D$, as estimated above, but $\mu \approx 4.0D$.

3.6 The Derivative Expansion

In general, the Wetterich equation cannot be solved exactly. The derivative expansion is an approximation scheme based on the fact that the initial condition, which is equal to the microscopic action $\Gamma_\Lambda = \mathcal{S}$, is analytic, since there are only nearest neighbor interactions. Since infrared singularities are suppressed by the cutoff R_κ, analyticity also holds for the effective average action $\Gamma_\kappa[\bar{\psi}, \psi]$ as long as $\kappa > 0$ [111]. It is therefore possible to perform the derivative expansion by expanding the functional $\Gamma_\kappa[\bar{\psi}, \psi]$ in orders of the temporal derivative ∂_t and the spatial derivative ∇ (for the remainder of this chapter the fields $\bar{\psi}(\mathbf{x}, t), \psi(\mathbf{x}, t)$ are taken as continuous functions of $\mathbf{x}$; correspondingly sums over $\mathbf{x}$ are replaced by integrals). In Fourier space this corresponds to factors of the frequency ω and the momentum $\mathbf{p}$, respectively. One then can simplify matters by truncating the functional $\Gamma_\kappa[\bar{\psi}, \psi]$ at a certain order. The

general idea is that this approach allows for an accurate description in the long time (low frequency ω) and large distance (small momentum $\mathbf{p}$) regime [111, 125], which is at the center of our interest.

For practical purposes it is very difficult to go beyond first order in the derivative ∂_t in time and beyond second order in the derivative ∇ in space. Canet shows that to this order the effective average action can be written as [125]

$$\Gamma_\kappa[\bar{\psi},\psi]=\int \mathrm{d}^d x\,\mathrm{d}t\,\Big[U_\kappa(\bar{\psi},\psi)+Z_\kappa(\bar{\psi},\psi)\bar{\psi}\partial_t\psi+D_\kappa(\bar{\psi},\psi)\nabla\bar{\psi}\nabla\psi+ \\ +\ \frac{1}{2}Y^1_\kappa(\bar{\psi},\psi)\left(\nabla\bar{\psi}\right)^2+\frac{1}{2}Y^2_\kappa(\bar{\psi},\psi)\left(\nabla\psi\right)^2\Big]\ . \tag{3.96}$$

Here, $U_\kappa, D_\kappa, Y^1_\kappa$ and Y^2_κ are analytic functions in the fields $\bar{\psi},\psi$. First order terms in the derivative in space ∇ can be ruled out for symmetry reasons. For instance, the symmetry under reflection along the plane $\mathbf{x}=0$ of a cubic lattice (created by the canonical lattice vectors $(1,0,0)$, $(0,1,0)$ and $(0,0,1)$, which start from the origin) immediately implies that terms involving only one derivatives ∂_x in space are forbidden. Also, if all three principal directions of the cubic lattice are equivalent, the derivatives ∂_x, ∂_y and ∂_z can be treated on equal footing and subsumed in the nabla operator ∇. Notice that since we only go to second order in ∇, the above action fulfills rotational symmetry and not just, say, the cubic, or hexagonal symmetry of the underlying lattice. This should be alright as long as we are to study the universal behavior below the critical dimension, which is independent of the lattice structure, see next chapter. There are other possible terms which involve second order derivatives in space, such as $Y^3_\kappa(\bar{\psi},\psi)\bar{\psi}\nabla^2\psi$ with analytic Y^3_κ, but that are not included in the above action. However they are redundant since they are readily re-expressed with the available terms employing partial integration.

The full action (3.96), although only lowest order derivatives are retained, still renders the flow equations very complicated and therefore one usually employs an even more crude approximation. This is achieved by a field expansion of the potentials $U_\kappa, Z_\kappa, D_\kappa, Y^1_\kappa$, and Y^2_κ, and keeping only terms up to a certain order. For the purposes of the next chapter we needed to calculate the "effective average potential" U_κ very precisely, i.e. to high order in the fields $\bar{\psi},\psi$. This was only feasible by keeping the other potentials only to zeroth order,

$$Z_\kappa(\bar{\psi},\psi)\equiv Z_\kappa\,,\ D_\kappa(\bar{\psi},\psi)\equiv D_\kappa\,,\ Y^1_\kappa(\bar{\psi},\psi)\equiv Y^1_\kappa\,,\ Y^2_\kappa(\bar{\psi},\psi)\equiv Y^2_\kappa\,, \tag{3.97}$$

which is known as the "leading order" approximation. It can be shown that in this case $Y^1_\kappa=Y^2_\kappa=0$ for all scales κ (if they vanish for $\kappa=\Lambda$), since in this approximation their flow is proportional to themselves [125].

In the following we shall employ the leading order approximation as our ansatz. The initial condition reduces to

$$\Gamma_\kappa[\bar{\psi},\psi]=\int \mathrm{d}^d x\,\mathrm{d}t\,\left[U_\kappa(\bar{\psi},\psi)+\bar{\psi}(Z_\kappa\partial_t-D_\kappa\nabla^2)\psi\right]\ . \tag{3.98}$$

This approximation is popular because it already allows to determine the anomalous dimension $\eta=-\kappa\,\partial_\kappa \ln Z_\kappa$ and the dynamic exponent $z=2+\kappa\partial_\kappa \ln D_\kappa-\kappa\partial_\kappa \ln Z_\kappa$. However, we

will show below that for the coagulation process this ansatz is equivalent to a lower order in the approximation, the so called "local potential" approximation,

$$\Gamma_\kappa[\bar{\psi},\psi] = \int \mathrm{d}^d x\, \mathrm{d}t \left[U_\kappa(\bar{\psi},\psi) + \bar{\psi}\left(\partial_t - \nabla^2\right)\psi\right] , \tag{3.99}$$

where only the renormalization of the local potential U_κ is taken into account. The reason is that, as proven in Chapter 4, for our particular process Z_κ and D_κ are not affected by the renormalization group flow, i.e. $Z_\kappa = D_\kappa = 1$ for all κ. Thus, for the coagulation process, η and z agree with the mean-field exponents 0 and 2, respectively. Incidentally, this is one reason why Smoluchowski's approach succeeds: Such a mean-field like approach cannot account for irrational exponents, which are usually found in critical systems [141].

In the following let us consider homogeneous fields $\bar{\psi}(x,t) \equiv \bar{\psi}$, $\psi(x,t) \equiv \psi$. The relation between the average effective action and the local potential then reads

$$\Gamma_\kappa[\bar{\psi},\psi] = VT \cdot U_\kappa(\bar{\psi},\psi) , \tag{3.100}$$

with the asymptotically large volumes of space and time $V = \int \mathrm{d}\mathbf{x} = (2\pi)^d \delta(\mathbf{p}=\mathbf{0})$ and $T = \int \mathrm{d}t = 2\pi\delta(\omega = 0)$, respectively. To obtain a flow equation for the local potential U_κ within the leading order truncation, Eq. (3.98), let us calculate the propagator $\hat{G}_\kappa[\bar{\psi},\psi] \equiv \left(\hat{\Gamma}^{(2)}_\kappa[\bar{\psi},\psi] + \hat{R}_\kappa\right)^{-1}$ in Fourier space, where it is diagonal because of translational invariance (assuming the cutoff R_κ is chosen such that it respects the translational invariance, see below). For concise notation, we express the combined vector of momentum $\mathbf{p}$ and frequency ω as $\mathrm{p} = (\mathbf{p},\omega)$. Notice that this allows to write the product of the volume of space and time in the short form $VT = (2\pi)^{d+1}\delta(\mathrm{p}=0)$. The bilinear form $\hat{\Gamma}^{(2)}_\kappa[\bar{\psi},\psi]$, becomes (as above, $m,n \in \{1,2\}$, "1" stands for the response field $\bar{\psi}$ and "2" for ψ):

$$\langle \mathrm{p}_1, m|\hat{\Gamma}^{(2)}_\kappa[\bar{\psi},\psi]|\mathrm{p}_2, n\rangle \equiv \hat{\Gamma}^{(2)}[\bar{\psi},\psi](\mathrm{p}_1, m; -\mathrm{p}_2, n) = \frac{\delta^2\Gamma[\bar{\psi},\psi]}{\delta\psi_m(-\mathrm{p}_1)\delta\psi_n(\mathrm{p}_2)} =$$

$$= \delta(\mathrm{p}_1 - \mathrm{p}_2)\left[\begin{pmatrix} U^{(2,0)}_\kappa(\bar{\psi},\psi) & U^{(1,1)}_\kappa(\bar{\psi},\psi) \\ U^{(1,1)}_\kappa(\bar{\psi},\psi) & U^{(0,2)}_\kappa(\bar{\psi},\psi)\end{pmatrix}_{m,n} + \begin{pmatrix} 0 & Z_\kappa i\omega_2 \\ -Z_\kappa i\omega_1 & 0\end{pmatrix}_{m,n} + \begin{pmatrix} 0 & D_\kappa p_2^2 \\ D_\kappa p_1^2 & 0\end{pmatrix}_{m,n}\right] . \tag{3.101}$$

For simplicity one usually chooses a cutoff function $R_\kappa(\mathbf{p},\omega) = R_\kappa(p^2)$ which is independent of the frequency ω [125]. This does not cause divergencies because stochastic processes need not have a "microscopic" scale in time [93]. Furthermore, we choose it to depend on the square p^2 of the momentum only, in order that the renormalization group flow conserves the rotational invariance of the initial, microscopic action $\mathcal{S}$. (This condition will be relaxed in later chapters.) Then, in particular, R_κ is translationally invariant in position and time, as we requested above. We have

$$\langle \mathrm{p}_1, m|\hat{R}_\kappa|\mathrm{p}_2, n\rangle = \delta(\mathrm{p}_1 - \mathrm{p}_2)\begin{pmatrix} 0 & R_\kappa(p_1^2) \\ R_\kappa(p_2^2) & 0\end{pmatrix}_{m,n} . \tag{3.102}$$

Thus,

$$\langle \mathrm{p}_1, m|(\hat{\Gamma}^{(2)}_\kappa[\bar{\psi},\psi] + \hat{R}_\kappa)|\mathrm{p}_2, n\rangle = \delta(\mathrm{p}_1 - \mathrm{p}_2)\begin{pmatrix} U^{(2,0)}_\kappa(\bar{\psi},\psi) & h_\kappa(\bar{\psi},\psi,\mathrm{p}_1) \\ h_\kappa(\bar{\psi},\psi,-\mathrm{p}_1) & U^{(0,2)}_\kappa(\bar{\psi},\psi)\end{pmatrix}_{m,n} , \tag{3.103}$$

with $h_\kappa(\bar{\psi},\psi,\mathrm{p}) = U_\kappa^{(1,1)}(\bar{\psi},\psi) + Z_\kappa i\omega + D_\kappa p^2 + R_\kappa(p^2)$. Since the propagator $\hat{G}_\kappa$ is diagonal in Fourier space it is not hard calculating its reciprocal

$$\begin{aligned}\hat{G}[\bar{\psi},\psi](\mathrm{p}_1,\mathrm{p}_2) &= \langle \mathrm{p}_1, m|\hat{G}_\kappa[\bar{\psi},\psi]|\mathrm{p}_2, n\rangle = \langle \mathrm{p}_1, m|(\hat{\Gamma}_\kappa^{(2)}[\bar{\psi},\psi] + \hat{R}_\kappa)^{-1}|\mathrm{p}_2, n\rangle = \\ &= -\delta(\mathrm{p}_1 - \mathrm{p}_2)\det[\bar{G}_\kappa(\bar{\psi},\psi,\mathrm{p}_1)] \begin{pmatrix} -U_\kappa^{(0,2)}(\bar{\psi},\psi) & h_\kappa(\bar{\psi},\psi,\mathrm{p}_1) \\ h_\kappa(\bar{\psi},\psi,-\mathrm{p}_1) & -U_\kappa^{(2,0)}(\bar{\psi},\psi)\end{pmatrix}_{m,n}, \end{aligned} \tag{3.104}$$

where $0 \overset{(!)}{<} -1/\det[\bar{G}_\kappa(\bar{\psi},\psi,\mathrm{p})] \equiv h_\kappa(\bar{\psi},\psi,\mathrm{p})h_\kappa(\bar{\psi},\psi,-\mathrm{p}) - U_\kappa^{(2,0)}(\bar{\psi},\psi)\,U_\kappa^{(0,2)}(\bar{\psi},\psi)$ is expected to be strictly larger than zero [125]. This property is the non-equilibrium analog to convexity (e.g. $U_\kappa^{(2)}(\psi) > 0$ when there is only one field ψ) in equilibrium physics.

Inserting the expression for the propagator, Eq. (3.104), into the Wetterich flow equation, we arrive at

$$\begin{aligned}\partial_\kappa \Gamma_\kappa[\bar{\psi},\psi] &\overset{\text{Wetterich Eq.}}{=} \frac{1}{2}\sum_{m,n}\int_{\mathrm{q},\mathrm{q}'} \langle \mathrm{q}, m|\partial_\kappa \hat{R}_\kappa|\mathrm{q}', n\rangle\langle \mathrm{q}', n|\hat{G}_\kappa[\bar{\psi},\psi]|\mathrm{q}, m\rangle = \\ &= (2\pi)^{d+1}\delta(\mathrm{p}=0)\int_{\mathrm{q}} -\det[\bar{G}_\kappa(\bar{\psi},\psi,\mathrm{p})]\left[h_\kappa(\bar{\psi},\psi,\mathrm{q})\partial_\kappa R_\kappa(q^2) + h(\bar{\psi},\psi,-\mathrm{q})\partial_\kappa R_\kappa(q^2)\right] = \\ &= (2\pi)^{d+1}\delta(\mathrm{p}=0)\int_{\mathrm{q}} \frac{\partial_\kappa R_\kappa(q^2)\left(U^{(1,1)}(\bar{\psi},\psi) + R_\kappa(q^2) + D_\kappa q^2\right)}{\left[U_\kappa^{(1,1)}(\bar{\psi},\psi) + R_\kappa(q^2) + D_\kappa q^2\right]^2 + Z_\kappa^2\omega^2 - U^{(2,0)}(\bar{\psi},\psi)U^{(0,2)}(\bar{\psi},\psi)}\,. \end{aligned} \tag{3.105}$$

After inserting $VT = (2\pi)^{d+1}\delta(\mathrm{p}=0)$ and Eq. (3.100), we finally obtain the Wetterich Equation for the potential U_κ within the leading order truncation

$$\partial_\kappa U_\kappa(\bar{\psi},\psi) = \int_{\mathrm{q}} \frac{\partial_\kappa R_\kappa(q^2)\left(U_\kappa^{(1,1)}(\bar{\psi},\psi) + R_\kappa(q^2) + D_\kappa q^2\right)}{\left(U_\kappa^{(1,1)}(\bar{\psi},\psi) + R_\kappa(q^2) + D_\kappa q^2\right)^2 + Z_\kappa^2\omega^2 - U_\kappa^{(2,0)}(\bar{\psi},\psi)U_\kappa^{(0,2)}(\bar{\psi},\psi)}\,. \tag{3.106}$$

Since R_κ is chosen to be independent of ω, the integration over ω can be carried out explicitly, and the flow equation becomes

$$\partial_\kappa U_\kappa(\bar{\psi},\psi) = \frac{1}{2Z_\kappa}\int_{\mathbf{q}} \frac{\partial_\kappa R_\kappa(q^2)\left(U_\kappa^{(1,1)}(\bar{\psi},\psi) + R_\kappa(q^2) + D_\kappa q^2\right)}{\sqrt{\left(U_\kappa^{(1,1)}(\bar{\psi},\psi) + R_\kappa(q^2) + D_\kappa q^2\right)^2 - U_\kappa^{(2,0)}(\bar{\psi},\psi)U_\kappa^{(0,2)}(\bar{\psi},\psi)}}\,. \tag{3.107}$$

In the following we will mostly employ the standard cutoff function [142]

$$R_\kappa(\mathbf{q},\omega) = R_\kappa(q^2) = D_\kappa(\kappa^2 - q^2)\Theta(\kappa^2 - q^2)\,. \tag{3.108}$$

It has the convenient property of rendering the integration over the momentum q trivial. Thus, neglecting also $\partial_\kappa D_\kappa$ (which indeed vanishes for the coagulation process), the flow equation for the effective average potential further simplifies to

$$\partial_\kappa U_\kappa(\bar{\psi},\psi) = \frac{\widetilde{V}_d\kappa^d D_\kappa}{Z_k}\frac{\kappa\left(U_\kappa^{(1,1)}(\bar{\psi},\psi) + D_\kappa\kappa^2\right)}{\sqrt{\left(U_\kappa^{(1,1)}(\bar{\psi},\psi) + D_\kappa\kappa^2\right)^2 - U_\kappa^{(2,0)}(\bar{\psi},\psi)U_\kappa^{(0,2)}(\bar{\psi},\psi)}}\,, \tag{3.109}$$

where $\widetilde{V}_d = V_d/(2\pi)^d$ and V_d is the volume of the d-dimensional unit sphere.

3.7 Dimensionless Flow Equation

In order to be able to study critical behavior, we need to resolve the fixed points of the flow. These are only found after appropriate rescaling of the fields and potentials. In this section, we rewrite the Wetterich equation with these new, rescaled quantities. To motivate the choice of our rescaling, let us consider the renormalized kinetic term

$$\Gamma_{\kappa,\mathrm{kin}}[\bar{\psi},\psi] = \int \mathrm{d}^d x\, \mathrm{d}t\, \bar{\psi}(\mathbf{x},t)\left(Z_\kappa \partial_t - D_\kappa \nabla^2\right)\psi(\mathbf{x},t)\,, \tag{3.110}$$

of the effective average potential. If we are looking for a fixed point then at least this expression should be constant under renormalization. This is realized if we introduce the dimensionless coordinates

$$\mathbf{x} = \kappa^{-1}\tilde{\mathbf{x}}\,, \quad t = \kappa^{-2}\frac{Z_\kappa}{D_\kappa}\tilde{t}\,, \tag{3.111}$$

and the renormalized dimensionless fields

$$\bar{\psi}(\mathbf{x},t) = \bar{\chi}(\tilde{\mathbf{x}},\tilde{t})\,, \quad \psi(\mathbf{x},t) = \kappa^d Z_\kappa^{-1}\chi(\tilde{\mathbf{x}},\tilde{t})\,. \tag{3.112}$$

The kinetic term is then rewritten as

$$\Gamma_{\mathrm{kin}}[\bar{\chi},\chi] = \int \mathrm{d}^d\tilde{x}\, \mathrm{d}\tilde{t}\, \bar{\chi}(\tilde{\mathbf{x}},\tilde{t})\left(\partial_{\tilde{t}} - \nabla_{\tilde{x}}\right)\chi(\tilde{\mathbf{x}},\tilde{t})\,. \tag{3.113}$$

The derivatives $\nabla_{\tilde{x}}$ and $\partial_{\tilde{t}}$ in space and time, respectively, are now with respect to the new, dimensionless coordinates. Indeed, with these rescalings the kinetic term keeps its form along the renormalization group flow.

There is a subtlety regarding the rescaling of the fields $\bar{\psi}$ and ψ. Our choice is the right one, because it turns out that it leads to a fixed point. In general however it is not clear which rescaling to opt for, since the only constraint is on the product $[\bar{\psi}\psi] = \kappa^d Z_\kappa^{-1}$ [137]. To study the possible implications of fixed point for a different choice of the rescaling, for simplicity let us provisionally set $Z_\kappa = 1$, as for the local potential approximation. In general then, $\bar{\psi} = \kappa^{\epsilon d}\bar{\chi}, \psi = \kappa^{(1-\epsilon)d}\chi$ where ϵ is an additional exponent. Its impact can be seen when one introduces a particle input field $\widetilde{J}$ ($\varnothing \xrightarrow{J} A$). Since it is associated with the auxiliary field $\bar{\psi}$ it is rescaled $J \to \kappa^{-\epsilon d+d+2}J$. Thus, at the critical point the stationary density behaves as

$$\psi \sim J^{\frac{d(1-\epsilon)}{d(1-\epsilon)+2}}\,, \text{ when } \epsilon > 0\,. \tag{3.114}$$

A special case is $\epsilon = 1/2$. This holds for the famous contact process, where the two fields $\bar{\psi}$ and ψ are linked by the so called rapidity symmetry [86]. At the critical dimension $d_c = 4$, we recover the mean-field scaling $\psi \sim \sqrt{J}$ of the contact process. For the coagulation and annihilation process we will see in the next chapter that $\epsilon = 0$ and that the critical dimension is $d_c = 2$. Indeed for $d = 2$ Eq. (3.114) gives the mean-field scaling, which here is also $\psi \sim \sqrt{J}$.

For reference, let us also note down the corresponding relations to Eqs. (3.111,3.112) in Fourier space. They turn to

$$\mathbf{q} = \kappa\tilde{\mathbf{q}}\,, \quad \omega = \kappa^{-2}\frac{Z_\kappa}{D_\kappa}\tilde{\omega}\,, \tag{3.115}$$

for the coordinates and

$$\bar{\psi}(\mathbf{q},\omega) = \kappa^{d+2} D_\kappa Z_\kappa^{-1} \bar{\chi}(\tilde{\mathbf{q}},\tilde{\omega})\,, \quad \psi(\mathbf{q},\omega) = \kappa^{2d+2} D_\kappa Z_\kappa^{-2} \chi(\tilde{\mathbf{q}},\tilde{\omega})\,, \tag{3.116}$$

for the fields.

The terms D_κ and Z_κ absorb divergencies that arise at the critical point, where the flow drives the system to the fixed point. In this case, as proven below, $D_\kappa \sim \kappa^{-x_D}$ and $Z_\kappa \sim \kappa^{-x_Z}$, for some constants x_D and x_Z. Thus, expressing the dimension of time in terms of the reciprocal lengthscale κ, one obtains

$$[t] = [\kappa^{-2} Z_\kappa D_\kappa^{-1}] = \kappa^{-(2+x_Z-x_D)} \equiv \kappa^{-z} = [x]^z\,, \tag{3.117}$$

where z is the dynamic critical exponent [125]. To put this into perspective, we note that for pure diffusional motion, without chemical reactions, the law of diffusion $\langle x^2\rangle = 2Dt$ implies $[t] \sim [x]^2$ (and $D \sim \kappa^0$), giving the "classical" dynamic critical exponent $z = 2$. Moreover, x_Z can be identified with the anomalous dimension $\eta = x_Z$, defined by the dimension of the product $[\bar{\psi}\psi] = \kappa^{d+\eta}$ of the fields [125, 143].

In addition to the kinetic term, we need to rescale the potentials which appear in the derivative expansion. Let us focus here on the leading order truncation, Eq. (3.98). Evidently, for the effective average potential U_κ the proper dimensionless and renormalized form of the local potential obeys

$$U_\kappa(\bar{\psi},\psi) = \kappa^{d+2} \frac{D_\kappa}{Z_\kappa} u_\kappa(\bar{\chi},\chi)\,, \tag{3.118}$$

so that the reaction part of the effective average action $\Gamma_\kappa = \Gamma_{\kappa,\mathrm{kin}} + \Gamma_{\kappa,\mathrm{react}}$ is rewritten as $\Gamma_{\kappa,\mathrm{react}}[\bar{\chi},\chi] = \int \mathrm{d}^d\tilde{x}\,\mathrm{d}\tilde{t}\,u_\kappa(\bar{\chi},\chi)$.

We also need to look at the cutoff term, which is most conveniently described in Fourier space, $\mathcal{S}_{\mathrm{cutoff}}[\bar{\psi},\psi] = \int_{\mathbf{q},\omega} R_\kappa(q^2)\bar{\psi}(-\mathbf{q},-\omega)\psi(\mathbf{q},\omega)$. We demand that

$$R_\kappa(q^2) = D_\kappa q^2 r(\tilde{q}^2)\,. \tag{3.119}$$

Notice that this is an additional constraint on the cutoff function. It is necessary, because at a fixed point, also the cutoff function, i.e. r must be fixed: In contrast to the potential u_κ, which at the critical point is expect to flow to some constant value $u^\star$, the function r must be enforced to be constant "by hand". (This requirement will be relaxed in later chapters, where, however, we will not be interested in fixed points.) The cutoff action then reads $\mathcal{S}_{\mathrm{cutoff}}[\bar{\chi},\chi] = \int_{\tilde{\mathbf{q}},\tilde{\omega}} \tilde{q}^2 r(\tilde{q})\bar{\chi}(-\tilde{\mathbf{q}},-\tilde{\omega})\chi(\tilde{\mathbf{q}},\tilde{\omega})$.

Let us now turn to the flow of the effective average action in the framework of the redefined quantities. The Wetterich equation is recast in the form

$$\partial_\kappa \Gamma_\kappa[\bar{\psi},\psi] = \frac{1}{2}\mathrm{Tr}\left[\left(\partial_\kappa \frac{\delta^2 \mathcal{S}_{\kappa,\mathrm{cutoff}}[\bar{\psi},\psi]}{\delta(\bar{\psi},\psi)\delta(\bar{\psi},\psi)}\right)\left(\frac{\delta^2(\Gamma_\kappa + \mathcal{S}_{\kappa,\mathrm{cutoff}})[\bar{\psi},\psi]}{\delta(\bar{\psi},\psi)\delta(\bar{\psi},\psi)}\right)^{-1}\right], \tag{3.120}$$

where $\frac{\delta^2}{\delta(\bar{\psi},\psi)\delta(\bar{\psi},\psi)}$ creates the 2×2 matrix of second order functional derivatives. Evidently, when the fields are rescaled on the right hand side, the factors cancel due to the reciprocal. Therefore, also

$$\partial_\kappa \Gamma_\kappa[\bar{\psi},\psi] = \frac{1}{2}\mathrm{Tr}\left[\left(\partial_\kappa \frac{\delta^2 \widetilde{\mathcal{S}}_{\kappa,\mathrm{cutoff}}[\bar{\chi},\chi]}{\delta(\bar{\chi},\chi)\delta(\bar{\chi},\chi)}\right)\left(\frac{\delta^2(\widetilde{\Gamma}_\kappa + \widetilde{\mathcal{S}}_{\kappa,\mathrm{cutoff}})[\bar{\chi},\chi]}{\delta(\bar{\chi},\chi)\delta(\bar{\chi},\chi)}\right)^{-1}\right] =$$

$$= \frac{1}{2}\mathrm{Tr}\left[\partial_\kappa \hat{\tilde{R}}\left(\hat{\tilde{\Gamma}}^{(2)}[\bar{\chi},\chi] + \hat{\tilde{R}}\right)^{-1}\right], \tag{3.121}$$

where the trace is over the 2×2 matrix and the rescaled coordinates $\tilde{\mathrm{x}}$ (or in Fourier space $\tilde{\mathrm{q}}$). Here, it is understood that the fields $\bar{\psi},\psi$ are fixed, i.e. independent of the scale κ, and we have introduced the notation

$$\widetilde{\Gamma}_\kappa[\bar{\chi},\chi] \equiv \Gamma_\kappa[\bar{\psi}(\bar{\chi}),\psi(\chi)], \quad \widetilde{\mathcal{S}}_{\kappa,\mathrm{cutoff}}[\bar{\chi},\chi] \equiv \mathcal{S}_{\kappa,\mathrm{cutoff}}[\bar{\psi}(\bar{\chi}),\psi(\chi)], \tag{3.122}$$

and

$$\hat{\tilde{R}}(\tilde{q}^2) := \hat{\tilde{\mathcal{S}}}^{(2)}_{\mathrm{cutoff}}(\tilde{\mathrm{q}},-\tilde{\mathrm{q}}) = \begin{pmatrix} 0 & \tilde{q}^2 r(\tilde{q}) \\ \tilde{q}^2 r(\tilde{q}) & 0 \end{pmatrix}. \tag{3.123}$$

The derivative of this rescaled cutoff function becomes

$$\partial_\kappa \hat{\tilde{R}}(\tilde{q}^2) = \frac{1}{\kappa}\begin{pmatrix} 0 & \tilde{q}^2 r'\left(\tilde{q}^2\right) \\ \tilde{q}^2 r'\left(\tilde{q}^2\right) & 0 \end{pmatrix}. \tag{3.124}$$

In the derivative of $\partial_\kappa \widetilde{\Gamma}_\kappa[\bar{\chi},\chi] = \partial_\kappa\left(\Gamma_\kappa[\bar{\psi}(\bar{\chi}),\psi(\chi)]\right)$, in addition to the above term describing the integration of degrees of freedom, there is also the term which is a consequence of the κ-dependence of the field $\psi\equiv\psi(\chi)$, c.f. (3.112),

$$\int \mathrm{d}^d x\,\mathrm{d}t\,\frac{\delta\Gamma[\bar{\psi},\psi]}{\delta\psi(\mathbf{x},t)}\frac{\partial\psi(\mathbf{x},t)}{\partial\kappa} = \int \mathrm{d}^d\tilde{x}\,\mathrm{d}\tilde{t}\,\frac{\delta\widetilde{\Gamma}[\bar{\chi},\chi]}{\delta\chi(\tilde{\mathbf{x}},\tilde{t})}\left(\frac{d}{\kappa} - \frac{\partial_\kappa Z_\kappa}{Z_\kappa}\right). \tag{3.125}$$

At the critical dimension we expect that $Z_\kappa \sim \kappa^{-x_Z}$, for some exponent x_Z. Therefore, we define $x_{\kappa,Z} = -\kappa\frac{\partial_\kappa Z_\kappa}{Z_\kappa}$. At a fixed point, the contribution of the flow equation $\partial_\kappa\widetilde{\Gamma}[\bar{\chi},\chi]$ behaves as κ^{-1}. This divergency can be dealt with by introducing the renormalization time

$$\tau = \ln(\kappa/\Lambda), \tag{3.126}$$

which, by definition, runs from 0 to $-\infty$.

We thus obtain the flow equation for the dimensionless action,

$$\partial_\tau\widetilde{\Gamma}_\tau[\bar{\chi},\chi] = (d+x_{\kappa,D})\int \mathrm{d}^d\tilde{x}\,\mathrm{d}\tilde{t}\,\frac{\delta\widetilde{\Gamma}_\tau[\bar{\chi},\chi]}{\delta\chi(\tilde{\mathbf{x}},\tilde{t})}\chi(\tilde{\mathbf{x}},\tilde{t}) + \frac{1}{2}\mathrm{Tr}\left[\partial_\tau\hat{\tilde{R}}\cdot\left(\hat{\tilde{\Gamma}}^{(2)}_\tau[\chi,\chi] + \hat{\tilde{R}}\right)^{-1}\right]. \tag{3.127}$$

This flow equation is incomplete since, in addition, we need to determine the flow of

$$D_\kappa = \frac{(2\pi)^{d+2}}{\delta(\mathrm{q}=0)}\frac{\partial}{\partial q^2}\frac{\delta^2}{\delta\bar{\psi}(-\mathrm{q})\delta\psi(\mathrm{q})}\Gamma_\kappa[\bar{\psi},\psi]\Big|_{\mathrm{q}=\bar{\psi}=\psi=0}, \tag{3.128}$$

and of

$$Z_\kappa = -i\frac{(2\pi)^{d+2}}{\delta(\mathrm{q}=0)}\frac{\partial}{\partial\omega}\frac{\delta^2}{\delta\bar{\psi}(-\mathrm{q})\delta\psi(\mathrm{q})}\Gamma_\kappa[\bar{\psi},\psi]\Big|_{\mathrm{q}=\bar{\psi}=\psi=0}. \tag{3.129}$$

Transforming to dimensionless, renormalized quantities, and inserting Eq. (3.121) we thus obtain

$$x_{D,\tau} := -\partial_\tau \ln D_\tau = -\frac{1}{2}\frac{(2\pi)^{d+2}}{\delta(\tilde{\mathrm{q}}=0)}\frac{\partial}{\partial\tilde{q}^2}\frac{\delta^2}{\delta\bar{\psi}(-\tilde{\mathrm{q}})\delta\psi(\tilde{\mathrm{q}})}\,\mathrm{Tr}\left[\hat{\tilde{R}}\cdot\left(\partial_\tau\hat{\tilde{\Gamma}}^{(2)}_\tau[\bar{\chi},\chi] + \hat{\tilde{R}}\right)^{-1}\right]\Bigg|_{\tilde{\mathrm{q}}=\bar{\chi}=\chi=0}, \tag{3.130}$$

and

$$x_{Z,\tau} = -\partial_\tau \ln Z_\tau = \frac{i}{2}\frac{(2\pi)^{d+2}}{\delta(\tilde{\mathrm{q}}=0)}\frac{\partial}{\partial\tilde{\omega}}\frac{\delta^2}{\delta\bar{\chi}(-\tilde{\mathrm{q}})\delta\psi(\tilde{\mathrm{q}})}\,\mathrm{Tr}\left[\hat{\tilde{R}}\cdot\left(\hat{\tilde{\Gamma}}_\tau^{(2)}[\bar{\chi},\chi]+\hat{\tilde{R}}\right)^{-1}\right]\Bigg|_{\tilde{\mathrm{q}}=\bar{\chi}=\chi=0}. \tag{3.131}$$

When the flow has reached a fixed point, the right hand sides attain constant values, say $-x_D$ and $-x_Z$. Therefore, in this case one observes the divergencies $D_\kappa \sim \kappa^{-x_D}, Z_\kappa \sim \kappa^{-x_Z}$, as already claimed above.

Eqs. (3.127,3.130,3.131) represent a complete description of the flow in the new, dimensionless framework. We remark that, although we considered the leading order approximation, these equations also hold to arbitrary order in the derivative expansion. Furthermore, we note that it is not strictly necessary to choose $\bar{\chi} = \chi = 0$ in Eqs. (3.130,3.131). For instance, for the contact process it was found more convenient to take the derivatives at the minimum of $\partial_{\bar{\chi}} u_\tau(\bar{\chi}=0,\chi)$ [125].

We can now easily deduce the flow equation for the dimensionless local potential u_τ. Inserting homogeneous fields $\bar{\chi}(\tilde{\mathbf{x}},\tilde{t}) \equiv \bar{\chi}$, $\chi(\tilde{\mathbf{x}},\tilde{t}) \equiv \chi$, the left hand side of Eq. (3.127) becomes $\partial_\tau\left[\widetilde{V}\widetilde{T}u_\tau(\bar{\chi},\chi)\right]$, where $\widetilde{V} = \kappa^d V$ and $\widetilde{T} = \kappa^2 D_\kappa Z_\kappa^{-1} T$ denote the dimensionless volumes of space and time, respectively. Just as the rescaled fields $\bar{\psi}$ and ψ these rescaled volumes are kept fixed along the renormalization group flow. Thus,

$$\partial_\tau u_\tau(\bar{\chi},\chi) = -\underbrace{(d+z_\tau)u_\tau(\bar{\chi},\chi)}_{\text{decrease of volume } \widetilde{V}\widetilde{T}} + \underbrace{(d+\eta_\tau)\chi u_\tau^{(0,1)}(\bar{\chi},\chi)}_{\text{increase of field } \chi} + \underbrace{\frac{1}{2\widetilde{V}\widetilde{T}}\mathrm{Tr}\left[\hat{\tilde{R}}\cdot\left(\hat{\tilde{\Gamma}}_\tau^{(2)}[\chi,\chi]+\hat{\tilde{R}}\right)^{-1}\right]}_{\text{integration of degrees of freedom}}, \tag{3.132}$$

where we have defined the τ-dependent dynamic exponent

$$z_\tau = 2 + \partial_\tau \ln D_\tau - \partial_\tau \ln Z_\tau = 2 + x_{Z,\tau} - x_{D,\tau}\,, \tag{3.133}$$

and the τ-dependent anomalous dimension

$$\eta_\tau = -\partial_\tau \ln Z_\tau = x_{Z,\tau}\,. \tag{3.134}$$

By the underbraces in Eq. (3.132) we indicate the origin of the three contributions. The first two are trivial, in the sense that they stem from the rescaling to our new variables. The Wetterich equation, which describes the gradual integration of degrees of freedom as the cutoff is decreased along the flow, only enters the third term.

Let us finally exploit that in the leading order approximation the new effective average action is of the form

$$\widetilde{\Gamma}_\tau[\bar{\chi},\chi] = \int \mathrm{d}^d\tilde{x}\,\mathrm{d}\tilde{t}\,\left[u_\tau(\bar{\chi},\chi) + \bar{\chi}(\tilde{\mathbf{x}},\tilde{t})\,(i\partial_{\tilde{t}} - \nabla_{\tilde{x}})\,\chi(\tilde{\mathbf{x}},\tilde{t})\right]. \tag{3.135}$$

By the same procedure as in the previous chapter one can work out the third term in Eq. (3.132) to arrive at an equation for the flow of the dimensionless effective average potential u_τ analogous to Eq. (3.107). Within the leading order approximation the flow equation reads

$$\partial u_\tau(\bar{\chi},\chi) = -(d+z_\tau)u_\tau(\bar{\chi},\chi) + (d+\eta_\tau)\chi\, u_\tau^{(0,1)}(\bar{\chi},\chi) -$$

$$- \frac{1}{2}\int_{\tilde{\mathrm{q}}} \frac{s(\tilde{q}^2)\left(u_\tau^{(1,1)}(\bar{\chi},\chi)+\tilde{q}^2 r(\tilde{q}^2)+q^2\right)}{\sqrt{\left(u_\tau^{(1,1)}(\bar{\chi},\chi)+\tilde{q}^2 r(\tilde{q}^2)+\tilde{q}^2\right)^2 - u_\tau^{(2,0)}(\bar{\chi},\chi)u_\tau^{(0,2)}(\bar{\chi},\chi)}}\,, \tag{3.136}$$

where

$$s(\tilde{q}^2) = -2\tilde{q}^4 r'\big(\tilde{q}^2\big) - x_{D,\tau}\tilde{q}^2 r\big(\tilde{q}^2\big)\ . \tag{3.137}$$

With the standard cutoff function (3.108), which now takes the form

$$r(\tilde{q}^2) = \left(\frac{1}{\tilde{q}^2}-1\right)\Theta\left(1-\tilde{q}^2\right)\ , \tag{3.138}$$

this reduces to

$$\begin{aligned}\partial_\tau u_\tau(\bar{\chi},\chi) &= -(d+z_\tau)u_\tau(\bar{\chi},\chi) + (d+\eta_\tau)\chi\, u_\tau^{(0,1)}(\bar{\chi},\chi) + \\ &+ \frac{d+2-x_{D,\tau}}{d+2}\frac{\widetilde{V}_d\left(u_\tau^{(1,1)}(\bar{\chi},\chi)+1\right)}{\sqrt{\left(u_\tau^{(1,1)}(\bar{\chi},\chi)+1\right)^2 - u_\tau^{(2,0)}(\bar{\chi},\chi)u_\tau^{(0,2)}(\bar{\chi},\chi)}}\,,\end{aligned} \tag{3.139}$$

where, as before, $\widetilde{V}_d$ denotes the volume of the d-dimensional sphere with radius $(2\pi)^{-1}$ (and not the rescaled volume $\widetilde{V} = \kappa^d V$).

Let us assume that we are at a critical point, such that, after an initial transient, the renormalization group flow reaches a fixed point. By standard renormalization group arguments one can then make a number of statements on the mathematical properties of the effective action $\Gamma[\bar{\psi},\psi]$ and in particular on the effective average potential $U_\kappa(\bar{\psi},\psi)$ [144, 145]. Alternatively, let us here deduce the scaling of the quantity $F(\psi) := \partial_{\bar{\psi}} U_\kappa(\bar{\psi}=0,\psi)$ (which will be of interest in the next chapter, since it determines the equation of motion of the particle density) directly from the flow equation (3.139). For large fields χ the term of the integration of the degrees of freedom becomes small and can be neglected. At the fixed point we therefore obtain $0 = -(d+z)u^\star(\bar{\chi},\chi) + (d+\eta)\chi\, u^{\star\,(0,1)}(\bar{\chi},\chi)$. Thus, $u^\star(\bar{\chi},\chi) = C\bar{\chi}\chi^{(d+z)/(d+\eta)}$, for some constant C and up to higher orders in $\bar{\chi}$ and $F(\psi)$ scales as $\psi^{z/(d+\eta)}$.

4 Renormalization of the Coagulation Process Below the Critical Dimension

Although the coagulation process does not display a phase transition, its long time approach to a vacant system with zero particle density can be described within the framework of critical phenomena. Indeed, the process is suitable for treatment with the perturbative renormalization group approach, as was demonstrated in the pioneering works of Peliti [76] and Lee [77]. Peliti established that the process displays an upper critical dimension and that its value is $d_c = 2$. This confirms predictions based on heuristic arguments and computer simulations [62, 64, 65, 79, 146–148]. Above the critical dimension, the mean-field decay $\rho \sim \mathcal{A}(Dt)^{-1}$ (for some dimension dependent amplitude $\mathcal{A}$ and diffusion constant D) is not destroyed by fluctuations. In contrast it is significantly retarded by fluctuations below the critical dimension, such that $\rho \sim \mathcal{A}(Dt)^{-d/2}$ when $d < 2$, and it is slowed down by a logarithmic term at the critical dimension $d_c = 2$, where $\rho \sim \ln(t)(4\pi Dt)^{-1}$.

Peliti's analysis was only concerned with the long time scaling. Employing the perturbative renormalization group, Lee showed that also the amplitude $\mathcal{A}$ can be calculated for $d = 2$ dimensions, and for $d < 2$ as an expansion in $\epsilon = 2 - d$ (the difference between the upper critical dimension $d_c = 2$ and the dimension d). It was found that,

$$\mathcal{A} = \begin{cases} \frac{\ln(t)}{4\pi} & \text{if } d = d_c = 2\,, \\ \frac{1}{2\pi\epsilon} + \frac{2\ln(8\pi)-5}{16\pi} + O(\epsilon) & \text{if } d < d_c\,. \end{cases} \tag{4.1}$$

The Landau $O(\epsilon)$ can in principle be obtained by going to higher and higher loops in the calculation, but the complexity of the problem does not seem to allow to go beyond one-loop order in the calculation of the density [77].

It is of course doubtful if the above result is of relevance for one dimension, where $\epsilon = 1$, since the expansion for the amplitude is only expected to be accurate when ϵ is small. Thus, in order to be able to verify Eq. (4.1) by simulation results, one needs to find a way to tune ϵ. This idea can be pursued by replacing the diffusional motion of the particles by Lévy flights. This allows one to shift the critical dimension d_c to a value close to $d = 1$ and to render $\epsilon = d_c - d$ small. An expansion of the amplitude $\mathcal{A}$ for this realization of the process can be obtained in complete analogy to Lee's calculations and is in good agreement with stochastic simulations [149].

In this chapter we will first study the mathematical properties of the effective average action Γ, exploiting special properties of the coagulation process. Similar to restrictions due to certain symmetries in, say, magnetic models, we will show that in the Taylor expansion of the effective average potential U_κ many terms are not created along the renormalization group flow. These properties can most conveniently be seen upon representing the flow by one-loop Feynman

diagrams. Having established these simplifications, we will prove that the coagulation process $A + A \to A$ is equivalent to the annihilation process $A + A \to \varnothing$, in the sense that their time dependent density and its moments are connected by a simple mapping. Therefore, all of the results that are derived for the coagulation process in this and the following chapters are also relevant for the annihilation process. We will further exploit the relative simplicity of the flow equations to study the coagulation process in one dimension. As opposed to the perturbative approach, the fact that $d_c - d = \epsilon = 1$ is not small does not pose a problem for NPRG, since the amplitude can be calculated directly for one dimension without the need of an expansion in a small parameter ϵ. As one might expect, the calculation cannot be carried out exactly. We will need to recur to an approximation scheme, as developed in the previous chapter, in order to reduce the complexity of the flow equation. We find that the coagulation process, due to its specific properties, permits us to go to a relatively high order of the approximation, therefore promising accurate results. Indeed, they compare well to the exact solution for one dimension. We also extend our analysis to general dimension $d \leq 2$ and thus reproduce results from perturbative calculations for small ϵ.

4.1 Mathematical Properties of the Effective Average Action

Symmetries which are obeyed by the effective average action Γ_κ usually play a central role in the discussion of the critical behavior of a system. Examples include the $O(N)$ symmetries in equilibrium statistical mechanics [111], and, in non-equilibrium reaction-diffusion systems, the KPZ-symmetries [130, 131], the time-reversal symmetries of "model A" [127, 140], or the so called "rapidity symmetry" of the contact process [125, 126] (the term "rapidity symmetry" was coined in the context of the related Reggeon field theory [150]), where the action is invariant under the transformation

$$\psi(\mathbf{x}, t) \to -\bar{\psi}(\mathbf{x}, -t)\,, \quad \bar{\psi}(\mathbf{x}, t) \to -\psi(\mathbf{x}, -t)\,. \tag{4.2}$$

Strikingly, at phase transitions there is a macroscopic breaking of these symmetries, as, for instance, the Z_2 symmetry of an Ising magnet is broken by spontaneous magnetization above the critical temperature. Nevertheless, it is important that symmetries be preserved along the renormalization group flow by adequate choice of the cutoff function R_κ and the truncation. For the rapidity symmetry this can be ensured by expressing the potentials in the derivative expansion (in particular the effective average potential $U_\kappa(\bar{\psi}, \psi)$) as functions of $\rho = \bar{\psi}\psi$ and $\chi = \psi - \bar{\psi}$, which (for stationary fields) are invariants under the above transformation. Thus, the flow cannot leave the manifold defined by the rapidity symmetry.

Similarly, one can make statements on the mathematical properties of the effective average action Γ_κ for the coagulation process. They do not come as an invariance with respect to a symmetry transformation of the fields $\bar{\psi}$ and ψ, as it is the case for the contact process. Rather, they become apparent upon expanding the effective average action Γ_κ, which is rendered analytic by the infrared cutoff as long as the scale $\kappa > 0$ [111]. In particular, for a general reaction-diffusion process, the effective average potential $U_\kappa(\bar{\psi}, \psi) = (TV)^{-1}\,\Gamma_\kappa[\bar{\psi}, \psi]$ (for homogeneous fields $\bar{\psi}(\mathbf{x}, t) \equiv \bar{\psi}$, $\psi(\mathbf{x}, t) = \psi$, with the volume V and T of space and time, respectively) and its rescaled counterpart $u_\tau(\bar{\chi}, \chi) = \kappa^{-d-2} D_\kappa^{-1} Z_\kappa U_\kappa(\bar{\psi}, \psi)$ (with $\bar{\chi} = \bar{\psi}$,

$\chi = \kappa^{-d}\psi$, and $\tau = \ln(\kappa/\Lambda)$), can be expressed as the power series

$$U_\kappa(\bar{\psi},\psi) = \sum_{m\geq 1,n\geq 1} \frac{1}{m!n!} g_\kappa^{(m,n)} \bar{\psi}^m \psi^n \,, \quad u_\tau(\bar{\chi},\chi) = \sum_{m\geq 1,n\geq 1} \frac{1}{m!n!} \tilde{g}_\tau^{(m,n)} \bar{\chi}^m \chi^n \,. \tag{4.3}$$

As proven by Canet et al. [140], and as shown below for the coagulation process, the terms are at least of order one in each field. According to Eqs. (3.112,3.118), there is the simple relation

$$g_\kappa^{(m,n)} = \kappa^{2+d(1-n)} Z_\kappa^{n-1} D_\kappa \tilde{g}_\tau^{(m,n)} \,, \tag{4.4}$$

between the coefficients $g_\kappa^{(m,n)}$ for the dimensionful potential U_κ and the coefficients $\tilde{g}_\tau^{(m,n)}$ for the dimensionless potential u_τ. Let us in the following consider the rescaled average effective potential $u_\tau(\bar{\chi},\chi)$, because it will also be employed for the concrete calculations later in this chapter.

To exploit the specific properties of the coagulation process, recall that, as discussed in Section 3.3, the fields $\bar{\psi}$ and ψ, and consequently their rescaled counterparts $\bar{\chi}$ and χ, are related to the creation and destruction operators $\hat{a}^\dagger$ and $\hat{a}$, respectively. For the coagulation process, the number of particles can only decrease. Hence, we expect that the expansion of $u_\tau(\bar{\chi},\chi)$ only includes monomials $\bar{\chi}^m\chi^n$ with $m \leq n$. Furthermore, there are no single particle reactions, such as the spontaneous decay $A \to \varnothing$ for the contact process, which would give rise to monomials with $n = 1$. In contrast, reactions of three or more particles may arise along the renormalization group flow by a combination of reactions (the sequence $3A \to 2A \to A$ effectively gives $3A \to A$). Hence, it seems reasonable to demand, in addition to $m \leq n$, that $n > 1$.

To put the above assertions on firm ground, one has to look at the flow equation for u_τ, c.f. Eq. (3.139). Here, we shall employ the local potential approximation, as introduced in Section 3.6, where the diffusion constant D_κ and the field amplitude Z_κ are not renormalized and the exponents z_τ, η_τ and $x_{D,\tau}$ in Eq. (3.139) are zero. (Below, it is shown that for our process this is in fact exact, because the renormalization group flow for D_κ and Z_κ vanishes.) Thus, the flow equation studied in this chapter is

$$\partial_\tau u_\tau(\bar{\chi},\chi) = -(d+2)u_\tau(\bar{\chi},\chi) + d\chi u_\tau^{(0,1)}(\bar{\chi},\chi) + \frac{\widetilde{V}_d \left(u_\tau^{(1,1)}(\bar{\chi},\chi)+1\right)}{\sqrt{\left(u_\tau^{(1,1)}(\bar{\chi},\chi)+1\right)^2 - u_\tau^{(2,0)}(\bar{\chi},\chi)u_\tau^{(0,2)}(\bar{\chi},\chi)}} \,, \tag{4.5}$$

with the microscopic action (3.60) (zero rate $\lambda' = 0$ for annihilation) as the initial condition, i.e.

$$u_{\tau=0}(\bar{\chi},\chi) = \tilde{\lambda}_{\tau=0}\bar{\chi}^2\chi^2 + \tilde{\lambda}_{\tau=0}\bar{\chi}\chi^2 \,, \tag{4.6}$$

where $\tilde{\lambda}_{\tau=0} = \Lambda^{d-2}\lambda$ is the rescaled coagulation rate. For the purposes of this section, we rewrite Eq. (4.5) for small $\bar{\chi}$ and χ (so that, in particular, $u_\tau^{(1,1)}(\bar{\chi},\chi)+1 > 0$) as

$$\partial_\tau u_\tau(\bar{\chi},\chi) = -(d+2)u_\tau(\bar{\chi},\chi) + d\chi u_\tau^{(0,1)}(\bar{\chi},\chi) + \frac{\widetilde{V}_d}{\sqrt{1 - \frac{u_\tau^{(2,0)}(\bar{\chi},\chi)u_\tau^{(0,2)}(\bar{\chi},\chi)}{1+u_\tau^{(1,1)}(\bar{\chi},\chi)}}} \,. \tag{4.7}$$

Let us ignore for a moment the trivial, "dimensional" first two terms of this equation and for the "dynamic" part, the third term, perform the expansion

$$\frac{\partial_\tau u_\tau(\bar\chi,\chi)|_{\mathrm{dyn}}}{\widetilde{V}_d}=1+\frac{1}{2}\frac{u_\tau^{(2,0)}(\bar\chi,\chi)u_\tau^{(0,2)}(\bar\chi,\chi)}{1+u_\tau^{(1,1)}(\bar\chi,\chi)}+\frac{3}{8}\left(\frac{u_\tau^{(2,0)}(\bar\chi,\chi)u_\tau^{(0,2)}(\bar\chi,\chi)}{1+u_\tau^{(1,1)}}\right)^2+\ldots=$$
$$=\sum_{j=0}^{\infty}\binom{-\frac{1}{2}}{j}(-1)^j\left(\frac{u_\tau^{(2,0)}(\bar\chi,\chi)u_\tau^{(0,2)}(\bar\chi,\chi)}{1+u_\tau^{(1,1)}(\bar\chi,\chi)}\right)^j. \tag{4.8}$$

The base itself of this binomial expansion can also be written as a power series,

$$\frac{u_\tau^{(2,0)}(\bar\chi,\chi)u_\tau^{(0,2)}(\bar\chi,\chi)}{1+u_\tau^{(1,1)}(\bar\chi,\chi)}=u_\tau^{(2,0)}(\bar\chi,\chi)u_\tau^{(0,2)}(\bar\chi,\chi)\sum_{j=0}^{\infty}(-1)^j\left(u_\tau^{(1,1)}(\bar\chi,\chi)\right)^j. \tag{4.9}$$

Since the assertions on the power series of $u_\tau(\bar\chi,\chi)$ also hold true for the initial condition, it is now easily verified that they must also hold along the renormalization group flow: Ignoring the physically irrelevant constant (i.e. independent of the fields $\bar\chi,\chi$) contribution to the flow, all the terms in the dynamic part of the flow equation are multiplied by $u_\tau^{(2,0)}(\bar\chi,\chi)u_\tau^{(0,2)}(\bar\chi,\chi)$. Therefore, in the flow equation neither the power in $\bar\chi$ nor the power in χ can be lower than the lowest powers present in $u_\tau(\bar\chi,\chi)$, which, initially, are 1 for $\bar\chi$ and 2 for χ. Furthermore, the terms in the dynamic part are made up only of the factors $u_\tau^{(2,0)}(\bar\chi,\chi)u_\tau^{(0,2)}(\bar\chi,\chi)$ and $u_\tau^{(1,1)}(\bar\chi,\chi)$, which evidently cannot lead to monomials $\bar\chi^m\chi^n$ with $m>n$ if they were not already present in $u_\tau(\bar\chi,\chi)$. These properties of the flow are obviously not destroyed by the dimensional part of Eq. (4.7). So indeed we have

$$u_\tau(\bar\chi,\chi)=\sum_{m,n}\frac{1}{m!n!}\tilde g_\tau^{(m,n)}\bar\chi^m\chi^n\,,\ \text{where } n\geq m\geq 1 \text{ and } n\geq 2\,. \tag{4.10}$$

4.2 The One-Loop Expansion and Restrictions on the Flow Equation

In addition to this restriction on the form of the potential, we can make statements on which terms enter the flow equation of each coefficient $\tilde g_\tau^{(m,n)}$. For instance, the flow for $\tilde g_\tau^{(1,3)}$, related to the reaction $3A\to A$, should involve itself and $\tilde g_\tau^{(1,2)}$ to the square, because the reaction may be effectively created by two consecutive reactions $3A\to 2A\to A$, but clearly there should be no terms corresponding to four or more initial particles, i.e. $\tilde g_\tau^{(1,n)}$ with $m\geq 4$. In principle, this can be proven by careful study of the flow equation (4.5) for u_τ. But although this equation will be most adequate for our concrete calculations in the following sections, here it is more elegant to go back to the full Wetterich equation for the effective average action Γ_κ and recast it in a form that is amenable to a diagrammatic analysis and thus reveals the mathematical structure more immediately,

$$\partial_\kappa\Gamma_\kappa[\bar\psi,\psi]=\tilde\partial_\kappa\underbrace{\frac{1}{2}\mathrm{Tr}\left[\ln\left(\hat\Gamma_\kappa^{(2)}[\bar\psi,\psi]+\hat R_\kappa\right)\right]}_{\mathcal{D}_\kappa}, \tag{4.11}$$

where $\tilde{\partial}_\kappa := \partial_\kappa R_\kappa \cdot \partial_{R_\kappa}$ acts only on the κ-dependence of the cutoff function R_κ.

The function $\mathcal{D}_\kappa$ on the right hand side in Eq. (4.11) is known from perturbative analysis as the creator of one-loop Feynman diagrams [111, 151–153]. Therefore, the renormalization group flow of the (m,n)-point vertex functions $\Gamma^{(m,n)}$, in Fourier space obtained by taking the functional derivative with respect to $\bar{\psi}(\mathbf{p}_i,\omega_i)$, $i \in \{1,\dots,m\}$ and $\psi(\mathbf{p}_j,\omega_j)$, $j \in \{m+1,\dots,m+n\}$ at zero fields $\bar{\psi}=\psi=0$,

$$\Gamma^{(m,n)}_{\kappa\,(\mathbf{p}_1,\omega_1;\dots;\mathbf{p}_{m+n},\omega_{m+n})} = \frac{\delta^{m+n}\Gamma_\kappa[\bar{\psi}=0,\psi=0]}{\delta\bar{\psi}(\mathbf{p}_1,\omega_1)\cdots\delta\bar{\psi}(\mathbf{q}_m,\omega_m)\delta\psi(\mathbf{p}_{m+1},\omega_{m+1})\cdots\delta\psi(\mathbf{q}_{m+n},\omega_{m+n})}\,, \tag{4.12}$$

can be represented by the one-loop Feynman diagrams for the (m,n)-vertex.

In this way, we also obtain the flow of the coefficients $\tilde{g}^{(m,n)}_\tau$, since, evidently, they are proportional to the momentum- and frequency-independent part of $\Gamma^{(m,n)}_{\kappa\,(\mathbf{p}_1,\omega_1;\dots;\mathbf{p}_{m+n},\omega_{m+n})}$. Indeed, functional differentiation at zero momenta and frequencies yields

$$g^{(m,n)}_\kappa = \frac{(2\pi)^{(d+1)(m+n)}}{TV}\Gamma^{(m,n)}_{\kappa\,(\mathbf{0},0;\dots;\mathbf{0},0)}\,, \tag{4.13}$$

and $g^{(m,n)}_\kappa$ is related to the rescaled coefficients $\tilde{g}^{(m,n)}_\tau$ by Eq. (4.4).

Now, the fact that the propagator, due to causality, can only connect earlier to later vertices, together with the fact that the number of legs can only decrease as time passes, drastically restricts the number of possible Feynman diagrams. We can at once deduce that the flow of $\Gamma^{(1,1)}_\kappa(\mathbf{p},\omega;\mathbf{p}',\omega')$ vanishes, since there is no diagram of the form

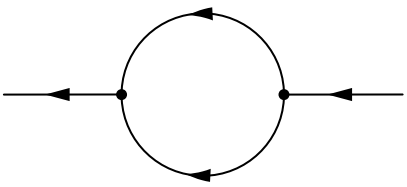

(The arrows indicate the direction of increasing time.) As a consequence, similar to the absence of propagator renormalization in perturbative renormalization [76], the diffusion constant D_κ and field amplitude Z_κ are constant

$$D_\kappa = Z_\kappa = 1\,. \tag{4.14}$$

Therefore, the local potential approximation and the leading order approximation are equivalent for the coagulation process.

Explicitly, at all scales κ, the propagator reads

$$\begin{aligned}\langle\mathbf{p}',\omega',m|\hat{G}_\kappa[\bar{\psi}=0,\psi=0]|\mathbf{p},\omega,n\rangle &= \langle\mathbf{p}',\omega',m|(\hat{\Gamma}^{(2)}_\kappa[0,0]+\hat{R}_\kappa)^{-1}|\mathbf{p},\omega,n\rangle = \\ &= \frac{1}{2}\delta(\mathbf{p}-\mathbf{p}')\delta(\omega-\omega')\begin{pmatrix} 0 & \frac{1}{p^2+R_\kappa+i\omega} \\ \frac{1}{p^2+R_\kappa-i\omega} & 0\end{pmatrix}_{m,n}\,.\end{aligned} \tag{4.15}$$

Transforming to momentum- and time-space,

$$\langle \mathbf{p}', t', m|\hat{G}_\kappa[0,0]|\mathbf{p}, t, n\rangle = \frac{\delta(\mathbf{p}-\mathbf{p}')}{4\pi} \begin{pmatrix} 0 & e^{-(p^2+R_\kappa)(t-t')}\Theta(t-t') \\ e^{-(p^2+R_\kappa)(t'-t)}\Theta(t'-t) & 0 \end{pmatrix}_{m,n} . \tag{4.16}$$

with Heaviside's step function $\Theta(t)$,

$$\Theta(t) = \begin{cases} 1 & \text{if } t > 0, \\ 0 & \text{if } t < 0, \end{cases} \tag{4.17}$$

which ensures the propagator only connects earlier $\bar{\psi}$ to later ψ, such that causality is obeyed.

There arises a subtlety, since the propagator is ill-defined at $t' - t = 0$. One might wonder if tadpole diagrams, i.e. loops that close on themselves, such as

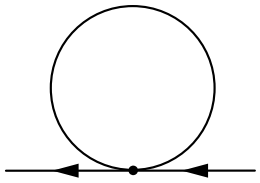

need to be taken into account and there is propagator renormalization after all. However, in the derivation of the field theory in Section 3.3, it is understood that in the products $\bar{\psi}(\mathbf{x}, t)^m \psi(\mathbf{x}, t)^n$, the response field $\bar{\psi}$ follows ψ by an infinitesimally small time interval. In the perturbative approach, therefore, it is important that these diagrams be excluded in order to guarantee causality [154]. In contrast, in the non-perturbative approach it is not possible to remove these diagrams "by hand". Sometimes, it is necessary to introduce a regularization scheme which deals with this problem [140]. In our case however, the contributions of these tadpole diagrams are harmless. Indeed, the loop in the above diagram gives

$$\delta(\mathbf{p}-\mathbf{p}')\delta(\omega-\omega')\frac{p^2+R_\kappa}{(p^2+R_\kappa)^2+\omega^2}\,, \tag{4.18}$$

in $(\mathbf{p}, \omega)$-space. Transforming to $(\mathbf{p}, t)$-space this becomes

$$\begin{cases} \frac{1}{2}\delta(\mathbf{p}-\mathbf{p}') & \text{if } t = t'\,, \\ 0 & \text{otherwise}\,. \end{cases} \tag{4.19}$$

Since this is non-zero only on a null set of the time axis, it is irrelevant. We remark that, as argued in [140], in general the contributions of such tadpole diagrams are not negligible since they can involve delta functions of time, or derivatives thereof (this is clearly not the case here).

Let us now consider the flow of general (m, n)-point vertex functions. Since in the initial action the number n of incoming legs is larger than the number m of outgoing legs for all non-zero vertex functions, it follows that no one-loop diagrams with $m > n$ can be constructed from these vertices and therefore the flow of the vertex functions with $m > n$ is zero. Similarly,

the minimum number of incoming legs in the Feynman diagrams, which is $n = 2$, and the minimum number of outgoing legs, which is $m = 1$, is inherited to all scales because no one-loop diagram can be created breaching these minimum numbers. Thus, we recover the result stated in Eq. (4.10). But by looking at the one-loop diagrams, we can learn even more about the flow of (m, n)-vertex functions, which goes beyond the findings of the previous section. The flow equation must not contain (m', n')-vertices with $m' - n' > m - n$, since too many "particles" would be annihilated. As an illustration, consider the vertex

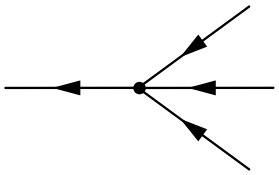

The three incoming lines are reduced to one line by a $(1, 3)$-point vertex function. With the available vertices, one cannot complete this diagram to a one-loop diagram in a way that it would connect to two or three outgoing vertices. Therefore, it cannot contribute to the flow equations of $\Gamma_\kappa^{(2,3)}$ and $\Gamma_\kappa^{(3,3)}$. As a corollary, it again follows that $\Gamma_\kappa^{(m,n)} = 0$ if $m > n$. Moreover, when $m \leq n$ (except for $m = n = 2$), the flow $\partial_\kappa \Gamma_\kappa^{(m,n)}$ is linear in $\Gamma_\kappa^{(m,n)}$: When $m < n$ the corresponding vertex has only m outgoing lines, which evidently cannot connect again to a vertex with n incoming lines. When $m = n > 2$ one loop would not suffice to include a second (m, n)-vertex in the diagram.

In general, one-loop diagrams for the flow of the vertex function $\Gamma_\kappa^{(m,n)}$ which contain one (m, n)-vertex can only involve exactly one additional vertex, which must be a $(2, 2)$-vertex, so that the result is the number of ways the $(2, 2)$-vertex can be attached times the value of the single diagrams. For the $(1, 3)$-vertex this would be

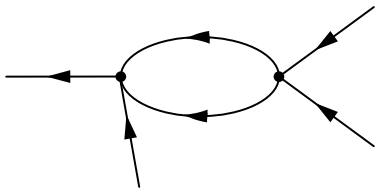

Therefore, the term linear in $\Gamma_\kappa^{(m,n)}$ cannot vanish, so that the stationary flow equation can always be resolved for a finite $\Gamma_\kappa^{(m,n)}$. Exceptionally, when $m = n = 2$ the differential equation is quadratic, because the flow is determined by the one-loop diagram

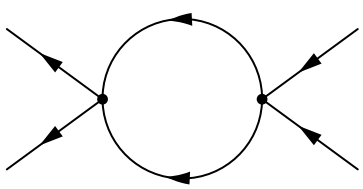

Note that the renormalization group flow of $\Gamma_\kappa^{(2,2)}$ is "self-contained", i.e. it only depends on itself.

Let us apply our findings to the dimensionless potential $u_\tau(\bar\chi,\chi)$. Expanding this analytic function

$$u_\tau(\bar\chi,\chi)=\sum_{m\geq 1,n\geq 2,m\leq n}\frac{1}{m!n!}\tilde g_\tau^{(m,n)}\bar\chi^m\chi^n\,, \tag{4.20}$$

we can calculate the coefficients $\tilde g^{\star(m,n)}$ of the fixed point potential $u^\star$ (giving zero flow when it is inserted in Eq. (4.5)) within the local potential approximation step by step as follows (also see Fig. 4.1): We start with $\tilde g^{\star(2,2)}$, which is easily obtained because $\partial_\tau\tilde g_\tau^{(2,2)}$ depends only on $\tilde g_\tau^{(2,2)}$. We then turn to $\tilde g^{\star(1,2)}$, whose flow $\partial_\tau\tilde g_\tau^{(1,2)}$ is a function of $\tilde g_\tau^{(2,2)}$ and $\tilde g_\tau^{(1,2)}$. Assuming that we know the fixed point values of $\tilde g^{\star(m,n)}$ for all $m<n$ we can go on to treat $\tilde g^{\star(m,n)}$ successively for $m=n,n-1,\ldots,1$. In each step one simply needs to solve the linear equation

$$0\stackrel{!}{=}c_1(m,n)+c_2(m,n)\cdot\tilde g^{\star(m,n)}\,, \tag{4.21}$$

given some $c_1(m,n)$ and $c_2(m,n)\neq 0$.

To conclude this section, let us look more closely at the flow of the lowest order vertex functions $\Gamma^{(1,2)}_{\kappa\,(\mathbf{p}_1,\omega_1;\mathbf{p}_2,\omega_2;\mathbf{p}_3,\omega_3)}$ and $\Gamma^{(2,2)}_{\kappa\,(\mathbf{p}_1,\omega_1;\mathbf{p}_2,\omega_2;\mathbf{p}_3,\omega_3;\mathbf{p}_4,\omega_4)}$. We will be most interested in homogeneous states, where the external momenta vanish, $\mathbf{p}_i=\mathbf{0},\omega_i=0$. For the (2,2)-vertex it turns out to be convenient to look at the slightly more general case $\Gamma^{(2,2)}_{\kappa\,(\mathbf{p}',\omega';-\mathbf{p}',-\omega';\mathbf{p},\omega;-\mathbf{p},-\omega)}$, whose flow is determined by the diagram

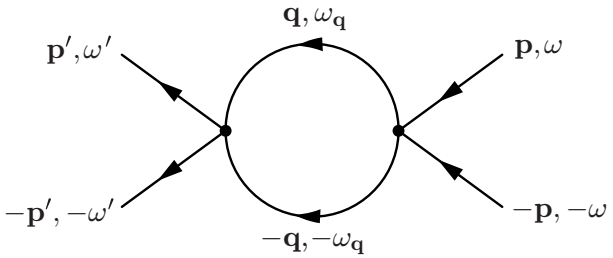

Interestingly, the renormalization group flow of $\Gamma^{(2,2)}_{\kappa\,(\mathbf{p}',\omega';-\mathbf{p}',-\omega';\mathbf{p},\omega;-\mathbf{p},-\omega)}$ is a function of itself. Now, the initial value $\Gamma^{(2,2)}_{\Lambda\,(\mathbf{p}',\omega';-\mathbf{p}',-\omega';\mathbf{p},\omega;-\mathbf{p},-\omega)}$ is independent of the external momenta and frequencies $\mathbf{p},\omega$, and $\mathbf{p}',\omega'$. Thus, this property is inherited to all scales κ and we have that

$$\Gamma^{(2,2)}_{\kappa\,(\mathbf{p}',\omega';-\mathbf{p}',-\omega';\mathbf{p},\omega;-\mathbf{p},-\omega)}\equiv\Gamma^{(2,2)}_{\kappa\,(\mathbf{0},0;\mathbf{0},0;\mathbf{0},0;\mathbf{0},0)}\propto U_\kappa^{(2,2)}(0,0)\,. \tag{4.22}$$

This fact puts us in a rather comfortable position: The renormalization group flow for $\Gamma^{(2,2)}_{\kappa\,(\mathbf{0},0;\mathbf{0},0;\mathbf{0},0;\mathbf{0},0)}$ is a function of itself and is not affected by our truncation (the local potential approximation). Therefore, it is possible to calculate its flow exactly, which will be carried out later in this chapter.

Of particular importance will be the vertex functions $\Gamma_\kappa^{(1,n)}$ because they determine the kinetic equation via the extremal principle, c.f. Eq. (3.93) (the first condition simply implies $\bar\psi=0$,

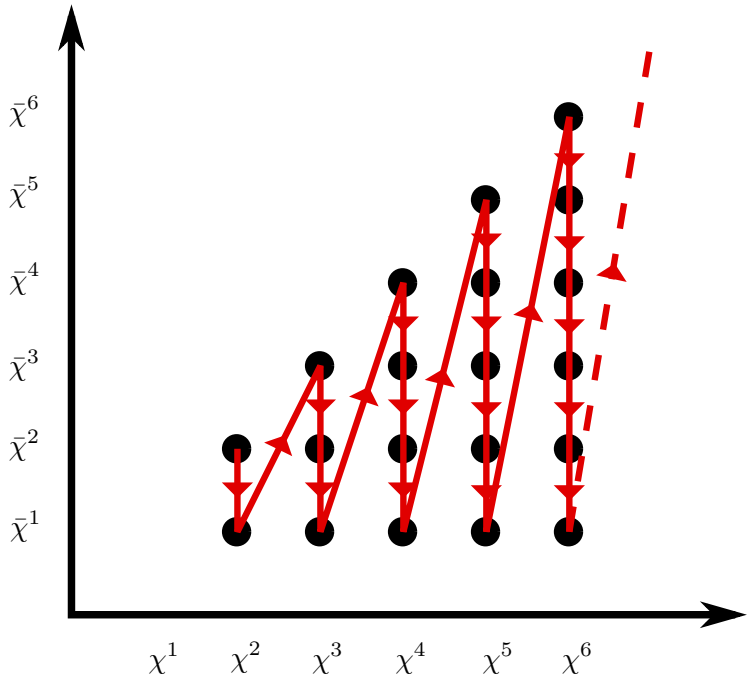

Figure 4.1: Illustration of the order for calculating the non-zero fixed point coefficients $\tilde{g}^{\star(m,n)}$ in the power series of the dimensionless fixed point potential $u^\star(\bar{\chi},\chi) = \sum_{m\geq 1,n\geq 2,m\leq n} \frac{1}{m!n!}\tilde{g}^{\star(m,n)}\bar{\chi}^m\chi^n$. In each step the flow equation for the coefficient that is calculated, is independent of the coefficients to follow. This can be shown by looking at all possible one-loop diagrams, which determine the flow of the vertex function $\Gamma_\kappa^{(m,n)}$. Alternative orders in which one calculates the coefficients are conceivable. For instance, one could first calculate the line $m = n$ up to a some maximal n, since the diagonal elements $\tilde{g}^\star(n,n)$ only depend on $\tilde{g}^{\star(n',n')}$ with $n' < n$. One could then go on to resolve the line $m + 1 = n$ and so on. Remarkably, in terms of computational effort the physically relevant line $\sim \bar{\chi}^1$ is the most expensive—all the other coefficients $\tilde{g}^\star(m',n')$ with $n' \leq n$ must be known.

such that vertex functions $\Gamma_\kappa^{(m,n)}$ with $m > 1$ are irrelevant for the kinetics). It turns out that, despite of the truncation, the first of these "physically relevant" vertex functions, $\Gamma_\kappa^{(1,2)}$, which describe the decay for small densities, is calculated exactly at zero momenta and frequencies, for the same reasons as for the (2,2)-vertex. The corresponding one-loop diagram is

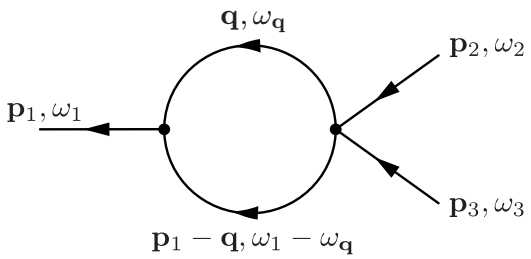

(which is non-zero only if $\mathbf{p}_1 = \mathbf{p}_2 + \mathbf{p}_3, \omega_1 = \omega_2 + \omega_3$). Since this is identical to the (2,2)-diagram with the left (2,2)-vertex replaced by a (1,2)-vertex, it follows for coagulation, that the relation

$$\Gamma^{(1,2)}_{\kappa\,(\mathbf{p}_1,\omega_1;\mathbf{p}_2,\omega_2;\mathbf{p}_3,\omega_3)} \equiv \frac{1}{2}(2\pi)^{d+1}\Gamma^{(2,2)}_{\kappa\,(\mathbf{p}_1-\mathbf{p}',\omega_1-\omega';\mathbf{p}',\omega';\mathbf{p}_2,\omega_2;\mathbf{p}_3,\omega_3)}\,, \tag{4.23}$$

which holds initially, at $\kappa = \Lambda$, is conserved along the renormalization group flow. In particular, for zero momenta and frequencies both vertex functions are obtained exactly.

4.3 Relation Between the Coagulation Process and the Annihilation Process

We are now able to verify that the coagulation process and the annihilation process are in the same universality class [76, 155, 156]. Consider the coagulation process, $A + A \to A$, with rate $\hat{\lambda}$ and annihilation $A + A \to \varnothing$ with equal rate $\hat{\lambda}$. The microscopic action is given by Eq. (3.53) with $\lambda = \hat{\lambda}$, $\lambda' = 0$ for coagulation, and $\lambda = 0$, $\lambda' = \hat{\lambda}$ for annihilation. Thus it follows that for the microscopic scale Λ we have the identity $\Gamma^{(1,2)}_{\Lambda,\mathrm{coag}} = \frac{1}{2}\Gamma^{(1,2)}_{\Lambda,\mathrm{annih}}$. As remarked in the previous section, c.f. Eq. (4.23), there is a simple relation between the (1,2)- and (2,2)-vertex functions for the coagulation process. In complete analogy, for the annihilation process one has instead that

$$\Gamma^{(1,2)}_{\kappa,\mathrm{annih}\,(\mathbf{p}_1,\omega_1;\mathbf{p}_2,\omega_2;\mathbf{p}_3,\omega_3;\mathbf{p}_4,\omega_4)} = (2\pi)^{d+1}\Gamma^{(2,2)}_{\kappa,\mathrm{annih}\,(\mathbf{p}_1,\omega_1;\mathbf{p}_2,\omega_2;\mathbf{p}_3,\omega_3;\mathbf{p}_4,\omega_4)}\,. \tag{4.24}$$

Therefore, when the microscopic rates for coagulation and annihilation are equal, we have that the identity $\Gamma^{(1,2)}_{\kappa,\mathrm{coag}} = \frac{1}{2}\Gamma^{(1,2)}_{\kappa,\mathrm{annih}}$ is conserved along the flow.

More generally we assert that

$$\Gamma^{(m,n)}_{\kappa,\mathrm{coag}} = 2^{m-n}\Gamma^{(m,n)}_{\kappa,\mathrm{annih}}\,, \tag{4.25}$$

exactly at all scales κ. This can be proven by induction: At the microscopic scale Λ the equation is certainly true. The flow of the (m,n)-point vertex functions, determined by the corresponding one-loop diagrams, is a sum of products of vertex-functions with $n_1, \ldots, n_j$ $(n_1 + \ldots + n_j = n)$ incoming and $m_1, \ldots, m_j$ $(m_1 + \ldots + m_j = m)$ outgoing legs, such that $(n_1 - m_1) + \ldots + (n_j - m_j) = n - m$. Therefore, assuming that Eq. (4.25) holds, the flow of the vertex functions for annihilation is accelerated by the factor $2^{(n-m)}$ as compared to the flow for coagulation. Thus, Eq. (4.25) holds for all vertex functions and at all scales κ.

It follows that, due to the extremal princple, c.f. Eq. (3.93), the kinetics for annihilation and coagulation are simply related. If $\Gamma[\bar{\psi} = 0, \psi = \rho]$ is a solution of the extremal principle for the coagulation process with particle input J, then $\Gamma[\bar{\psi} = 0, \psi = \rho/2]$ is a solution for the annihilation process with particle input $J/2$. Of course one can proceed in an analogous fashion for a mixed annihilation and coagulation process, the "α-process", $A + A \to \varnothing$ with rate $(\alpha - 1)\hat{\lambda}$ and $A + A \to A$ with rate $(2 - \alpha)\hat{\lambda}$ $(\alpha \in [1, 2])$, to find that the decay is accelerated by a factor α instead,

$$\rho_{\mathrm{coag}}(t) = \alpha\rho_\alpha(t)\,, \tag{4.26}$$

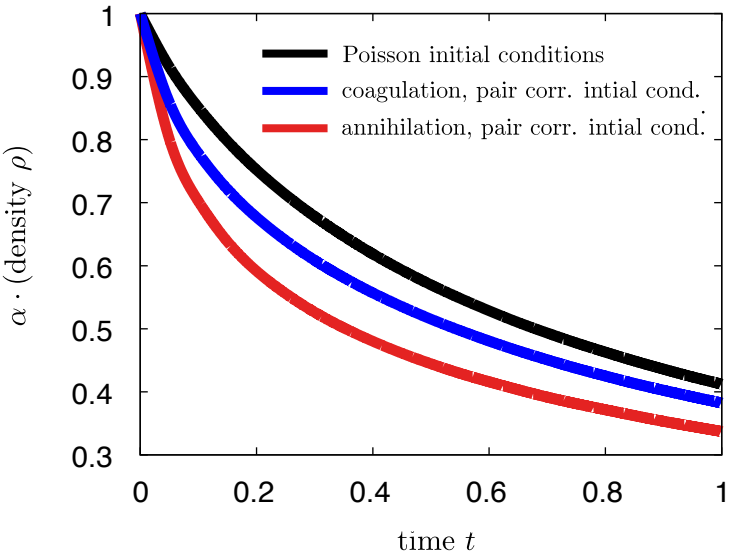

Figure 4.2: Comparison of the decay for a pure coagulation process, $A + A \to A$ with rate $\hat{\lambda}$, and a pure annihilation process, $A + A \to \varnothing$ with the same rate $\hat{\lambda}$. For Poissonian initial conditions the result agrees with Eq. (4.26) (black line, $\alpha = 1$ for coagulation, $\alpha = 2$ for annihilation). When the particles are distributed in pairs on the lattice (on each site the probability to find $2n$ particles is $\cosh(\rho)\frac{\rho^{2n}}{(2n)!}$, with no correlations between the sites), this symmetry between coagulation (blue line) and annihilation (red line) is broken. It has been shown that strongly correlated initial condition affect the long time behavior for the annihilation process in one dimension. The long time decay for the coagulation process, however, is universal [156].

if the equation holds initially. Thus, not only are the processes in the same universality class, but there is a simple, exact relation between their dynamics which is always true and not just in the long time and low density limit (also see [66, 156–158]).

However, we must add an important caveat to this neat result. There are initial conditions which cannot be created by particle input. This is the case for instance, when particles are initially distributed in pairs (two particles on the lattice site), with the probability $\cosh(\rho)\frac{\rho^{2n}}{(2n)!}$ to have n pairs, giving an initial density ρ. This state can be created by linear combination of the coherent states $|\rho\rangle$ and $|-\rho\rangle$. The former state, $|\rho\rangle$, would just imply a Poissonian distribution, which can be created by particle input $J(\mathbf{x}, t) = \rho\,\delta(t)$. Our above analysis applies to both of these coherent states $|\rho\rangle$, $|-\rho\rangle$ separately. For the sum, however, the computer simulations clearly show that there are strong deviations from Eq. (4.26), c.f. Figure 4.2. In fact, one can show that Eq. (4.26) only holds if initially the n-point correlation functions fulfill [156]

$$\langle \psi(\mathbf{x}_1) \cdot \ldots \cdot \psi(\mathbf{x}_n) \rangle_{\text{coag}} = \alpha^n \langle \psi(\mathbf{x}_1) \cdot \ldots \cdot \psi(\mathbf{x}_n) \rangle_{\alpha}\,. \tag{4.27}$$

(Notice that this is true, in particular, for Poissonian initial conditions, so long as $\rho_{\text{coag}} = 2\rho_{\text{annih}}$). These can be generated in our model by particle input of the form $J(t) = \rho_{\text{coag}}\delta(t)$ for the coagulation process and $J(t) = \rho_\alpha \delta(t)$ for the α-process, with $\rho_{\text{coag}} = \alpha\rho_\alpha$.

In general Eq. (4.26) need not even be true in the long time limit. The fact that the long

time behavior depends on the initial conditions, can perhaps be best understood for the one-dimensional annihilation model, after a mapping to a zero temperature, dynamic Ising model [159]. It was found that on condition that the initial magnetization m_0 vanishes, the long time behavior coincides with the long time behavior for Poissonian initial conditions. However, when m_0 is non-zero, corresponding to short range correlations in the annihilation model, one observes different behavior, which can be expressed as a lowering of the amplitude $\mathcal{A}$ for the long time decay $\mathcal{A}t^{-1/2}$ of the annihilation model. The annihilation model corresponds to the α-model with $\alpha = 2$. In contrast, as soon as there is a non-zero rate for coagulation, $1 \leq \alpha < 2$, the decay amplitude $\mathcal{A}$ is independent of the initial state [156].

4.4 The Fixed Point and the Upper Critical Dimension

Having established the equivalence of the annihilation and the coagulation process (apart from rather special initial conditions), from now on we will again focus on the latter. Let us have a closer look at the couplings for two-particle interaction, $\frac{1}{4}\tilde{g}_\tau(2,2) \equiv \frac{1}{2}\tilde{g}_\tau(1,2) =: \tilde{\lambda}_\tau$. From the flow equation for the rescaled potential, Eq. (4.5), we obtain

$$\partial_\tau \tilde{\lambda}_\tau = (d-2)\tilde{\lambda}_\tau + 2\widetilde{V}_d \tilde{\lambda}_\tau^2 \,. \tag{4.28}$$

At the upper critical dimension $d_c = 2$ there is a transcritical bifurcation, such that, when the dimension $d < 2$, there is an unstable fixed point at $\tilde{\lambda}^\star = 0$ (recall that τ flows in the negative direction) and a stable one at

$$\tilde{\lambda}^\star = \frac{2-d}{2\widetilde{V}_d} \,. \tag{4.29}$$

For $d > 2$ the stability of the fixed points is interchanged and at $d = 2$ they merge to one, marginally stable fixed point.

A similar behavior is obeyed by the other rescaled coefficients $g_\tau(m,n)$. As shown in Section 4.2, their flow is described by an equation of the form

$$\partial_\tau \tilde{g}_\tau^{(m,n)} = c_1(n,m) + c_2(m,n) \cdot \tilde{g}_\tau^{(m,n)} \,, \tag{4.30}$$

with non-zero $c_1(n,m)$ and $c_2(n,m)$, such that they tend to the finite value $\tilde{g}^{\star(m,n)} = -c_1(n,m)/c_2(n,m)$. As also discussed Section 4.2, we can calculate the fixed point coefficients subsequently in a way that $c_1(n,m), c_2(n,m)$ are functions of coefficients $\tilde{g}^{\star(m',n')}$ that are already known.

Thus, below the critical dimension, the flow drives the system automatically to a fixed point, in particular the rescaled potential flows to a fixed point potential $u_\tau \to u^\star$, which can be represented in the form

$$u^\star(\bar{\chi}, \chi) = \sum_{m\geq 1, n\geq 2, m\leq n} \frac{1}{m!n!} \tilde{g}^{\star(m,n)} \bar{\chi}^m \chi^n \,. \tag{4.31}$$

It will be our task in of the following sections to calculate the fixed point potential in order to extract the critical behavior of the system which arises in the long time and large distance

limit. In contrast, above the critical dimension u_τ goes to zero. In this case, we will have to consider the dimensionful potential U_κ instead (see next chapter). The critical dimension $d_c = 2$, where both potentials, u_τ and U_κ tend to zero along the flow, needs to be treated separately.

Finally, we remark that by generalizing the cutoff function (3.138) to

$$r(q^2) \to c^2 r(c^2 q^2) = (q^{-2} - c^2)\Theta(q^{-2} - c^2)\,, \tag{4.32}$$

the flow equation, Eq. (4.28), is replaced by

$$\partial_\tau \tilde{\lambda}_\tau = (d-2)\tilde{\lambda}_\tau + 2c^{d-2}\widetilde{V}_d \tilde{\lambda}_\tau^2\,, \tag{4.33}$$

indicating that the flow is independent of the cutoff if and only if the dimension is two. This is also confirmed by the analytic result for perturbative RG calculation [77],

$$\partial_\tau \tilde{\lambda}_\tau = (d-2)\tilde{\lambda}_\tau + 4(2\pi)^{-d/2}\Gamma(2-d/2)\tilde{\lambda}_\tau^2\,, \tag{4.34}$$

with the Gamma function Γ (not to be confused with the effective action). This coincides with our result at the critical dimension $d_c = 2$. Indeed, we will see below that in two dimensions the flow of $\tilde{\lambda}_\tau$ completely determines the long time kinetics. Due to its direct physical significance it must not depend on the particular cutoff. This is in contrast to dimensions $d < 2$, where the long time kinetics will turn out to be determined by an infinite sum of terms: Whereas this sum must converge to a function which does not depend on the cutoff, the flow of each coefficient need not be independent, since it is not of direct physical significance.

4.5 Study in One Dimension

From the previous sections we can already draw the conclusion that, by standard renormalization arguments [4, 86, 144], the density will behave as

$$\rho \sim \mathcal{A} t^{-\frac{1}{2}}\,, \tag{4.35}$$

in the long time limit, when the dimension d is one, for some amplitude $\mathcal{A}$: The density ρ corresponds to the field ψ, such that under renormalization it scales as $\rho = \kappa\tilde{\rho}$, with the "dimensionless" density $\tilde{\rho}$, see Eq. (3.112), whereas time scales as $t = \kappa^{-2}\tilde{t}$, see Eq. (3.111).

To obtain a broader picture, let us also consider particle input J, which gives rise to an additional term $\int \mathrm{d}x\,\mathrm{d}t\, J(\mathbf{x},t)\bar{\psi}(\mathbf{x},t)$ in the action and is not renormalized (since there exist no relevant one-loop diagrams, cf. Section 4.2). In one dimension it therefore scales as $J = \kappa^3 j$, with the dimensionless particle input j. We expect that in the long time limit the density becomes independent of the initial condition (as discussed in Section 4.3). Moreover, we have just seen that the effective average action tends to a fixed point, in our approximation described by the fixed point potential $u^\star$. Thus, the density will not depend on the initial action, in particular it will be independent of the coupling λ. Therefore, it is a function only of the particle input (chosen to be homogeneous in space and time), the initial action and time,

$$\rho(\lambda, t, J) = \kappa\tilde{\rho}(u_\tau, \tilde{t}(t), j(J)) \xrightarrow{\kappa \text{ small}} \kappa\tilde{\rho}(u^\star, \kappa^2 t, \kappa^{-3} J)\,. \tag{4.36}$$

Since the result must be independent of the scale κ, the density is expected to behave as $\rho \sim J^{\frac{1}{3}}$ for finite J and as $\rho \sim t^{-\frac{1}{2}}$ when there is no particle input.

We also remark that the long time behavior of the density may be obtained after noting that, since time scales as $t \sim \kappa^{-2}$, the scaling of the coupling $\lambda_\kappa = \kappa\tilde{\lambda}_\tau \to \kappa\tilde{\lambda}^\star$ may be interpreted as a time dependent coupling $\lambda_\kappa \sim t^{-\frac{1}{2}}$. Thus, inserting this into the mean-field result $\rho \sim \lambda^{-1}t^{-1}$, we again obtain $\rho \sim \lambda_\kappa^{-1}t \sim t^{-\frac{1}{2}}$. In fact, this corresponds to the first approximation in the perturbative approach, where the density is calculated by only summing over tree diagrams (diagrams which contain no loops) [77, 137].

In the following, we turn to the question of how to estimate the amplitude $\mathcal{A}$. The expectation value ρ of the particle density is determined by the extremal principle, Eq. (3.93). Within our approximation, cf. Eq. (3.99), and seeking for a solution that is homogeneous in space, instead of the mean-field equation $\partial_t\rho = -\lambda\rho^2$, the extremal principle yields the kinetic equation

$$\partial_t\rho = -F(\rho)\,, \tag{4.37}$$

with the *non-equilbrium force* $F = F_{\kappa\to 0}$, where the renormalized non-equilibrium force F_κ is defined by

$$F_\kappa(\rho) := \left.\frac{\partial U_\kappa(\bar{\psi},\rho)}{\partial\bar{\psi}}\right|_{\bar{\psi}=0}\,. \tag{4.38}$$

We also define its dimensionless counterpart

$$f_\tau(\chi) := \left.\frac{\partial u_\tau(\bar{\chi},\chi)}{\partial\bar{\chi}}\right|_{\bar{\chi}=0}\,. \tag{4.39}$$

Just as the rescaled potential u_τ flows to $u^\star$, the renormalization group flow drives f_τ to its fixed point value $f^\star$, which according to Eq. (4.31) may be written as

$$f^\star(\chi) = \sum_{n\geq 2}\frac{1}{n!}\tilde{g}^{\star(1,n)}\chi^n\,. \tag{4.40}$$

The kinetic equation becomes

$$\partial_t\rho = -\lim_{\kappa\to 0}\kappa^3 f_\tau(\kappa^{-1}\psi) = -\lim_{\kappa\to 0}\kappa^3 f^\star(\kappa^{-1}\psi)\,. \tag{4.41}$$

The limit must not depend on κ, since, once the reciprocal scale $1/\kappa$ is much larger than the correlation length, the right hand side of the equation should have converged well. Hence, the fixed point will be of the form

$$f^\star(\chi) \sim c\chi^3\,, \tag{4.42}$$

when χ is large, for some universal factor c. This implies that the non-equilibrium force $F(\rho) = c\rho^3$ and we have for the kinetic equation

$$\partial_t\rho = -c\rho^3\,, \tag{4.43}$$

such that we indeed recover the decay law, Eq. (4.35), with $\mathcal{A} = (2c)^{-1/2}$. We remark that, whereas $f^\star$ is analytic, the non-equilibrium force $F(\rho)$ has a singular point $\rho = 0$. Phase transitions can be defined by non-analyticities in the free energy. Thus, our system displays a phase transition at vanishing particle density.

In order to derive the factor c, which determines the amplitude in Eq. (4.35) and therefore the long time kinetics, one needs to determine $f^\star(\chi)$ for large values of χ. This in turn affords a good knowledge of the rescaled effective average potential $u_\tau(\bar{\chi}, \chi)$, whose flow is given by Eq. (4.5) with the microscopic action for coagulation as the initial condition, c.f. Eq. (4.6). Typically, the goal of the numerical calculations is to extract critical exponents, by considering the flow in the region around the fixed point. In this case, to obtain a satisfactory result, it is often sufficient to perform a series expansion of the Wetterich equation to the first few orders in $\bar{\chi}$ and χ and then to consider the flow of the coefficients $\tilde{g}_\tau^{(m,n)}$. For our problem this clearly will not suffice, since the lower order coefficients only describe the behavior of the force $f^\star$ around the origin but not for large χ. Therefore, the question arises, if an expansion of the fields around the origin is a reasonable approach to our problem, or if one should resort to an approach where the functional dependence in χ is retained and go to large values of this field. For instance, similar to the approach in [125], one could consider

$$u_\tau(\bar{\chi}, \chi) = \bar{\chi} u_\tau^1(\chi) + \frac{\bar{\chi}^2}{2} u_\tau^2(\chi) + \frac{\bar{\chi}^3}{6} u_\tau^3(\chi) + \dots \tag{4.44}$$

derive the flow equations for $u_\tau^1, u_\tau^2, u_\tau^3, \dots$ to some order, and then solve it "directly" by finite difference methods, as demonstrated in [127, 160]. In principle, the amplitude $\mathcal{A} = (2c)^{-1}$ can then be determined by computing the non-equilibrium force $f^\star(\chi) = u^{1,\star}(\chi)$ at the fixed point up to large values of χ and exploiting Eq. (4.50).

However, the special simplifications of our process, as discussed in Section 4.2, are only obvious in the expansion in the fields. For this reason, instead of calculating $f^\star(\chi) = u^{1,\star}(\chi)$ by solving the flow equation for u_τ^1 numerically, we have exploited these properties to calculate a large number of fixed point coefficients $g^{\star(m,n)}$ exactly (yet of course within our truncation, Eq. (3.99), and we could thus determine the expansion $f^\star(\chi) = \sum_{n\geq 2} g^{\star(1,n)} \chi^n$ for the first 125 coefficients with the aid of a symbolic computation program. The power series has a finite radius of convergence. To be able to determine the amplitude $\mathcal{A} = (2c)^{-1}$, we enhanced the result by employing Padé extrapolation [152, 161], cf. Fig. 4.3. This method consists in calculating a rational function, with polynomials in the nominator and denominator, whose coefficients are determined by the derivatives around the origin.

For the first 125 coefficients $\tilde{g}^{\star(1,n)}$ one must obtain very many, i.e. $\sim 125^2/2$, coefficients $\tilde{g}^{\star(m,n)}$. Hence, for the concrete calculation we had to put some thought into decreasing the complexity of our algorithm to speed up the program. As illustrated in Figure 4.1, one can derive the flow equation for $\tilde{g}_\tau^{(m,n)}$ step by step. In each step the stationary value $\tilde{g}^{\star(m,n)} = \lim_{\tau\to-\infty} \tilde{g}_\tau^{(m,n)}$ is obtained by resolving the ensuing linear equation (4.21). We obtained these equations not from the one-loop diagrams, as we did for the theoretical considerations in Section 4.2 but "directly" from the flow equation (4.5), for the dimensionless potential $u_\tau(\bar{\chi}, \chi) = \sum \frac{1}{m!n!} \tilde{g}_\tau^{(m,n)} \bar{\chi}^m \chi^n$. In principle, differentiating Eq. (4.5) m times with respect to $\bar{\chi}$ and n times with respect to χ and setting $\bar{\chi} = \chi = 0$, yields the flow equation for $\tilde{g}_\tau^{(m,n)}$. Yet, in practice, this approach turned out infeasible since the expressions become too lengthy with increasing m and n. However, by exploiting the analyticity of the Wetterich equation, the problem of extracting the flow equations can be reduced to polynomial multiplication.

Let us rewrite the flow equation (4.5) for the rescaled potential employing the Taylor expansion

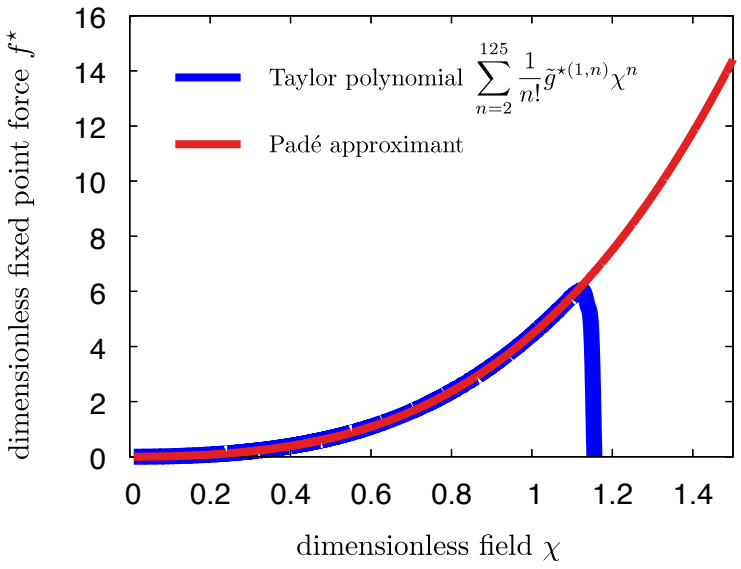

Figure 4.3: Dimensionless non-equilibrium force $f^\star(\chi) = \partial_{\bar{\chi}} u_{\tau\to-\infty}(\bar{\chi}=0,\chi) = \sum_{n=2}^{\infty} \frac{1}{n!}\tilde{g}^{\star(1,n)}\chi^n$ at the fixed point. Considering the series expansion of the flow, Eq. (4.5), for the rescaled effective average potential u_τ, we have calculated the expansion of $f^\star$ exactly up to order 125 and plotted the sum $\sum_{n=2}^{125} \frac{1}{n!}\tilde{g}^{\star(1,n)}\chi^n$ (thick blue line). Evidently, $f^\star(\chi)$ only has a finite radius of convergence of approximately 1.1 around the origin. To extrapolate beyond the region of convergence, we employed a Padé approximant (thin red line), which relies on so called rational functions, i.e. fractions of polynomials [152, 161].

$1/\sqrt{1+x} = \sum_j \binom{-1/2}{j} x^j$. A the fixed point

$$\begin{aligned} 0 &= -(d+2)u^\star(\bar{\chi},\chi) + d\chi u^{\star\,(0,1)}(\bar{\chi},\chi) + \frac{\widetilde{V}_d\left(u^{\star\,(1,1)}(\bar{\chi},\chi)+1\right)}{\sqrt{\left(u^{\star\,(1,1)}(\bar{\chi},\chi)+1\right)^2 - u^{\star\,(2,0)}(\bar{\chi},\chi)u^{\star\,(0,2)}(\bar{\chi},\chi)}} \\ &= -(d+2)u^\star(\bar{\chi},\chi) + d\chi u^{\star\,(0,1)}(\bar{\chi},\chi) + P(\bar{\chi},\chi)\cdot\sum_{j=0}^{\infty}\binom{-1/2}{j}Q(\bar{\chi},\chi)^j\,, \end{aligned} \tag{4.45}$$

with

$$P(\bar{\chi},\chi) = 1 + u^{\star\,(1,1)}(\bar{\chi},\chi)\,, \tag{4.46}$$

and

$$Q(\bar{\chi},\chi) = 2u^{\star\,(1,1)}(\bar{\chi},\chi) + \left(u^{\star\,(1,1)}(\bar{\chi},\chi)\right)^2 - u^{\star\,(2,0)}(\bar{\chi},\chi)u^{\star\,(0,2)}(\bar{\chi},\chi)\,. \tag{4.47}$$

Eq. (4.45) holds for a general reaction-diffusion process with one type of particles. It tells us that the expansion in the fields can be carried out, in practice, by polynomial multiplication. In general, the Fast Fourier Transform would provide an efficient algorithm to carry out these multiplications [161].

For our specific case, we have devised the following algorithm: The coefficients of $u^\star(\bar{\chi},\chi) = \sum_{m,n} \frac{1}{m!n!}\tilde{g}^{\star\,(m,n)}\bar{\chi}^m\chi^n$ are calculated successively, as illustrated in Fig. 4.1. In every step of the calculation we not only compute one new coefficient $\tilde{g}^{\star\,(m,n)}$, but we also obtain the

coefficient $q^{j,(m,n)}$ in the expansion of the powers of Q, $Q(\bar\chi,\chi)^j = \sum_{m,n} q^{j\,(m,n)} \bar\chi^m \chi^n$, and the coefficient $s^{(m,n)}$ in the expansion $S(\bar\chi,\chi) := \sum_{j=0}^{\infty} \binom{-1/2}{j} Q(\bar\chi,\chi)^j = \sum_{m,n} s^{(m,n)} \bar\chi^m \chi^n$. All other coefficients which are not yet known, need not be summed over and can provisionally be set to zero. Since the lowest order terms of $Q(\bar\chi,\chi)$ are χ and $\bar\chi\chi$, we only need to look at powers $Q(\bar\chi,\chi)^j$ up to order $j = n$ for calculation of $\tilde g^{\star\,(m,n)}$. Notice, that in contrast to the potential $u^\star(\bar\chi,\chi)$, the functions $Q(\bar\chi,\chi)^j$ and $S(\bar\chi,\chi)$ include monomials χ^n, which lack the response field $\bar\chi$. Although in the flow equation for $\tilde g_\tau^{(0,n)}$ they cancel, such that $\tilde g_\tau^{(0,n)} \equiv \tilde g^{\star(0,n)} = 0$, the coefficients $q^{j\,(0,n)}, s^{(0,n)}$ enter the equations for higher order coefficients $\tilde g^{\star\,(m,n')}$ $(n' > n)$. Therefore, after completing a vertical row in Fig. 4.1 for the coefficients $\tilde g^{\star\,(n,n)}, \tilde g^{\star\,(n-1,n)}, \ldots, \tilde g^{\star\,(1,n)}$ one must compute $p^{j\,(0,n)}$ for $1 \le j \le n$ and $s^{(0,n)}$ before one turns to the next vertical row of coefficients $\tilde g^{\star\,(n+1,n+1)}, \tilde g^{\star\,(n,n+1)}, \ldots, \tilde g^{\star\,(1,n+1)}$.

It was our experience that if we solve the ensuing linear equations (4.30) for $\tilde g^{\star\,(m,n)}$ numerically, the results become unstable quickly. This was the case although we used a stable method for each linear equation [162]. For this reason, the equations were solved exactly with a symbolic computation program. The behavior of $f(\chi)$ for large χ was evaluated in a double logarithmic plot, cf. Fig. 4.4. For large values of χ, the terms in the expansion indeed add up a to power law $\sim \chi^3$. We find that approximately

$$f(\chi) \sim 4.2\,\chi^3 \quad \Rightarrow \quad \rho(t) \sim 0.35\,t^{-1/2}\,. \tag{4.48}$$

As compared to the perturbative two-loop result $\mathcal{A} = \frac{1}{2\pi\epsilon} + \frac{2\ln(8\pi)-5}{8\pi} \approx 0.217$ [77] (with difference $\epsilon = d_c - d = 2 - 1$), this is much closer to the exact decay amplitude $\frac{1}{\sqrt{2\pi}} \approx 0.399$ [163].

Finally, we demonstrate that with our approach one can also derive the behavior of the coagulation process with particle input $\varnothing \xrightarrow{J} A$ directly from Eq. (4.50). The extremal principle, Eq. (3.93), yields $0 = \partial_t \rho = -c\rho^2 + J$. Thus, the density of the stationary state scales as

$$\rho \sim (cJ)^{\frac{1}{3}}\,, \tag{4.49}$$

in agreement with the corresponding result in [164].

4.6 Study for $d < d_c$

Formally one can extend the above approach to all "dimensions" d below the critical dimension $d_c = 2$ and calculate the corresponding amplitude $\mathcal{A}$ in the long time scaling of the density $\rho \sim \mathcal{A} \cdot t^{-d/2}$ (see Figure 4.5). In complete analogy to the previous section, we find that for large values of the field χ, the fixed point result of the non-equilibrium force must scale as

$$f^\star(\chi) \sim c_d \chi^{(d+2)/d}\,, \tag{4.50}$$

with the dimension-dependent but otherwise universal factor c_d. Hence for the kinetic equation we have

$$\partial_t \rho = -F(\rho) = -c_d \rho^{(d+2)/d}\,, \tag{4.51}$$

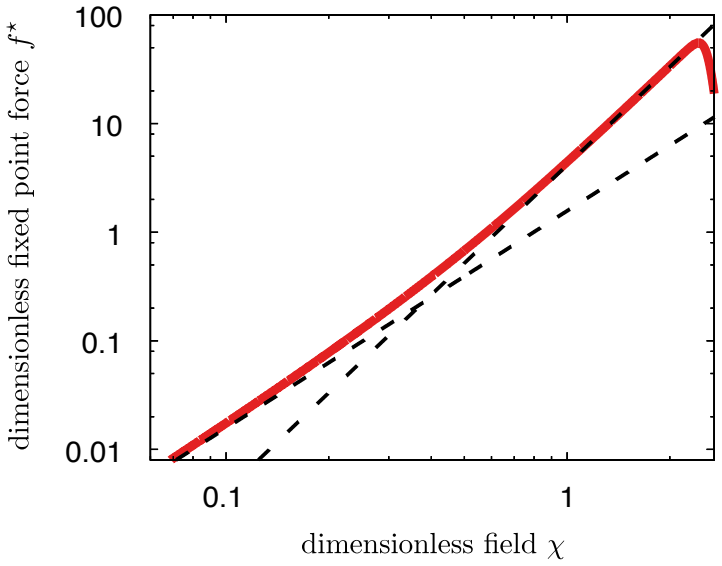

Figure 4.4: Double logarithmic plot of the rescaled non-equilibrium force $f^\star$ (solid red line) at the fixed point, within the local potential approximation, obtained by calculating its expansion up to order 125 in χ. For small χ, $f^\star(\chi) = \partial_{\bar{\chi}} u^\star(\bar{\chi} = 0, \chi) = \pi/2 \cdot \chi^2 + \pi^2/6 \cdot \chi^3 + \ldots$ obviously must follow the power law $\pi/2 \cdot \chi^2$ (flat dashed line). When χ is increased, one reaches a regime where f is described well by $4.2\,\chi^3$ (steep dashed line), before the Padé Approximation breaks down. As predicted by our theory, in addition to the third order term $\pi^2/6 \cdot \chi^3 \approx 1.64\,\chi^3$, the rest of the expansion of f generates another term proportional to $2.56\chi^3$.

or $\rho(t) \sim \left(\frac{2c_d t}{d}\right)^{-d/2}$ and for the stationary state with homogeneous particle input $\varnothing \xrightarrow{J} A$, we have

$$\rho \sim (c_d J)^{\frac{d}{d+2}} \ , \tag{4.52}$$

below the critical dimension, establishing a relation that was also derived in [164] by different means. The form of our results suggest that for the critical dimension one has logarithmic corrections and above the critical dimension, for $d > 2$, the density $\rho \sim J^{\frac{1}{2}}$, which will be confirmed in the next chapter.

We remark, that although d is a natural parameter of the renormalization flow (see Eq. (4.5)), our calculations need not have implications on lattices with an associated rational dimension d. For instance, in [79] d-independent behavior, $\rho \sim t^{-2/3}$, was found for certain kinds of fractals, in seeming contradiction to our theory. The problem is that there are various definitions of the dimension for fractals [165]. In [60] it is argued that the right choice for the process at hand is the so-called spectral dimension d_s, defined by the recurrence of a random walker; the probability of a (free) random walker to return to its initial position scales as $t^{-d_s/2}$. (This suggest that the fractals studied in [79] had a spectral dimension $d_s = 4/3$, so that $\rho \sim \tilde{c} t^{-2/3}$ if $d_s = 4/3$, with a proportionality factor $\tilde{c}$ that is not fully determined by d_s but depends on the specific fractal.)

As for the one-dimensional case, the factor c_d can be determined by calculating a sufficient number of coefficients in the expansion of the rescaled non-equilibrium force $f(\bar{\chi}, \chi)$,

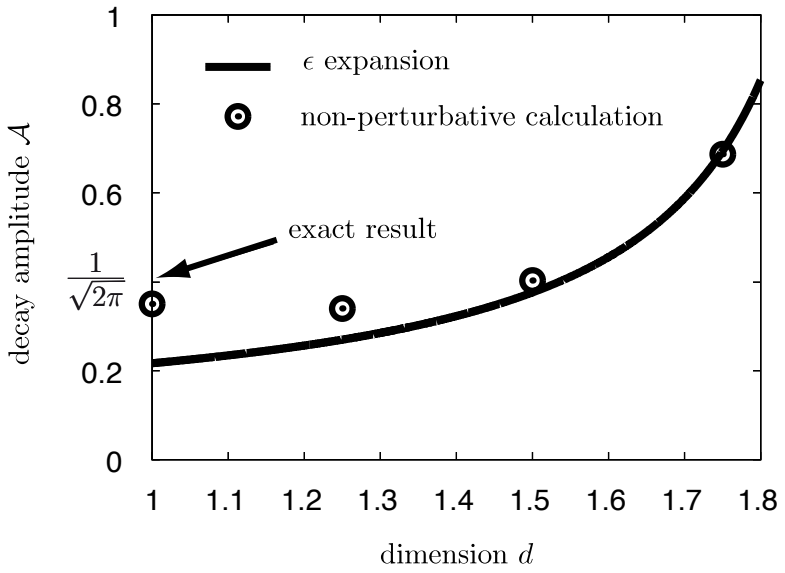

Figure 4.5: Results for the amplitude $\mathcal{A}$ of the long time decay $\rho \sim \mathcal{A}\rho^{-d/2}$, obtained by various means. The circles are our estimates from the non-perturbative renormalization group calculations within local potential approximation. They are compared to the exact result $\mathcal{A} = 1/\sqrt{2\pi}$ in one dimension [163] and to the perturbative two-loop result $\frac{1}{2\pi\epsilon} + \frac{2\ln(8\pi)-5}{8\pi}$ [77] (solid line). The latter is an expansion in the deviation ϵ from the upper critical dimension, $\epsilon = d_c - d$. It is doubtful whether $\epsilon = 1$ (corresponding to one dimension) can be considered small. Indeed, despite the relatively crude truncation, our non-perturbative approach provides a substantially better result.

cf. Fig. 4.5. One observes that the Padé approximation works the better, i.e. converges for larger values of χ, the closer one approaches the critical dimension. Indeed, from perturbation theory one expects that near the critical dimension only $\tilde{g}^{\star(2,2)}$ and $\tilde{g}^{\star(1,2)}$ are important, so that the approximation should converge quickly. Performing the limit $d_c - d = \epsilon \to 0$, we can make contact with a result from perturbation theory [77]. To this end, we assume that to lowest order

$$f^\star(\chi) \sim c\chi^{(4-\epsilon)/(2-\epsilon)} \sim \left(\tilde{g}^{\star\,(1,2)} + O(\epsilon^2)\right) \chi^{(4-\epsilon)/(2-\epsilon)}\,, \tag{4.53}$$

i.e. the constant c is, to good approximation, equal to the coupling $\tilde{g}^{\star\,(1,2)}$. This is plausible since the exponent $(4-\epsilon)/(2-\epsilon) \approx 2$, although of course not necessary. The assumption is justified, however, by that fact that it allows us to derive from Eq. (4.29) the relation $\widetilde{\mathcal{A}} = 2\pi\epsilon + O(\epsilon^2)$ and thus, to lowest order, we recover the result from perturbation theory $\mathcal{A} = \frac{1}{2\pi\epsilon}$.

4.7 Study for the Critical Dimension

At the critical dimension $d_c = 2$ the couplings $\tilde{g}_\tau^{(1,2)}, \tilde{g}_\tau^{(2,2)}$ behave as $1/\tau$ when $\tau \to -\infty$. Since the Feynman diagrams which determine the flow of $\tilde{g}_\tau^{(m,n)}$ involve n of these "elementary" couplings, the other coefficients go to zero as $1/\tau^n$. Therefore, the dimensionless potential

vanishes along the renormalization group flow, $u_\tau \to 0$, we cannot take the limit of Eq. (4.41) and a straightforward application of the analysis of the previous sections to determine the long time behavior of the density is not possible. Instead, we start, at finite renormalization time τ, with the dimensionless equation

$$\partial_{\tilde{t}}\chi = -\left(\chi + f_\tau(\chi)\right) \quad (\tilde{t} = \kappa^2 t)\,, \tag{4.54}$$

where the constant term $\sim \chi$ stems from the dimensionless cutoff function (3.138) at vanishing rescaled momentum $\tilde{q} = 0$ ($\lim_{\tilde{q}\to 0} \tilde{q}^2 r(\tilde{q}^2) \to 1$). In this equation the long range fluctuations have not yet been integrated out completely. At finite τ the results roughly correspond to those of a system of finite size, with edge length κ^{-1} (recall that $\kappa = \Lambda \exp(\tau)$). Thus, the equation becomes valid for large enough χ and short enough $\tilde{t}$.

We saw in the previous section that, as the critical dimension is approached, $d \to 2$, the decay amplitude $\mathcal{A}$ is determined by the lowest order coefficient $\tilde{g}_\tau^{(1,2)}$ (up to corrections in the difference $\epsilon = 2 - d$). Therefore, let us assume that we may set

$$f_\tau(\chi) = g_\tau^{(1,2)}\chi^2 = -\frac{2\pi}{\tau}\chi^2\,, \tag{4.55}$$

ignoring higher order coefficients (for a more rigorous analysis by means of the perturbative renormalization group, we refer to [77]). A constant initial density ρ_0 implies a diverging dimensionless initial density ρ_0/κ^2. Solving Eq. (4.54) for this initial condition, we obtain

$$\chi(\tilde{t}) = \frac{\rho_0 \tau}{-2\pi\tilde{t}\rho_0 + \tau\kappa^2}\,, \tag{4.56}$$

as long as χ is large enough so that the term $-\chi$ in Eq. (4.54) can be disregarded. (It destroys the algebraic behavior for large times, where $\chi(\tilde{t}) \sim \exp(-\tilde{t})$ decays exponentially, as one would also expect for finite size system.) Thus, after an initial transient time $\sim \tau\kappa^2$, which goes to zero exponentially fast as $\tau \to -\infty$ and can therefore be neglected, we have $\chi(\tilde{t}) = -\frac{\tau}{2\pi\tilde{t}}$. Inserting $\chi(\tilde{t}) = \rho(t)/\kappa^2$ and $\tilde{t} = \kappa^2 t$ (see Eqs. (3.111,3.112) with $\psi = \rho$) and $\tau = \ln(\kappa/\Lambda) \sim -\frac{\ln(t)}{2}$, we recover the result [77]

$$\rho(t) = \frac{\ln t}{4\pi t}\,, \tag{4.57}$$

for large times t.

By the same token we can derive the dependence of the stationary density $\rho(t) \equiv \rho = \kappa^2\chi$ for constant particle input $J(\mathbf{x}, t) \equiv J = \kappa^4 j$, where j is the dimensionless particle input. In this case Eq. (4.54) becomes

$$0 = \partial_{\tilde{t}}\chi = -\left(\chi + f_\tau(\chi)\right) + j \approx -\frac{2\pi}{\tau}\chi^2 + j\,. \tag{4.58}$$

Thus, $\rho^2 = \frac{-\tau}{2\pi} J$ and from $J = \kappa^4 j$ it follows that $\tau = \ln(\kappa/\Lambda) \sim \frac{1}{4}\ln(J)$. We find that, to lowest order in J, the stationary density behaves as

$$\rho(J) = -\frac{\ln(J) J^{\frac{1}{2}}}{8\pi}\,, \tag{4.59}$$

confirming the implicitly stated result in [166].

4.8 Conclusion

In general, due to the large number of degrees of freedom, solving the Wetterich equation is a formidable task, even within the local potential approximation. It is therefore crucial to exploit the symmetries and properties of the process at hand. For the decay process we could show that only terms $\sim \bar{\chi}^m \chi^n$ with $m \leq n$ in the power series of the dimensionless potential u_τ are nonzero. This is a consequence of the fact that for the coagulation process the particle number can only decrease, and that the fields $\bar{\chi}$ and χ are related to the creation operator and destruction operator, respectively. Invoking the diagrammatic one-loop representation of the Wetterich equation, it was demonstrated that, since the number of legs of the diagrams can only decrease, there is a drastic restriction of possible one-loop Feynman diagrams. In particular, this relative simplicity of the flow equations allowed us to prove that the coagulation process $A + A \to A$ and the annihilation process $A + A \to \varnothing$ are in essence equivalent and satisfy the simple relation $\rho_{\text{coag}}(t) = 2\rho_{\text{annih}}(t)$ (except for rather pathological initial conditions).

Studying the flow of the renormalized decay rate $\tilde{\lambda}_\tau = \frac{1}{2}\tilde{g}_\tau^{(1,2)}$, we could show that below the critical dimension $d_c = 2$, the flow drives the dimensionless effective average potential $u_\tau(\bar{\chi}, \chi)$ to a fixed point function $u^\star(\bar{\chi}, \chi)$ without tuning of parameters. This is the underlying reason why there is a universal scaling $\rho = \frac{D}{\sqrt{2\pi}} t^{-1/2}$ in one dimension (for large times t, with diffusion constant D), such that the type of the underlying lattice and the microscopic decay rate λ are immaterial for the long time behavior. (For instance, one could introduce next to nearest neighbor interactions, or a second lane with particles that are allowed to hop between the two lanes. The microscopic decay rate does not even need to be finite: The same results are expected when the coagulation reactions are instantaneous, i.e. $\lambda \to \infty$.) In order to calculate the dimension-dependent, universal decay amplitude $\mathcal{A}_d$, we had to work out the non-analytic behavior of the force $F(\psi) = c_d \psi^{(d+2)/d}$, or, equivalently, the behavior of the dimensionless fixed point force $f^\star(\chi) \sim c_d \chi^{(d+2)/d}$ for large fields χ. To achieve this, an algorithm for the successive calculation of the coefficients in the power series of the fixed point potential $u^\star$ was devised and implemented with a symbolic computation program. This allowed to determine $f^\star(\chi)$ up to high orders (≈ 100) in χ. Thus, by extrapolating $f^\star(\chi)$ to large χ by a Padé approximant, the coefficient c_d and hence the decay amplitude $\mathcal{A}_d$ could be extracted. As opposed to perturbative renormalization group calculations, our approach does not rely on a small difference $\epsilon = 2 - d$ to the critical dimension, and indeed the results for $d = 1$ and $\epsilon = 1$ compare very well to the known exact values for the decay amplitude. Finally, we showed that the NPRG approach is capable of recovering analytic results for small ϵ and at the critical dimension.

5 Non-Universality Above the Critical Dimension

In the previous chapter we saw that below the critical dimension two, the renormalization group flow drives the renormalized decay rate $\lambda_\kappa := \frac{1}{2} g_\kappa^{(1,2)}$ to zero. In order to treat this singularity, we introduced the dimensionless couplings $\tilde{g}_\kappa^{(m,n)} = \kappa^{-2+d(n-1)} g_\kappa^{(m,n)}$, which tend to a finite, universal value $\tilde{g}^{\star(n,m)}$ as the infrared cutoff scale κ becomes small. Without tuning of parameters the couplings flow to a fixed point, which implies an anomalous long time behavior $\rho \sim \mathcal{A}_d t^{-d/2}$ with a universal amplitude $\mathcal{A}_d$. We shall see in the following that in contrast to this, above the critical dimension the renormalized decay rate $\lambda_\kappa := g_\kappa^{(1,2)}$ attains a finite, non-universal value as the scale κ goes to zero. This turns out to depend on the microscopic decay rate λ, on the structure of the lattice, and on the shape and size of the particles. Thus, above the critical dimension the long time behavior is fully determined by the "classical", i.e. mean-field relation

$$\partial_t \rho \sim -\mu \rho^2 \,, \tag{5.1}$$

with a macroscopic decay rate $\mu := \lambda_{\kappa=0}$. Hence at long times the particle density fulfills the classical scaling

$$\rho \sim \mu^{-1} t^{-1} \,. \tag{5.2}$$

The amplitude μ^{-1} of this long time decay, however, is non-universal and disagrees with the mean-field value (the inverse microscopic decay rate λ^{-1}). It is lowered by fluctuations, which—as we shall see below—monotonically drive the coupling to smaller values as they are integrated out. The renormalization group flow of the decay rate λ_κ for various dimensions d is illustrated in Figure 5.1.

To obtain an intuitive understanding of the kinetics in high dimensions, it is important to note that the random walk above the critical dimension two is not recurrent, i.e. two point particles starting at the same place at a certain time will never meet again [138]. Thus an ultraviolet cutoff, induced by a lattice or a finite extension of the particles, is absolutely necessary in order to render the probability for two particles to meet finite and to obtain a non-zero decay rate. Nevertheless, also if this requirement of an ultraviolet cutoff is fulfilled, above the critical dimension the average time it takes for two particles (on an otherwise empty lattice) to meet still goes to infinity very quickly as their initial distance is increased. This is the underlying reason why strong long range correlations which imply anomalous long time scaling in one and two dimension, cannot build up above the critical dimension.

In the following we restrict our discussion to the leading term $\sim \rho^2$ in the kinetic equation for the time evolution of the density. This term agrees with the law of mass action, stating that the rate of an elementary reaction is proportional to the product of the concentrations of the

participating molecules. We will indeed be able to prove that above the critical dimension fluctuations are not strong enough to breach this law for asymptotically low densities. The treatment of violations of this classical term for finite densities is deferred to the next chapter. We shall focus on the case of a three-dimensional system. As a first approximation we artificially introduce an ultraviolet cutoff Λ (approximately corresponding to a lattice spacing $a = \Lambda^{-1}$) into the flow equations, to obtain crude results for the macroscopic decay rate μ. We then proceed with a more careful analysis, where we introduce the ultraviolet cutoff in terms of the lattice structure and the shape and size of the particles into the flow equation. The exact flow equation is solved for a number of examples and the results are compared to stochastic lattice simulations. The precision of our numeric results will be an important requirement for the verification of deviations from the law of mass action by stochastic lattice simulations in the next chapter. Finally, we discuss the possibility of adapting our findings to similar decay processes for three and more reactants. Parts of this chapter have been published in our article "On the validity of the law of mass action in three dimensional coagulation processes", which appeared in Physical Review Letters [167].

5.1 One-Site Objects on a Cubic Lattice

The dimensionful flow equation for the renormalized decay rate $\lambda_\kappa := \frac{1}{2} g_\kappa^{(1,2)}$ is straightforwardly derived from Eq. (3.109), with $D_\kappa = Z_\kappa = 1$, by Taylor expansion. It reads

$$\partial_\kappa \lambda_\kappa = 2\widetilde{V}_d \kappa^d \frac{\lambda_\kappa^2}{\kappa^3} = \frac{2\lambda_\kappa^2 \kappa^{d-3}}{\Gamma\left(1+\frac{d}{2}\right)(4\pi)^{\frac{d}{2}}}\,, \tag{5.3}$$

where Γ denotes the Γ-function and not the effective action. With the initial (microscopic) value $\lambda_{\kappa=\Lambda} = \lambda$, where $\Lambda > 0$ is the "explicit" ultraviolet cutoff, this gives

$$\lambda_\kappa = \frac{2\pi\lambda}{2\pi + \lambda\left(\ln(\Lambda) - \ln(k)\right)}\,, \tag{5.4}$$

for a two-dimensional system and

$$\lambda_\kappa = \frac{2^d(d-2)\pi^{\frac{d}{2}}\,\Gamma\left(1+\frac{d}{2}\right)\lambda}{2\left(\Lambda^{d-2} - \kappa^{d-2}\right)\lambda + 2^d(d-2)\pi^{\frac{d}{2}}\Gamma\left(1+\frac{d}{2}\right)}\,, \tag{5.5}$$

otherwise, cf. Figure 5.1. Thus, below the critical dimension $d_c = 2$ the renormalized decay rate tends to zero as $\lambda_\kappa \sim \kappa^{2-d}$. (Notice that the universality below the critical dimension $d < 2$ is expressed in the fact that in the denominator κ^{d-2} diverges for small κ and the non-universal microscopic decay rate λ in the nominator and denominator cancels, so that there only remains a d-dependent proportionality factor $2^{d-1}(2-d)\pi^{d/2}\Gamma\left(1+\frac{d}{2}\right)$.) In contrast, for large d, long range fluctuations (κ small) are suppressed by a the factor κ^{d-3} in the flow equation (5.3), such that there exists a finite macroscopic decay rate $\mu = \lambda_{\kappa\to 0}$. However, above the critical dimension $d > d_c = 2$, it is the short range fluctuations (κ large) which force the renormalized decay rate λ_κ to tend to zero, if we let the ultraviolet cutoff Λ go to infinity. This correctly implies a trivial, vanishing decay rate for point particles in continuous space.

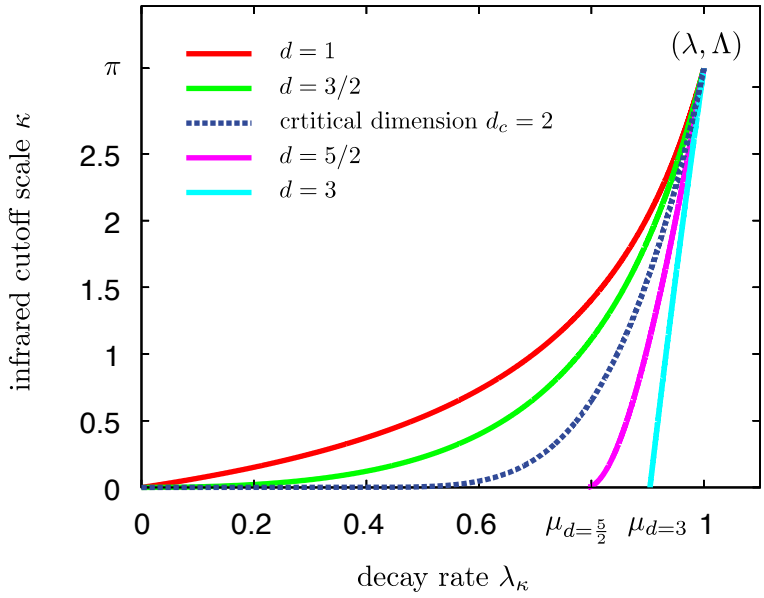

Figure 5.1: Illustration of the flow of the renormalized macroscopic decay rate λ_κ (with $\lambda_{\kappa=\Lambda} = \lambda$, $\mu = \lambda_{\kappa=0}$) for a range of dimensions. The flow for the critical dimension $d_c = 2$ (dashed curve), where $\lambda_\kappa \sim \ln(1/\kappa)$ for small κ, separates the curves into two qualitatively different regimes: When $d < 0$ the function λ_κ tends to zero as $c(d)\kappa^{2-d}$, when the long range fluctuations are integrated, $\kappa \ll 1$, with a universal function $c(d)$. Above the critical dimension the renormalized decay rate λ_κ meets the axis at a finite value $\mu = \lambda_0$, which critically depends on the cutoff Λ. Here we have chosen $\Lambda = \pi$ as an "explicit" ultraviolet cutoff. In the course of this chapter we show how the ultraviolet cutoff is defined implicitly by the lattice structure and the shape and size of the particles. Also notice that the larger the dimension the less impact the fluctuations have on the decay rate: as $d \to \infty$ mean-field becomes exact, $\mu \to \lambda$.

These systems with an ultraviolet cutoff Λ do not have a one-to-one correspondence with a concrete realization of the model, where the ultraviolet cutoff is provided "implicitly" by the structure of the lattice or the extension of the particles. For instance, when particles which each occupy one site on a regular lattice, diffuse by hopping to one of their nearest neighbors with rate one, the ultraviolet cutoff is related to the inverse lattice spacing. This system is a convenient choice for stochastic simulations, since regular, i.e. hypercubic lattices, are naturally implemented by the standard arrays provided by the programming languages and we do not need to introduce discretization artificially as for reactions in continuous space [168]. Our simulations in three dimensions confirm the classical scaling $\rho \sim \mu^{-1}t^{-1}$ for microscopic decay rates $\lambda = 1$ and $\lambda = \infty$ (an infinite rate implies that two particles coagulate immediately upon contact) and yield for the decay amplitudes $\mu^{-1} \approx 0.25$ and $\mu^{-1} \approx 1.25$, respectively (see Figure 5.3).

In a first attempt to explain these amplitudes, let us naively set the ultraviolet cutoff Λ to π, approximately corresponding to a lattice spacing of one. (For a cubic lattice with lattice spacing a, the reciprocal lattice is again cubic with lattice spacing $2\pi a^{-1}$. We need to integrate over momenta in the first Brillouin zone, which is a cube with edge length $2\pi a^{-1}$ centered at

the origin [169], i.e. the components of the momentum fulfill $-\pi/a < q_\nu \leq \pi/a$. By setting $\Lambda = \pi$ we constrict the momenta to a ball of radius π which is contained in this cube, but even if we were to set $\Lambda = \sqrt{3}\pi$ and thus extended the domain of integration to a ball that contains the cube, the result for the macroscopic amplitude would still be significantly too small.) In three dimensions this yields $\mu^{-1} = \lambda_0^{-1} = \lambda^{-1} + \frac{1}{3\pi}$, that is $\mu^{-1} \approx 0.11$ when $\lambda \to \infty$ and $\mu^{-1} \approx 1.11$ when $\lambda = 1$. This is certainly not a satisfactory result. Nevertheless, as a consistency check, we can indeed verify that the mean-field result $\mu = \lambda_0 = \lambda_\Lambda = \lambda$ is recovered in the reaction limited regime $\lambda \to 0$. The same holds true, as expected, when one lets the dimension d go to infinity for fixed λ.

To improve our results, we must not perform the continuum limit in the Doi formalism, but incorporate the structure of the cubic lattice in our equations. To this end we need to work out the Fourier transform of the diffusion term in the microscopic action,

$$\begin{aligned}
\mathcal{S}_\epsilon[\bar\psi,\psi] &= D\int \mathrm{d}t \sum_{\mathbf{x},\mathbf{y}} \big(\bar\psi(\mathbf{x},t) - \bar\psi(\mathbf{y},t)\big)\,(\psi(\mathbf{x},t) - \psi(\mathbf{y},t)) = \\
&= D\int \mathrm{d}t \sum_{\mathbf{x},\nu} \big(\bar\psi(\mathbf{x},t) - \bar\psi(\mathbf{x}+\mathbf{a}_\nu,t)\big)\,(\psi(\mathbf{x},t) - \psi(\mathbf{x}+\mathbf{a}_\nu,t)) = \\
&= D\int \mathrm{d}t \sum_{\nu} \int_{\mathbf{q}} e^{iq_\nu(x_\nu+a/2)} 2\sin\Big(\frac{q_\nu a}{2}\Big)\,\bar\psi(q_\nu)\cdot \int_{\mathbf{q}'} e^{iq'_\nu(x_\nu+a/2)} 2\sin\Big(\frac{q'_\nu a}{2}\Big)\,\psi(q'_\nu) = \\
&= \int_{\mathbf{q},\omega} \epsilon(\mathbf{q})\bar\psi(-\mathbf{q},-\omega)\psi(\mathbf{q},\omega)\,, \qquad (5.6)
\end{aligned}$$

with the dispersion relation

$$\epsilon(\mathbf{q}) = 4D\sum_{\nu=1}^{d}\Big[\sin\Big(\frac{q_\nu a}{2}\Big)\Big]^2\,. \qquad (5.7)$$

Here D is the diffusion rate, a is the lattice spacing, $\mathbf{a}_\nu$ is a times the unit vector along the νth coordinate, $\int_\omega := \int \frac{\mathrm{d}\omega}{2\pi}$, and $\int_{\mathbf{q}} := \int \frac{\mathrm{d}^3 q}{(2\pi)^3}$ runs over the first Brillouin zone, cf. Figure 5.2. Notice that the expression can easily be generalized to arbitrary Bravais lattices.

Therefore, to take account of the lattice structure, in flow equation (3.107) we need to substitute $Dq^2 \to \epsilon(\mathbf{q})$ (for the local potential approximation, where $D_\kappa = D$, and $Z_\kappa = 1$),

$$\partial_\kappa U_\kappa[\bar\psi,\psi] = \frac{1}{2}\int_{\mathbf{q}} \frac{\partial_\kappa R(\mathbf{q})\left(U_\kappa^{(1,1)}[\bar\psi,\psi] + \epsilon(\mathbf{q}) + R_\kappa(\mathbf{q})\right)}{\sqrt{\left(U_\kappa^{(1,1)}[\bar\psi,\psi] + \epsilon(\mathbf{q}) + R_\kappa(\mathbf{q})\right)^2 - U_\kappa^{(2,0)}[\bar\psi,\psi]U_\kappa^{(0,2)}[\bar\psi,\psi]}}\,. \qquad (5.8)$$

With the cutoff [170, 171]

$$R_\kappa(\mathbf{q}) = (\kappa^2 - \epsilon(\mathbf{q}))\Theta(\kappa^2 - \epsilon(\mathbf{q}))\,, \qquad (5.9)$$

we obtain

$$\partial_\kappa U_\kappa[\bar\psi,\psi] = \widetilde{\mathcal{V}}_3(\kappa)\cdot \frac{\kappa\left(U_\kappa^{(1,1)}[\bar\psi,\psi] + \kappa^2\right)}{\sqrt{\left(U_\kappa^{(1,1)}[\bar\psi,\psi] + \kappa^2\right)^2 - U_\kappa^{(2,0)}[\bar\psi,\psi]U_\kappa^{(0,2)}[\bar\psi,\psi]}}\,, \qquad (5.10)$$

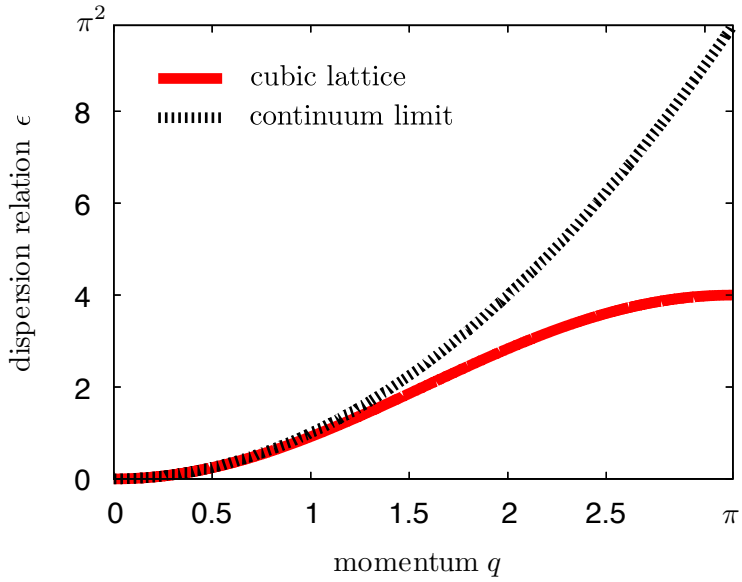

Figure 5.2: Dispersion relation $\epsilon(\mathbf{q}) = 4D\sum_{\nu=1}^{d}\sin^2(q_\nu a/2)$, $\mathbf{q} \in]-\pi/a, \pi/a]^3$ for the cubic lattice, with lattice spacing $a = 1$ and diffusion constant $D = 1$, along one of the principal axes (solid red line) in comparison with the dispersion relation $\epsilon(\mathbf{q}) = Dq^2$ (with diffusion constant $D = 1$) in the continuum limit (dashed line). The larger the dispersion relation ϵ, the stronger the fluctuations with momentum q are suppressed. The dispersion relation ϵ of the continuum limit is strictly larger than the exact relation for the cubic lattice. Therefore, in the continuum limit, fluctuations are suppressed too strongly and this is the reason why the macroscopic decay rate μ is overestimated (see text).

where

$$\widetilde{\mathcal{V}}_3(\kappa) = \int_{\mathbf{q}} \Theta(\kappa^2 - \epsilon(\mathbf{q}))\,, \tag{5.11}$$

is a volume in reciprocal space. Note that $\widetilde{\mathcal{V}}_3(\kappa) \overset{\kappa\to 0}{\sim} \kappa^3\widetilde{V}_3$ (where $\widetilde{V}_3$ is the volume of a three-dimensional ball with radius $(2\pi)^{-1}$) so that Eq. (3.107) is recovered for small κ.

For coagulation with rate λ, the reaction part of the microscopic action reads $\mathcal{S}_\lambda[\bar\psi,\psi] = \sum_{\mathbf{x}}\int \mathrm{d}t\,\left[\lambda\bar\psi(\mathbf{x},t)^2\psi(\mathbf{x},t)^2 + \lambda\bar\psi(\mathbf{x},t)\psi(\mathbf{x},t)^2\right]$, see Eq. (3.56). Therefore, the initial condition for the effective average potential becomes

$$U_{\kappa=\infty}(\bar\psi,\psi) = \lambda\bar\psi^2\psi^2 + \lambda\bar\psi\psi^2\,. \tag{5.12}$$

We consider the expansion $U_\kappa(\bar\psi,\psi) = \lambda_\kappa\bar\psi^2\psi^2 + \lambda_\kappa\bar\psi\psi^2$, truncating terms which are not present in the initial action, such as terms of third order in ψ. It turns out that they do not enter the flow equation, as is discussed in the next section. Thus, expanding Eq. (5.10), we arrive at the flow equation for the renormalized decay rate

$$\partial_\kappa\lambda_\kappa = 2\frac{\widetilde{\mathcal{V}}_3(\kappa)}{\kappa^3}\lambda_\kappa^2\,. \tag{5.13}$$

For the (three dimensional) cubic lattice with lattice spacing $a = 1$ and diffusion constant

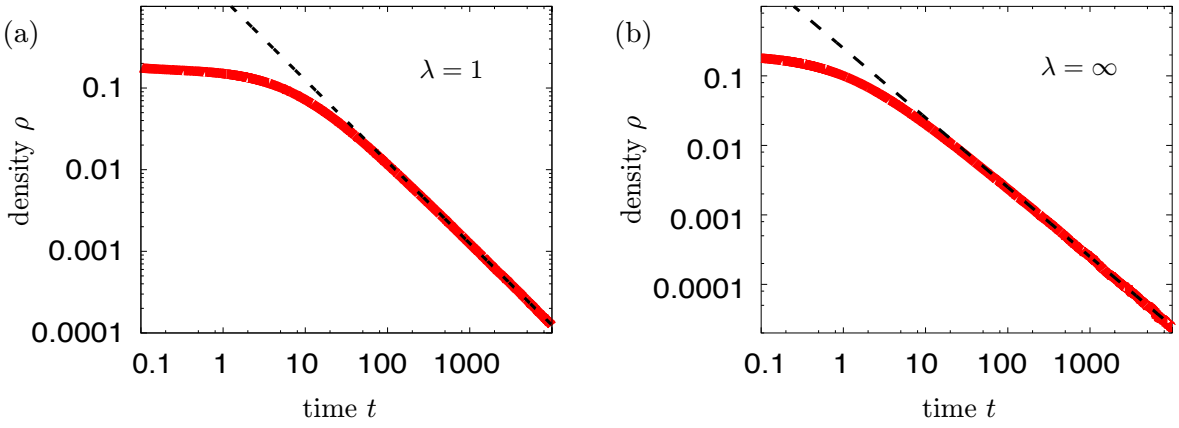

Figure 5.3: Relaxation of the particle density ρ for one-site objects. On double logarithmic plots, data of stochastic simulations (solid red) are compared to the theoretical prediction for the density decay $\rho(t) \sim \mu^{-1} t^{-1}$ (dashed line), with the reciprocal macroscopic decay rate $\mu^{-1} = \lambda^{-1} + 0.252731009858$, cf. Eq. (5.26). Here λ is the microscopic reaction rate, which determines the rate of the coagulation reaction $A + A \to A$ once two particles meet on the same site. An infinite rate $\lambda = \infty$ implies instantaneous reaction. The initial states in both plots were randomly distributed (each site independent and Poissonian) with $\rho(0) = 0.2$.

$D = 1$, let us calculate an explicit formula for the amplitude,

$$\frac{1}{\mu} = \frac{1}{\lambda_0} = \frac{1}{\lambda} + 2\int_0^\infty \mathrm{d}\kappa \int_{\mathbf{q}} \frac{\Theta\Big(\big(\frac{\kappa}{2}\big)^2 - \sum_{\nu=1}^3 \big[\sin\big(\frac{q_\nu}{2}\big)\big]^2\Big)}{\kappa^3} =$$

$$= \frac{1}{\lambda} + 2\int_{\mathbf{q}} \int_{\sqrt{4\sum_{\nu=1}^3 [\sin(\frac{q_\nu}{2})]^2}}^\infty \frac{\mathrm{d}\kappa}{\kappa^3} = \frac{1}{\lambda} + \int_{\mathbf{q}} \frac{1}{\sum_{\nu=1}^3 4\,\big[\sin\big(\frac{q_\nu}{2}\big)\big]^2}\,. \tag{5.14}$$

The integral in the second term can be evaluated numerically to high precision,

$$\frac{1}{\mu} \approx \frac{1}{\lambda} + 0.252731009858(3)\,. \tag{5.15}$$

Within the boundaries of the statistical error this is in accordance with the stochastic simulations, cf. Figure 5.3.

5.2 Proof of the Exactness of the Local Potential Approximation for One-Site Objects

The fact that our result for the macroscopic decay rate μ perfectly describes our empirical simulation results, raises the question whether the approach is exact, despite restricting ourselves to the lowest order approximation, i.e. the local potential approximation. First we note that the above calculation of the macroscopic density gives the same result for every choice of the cutoff function. Indeed, from Eq. (5.8) it follows the flow equation $\partial_\kappa \lambda_\kappa = \lambda_\kappa^2 \int_{\mathbf{q}} \frac{\partial_\kappa R_\kappa(\mathbf{q})}{R_\kappa(\mathbf{q}) + \epsilon(\mathbf{q})}$ and thus

$$\frac{1}{\lambda_\kappa} = \frac{1}{\lambda} + \int_{\mathbf{q}} \frac{1}{R_\kappa(\mathbf{q}) + \epsilon(\mathbf{q})}\,. \tag{5.16}$$

When the scale $\kappa = 0$ ($\mu = \lambda_{\kappa=0}$), such that all fluctuations are integrated out, a general cutoff function vanishes by definition ($R_\kappa = 0$, see the constraint (3.73)), so the result becomes independent of the specific choice of R_κ. The independence from the cutoff function is necessary for the exactness of our result. Moreover, the deviations for different cutoff functions are sometimes used to optimize the result and to estimate the error [142, 172, 173]. The fact that there are no deviations should therefore be regarded as a strong indication that Eq. (5.16) is exact.

To prove this assertion, let us go back to the original Wetterich flow equation, see Eq. (3.90). Its initial condition is the microscopic action, which here reads

$$\mathcal{S}[\bar\psi,\psi] = \sum_{\mathbf{x}} \int \mathrm{d}t \left(\lambda\left(\bar\psi(\mathbf{x},t)+1\right)\bar\psi(\mathbf{x},t)\psi(\mathbf{x},t)^2 + \bar\psi(\mathbf{x},t)\partial_t\psi(\mathbf{x},t)\right) + \\ + \int_{\mathbf{q},\omega} \epsilon(\mathbf{q})\bar\psi(-\mathbf{q},-\omega)\psi(\mathbf{q},\omega)\,. \tag{5.17}$$

As in the previous chapter, we define the (m,n)-vertex functions $\Gamma^{(m,n)}_{\kappa\,(\mathbf{p}_1,\omega_1;\ldots;\mathbf{p}_{m+n},\omega_{m+n})}$ (related to one-loop Feynman diagrams with n incoming and m outgoing legs) by taking the functional derivative with respect to $\bar\psi(\mathbf{p}_i,\omega_i)$, $i \in \{1,\ldots,m\}$ and $\psi(\mathbf{p}_j,\omega_j)$, $j \in \{m{+}1,\ldots,m{+}n\}$ at vanishing fields $\bar\psi = \psi = 0$. The renormalized reaction rate λ_κ is given by

$$\lambda_\kappa = \frac{1}{2}\frac{(2\pi)^{12}\,\Gamma^{(1,2)}_{\kappa\,(\mathbf{0},0;\mathbf{0},0;\mathbf{0},0)}}{VT}\,. \tag{5.18}$$

Here, $V = \sum_{\mathbf{x}} = (2\pi)^3\delta(\mathbf{q}=\mathbf{0})$ and $T = \int \mathrm{d}t = 2\pi\delta(\omega = 0)$ denote the asymptotically large volumes in space and time which are summed and integrated over, respectively (in the final result they drop out). The flow of $\Gamma^{(1,2)}_{\kappa\,(\mathbf{0},0;\mathbf{0},0;\mathbf{0},0)}$ is associated with the diagram

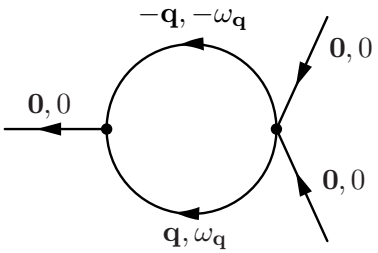

which includes, in addition to the (1,2)-vertex, a (2,2)-vertex with non-zero momenta and frequencies (right vertex of the graph). Let us therefore also consider the flow of the vertex function $\Gamma^{(2,2)}_{\kappa\,(\mathbf{p}',\omega';-\mathbf{p}',-\omega';\mathbf{p},\omega;-\mathbf{p},-\omega)}$, determined by the diagram

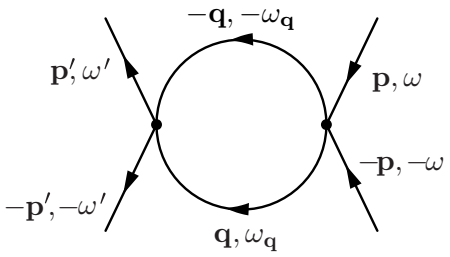

Evidently, it is a closed function of itself. The vertices and the internal momenta and frequencies are independent of the external ones. Since this also holds for the initial conditions, we have $\Gamma^{(2,2)}_{\kappa\,(\mathbf{p}',\omega';-\mathbf{p}',-\omega';\mathbf{p},\omega;-\mathbf{p},-\omega)} = \Gamma^{(2,2)}_{\kappa\,(\mathbf{0},0;\mathbf{0},0;\mathbf{0},0;\mathbf{0},0)}$, for all κ. Similarly, the identity $\Gamma^{(2,2)}_{\kappa\,(\mathbf{0},0;\mathbf{0},0;\mathbf{0},0;\mathbf{0},0)} = \frac{2}{(2\pi)^4}\Gamma^{(1,2)}_{\kappa\,(\mathbf{0},0;\mathbf{0},0;\mathbf{0},0)}$, which holds initially, is inherited to all scales κ. Thus,

$$\Gamma^{(2,2)}_{\kappa\,(\mathbf{p}',\omega';-\mathbf{p}',-\omega';\mathbf{p},\omega;-\mathbf{p},-\omega)} = \frac{4VT}{(2\pi)^{16}}\lambda_\kappa\,. \tag{5.19}$$

The evaluation of the flow of λ_κ through the corresponding one-loop diagram for the (1,2)-vertex function $\Gamma^{(1,2)}$ at zero momenta and frequencies therefore involves no approximation. With our standard cutoff mass $R_\kappa(\mathbf{q}) = (\kappa^2 - \epsilon(\mathbf{q}))\,\Theta(\kappa^2 - \epsilon(\mathbf{q}))$ it yields (recall that $\tilde{\partial}_\kappa = \partial_\kappa R_\kappa \cdot \partial_{R_\kappa}$)

$$\partial_\kappa \lambda_\kappa = -2\tilde{\partial}_\kappa \int_{\mathbf{q},\omega} \lambda_\kappa \frac{1}{R_\kappa(\mathbf{q}) + \epsilon(\mathbf{q}) - i\omega}\lambda_\kappa \frac{1}{R_\kappa(\mathbf{q}) + \epsilon(\mathbf{q}) + i\omega} = 2\lambda_\kappa^2 \frac{\int_{\mathbf{q}} \Theta(\kappa^2 - \epsilon(\mathbf{q}))}{\kappa^3}\,. \tag{5.20}$$

Thus the exact solution for the macroscopic decay rate is

$$\frac{1}{\mu} = \frac{1}{\lambda_0} = \frac{1}{\lambda} + \int_{\mathbf{q}} \frac{1}{\epsilon(\mathbf{q})}\,. \tag{5.21}$$

We remark that one arrives at the same result by summing over a sequence of bubble diagrams, analogous to calculations in [64, 166] for spheres. One needs to consider

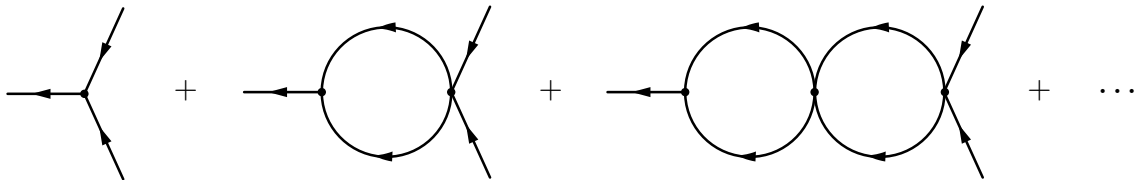

For one-site objects these bubble diagrams factorize, such that one obtains the geometric series

$$\mu = 2\lambda + (-\lambda)\int_{\mathbf{q},\omega} \frac{1}{\epsilon(\mathbf{q})^2 + \omega^2} 2\lambda + \left[(-\lambda)\int_{\mathbf{q},\omega} \frac{1}{\epsilon(\mathbf{q})^2 + \omega^2}\right]^2 2\lambda + \ldots \tag{5.22}$$

When $\lambda \int_{\mathbf{q},\omega} \frac{1}{\epsilon(\mathbf{q})^2+\omega^2} < 1$ the geometric series converges, while for the range $\lambda \int_{\mathbf{q},\omega} \frac{1}{\epsilon(\mathbf{q})^2+\omega^2} \geq 1$ one exploits analytic continuation, thus confirming Eq. (5.21)

Finally we remark that, in general, the one-loop diagram of the (1,2)-vertex, which in position- and time-space is of the form

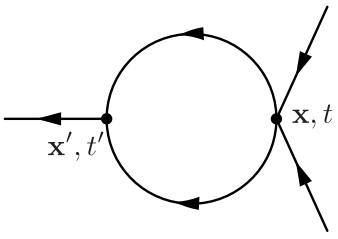

gives rise to a term $\sum_{\mathbf{x},\mathbf{x}'} \int \mathrm{d}t\, \mathrm{d}t'\, \lambda_\kappa(\mathbf{x}'-\mathbf{x}, t'-t)\bar{\psi}(\mathbf{x}', t')\psi^2(\mathbf{x}, t)$ in the effective average action Γ_κ. The local potential approximation is tantamount to taking a rate

$$\lambda_\kappa(\mathbf{x}' - \mathbf{x}, t' - t) \approx \delta(\mathbf{x}' - \mathbf{x})\delta(t' - t)\lambda_\kappa\,, \tag{5.23}$$

which is local in space and time. While this equation is only approximately true, we find for our case that summing over space an integrating over time again gives an exact result,

$$\sum_{\mathbf{x}} \int \mathrm{d}t\, \lambda_\kappa(\mathbf{x}, t) = \lambda_\kappa\,. \tag{5.24}$$

Moreover, for the flow λ_κ we do not need the full information in $\lambda_\kappa(\mathbf{x}, t)$, but it already suffices to know λ_κ, i.e. the error made by approximating $\lambda_\kappa(\mathbf{x}, t)$ as local (see Eq. (5.23)) cancels in the flow for λ_κ. This quality is rather exceptional and the underlying reason why for the coagulation process the macroscopic decay rate $\mu = \lambda_{\kappa=0}$ can be calculated exactly to high numerical precision.

5.3 Direct Measurement of the Non-Equilibrium Force

The theoretical finding that our result for the macroscopic decay rate μ is exact, calls for a more reliable "empirical" check than is provided by examining the slope of the particle decay, c.f. Figure 5.3. To determine the decay rate in the simulations more accurately, we introduced homogeneous particle input with rate J. This gives rise to a term $J\sum_{\mathbf{x}} \int dt\, \bar{\psi}(\mathbf{x}, t)$ in the action $\mathcal{S}[\bar{\psi}, \psi]$. For a homogenous initial distribution, it follows from the extremum principle, Eq. (3.93), that the density $\rho(\mathbf{x}, t) \equiv \rho(t)$ obeys the kinetic equation $\partial_t\rho = -F(\rho) + J$, with the non-equilibrium force $F(\rho) = \partial_{\bar{\psi}} U_{\kappa=0}(\bar{\psi} = 0, \psi = \rho)$. Therefore, for stationary states the non-equilibrium force equals the input rate, $F(\rho) = J$, exactly. For fixed input rate J, we waited in the stochastic simulations for the particle density to relax and then averaged over time. The time interval between the measurements was based on the relaxation time and supposed to be large enough for the densities to be uncorrelated.

In order to measure the macroscopic decay rate accurately, one is obliged to go to very low densities in the simulations. At the same time, the average number of particles needs to be kept at a sufficiently large value by accordingly increasing the system size, in order to eliminate finite sizes effects. (We considered systems containing around ten thousand particles on average.) For larger densities one can describe the state of the system by an array whose elements are the number of particles on each site, and let it evolve in time by random sequential updates [7]. However, this would have surpassed the memory resources. Moreover, such an algorithm would be very inefficient since most updates would be idle, because there can only be a particle hopping if the randomly chosen site is not empty. Therefore, it is convenient to memorize the configuration of the system by a one-dimensional array where each element corresponds to a particle and saves its position on the lattice. In a naive implementation, every time a particle has hopped to a neighboring site, one would have to check if the new site is empty or occupied by one of the other particles. If there are N particles in the system, this implies the need to perform $\sim N^2$ of these checks until on average every particle has moved once. To be able to simulate a system with large particle numbers, it was necessary

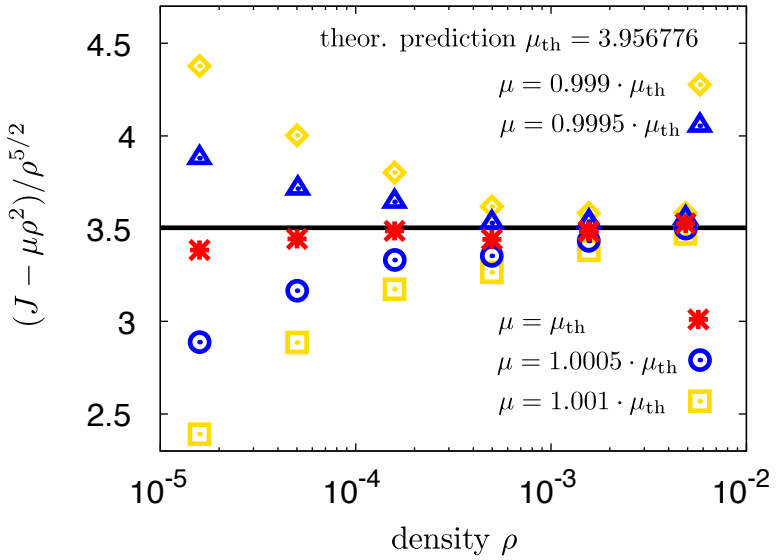

Figure 5.4: Numerical confirmation of the theoretical prediction $\mu_{\rm th} = 3.956776$ for the macroscopic decay rate. For stationary states the density should behave as $\partial_t \rho = 0 = -F(\rho) + J$, with $F(\rho) = \mu\rho^2$ to lowest order in ρ. It is observed that the difference $J - \mu^2\rho^2$ scales as $\rho^{5/2}$, which is proven in the next chapter by analytical means. For this reason it is convenient to plot the scaled difference $(J - \mu^2\rho^2)/\rho^{5/2}$. In theory this should become constant for small densities, which is in good agreement with the data when $\mu = \mu_{\rm th}$ and can be ruled out already if the deviations is larger than 0.05%. In this plot the standard deviation is comparable to (for low densities) or much smaller than (for high densities) the size of the data points.

to introduce some sort of topology. For this purpose, the lattice was divided up into boxes, and an array was introduced which for every box memorizes the locations of the particles contained in this box. When a particle hops, one only needs to check if it shares a site with the other particles in the same box. The size of the boxes should be chosen in a way that on average no more than a few particles are contained in one box. Thus the problem of increasing computational complexity is circumvented while not exhausting the memory resources.

To determine the macroscopic decay rate from the numerical data, we found it convenient to consider the difference $J - \mu^2\rho^2$. It is observed that it obeys a power law $\sim \rho^{5/2}$, which will be discussed in detail and confirmed by analytical means in the next chapter. In Figure 5.4 the validity of $\mu = 3.956776$ is confirmed up to deviations smaller than 0.001, by verifying that the data only conforms with this power law when μ is very close the theoretical prediction.

5.4 Generalization to Extended Objects on Bravais Lattices

For a coagulation process with particles that are embedded on a lattice, the initial action is of the form $\mathcal{S}[\bar{\psi}, \psi] = \mathcal{S}_\lambda[\bar{\psi}, \psi] + \mathcal{S}_\epsilon[\bar{\psi}, \psi] + \sum_{\mathbf{x}} \int \mathrm{d}t \bar{\psi}(\mathbf{x}, t) \partial_t \psi(\mathbf{x}, t)$, with a reaction term $\mathcal{S}_\lambda$, a diffusion term $\mathcal{S}_\epsilon$, and a term for the time evolution. Up to now, we have restricted the

analysis to particles that occupy only one lattice site. The lattice structure and the ultraviolet cutoff is implicitly defined by the diffusion term

$$\mathcal{S}_\epsilon[\bar\psi,\psi] = \int_{\mathbf{q},\omega} \epsilon(\mathbf{q})\bar\psi(-\mathbf{q},-\omega)\psi(\mathbf{q},\omega)\,. \tag{5.25}$$

Although, we considered cubic lattices in the previous sections, our results straightforwardly generalize to arbitrary Bravais lattices and dimension. In particular, the formula

$$\frac{1}{\mu} = \frac{1}{\lambda_0} = \frac{1}{\lambda} + \int_{\mathbf{q}} \frac{1}{\epsilon(\mathbf{q})}\,, \tag{5.26}$$

is valid for general Bravais lattices. Thus the microscopic decay rate λ is connected with its macroscopic analog μ by a term that depends on the lattice structure via the dispersion relation ϵ. The only restriction is that the dimension d must be larger than the critical dimension $d_c = 2$, since otherwise the expression diverges. Indeed, at $d = 2$ the density is known to behave as $t \ln t$, which may be interpreted by a macroscopic rate μ which becomes infinitely small [137]. Notice, that the result also covers anisotropic diffusion. For a cubic lattice, for example, one only needs to insert the adapted dispersion relation $\epsilon(\mathbf{q}) = 4\sum_{\nu=1}^{d} D_\nu \left[\sin\!\left(\frac{q_\nu a}{2}\right)\right]^2$ into Eq. (5.26).

To render our approach more versatile and realistic, we would also like to be able to consider extended particles in space. This is achieved with a generalized coagulation term

$$\mathcal{S}_\lambda(\bar\psi,\psi) = \sum_{\mathbf{x},\mathbf{y}} \int \mathrm{d}t\, \lambda(\mathbf{y}-\mathbf{x}) \left(\bar\psi(\mathbf{y},t)+1\right) \bar\psi(\mathbf{x},t)\psi(\mathbf{y},t)\psi(\mathbf{x},t)\,. \tag{5.27}$$

The "reaction kernel" $\lambda(\mathbf{z})$ allows for a finite range of the interactions instead of only local interactions. In addition to the lattice structure it implicitly imposes an ultraviolet cutoff, since its Fourier transform $\lambda(\mathbf{q})$ is negligible when the inverse momentum q^{-1} is much smaller than the typical length scale of the reaction kernel. The corresponding vertices are represented as

where the wiggly lines stand for $\lambda(\mathbf{z})$.

As the ansatz for the effective average action, let us take the "minimal" truncation

$$\Gamma_\kappa[\bar\psi,\psi] = \mathcal{S}_{\lambda_\kappa}[\bar\psi,\psi] + \mathcal{S}_{\epsilon_\kappa}[\bar\psi,\psi] + \mathcal{S}_{Z_\kappa}[\bar\psi,\psi]\,, \tag{5.28}$$

where $\mathcal{S}_{Z_\kappa} = \sum_{\mathbf{x}} \int \mathrm{d}t Z_\kappa \bar\psi(\mathbf{x},t)\partial_t\psi(\mathbf{x},t)$ denotes the term for the time evolution. This truncation contains only terms which are already present in the initial action. Just as for one-site objects, the field amplitude Z_κ and the dispersion relation ϵ_κ are not renormalized, $Z_\kappa \equiv 1$, $\epsilon_\kappa \equiv \epsilon$. In Fourier space the reaction part $\mathcal{S}_{\lambda_\kappa}[\bar\psi,\psi]$ reads

$$\int_{\mathbf{p},\omega,\mathbf{p}',\omega',\mathbf{q},\omega''} \lambda_\kappa(\mathbf{q}) \left(\bar\psi(-\mathbf{p}-\mathbf{q},-\omega-\omega'-\omega'') + (2\pi)^4\delta(-\mathbf{p}-\mathbf{q})\delta(-\omega-\omega'-\omega'')\right) \cdot \\ \cdot\, \bar\psi(-\mathbf{p}'+\mathbf{q},\omega'')\psi(\mathbf{p}',\omega')\psi(\mathbf{p},\omega)\,. \tag{5.29}$$

The renormalized reaction kernel is given by

$$\lambda_\kappa(\mathbf{p}) = \frac{1}{2}\frac{(2\pi)^{12}\,\Gamma^{(1,2)}_{\kappa\,(\mathbf{0},0;\mathbf{p},0;-\mathbf{p},0)}}{VT}\,. \tag{5.30}$$

In analogy to one-site objects,

$$\Gamma^{(2,2)}_{\kappa\,(\mathbf{p}',\omega';\mathbf{p}',\omega';-\mathbf{p}',-\omega';\mathbf{p},\omega;-\mathbf{p},-\omega)} = \frac{4VT}{(2\pi)^{16}}\lambda(\mathbf{p}+\mathbf{p}')\,. \tag{5.31}$$

Thus evaluating the flow of $\lambda_\kappa(\mathbf{p})$ given by the one-loop diagram

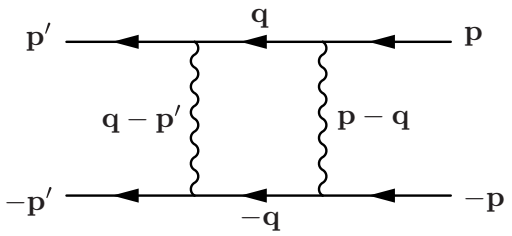

for $\mathbf{p}' = \mathbf{0}$ yields

$$\partial_\kappa\lambda_\kappa(\mathbf{p}) = 2\int_{\mathbf{q}} \lambda_\kappa(\mathbf{p}-\mathbf{q})\lambda_\kappa(\mathbf{q})\frac{\Theta(\kappa^2-\epsilon(\mathbf{q}))}{\kappa^3}\,. \tag{5.32}$$

Equivalently, in position space

$$\partial_\kappa\lambda_\kappa(\mathbf{x}) = \frac{2\lambda_\kappa(\mathbf{x})\,(\mathcal{P}\circ\lambda_\kappa)(\mathbf{x})}{\kappa^3}\,, \tag{5.33}$$

with the projection $(\mathcal{P}\circ\lambda_\kappa)(\mathbf{x}) = \int_{\mathbf{q}}\exp(i\mathbf{q}\cdot\mathbf{x})\lambda_\kappa(\mathbf{x})\Theta(\kappa^2-\epsilon(\mathbf{q}))$.

Eq. (5.33) conserves the support of the reaction kernel $\lambda_\kappa(\mathbf{z})$, which is particularly convenient when the microscopic kernel $\lambda(\mathbf{z})$ has a "simple" support (see next section). For large scales κ (i.e. when there is a lattice, κ should be larger than the maximum value in the first Brillouin zone, and for continuous objects it should be much larger than the typical reciprocal length scale of the reaction kernel in continuous space), the equation decouples in $\mathbf{x}$. This is advantageous for concrete numerical solutions, since this disposes of the problem of treating strongly diverging functions $\exp(i\mathbf{q}\cdot\mathbf{x})$ for large q. On the other hand, when κ is much smaller than the reciprocal typical length scale of the reaction kernel, the projection is just the sum $\sum_{\mathbf{x}}\lambda_\kappa(\mathbf{x}) = \lambda_\kappa(\mathbf{p}=\mathbf{0})$.

5.5 Examples of Extended Objects

Let us first apply the flow equation (5.33) for the reaction kernel to study the reaction kinetics of objects in continuous space. This is achieved by simply considering the limit where the lattice spacing goes to zero. In contrast to lattice models, where momenta are restricted to the finite, first Brillouin zone, the integration of the momenta $\mathbf{q}$ now runs over the whole

$\mathbb{R}^d$. The ultraviolet cutoff is solely imposed by the reaction kernel $\lambda_\kappa(\mathbf{q})$, which suppresses momenta $\mathbf{q}$ much larger than the typical reciprocal length scale.

As an application we would like to verify Smoluchowski's result, who studied spheres that coagulate instantaneously. The reaction kernel reads

$$\lambda_\kappa(\mathbf{x}) = \tilde{\lambda}_\kappa \, \Theta(R - x) \,, \tag{5.34}$$

in the limit $\tilde{\lambda} = \tilde{\lambda}_{\kappa\to\infty} \to \infty$, where x denotes the modulus of $\mathbf{x}$. Despite the fact that the reaction kernel $\lambda_\kappa(\mathbf{x})$ is effectively one-dimensional, since it only depends on the distance x, and the complexity of the Eq. (5.33) is thus reduced, it is not obvious how to obtain an analytical solution for this problem. However, we can exploit the conservation of the support of the reaction kernel $\lambda_\kappa(\mathbf{x})$ along the flow. Evidently, for instantaneous reactions, i.e. in the limit of an infinitely large microscopic decay rate, we may just as well consider the reaction kernel to be the surface of a sphere,

$$\lambda_\kappa(\mathbf{x}) = \tilde{\lambda}_\kappa \, \delta(R - x) \,. \tag{5.35}$$

In the limit $\tilde{\lambda} = \tilde{\lambda}_{\kappa\to\infty} \to \infty$ this must give the same results as for spheres that coagulate instantaneously on contact.

Without loss of generality, we set the radius $R = 1$ in the following calculation. Utilizing spherical coordinates,

$$\begin{aligned}
\left(\mathcal{P} \circ \lambda_\kappa\right)(\mathbf{x}) &= \frac{1}{(2\pi)^3} \int \mathrm{d}q \, \mathrm{d}\vartheta \, \mathrm{d}\phi \, q^2 \sin(\vartheta) e^{iqx\cos(\vartheta)} \Theta\big(\kappa^2 - q^2\big) \cdot \\
&\quad \cdot \int \mathrm{d}r \, \mathrm{d}\tilde{\vartheta} \, \mathrm{d}\tilde{\phi} \, r^2 \sin(\tilde{\vartheta}) e^{-iqr\cos(\tilde{\vartheta})} \tilde{\lambda}_\kappa \, \delta(1 - r) = \\
&= \tilde{\lambda}_\kappa \underbrace{\frac{2}{\pi} \int_0^k \mathrm{d}q \, \frac{1}{x} \sin(qx) \sin(q)}_{=: f_\kappa(x)} \,.
\end{aligned}$$

$$\begin{aligned}
&\Longrightarrow \quad \partial_\kappa \tilde{\lambda}_\kappa = 2\tilde{\lambda}_\kappa^2 \frac{f_\kappa(1)}{\kappa^3} \\
&\Longrightarrow \quad \frac{1}{\tilde{\lambda}_0} = \frac{1}{\tilde{\lambda}_\infty} + 2\int_0^\infty \mathrm{d}k \, \frac{f_\kappa(1)}{\kappa^3} = \frac{1}{\tilde{\lambda}_\infty} + 1 \,.
\end{aligned} \tag{5.36}$$

The macroscopic decay rate becomes

$$\frac{1}{\mu} = \frac{1}{\lambda} + \frac{1}{4\pi} \,, \tag{5.37}$$

where $\lambda = 4\pi\tilde{\lambda}_\infty$. Therefore,

$$\mu = 4\pi D R \,, \tag{5.38}$$

with diffusion constant D and radius R. This confirms Smoluchowski's result [54], proved to be exact by Doi [64].

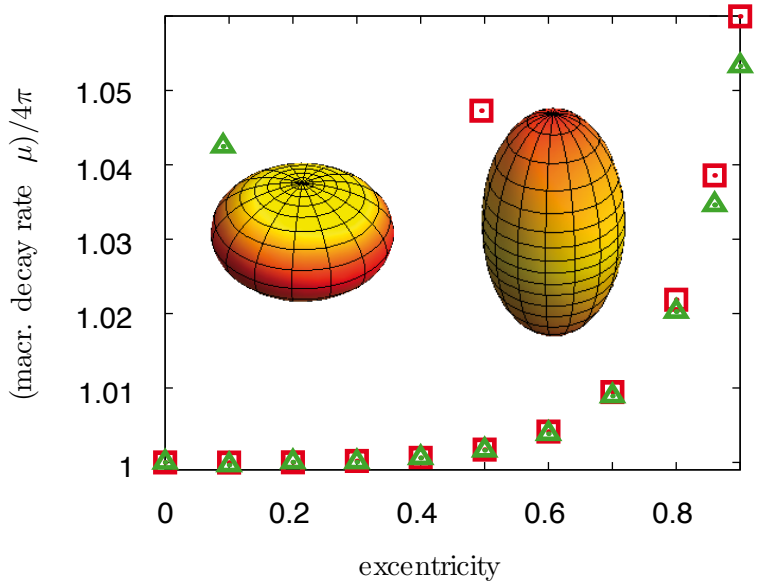

Figure 5.5: Numerical solution to the flow equation, Eq. (5.33), for spheroids of volume $\frac{4}{3}\pi$ as a function of their eccentricity. Let $\frac{a}{2}$ be the equatorial diameter and $\frac{b}{2}$ the polar axis, so that the volume is $\frac{4}{3}\pi a^2 b = 1$. One speaks of oblates when $a > b$, in which case the eccentricity is defined as $\sqrt{1 - b^2/a^2}$, and one speaks of prolates when $a < b$, with the eccentricity defined as $\sqrt{1 - a^2/b^2}$. We observe that the macroscopic decay rate μ increases with the eccentricity and, at a given eccentricity, is larger for prolates. In the images, as yellow turns to orange and red, the $\mathbf{x}$-dependent macroscopic rate $\lambda_0(\mathbf{x})$ grows. As a rule of thumb, the more jagged the reaction kernel, the higher the macroscopic decay rate μ becomes.

To further illustrate the potential and versatility of our approach, we have solved Eq. (5.33) numerically for spheroids of equal volume $\frac{4}{3}\pi$, c.f. Figure 5.5. We find that the largest values of the macroscopic rates $\lambda_0(\mathbf{x})$ are attained at the sharp ends and edges of the prolates and oblates, respectively. This can be traced back to the fact that large momenta $q^2 > \kappa^2$ do not contribute to the projection $\mathcal{P}$.

As long as the support of the reaction kernel is finite, flow equation (5.33) reduces to a finite set of coupled ordinary differential equations, with dimension equal to the number of sites that make up the reaction kernel. We will now treat reaction kernels that allow for a particularly precise numerical solution, because they can be described by only one degree of freedom. Incidentally, this is the underlying reason why the flow equation for the law of mass action term is exact, as is proven in Section 5.7.

Let us consider the two reaction kernels whose two-dimensional versions are depicted in Fig. 5.6. Extended object 1 can be considered as a discrete version of a sphere. The lattice sites that these two objects consist of (i.e. the part where reaction kernel $\lambda(\mathbf{x})$ is non-zero) are all equivalent. This symmetry must hold along the renormalization group flow. Furthermore, the flow equation conserves the support of the reaction kernel in position space. Thus the objects also keep their shape. Explicitly, in three dimensions the renormalized reaction kernel

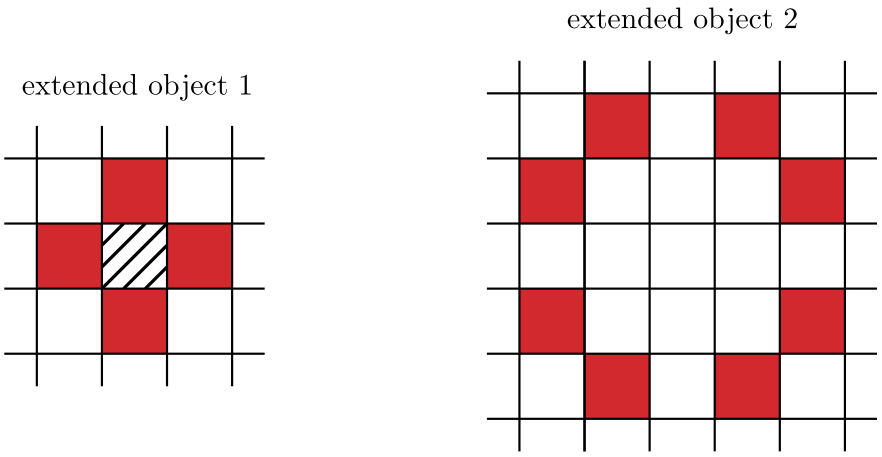

Figure 5.6: Two-dimensional versions of the reaction kernels of extended objects (solid red). The three-dimensional version of extended object 1 is obvious. It is a discretization of the sphere. The three-dimensional version of extended object 2 is created by the sites $(1,1,2),(1,2,1),(2,1,1)$ and their mirror image in each octant. The two objects encompass 6 and 24 sites, respectively. For instantaneous reactions, the striped square can be regarded as part of extended object 1. Since the flow conserves the support of the reaction kernel, their shape remains the same. The reaction kernel of the two objects can be described by one degree of freedom λ_κ because all the nonzero parts are equivalent. For infinite reaction rates, the striped squares can be regarded as part of the objects.

of extended object 1 can be expressed as

$$\lambda_\kappa(\mathbf{p}) = \frac{\lambda(\mathbf{q}=\mathbf{0})}{6}\sum_{\nu=1}^{3}\left(e^{+ip_\nu}+e^{-ip_\nu}\right) = \frac{\lambda(\mathbf{p}=\mathbf{0})}{3}\sum_{\nu=1}^{3}\cos(p_\nu)\,. \tag{5.39}$$

The microscopic decay rate is $\lambda := \lambda_\infty(\mathbf{p}=\mathbf{0}) = 6\tilde{\lambda}$ (each site of the kernel is associated the same microscopic reaction rate $\tilde{\lambda}$). Solving Eq. (5.32) at $\mathbf{p}=\mathbf{0}$, one obtains the macroscopic decay rate

$$\begin{aligned}\frac{1}{\mu} = \frac{1}{\lambda_0(\mathbf{0})} = \frac{1}{\lambda_\infty(\mathbf{0})} + 2\int_0^\infty \mathrm{d}k \int_{\mathbf{q}} \left(\frac{1}{3}\sum_{\nu=1}^{3}\cos(q_\nu)\right)^2 \frac{\Theta\big(\kappa^2-\epsilon(\mathbf{q})\big)}{\kappa^3} = \\ = \frac{1}{\lambda} + \underbrace{\int_{\mathbf{q}} \frac{\left(\sum_{\nu=1}^{3}\cos(p_\nu)\right)^2}{36\sum_{\nu=1}^{3}\sin^2(q_\nu/2)}}_{0.086064343192(3)}\,.\end{aligned} \tag{5.40}$$

In the last step we inserted the dispersion relation $\epsilon(\mathbf{p}) = 4\sum_{\nu=1}^{3}\sin^2(p_\nu/2)$ for the cubic lattice with lattice spacing $a=1$ and diffusion constant $D=1$.

The calculation for extended object 2 is similar. If each of the 24 sites effects a reaction with

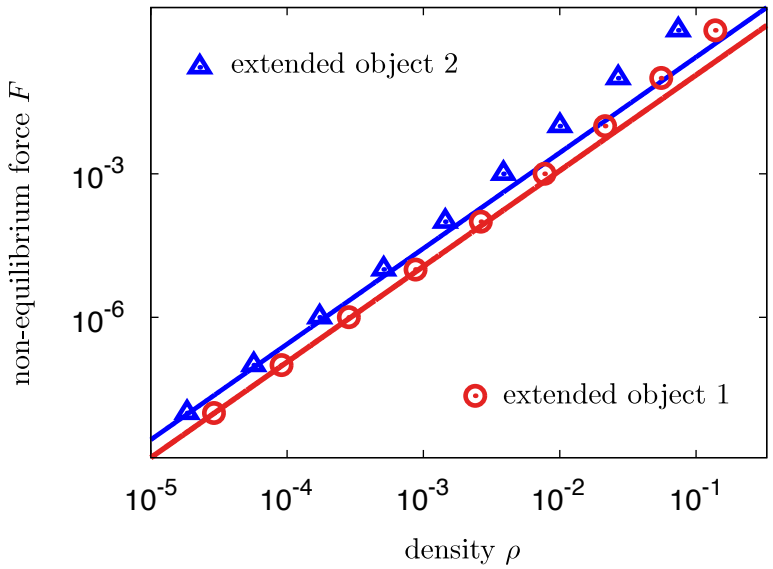

Figure 5.7: The non-equilibrium force for the two extended objects (see Figure 5.6), measured in the stationary state at constant particle input J, such that $0 = \partial_t \rho(t) = -F(\rho) + J$. The data of the stochastic simulations collapse well on the function $F(\rho) = \mu\rho^2$ (solid red for extended object 1, solid blue for extended object 2), with $\mu^{-1} = \lambda^{-1} + 0.0861\ldots$ (extended object 1) and $\mu^{-1} = \lambda^{-1} + 0.0363\ldots$ (extended object 2). For this plot we have chosen an infinitely large microscopic decay rate $\lambda = \infty$, where the particles react instantaneously on contact.

the same microscopic rate $\tilde{\lambda}$, then the flow dependent reaction kernel can be expressed as

$$\begin{aligned}\lambda_\kappa(\mathbf{p}) = \frac{\lambda(\mathbf{q}=\mathbf{0})}{12}\,&[(\cos(p_1+p_2+2p_3)+\cos(p_1+2p_2+p_3)+\cos(2p_1+p_2+p_3))+\\ &+(\cos(p_1+p_2-2p_3)+\cos(p_1+2p_2-p_3)+\cos(2p_1+p_2-p_3))+\\ &+(\cos(p_1-p_2+2p_3)+\cos(p_1-2p_2+p_3)+\cos(2p_1-p_2+p_3))+\\ &+(\cos(-p_1+p_2+2p_3)+\cos(-p_1+2p_2+p_3)+\cos(-2p_1+p_2+p_3))]\\ &\equiv \lambda_\kappa(\mathbf{q}=\mathbf{0}) f(\mathbf{p})\,,\end{aligned} \tag{5.41}$$

with only one degree of freedom. Solving Eq. (5.32) then yields

$$\frac{1}{\mu} = \frac{1}{\lambda} + \underbrace{\int_{\mathbf{q}} \frac{f(\mathbf{q})^2}{4\sum_{\nu=1}^{3}\sin^2(q_\nu/2)}}_{0.036287603611(2)}\,. \tag{5.42}$$

These results are in excellent agreement with the stochastic simulations, c.f. Figure 5.7.

5.6 General Exact Flow Equation

The derivation of the flow equations for extended objects, Eq. (5.32,5.33), was not rigorous, but valid only within the minimal truncation, cf. Eq. (5.28), for the average action $\Gamma_\kappa[\bar{\psi}, \psi]$.

We are primarily interested in the effective, macroscopic decay rate for homogeneous and stationary states. Thus, it is our goal to calculate the vertex $\Gamma^{(1,2)}_{\kappa\,(\mathbf{0},0;\mathbf{0},0;\mathbf{0},0)}$ represented by the graph

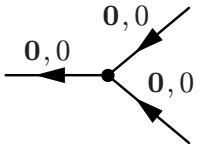

In this notation we have disposed of the wiggly line employed above, with the understanding that the vertex depends on the momenta and frequencies of the incoming and outflowing lines (which, in this diagram, are all equal to 0). Its flow is associated with the one-loop diagram

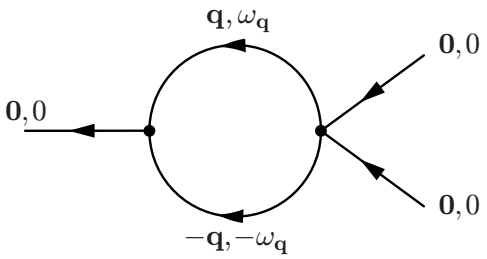

We therefore also need to calculate the (2,2)-vertex function $\Gamma^{(2,2)}_{\kappa\,(\mathbf{p}',\omega';-\mathbf{p}',-\omega';\mathbf{0},0;\mathbf{0},0)}$, whose flow is determined by the one-loop diagram

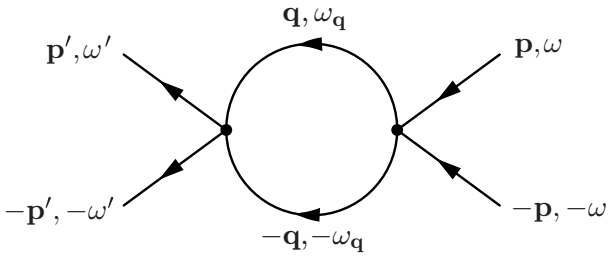

for $\mathbf{p} = \mathbf{0}, \omega = 0$. This in turn requires the knowledge of $\Gamma^{(2,2)}_{\kappa\,(\mathbf{p}',\omega';-\mathbf{p}',-\omega';\mathbf{p},\omega;-\mathbf{p},-\omega)}$ for general $\mathbf{p}', \omega', \mathbf{p}, \omega$.

The identity

$$\Gamma^{(2,2)}_{\kappa\,(\mathbf{0},0;\mathbf{0},0;\mathbf{p},\omega;-\mathbf{p},-\omega)} = \frac{2}{(2\pi)^4}\Gamma^{(1,2)}_{\kappa\,(\mathbf{0},0;\mathbf{p},\omega;-\mathbf{p},-\omega)}\,, \tag{5.43}$$

which holds at the microscopic scale $\kappa = \infty$, is evidently conserved along the renormalization group flow. Thus, by the same string of arguments as for one-site objects, it suffices to calculate the (2,2)-vertex function $\Gamma^{(2,2)}_{\kappa\,(\mathbf{p}',\omega';-\mathbf{p}',-\omega';\mathbf{p},\omega;-\mathbf{p},-\omega)}$, with the important difference however that in general this vertex function will depends explicitly on both of the momenta $\mathbf{p}'$ and $\mathbf{p}$

$$\Gamma^{(2,2)}_{\kappa\,(\mathbf{p}',\omega';-\mathbf{p}',-\omega';\mathbf{p},\omega;-\mathbf{p},-\omega)} \equiv \frac{4VT}{(2\pi)^{16}}\lambda(\mathbf{p}',\mathbf{p})\,. \tag{5.44}$$

Notice that there is no dependence on ω' and ω. We obtain

$$\partial_\kappa \lambda_\kappa(\mathbf{p}', \mathbf{p}) = 2\tilde{\partial}_\kappa \int_{\mathbf{q},\omega} \lambda_\kappa(\mathbf{p}', \mathbf{q}) \frac{1}{R_\kappa(\mathbf{q}) + q^2 + i\omega} \frac{1}{R_\kappa(\mathbf{q}) + q^2 - i\omega} \lambda_\kappa(\mathbf{q}, \mathbf{p}) \,, \tag{5.45}$$

where $\tilde{\partial}_\kappa$ acts only on the κ-dependence of R_κ. With our usual cutoff function $R_\kappa(\mathbf{q}) = (\kappa^2 - \epsilon(\mathbf{q}))\Theta(\kappa^2 - \epsilon(\mathbf{q}))$ this evaluates to

$$\partial_\kappa \lambda_\kappa(\mathbf{p}', \mathbf{p}) = 2 \int_{\mathbf{q}} \lambda_\kappa(\mathbf{p}', \mathbf{q}) \lambda_\kappa(\mathbf{q}, \mathbf{p}) \frac{\Theta(\kappa^2 - \epsilon(\mathbf{q}))}{\kappa^3} \,. \tag{5.46}$$

In position space

$$\partial_\kappa \lambda_\kappa(\mathbf{x}, \mathbf{y}) = 2 \int_{\mathbf{q}} \lambda_\kappa(\mathbf{x}, \mathbf{q}) \lambda_\kappa(\mathbf{q}, \mathbf{y}) \frac{\Theta(\kappa^2 - \epsilon(\mathbf{q}))}{\kappa^3} \,, \tag{5.47}$$

which may be rewritten as

$$\partial_\kappa \lambda_\kappa(\mathbf{x}, \mathbf{y}) = 2 \sum_z \lambda_\kappa(\mathbf{x}, \mathbf{z}) \left(\mathcal{P}_1 \circ \lambda_\kappa\right)(\mathbf{z}, \mathbf{y}) \tag{5.48}$$

$$= 2 \sum_z \left(\mathcal{P}_2 \circ \lambda_\kappa\right)(\mathbf{x}, \mathbf{z}) \lambda_\kappa(\mathbf{z}, \mathbf{y}) \,, \tag{5.49}$$

where the projections $\mathcal{P}_1$ and $\mathcal{P}_2$ are defined by

$$\left(\mathcal{P}_1 \circ \lambda_\kappa\right)(\mathbf{z}, \mathbf{y}) = \int_{\mathbf{q}} \exp(i\mathbf{q} \cdot \mathbf{z}) \lambda_\kappa(\mathbf{q}, \mathbf{y}) \Theta(\kappa^2 - \epsilon(\mathbf{q})) \,, \tag{5.50}$$

and

$$\left(\mathcal{P}_2 \circ \lambda_\kappa\right)(\mathbf{x}, \mathbf{z}) = \int_{\mathbf{q}} \exp(i\mathbf{q} \cdot \mathbf{z}) \lambda_\kappa(\mathbf{x}, \mathbf{q}) \Theta(\kappa^2 - \epsilon(\mathbf{q})) \,. \tag{5.51}$$

The initial condition is $\lambda_\infty(\mathbf{x}, \mathbf{y}) = \lambda(\mathbf{x}) \delta_{\mathbf{x},\mathbf{y}}$.

For numerical calculations it is an important simplification that the support of $\lambda_\kappa(\mathbf{x}, \mathbf{y})$ is contained in $S \times S$, where S is the support of $\lambda(\mathbf{x})$. This statement immediately follows from Eq. (5.47).

5.7 Three Types of Exact Flow Equations

By now we have arrived at three types of flow equations for the macroscopic decay rate. We began with the case of local, one-point objects, whose flow equation (5.20) has already been shown to be exact. The treatment in the last section of extended objects, which led to Eqs. (5.46,5.47,5.48,5.49), was rigorous as well. We have employed Eq. (5.32,5.33) as an approximation for extended objects. We shall now provide the proof that in certain cases these equations are indeed exact.

Suppose that the kernel $\lambda_\kappa(\mathbf{x}) = \sum_{\mathbf{y}} \lambda_\kappa(\mathbf{x}, \mathbf{y}) = \sum_{\mathbf{y}} \lambda_\kappa(\mathbf{y}, \mathbf{x})$ can be described by only one degree of freedom, i.e. on its support S, the reaction kernel $\lambda_\kappa(\mathbf{x})$ is a constant (for fixed scale κ) and all the elements of the support are equivalent, in the sense that under rotations and

reflections that conserve the symmetry of the lattice, the kernel is also conserved. This is the case, for example, for the surface of a sphere or the two kernels depicted in Figure 5.6.

According to Eq. (5.48)

$$\partial_\kappa \lambda_\kappa(\mathbf{x}) = 2\sum_{\mathbf{z}} \lambda_\kappa(\mathbf{x},\mathbf{z}) \sum_{\mathbf{y}} (\mathcal{P}_1 \circ \lambda_\kappa)(\mathbf{z},\mathbf{y}) = 2\sum_{\mathbf{z}\in S} \lambda_\kappa(\mathbf{x},\mathbf{z})(\mathcal{P}\circ\lambda_\kappa)(\mathbf{z})\,. \tag{5.52}$$

Exploiting the symmetry our kernel, $(\mathcal{P}\circ\lambda_\kappa)(\mathbf{z})$ is a constant on S. Thus the sum is trivial and we recover Eq. (5.33) which also implies Eq. (5.32).

5.8 Three-Particle Coagulation

Finally we turn to the question if we can exploit our findings to particle decay with three (or more) reactants. Consider, for instance, diffusing particles that undergo the reaction $3A \to A$ with rate λ (or equivalently $3A \to 2A$, or $3A \to \varnothing$). The reaction part of the action is given by

$$\mathcal{S}_\lambda[\bar\psi,\psi] = \int \mathrm{d}\mathbf{x}\,\mathrm{d}t\,\lambda\left[\bar\psi(\mathbf{x},t)^3\psi(\mathbf{x},t)^3 + 3\bar\psi(\mathbf{x},t)^2\psi(\mathbf{x},t)^3 + 2\bar\psi(\mathbf{x},t)\psi(\mathbf{x},t)^3\right], \tag{5.53}$$

in the continuum limit. Along the same lines as for the binary reaction $A + A \to A$, the renormalization group flow creates terms $\sim \bar\psi(\mathbf{x},t)^m\psi(\mathbf{x},t)^n$ with $n \geq 3$, $n \geq m \geq 1$. Above the critical dimension $d_c = 1$ these terms can be neglected to leading order [76, 77]. Curiously however, the initial terms, corresponding to vertices with three incoming legs, are not renormalized, because one cannot construct one-loop diagrams with three incoming legs from the available vertices. This seemingly implies that the macroscopic rate μ equals the microscopic rate λ,

$$\mu = \lambda_\kappa = \lambda\,. \tag{5.54}$$

But this cannot possibly be true: Similar as for binary coagulation, c.f. Section 3.5, we can obtain an upper bound for the effective, macroscopic decay rate. Suppose, for instance, we have a cubic lattice, where the particles hop with diffusion constant D to one of their nearest neighbors and coagulate instantaneously, $\lambda = \infty$. On one site there can be at most two particles. For an upper limit of the reaction rate, we can neglect anti-correlation and instead assume that the occupation of different lattice sites is uncorrelated. Then for low densities, the squared density ρ^2 is the probability to find two particles on a particular lattice site. If from one of the six neighboring sites a particle hops onto this site, there occurs the coagulation reaction, implying the kinetic equation $\partial_t\rho = -12D\rho^3$ and an effective reaction rate of $6D$. This is to be compared with the mean-field solution $\partial_t\rho = -2\lambda\rho^3$. Thus the reaction rate is diffusion limited and cannot be larger than $6D$ so that evidently there is a flaw in the renormalization group calculation. (Obviously, the same problem occurs for coagulation reactions involving more than three particles.)

In fact, the reason why NPRG fails for the action of Eq. (5.53) has already been discussed in Section 3.4. To prove that at the ultraviolet cutoff Λ the effective average action $\Gamma_{\kappa=\Lambda}$ equals the action $\mathcal{S}$, it was demanded that $\mathcal{S}$ is only quadratic in $\bar\psi$. The fact that the approach fails here shows that this is indeed a necessary requirement. A way to work around

this problem is to exploit that every multi-particle reaction can be broken down to a set of binary reaction (from a microscopic point of view it is, in fact, rather realistic that there is a transient, unstable formation of two particles, before a third particle attaches [57]). In our case we could replace the three particle coagulation $3A \to A$ by the two reaction $2A \to B$, $A + B \to A$, thus introducing further particles B, which stand for a complex of two particles A. The corresponding action then fulfills the requirements for the initial condition, Eq. (3.74), to hold. However, we did not pursue this approach in our work.

5.9 Conclusion

Above the critical dimension $d_c = 2$, to lowest order the kinetics of the coagulation process $A + A \to A$ is determined by the macroscopic decay rate μ. As opposed to the case below the critical dimension, the long time behavior is not only determined by long range fluctuations. Rather, fluctuations at all scales κ decrease the microscopic decay rate $\lambda > \mu$. Therefore, details in the shape and size of the particles, and the dispersion relation (which determines the structure of the lattice) have a strong impact on the kinetics. The Wetterich equation allows us to systematically integrate the contribution of the fluctuations, thus establishing an exact relation between the microscopic physics and the effective physics at the macroscopic scale. We solved this relation for a number of concrete realizations of the model. Objects on discrete lattices lend themselves very well to stochastic simulations (as opposed to objects in continuous space), which allowed us to empirically confirm the equation for the macroscopic decay rate to high accuracy. Finally, we showed that a naive adaption to three (and more) particle interaction is impossible, because the initial condition for the Wetterich equation is invalidated.

6 Violation of the Law of Mass Action in Three and Higher Dimensions

The law of mass action is the fundamental law in chemical reaction kinetics. It states that the rate of an elementary reaction is proportional to the product of the concentrations of the participating molecules. In a seminal article that helped lay the foundations of a stochastic theory of chemical reaction kinetics, Smoluchowski provided a framework for calculating the proportionality factor of the law of mass action, the macroscopic decay rate, and supported the validity of this law for three-dimensional systems [54, 63]. In the 1980s much effort was put in studying low dimensional systems, where it was found that strong correlations can lead to deviations from the law of mass action [59, 60, 62, 146, 147]. This anomalous behavior was observed, in particular, for the classical problem of coalescence, $A + A \to A$, where diffusing particles clot upon contact with a rate λ. By an approach designed for one dimension, one could even obtain exact solutions [67, 68]. This was complemented by results of the perturbative renormalization group at and below the critical dimension $d_c = 2$ [76, 77]. In contrast to this progress in low dimensions, advances for three-dimensional coagulation systems have remained largely elusive. In the experimental analysis, the law of mass action is still the "gold standard" [55, 57, 83]. Indeed, it has obtained further support by field theoretic analysis proving the validity of Smoluchowski's heuristic arguments for asymptotically long times and low densities [64, 166, 174–176]. In this regime the density ρ obeys the law of mass action rate equation $\partial_t \rho = -\mu\rho^2$, with a macroscopic decay rate μ which is a function of the microscopic rate λ and of the size and shape of the particles.

Having devoted the last chapter to the calculation of the macroscopic decay rate μ, by establishing a relation between the microscopic physics and the macroscopic physics, we now study the implications of fluctuations on the validity of the law of mass action. We first show that the density fulfills a generalized equation of motion, $\partial_t \rho = -F(\rho)$, where the non-equilibrium "force" F is derived from the effective potential Γ, the non-equilibrium analog of a thermodynamic potential. For low densities we recover the result from the law of mass action, $F(\rho) \approx \mu\rho^2$. However, for finite densities we find that there are marked deviations from the law of mass action, which become more pronounced as the density is increased. The most relevant additional term $c(\mu)\rho^{5/2}$ can be attributed to long range and many-particle fluctuations. Strikingly, $c(\mu)$ is a simple, universal function of the macroscopic rate μ. It depends on the microscopic features of the lattice and the particles only indirectly through its argument μ. This universality is remarkable since the system is not critical, as, for instance, in the analysis of the low dimensional systems ($d < 2$) of Chapter 4. The extra term is corroborated by stochastic lattice simulations. We will further discuss higher order contributions to the kinetic equation. Just as the first two terms, they can be separated in two groups: Non-universal contributions, depending on the concrete realization of the model, and universal contributions which are created by long range fluctuations and many-particle

couplings. Finally, we will show how our findings can be generalized to arbitrary dimensions $d > d_c = 2$. Parts of this chapter are found in our article "On the validity of the law of mass action in three-dimensional coagulation process", which was published in Physical Review Letters [167].

6.1 The Kinetic Equation

In the previous chapters we treated the "classical" regime, where the particle decay is determined by the law of mass action, such that the time evolution of the density obeys the rate equation $\partial_t \rho(t) = -\mu \rho(t)^2$, whereas the central formula in Chapter 4 was $\partial_t \rho(t) = -c_d \rho(t)^{\frac{d}{2}}$ (with some d-dependent, but otherwise universal factor c_d), which determines the anomalous kinetics below the critical dimension. In this chapter we intend to go beyond the lowest order in the kinetic equation. To this end we first derive from our field theoretic formalism the general kinetic equation governing the decay in a system with a particle density that is homogenous in space.

The effective average action Γ_κ can be written in an expansion in the fields $\bar{\psi}$, ψ, and multiple derivatives in space and time thereof [111]. For our purposes, we only need to consider the time evolution of homogeneous fields, i.e. $\psi(\mathbf{x}, t) \equiv \psi(t)$. This discards derivatives in space. Neglecting also derivatives in time except for the term $\bar{\psi}\partial_t\psi$, which is already present in the initial action, the general form of the effective average action then reads

$$\Gamma_\kappa[\bar{\psi}, \psi] = \sum_{\mathbf{x}} \int \mathrm{d}t \, U_\kappa(\bar{\psi}(\mathbf{x}, t), \psi(t)) + \sum_{\mathbf{x}} \int \mathrm{d}t \, \bar{\psi}_{\mathbf{x}}(t) \partial_t \psi(t) \,,$$

with the local potential U_κ, which can be defined for constant fields $\bar{\psi}, \psi$ by $\Gamma_\kappa[\bar{\psi}, \psi] = VT\, U_\kappa(\bar{\psi}, \psi)$, and with the volume in space and time $V = \sum_{\mathbf{x}}$, $T = \int \mathrm{d}t$. (Strictly speaking $\sum_{\mathbf{x}}$ is only the volume if the volume of an elementary cell is one. This, in particular, is the case for a cubic lattice with lattice spacing $a = 1$, which we usually consider.) The extremal principle (see Eq. (3.93)) yields

$$0 = \left. \frac{\delta \Gamma[\bar{\psi}, \rho]}{\delta \bar{\psi}(\mathbf{x}, t)} \right|_{\bar{\psi}=0} = \partial_{\bar{\psi}} U_{\kappa=0}(\bar{\psi}, \rho)|_{\bar{\psi}=0} + \partial_t \rho \,. \tag{6.1}$$

With the non-equilibrium force

$$F(\rho) = \partial_{\bar{\psi}} U_{\kappa=0}(\bar{\psi}, \rho)|_{\bar{\psi}=0} \,, \tag{6.2}$$

this gives the kinetic equation

$$\partial_t \rho(t) = -F(\rho(t)) \,. \tag{6.3}$$

The non-equilibrium force F can be determined directly in the simulations, by introducing homogeneous particle input with rate J. This gives rise to a term $J \sum_{\mathbf{x}} \int \mathrm{d}t \bar{\psi}(\mathbf{x}, t)$ in the effective action $\Gamma[\bar{\psi}, \psi]$. From the extremal principle it follows that $\partial_t \rho = -F(\rho) + J$, such that for stationary states the non-equilibrium force equals the input rate, $F(\rho) = J$, exactly. We remark that these stationary states created by constant particle input are not only interesting because of their implications on time-dependent systems, but also of direct relevance for experiments [177].

6.2 Universal Correction in Three Dimensions

To study the corrections to the law of mass action, let us represent the non-equilibrium force as the limit of a power series

$$F(\rho) = \lim_{\kappa\to 0} \sum_{n\geq 2} \frac{1}{n!} g_\kappa^{(1,n)} \rho^n \,, \tag{6.4}$$

exploiting the fact that Γ_κ is analytic if $\kappa > 0$ [111]. The lowest order coefficient $g_\kappa^{(1,2)} = 2\lambda_\kappa$ was treated in the previous chapter and converges to a constant value, the macroscopic decay rate $\mu = \frac{1}{2} g_{\kappa=0}^{(1,2)}$. Thus, assuming that the higher order terms $\frac{1}{n!} g_\kappa^{(1,n)} \rho^n$ $(n > 2)$ can be neglected, we would recover $F(\rho) = \mu\rho^2$. It is interesting that the most relevant term beyond $\frac{1}{2} g_{\kappa=0}^{(1,2)} \rho^2 = \mu\rho^2$ is not $\frac{1}{3!} g_{\kappa=0}^{(1,3)} \rho^3$ as one might naively expect. Rather, in three dimensions *all* coefficients $g_\kappa^{(1,n)}$ $(n > 2)$ turn out to diverge as κ goes to zero. In the following analysis, we show that the infinite sum of these diverging terms converges and gives the finite contribution $\sum_{n\geq 3} \frac{1}{n!} g_\kappa^{(1,n)} \rho^n \sim \rho^{\frac{5}{2}}$.

According to Eq. (6.2), the non-equilibrium force F contains only the terms of first order in the response field $\bar{\psi}$ of the Taylor expansion of the effective potential

$$U_\kappa(\bar{\psi}, \psi) = \sum_{m,n} \frac{1}{m!n!} g_\kappa^{(m,n)} \bar{\psi}^m \psi^n \,, \tag{6.5}$$

whose flow is determined by the Wetterich equation. As discussed in Chapter 4, the flow for each coupling $g_\kappa^{(m,n)}$ is associated with a one-loop diagram, where n is the number of incoming and m the number of outgoing legs. Thus, the flow of the physically relevant couplings $g_\kappa^{(1,n)}$ of the non-equilibrium force F is calculated from diagrams with n incoming and one outgoing leg. To lowest order, their divergency stems from the contribution to the flow of diagrams which only contain (1,2)- and (2,2)-vertices and follows from power counting. Let us exemplify this for the (1,3)-coupling $g_\kappa^{(1,3)}$, with the associated one-loop diagram

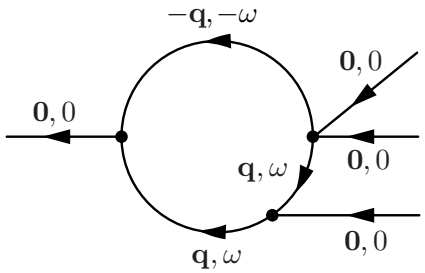

For any finite scale κ, also the couplings must be finite. Therefore, the divergency in κ of $g_\kappa^{(1,3)}$ is created in the limit of small κ, where only long wavelength and short frequency fluctuations, $q \lesssim \kappa$, and $\omega \lesssim \kappa^2$, contribute to the flow. From the previous chapter, we know that in three dimension the (1,2)- and (2,2)-vertex functions are not divergent for $\kappa = \mathbf{q} = \omega = 0$, but attain a finite value, which is equal to the macroscopic decay rate μ, up to an irrelevant constant factor. (The vertex functions corresponding to the left vertex in the above diagram, and the one for the top right vertex were treated in Section 5.2. Up to some constant factor

they equal the renormalized decay rate $\lambda_\kappa(\mathbf{q})$. The vertex function for the bottom right vertex reads $\Gamma^{(1,2)}_{\kappa\,(\mathbf{q},\omega;\mathbf{q},\omega;\mathbf{0},0)}$.) Since the vertex functions are continuous, we can take their value at $\kappa = \mathbf{q} = \omega = 0$, if we are only interested in the strongest divergence. The evaluation of the diagram then yields

$$\partial_\kappa g_\kappa^{(1,3)} = \frac{1}{2}\tilde{\partial}_\kappa 16 \int_{\mathbf{q},\omega} G_\kappa(\mathbf{q},\omega)^2 G_\kappa(-\mathbf{q},-\omega)\mu^3\,, \tag{6.6}$$

where, as usual, the macroscopic reaction decay rate $\mu := \mu(\mathbf{q}=0)$. The propagator reads

$$G_\kappa(\mathbf{q},\omega) = \frac{1}{\left(\kappa^2-\epsilon(\mathbf{q})\right)\Theta\left(\kappa^2-\epsilon(\mathbf{q})\right)+\epsilon(\mathbf{q})+i\omega}\,, \tag{6.7}$$

where we have inserted the standard cutoff function $R_\kappa(\mathbf{q}) = (\kappa^2-\epsilon(\mathbf{q}))\Theta\left(\kappa^2-\epsilon(\mathbf{q})\right)$. (Our results are of course independent of the choice of the cutoff function.) Due to the derivative $\tilde{\partial}_\kappa = \partial_\kappa R_\kappa \cdot \partial_{R_\kappa}$, the integration is restricted to the domain $\epsilon(\mathbf{q}) < \kappa^2$, where the propagator is independent of $\mathbf{q}$, i.e.

$$\tilde{\partial}_\kappa \int_{\mathbf{q}} = \tilde{\partial}_\kappa \int_{\epsilon(\mathbf{q})<\kappa^2}\,, \tag{6.8}$$

such that within the domain of integration the propagator simplifies to

$$G_\kappa(\mathbf{q},\omega) = \frac{1}{\kappa^2+i\omega}\,. \tag{6.9}$$

The fact that the integral, Eq. (6.6), does not depend on the full reaction kernel $\mu(\mathbf{q})$, already indicates that these divergencies cannot depend on the shape and size of the objects: Originating in long wavelength fluctuations around $q = 0$, they do not resolve the details of the reaction kernel.

For small κ, the dispersion relation $\epsilon(\mathbf{q})$ can be approximated by the "continuum limit" $\epsilon(\mathbf{q}) \approx Dq^2 = q^2$ (with diffusion constant $D = 1$). Therefore, the divergencies are not only unaffected by the shape and size of the particles, but also independent of the structure of the lattice; it is as if the divergent terms only "see" structureless point particles (for which $\mu(\mathbf{q}) = \mu$, independent of the momentum) that are embedded in continuous space (where according to Eq. (3.58), $\epsilon(\mathbf{q}) = q^2$). The integration over the momentum $\mathbf{q}$ then approximately yields the volume of the three-dimensional ball, $\frac{4}{3}\pi\kappa^3$ with radius κ, multiplied by the factor $1/(2\pi)^3$ from the definition of the integration in Fourier space. Thus, up to some constant factor, Eq. (6.6) becomes

$$\partial_\kappa g_\kappa^{(1,3)} = \mu^3\kappa^3 \int_\omega \partial_\kappa \frac{1}{\left(\kappa^2+i\omega\right)^2\left(\kappa^2-i\omega\right)} = \mu^3\kappa^3 \int \mathrm{d}\nu\, \frac{\kappa^2}{\left(1+i\nu\right)^2\left(1-i\nu\right)} \partial_\kappa \left(\frac{1}{\kappa^2}\right)^3\,. \tag{6.10}$$

In the integral we substituted $\frac{\omega}{\kappa^2} = \nu$. Thus,

$$\partial_\kappa g_\kappa^{(1,3)} \sim c\mu^3\kappa^5 \partial_\kappa \left(\frac{1}{\kappa^2}\right)^3 = c'\mu^3\kappa^{-2}\,, \text{ and } g_\kappa^{(1,3)} \sim c''\mu^3\kappa^{-1}\,, \tag{6.11}$$

for some constants c, c', c''

In summary, and generalizing to arbitrary couplings, the strongest divergency of a diagram is obtained by the following prescription. Each propagator gives a factor

$$G_\kappa(\mathbf{q},\omega) \sim \frac{1}{\kappa^2}\,. \tag{6.12}$$

The resulting divergency is attenuated by the integration over the momenta $\mathbf{q}$ and frequencies

$$\int_{\mathbf{q}} \sim \kappa^3\,, \quad \int_{\omega} \sim \kappa^2\,, \tag{6.13}$$

where in the left hand formula the exponent 3 is simply the dimension. Finally, the lowest order contribution in κ of the vertices must be multiplied with the result, in particular (1,2)- and (2,2)-vertices give rise to the constant factor $\mu \sim \kappa^0$.

To further illustrate this mehod, let us consider a second diagram that contributes to the coupling $g^{(1,3)}$,

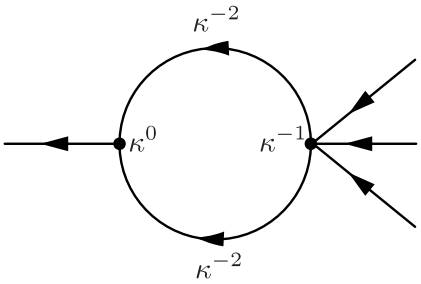

According to our prescription, this gives a term of order κ^0, which should be compared to the κ^{-1} divergency for the diagram which contains only (1,2)-vertices. (Actually, this diagrams contributes a term $\sim \ln(\kappa)$ which diverges, if only logarithmically. The reason is that, strictly speaking, one needs to perform the derivative by $\tilde{\partial}_\kappa$, which produces another factor κ^{-1}, before the flow is integrated over κ. For divergencies of order $\kappa^{-\alpha}$ with $\alpha > 0$, the two operations cancel, but here they imply a logarithmic factor.)

It is now straightforward to determine the strongest divergencies of the couplings $g_\kappa^{(m,n)}$. We need to consider the one-loop diagrams with n incoming and m outgoing legs that contain only (1,2)- (2,2)-vertices. Clearly, they contain n of these vertices, connected by n propagators, which gives a factor $\mu^n\kappa^{-2n}$. After integrating over the momenta and frequencies, c.f. Eq. (6.13), this gives a divergency for $g_\kappa^{(m,n)}$ of the order κ^{5-2n} ($n > 2$, $m \le n$). Diagrams with higher order vertices can be neglected. Suppose, for instance, that such a one-loop diagram contains a $(1,n')$-vertex ($n' > 2$), which contributes a factor $\kappa^{5-2n'}$. However, if we replace this vertex by a string of $n'-1$ (1,2)-vertices, connected one by one with $n'-2$ propagators, for instance if

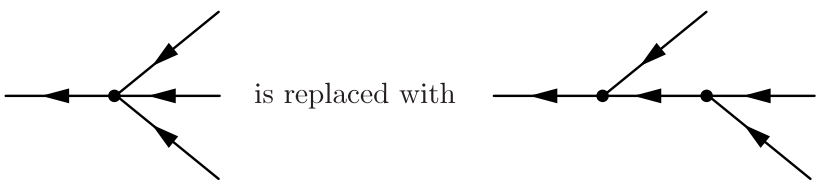

this gives the more relevant factor $\kappa^{-2(n'-2)}$.

Let us look at the prefactors of the divergencies more carefully. The one-loop diagrams are created upon functional derivatives of $\ln\left(\hat{\Gamma}_\kappa^{(2)}[\bar{\psi},\psi]+\hat{R}_\kappa\right)$ at $\bar{\psi}=\psi=0$, c.f. Eq. (4.11). Thus, every additional vertex affords a further differentiation of the propagator $\left(\hat{\Gamma}_\kappa^{(2)}[\bar{\psi},\psi]+\hat{R}_\kappa\right)^{-1}$. This can be effected with the formula [111]

$$\partial M^{-1} = -M^{-1}\partial M M^{-1}\,, \tag{6.14}$$

for some functional M (in our case $M=\hat{\Gamma}_\kappa^{(2)}[\bar{\psi},\psi]+\hat{R}_\kappa$). Thus, every propagator comes with a factor -1 so that

$$g^{(m,n)} \sim \begin{cases} -c_{m,n}\mu^n/\kappa^{2n-(d+2)} & \text{if } n \text{ even},\\ +c_{m,n}\mu^n/\kappa^{2n-(d+2)} & \text{if } n \text{ odd}, \end{cases}$$

for positive constants $c_{m,n}$.

The fact that we have an alternating sequence is not surprising, given that, quite generally, one also obtains such sequences when one takes the Taylor expansion, of the non-analytic function x^α for a non-integer $\alpha>0$ around, say, $x=1$. Indeed, we are on the lookout for such non-analytic terms. The infinite sum of diverging terms can be written as

$$\sum_{n\geq 3}\frac{1}{n!}g_\kappa^{(1,n)}\rho^2 \sim \kappa^5 f\left(\frac{\mu\rho}{\kappa^2}\right)\,, \tag{6.15}$$

for some scaling function f. Since for large systems the non-equilibrium force must become independent of the system size, corresponding to the reciprocal scale κ^{-1}, one obtains

$$f(x) \sim c x^{\frac{5}{2}}\,, \tag{6.16}$$

for some constant c. This adds a non-analytic term $\sim c(\mu\rho)^{\frac{5}{2}}$ to the force F.

Let us finally exploit our findings to calculate this term *exactly* from the Wetterich equation. We choose the ansatz

$$\Gamma_\kappa[\bar{\psi},\psi] = \sum_x \int \mathrm{d}t\, U_\kappa(\bar{\psi},\psi) + \mathcal{S}_{\epsilon_\kappa=\epsilon} + \mathcal{S}_{Z_\kappa=1}\,, \tag{6.17}$$

with the diffusion term $\mathcal{S}_{\epsilon_\kappa}\int_{\mathbf{q},\omega}\epsilon_\kappa(\mathbf{q})\bar{\psi}(-\mathbf{q},-\omega)\psi(\mathbf{q},\omega)$, where ϵ_κ is the renormalized dispersion relation, and the term $\mathcal{S}_{Z_\kappa}=\sum_{\mathbf{x}}\int \mathrm{d}t Z_\kappa\bar{\psi}(\mathbf{x},t)\partial_t\psi(\mathbf{x},t)$ for the time evolution, where Z_κ is the field amplitude. From the reaction part of the microscopic action, see Eq. (5.27), it follows that the initial condition for the effective average potential $U_{\kappa=\infty}(\bar{\psi},\psi)=\lambda\bar{\psi}^2\psi^2+\lambda\bar{\psi}\psi^2$, with $\lambda=\lambda(\mathbf{q}=0)=\sum_{\mathbf{x}}\lambda(\mathbf{x})$. According to our above discussion the renormalization group flow for ϵ_κ and Z_κ vanishes, and that Eq. (6.17) includes all the terms needed to determine the correction exactly. The local potential U_κ is related to the non-equilibrium force via $F(\rho)=\partial_{\bar{\psi}}U_0(\bar{\psi},\rho)|_{\bar{\psi}=0}$. Its flow is governed by Eq. (5.10), which for convenience is restated here

$$\partial_\kappa U_\kappa[\bar{\psi},\psi] = \frac{\widetilde{\mathcal{V}}_3(\kappa)\kappa\left(U_\kappa^{(1,1)}[\bar{\psi},\psi]+\kappa^2\right)}{\sqrt{\left(U_\kappa^{(1,1)}[\bar{\psi},\psi]+\kappa^2\right)^2 - U_\kappa^{(2,0)}[\bar{\psi},\psi]U_\kappa^{(0,2)}[\bar{\psi},\psi]}}\,, \tag{6.18}$$

where $\widetilde{\mathcal{V}}_3(\kappa) = \int_{\mathbf{q}} \Theta(\kappa^2 - \epsilon(\mathbf{q})) \sim \frac{4}{3}\pi \left(\frac{\kappa}{2\pi}\right)^3$. Since we are interested in long range fluctuations, i.e. small κ, we may replace the reciprocal volume $\widetilde{\mathcal{V}}_3(\kappa)$ in in this equation by $\frac{4\pi}{3(2\pi)^3}\kappa^3$. Further substituting

$$U_\kappa(\bar{\psi}, \psi) \to \mu\bar{\psi}^2\bar{\psi}^2 + \mu\bar{\psi}\psi^2\,, \tag{6.19}$$

on the right side of Eq. (6.18) then yields for the renormalized non-equilibrium force $F_\kappa = \frac{\partial U_\kappa(\bar{\psi}=0,\psi)}{\partial\bar{\psi}}$,

$$\partial_\kappa F_\kappa(\rho) \approx \frac{\mu^2\kappa^4\rho^2}{3\pi^2\left(\kappa^2 + 2\mu\rho\right)^2}\,. \tag{6.20}$$

Although this equation is not exact, it still delivers the correct non-analytic contribution $\sim \rho^{\frac{5}{2}}$, because it treats all the terms which give rise to it exactly. Indeed, integrating Eq. (6.20) from any $\kappa = \Lambda > 0$ to $\kappa = 0$ yields a contribution $\frac{\mu^{\frac{5}{2}}}{2\sqrt{2}\pi}\rho^{\frac{5}{2}}$ to the non-equilibrium force F.

It should be remarked that the correction term can also be obtained by a perturbative calculation (we thank K. Wiese for pointing out this solution to us). Assuming that the relevant diagrams which need to be resummed are of the form

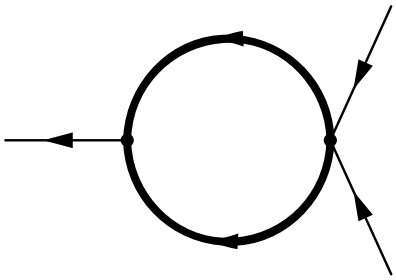

with the response function

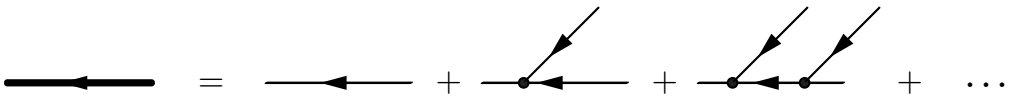

one finds a contribution

$$-\int_{\mathbf{q}}\int_{t>0} \mathrm{d}t\, e^{-t(q^2+2\mu\psi)}\bar{\psi}\psi^2\mu^2\,.$$

In writing this we have replaced the vertices by their macroscopic value μ. Thus again there arises the correction $\frac{\mu^{\frac{5}{2}}}{2\sqrt{2}\pi}\rho^{5/2}$ to F.

Overall we find for the non-equilibrium force (exact up to higher orders in ρ):

$$F(\rho) = \mu\rho^2 + \frac{\mu^{\frac{5}{2}}}{2\sqrt{2}\pi}\rho^{\frac{5}{2}}\,. \tag{6.21}$$

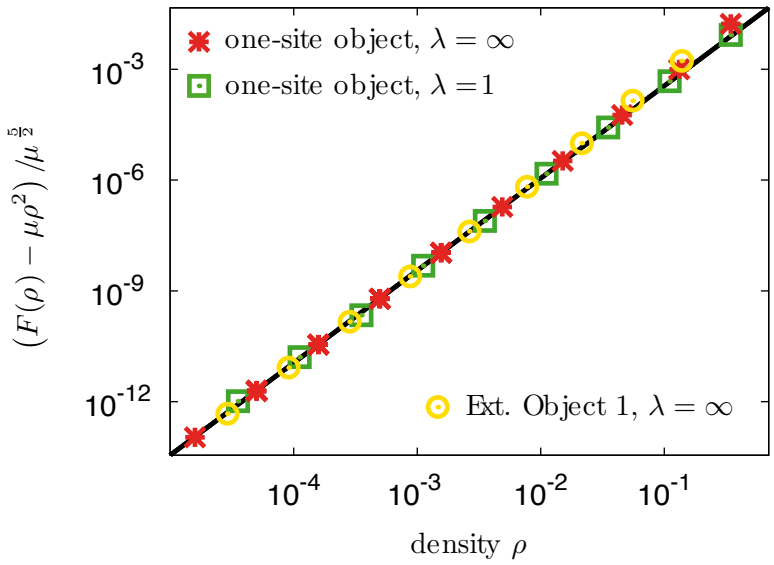

Figure 6.1: Rescaled data for the universal correction to the non-equilibrium force F. In the stochastic simulations, F was determined directly by introducing homogeneous particle input and considering stationary states. On this double logarithmic plot, we show the rescaled data for $\left(F(\psi) - \mu\rho^2\right)/\mu^{\frac{5}{2}}$ for a range of models. We predict this term to be of the universal form $\rho^{\frac{5}{2}}/\left(2\sqrt{2}\pi\right)$ (solid black line), independent of the model, cf. Eq. (6.21). The data evidently corroborate our theoretical results. For instantaneous reactions ($\lambda = \infty$) there are slight deviations from the curve for densities close to the maximum value of one. Extended object 1 is a discretization of the sphere made up of seven sites. Together with a further extended object (Extended Object 2), it was discussed in the Section 5.5. The data for extended object 2 is in excellent agreement with the theory as well, but not shown here for clarity.

We have run simulations for a range of different models (one-site objects with both finite and infinitely large reaction rates, and two examples of extended objects that react immediately on contact), cf. Fig. 4, which clearly corroborate our theoretical findings.

Eq. (6.21) holds for diffusion with diffusion constant $D = 1$. More generally, we can allow for anisotropic diffusion, where to lowest order in the momentum, the expansion of the dispersion relation along its principal axes reads $\epsilon(\mathbf{q}) = \sum_{\nu=1}^{3} D_\nu q_\nu^2$. Then the reciprocal volume behaves as

$$\widetilde{\mathcal{V}}_3(\kappa) = \int_{\mathbf{q}} \Theta(\kappa^2 - \epsilon(\mathbf{q})) \sim \frac{4}{3}\pi \prod_{\nu=1}^{3} \frac{\kappa}{2\pi\sqrt{D_\nu}}\,, \tag{6.22}$$

and our analysis yields

$$F(\rho) = \mu\rho^2 + \frac{\mu^{\frac{5}{2}}}{2\sqrt{2D_1D_2D_3}\pi}\rho^{\frac{5}{2}}\,. \tag{6.23}$$

As a consistency check, consider the case $D_1 = D_2 = D_3 = D$. Since D sets the time scale, the force F should depend linearly on D. This is indeed recovered for the correction term in Eq. (6.23), if we exploit that μ must also depends linearly on D.

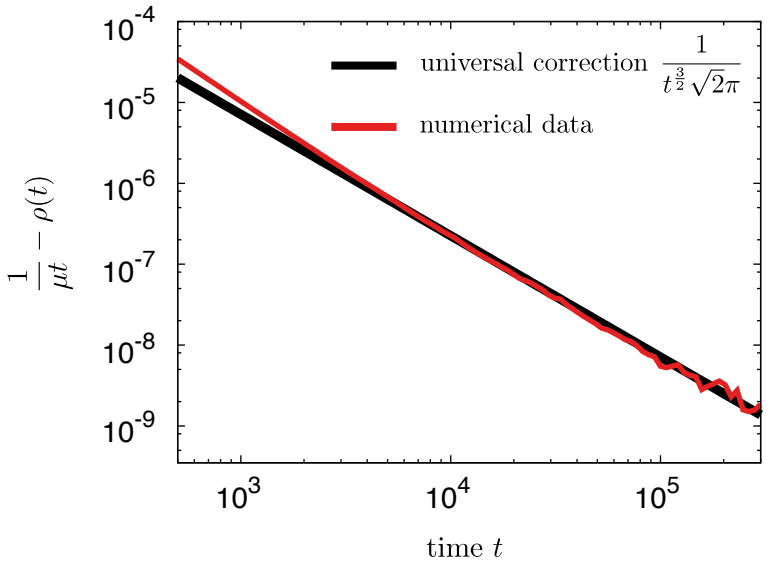

Figure 6.2: Deviation of the long time decay of the particle density from classical behavior $\rho(t) = \frac{1}{\mu t}$ that would follow from the law of mass action. Our findings show that long range and many-particle interaction imply a universal correction term which is independent of the microscopic physics, such that $\rho(t) = \frac{1}{\mu t} - \frac{1}{\sqrt{2}\pi t^{\frac{3}{2}}}$, up to order t^{-2}. The numerical data was obtained for a cubic lattice with instantaneous coagulation ($\lambda = \infty$), starting from a randomly distributed state with density $\rho(t = 0) = 0.01$.

For the time-dependent solution, starting from some finite density at time $t = 0$, we obtain for isotropic diffusion with diffusion constant $D = 1$

$$\rho(t) = \frac{1}{\mu t} - \frac{1}{\sqrt{2}\pi t^{\frac{3}{2}}}\,, \tag{6.24}$$

up to terms of order t^{-2}. This is corroborated by the data of our numerical simulations, c.f. Figure 6.2. Strikingly the additional term of order $t^{-\frac{3}{2}}$ is universal, and, in contrast to the correction term to non-equilibrium force F, it is independent of the macroscopic decay rate μ.

6.3 Universal and Non-Universal Effects in Arbitrary Dimensions

In the following, we analyze the impact of the interplay between the microscopic features (i.e. the lattice structure, the shape of the particles and their size) and long range fluctuations on the effective, macroscopic description of the kinetics. We argue that the microscopic structure is encoded in the effective action Γ by an infinite set of non-universal Taylor coefficients, each associated with the convergent part of an (m, n)-vertex function $\Gamma_\kappa^{(m,n)}$, which can be Taylor expanded not only if $\kappa > 0$ but also at $\kappa = 0$. These coefficients can, in principle, be calculated by the NPRG approach, in analogy to the calculation of the reaction kernel $\mu(\mathbf{q}) = \mu(\mathbf{q} = 0) + \frac{1}{2}\partial_{q_1}^2\mu(\mathbf{q} = 0)q_1^2 + \ldots$ in Chapter 5 (notice that the kernel should be

symmetric under reflection at the origin, so that $\mu(\mathbf{q}) = \mu(-\mathbf{q})$ and the Taylor expansion contains only even terms). The reaction kernel is related to $\Gamma_\kappa^{(1,2)}$, which converges as long as the dimension $d > d_c = 2$. We will show that, in addition to these non-analytic terms, there are contributions which stem from infinite sums of divergent terms in the Taylor expansion of Γ_κ, analogous to Eq. (6.15). It will be demonstrated that each of these sums only depends on a finite number of non-universal Taylor coefficients. Thus, the effective action $\Gamma[\bar{\psi}, \psi]$ can be expressed as a universal function of the non-universal coefficients, as a blueprint, as it were, of all possible realizations of the system.

6.3.1 Analysis up to the First Correction Caused by Long Range Fluctuations

Here we focus on the study of the effective potential $U(\bar{\psi}, \psi) = \frac{1}{TV}\Gamma[\bar{\psi}, \psi]$ (for homogenous fields $\bar{\psi}(\mathbf{x}, t) \equiv \bar{\psi}$, $\psi(\mathbf{x}, t) = \bar{\psi}$, and the volumes of space and time, V and T, respectively). From the previous section we know that in three dimensions, in additions to the non-universal terms $\mu\bar{\psi}^2\psi^2 + \mu\bar{\psi}\psi^2$, there is a term $\frac{\mu^{\frac{5}{2}}}{2\sqrt{2}\pi}\bar{\psi}\psi^{\frac{5}{2}}$, which originates in long wavelength, high frequency fluctuations. Let us now generalize this result to arbitrary dimension $d > 2$.

Adapting the prescription of the last section, c.f. Eqs. (6.12,6.13), the lowest order divergency of a coefficient $g_\kappa^{(m,n)}$ in the expansion (6.5) of the effective average potential U_κ is obtained from the corresponding one-loop diagrams with only (1,2)- and (2,2)-vertices. As discussed in the previous section, to each propagator we need to attribute a factor $-\kappa^{-2}$, and a factor κ^d for the integration over $\mathbf{q}$ and another κ^2 for the integration over ω. Furthermore, to obtain the flow $\partial_\kappa g_\kappa^{(m,n)}$, we need to perform the derivative $\tilde{\partial}_\kappa$, which gives another factor κ^{-1}. (The integration usually cancels with the $\tilde{\partial}_\kappa$ derivative, but implies a logarithmic contribution if $\partial_\kappa g_\kappa^{(m,n)}$ diverges as κ^{-1}.) The one-loop diagram for the coefficient $g_\kappa^{(m,n)}$ has n incoming and m outgoing legs, and is comprised of n propagators, $n-m$ (1,2)-vertices and m (2,2)-vertices. Thus, the coefficient behaves as

$$\partial_\kappa g_\kappa^{(m,n)} \sim \tilde{c}_{m,n} \left(\frac{-1}{\kappa^2}\right)^n \kappa^d \kappa^2 \kappa^{-1} \lambda_\kappa^n \,, \tag{6.25}$$

for a positive constant $\tilde{c}_{m,n}$. From Chapter 4 we know that below the critical dimension λ_κ behaves as κ^{d-2}. Thus, as long as $d < 2$ the coefficients $g_\kappa^{(m,n)}$ diverge in agreement with their scaling dimension $\kappa^{2+(1-n)d}$. In contrast, above the critical dimension, λ_κ converges to a constant value μ and we conclude that

$$g_\kappa^{(m,n)} \sim (-1)^{n+1} c_{m,n} \begin{cases} \kappa^0 & \text{if } 2n-(d+2) < 0\,, \\ \mu^n \ln(\kappa) & \text{if } 2n-(d+2) = 0\,, \\ \mu^n \kappa^{(d+2)-2n} & \text{if } 2n-(d+2) > 0\,. \end{cases} \tag{6.26}$$

In analogy to the previous section, to determine the corrections to the potential $U(\bar{\psi}, \psi)$ that are induced by these most divergent terms, one needs to sum up

$$\sum_{n>d/2+1} g_\kappa^{(m,n)} \bar{\psi}^m \psi^n \sim \sum_{n \geq d/2+1} \frac{(-1)^{n+1} c_{m,n} \mu^n}{\kappa^{2n-(d+2)}} \bar{\psi}^m \psi^n = \kappa^{d+2} \bar{\psi}^m f_\kappa\left(m, \frac{\mu\psi}{\kappa^2}\right), \tag{6.27}$$

for some function f_κ. When the system is large, the potential must be independent of the system size $\sim 1/\kappa$. This suggests

$$f_\kappa\left(m,x\right) \sim c_m \cdot x^{\frac{d}{2}+1}\,,$$

for some constants c_m, implying that the infinite sum of diverging terms int Eq. (6.27) attains the value $c_m \mu^{\frac{d}{2}+1}\bar{\psi}^m \psi^{\frac{d}{2}+1}$. In fact, we cannot strictly rule out that the sum does depend on κ. If so, however, the κ-dependent term must cancel with some other correction term (or terms) to the potential. Actually, this can rectify the problem of the logarithmic correction in even dimension. Assuming that

$$f_\kappa\left(m,x\right) \sim c_m \cdot x^{\frac{d}{2}+1}\ln(x)\,, \tag{6.28}$$

for even dimensions d, then the sum in Eq. (6.27), in addition to a κ-independent term $c_m\bar{\psi}^m(\mu\psi)^{\frac{d}{2}+1}\ln(\mu\psi)$, gives rise to a term $-2c_m\bar{\psi}^m(\mu\psi)^{\frac{d}{2}+1}\ln(\kappa)$. This term can cancel with the term that is logarithmic in κ, c.f. Eq. (6.26).

The concrete solution of the Wetterich equation shows that this is indeed the case. It is obtained upon replacing

$$U_\kappa(\bar{\psi},\psi) \to \lambda_{\kappa=0}\bar{\psi}^2\psi^2 + \lambda_{\kappa=0}\bar{\psi}\psi^2 = \mu\bar{\psi}^2\psi^2 + \mu\bar{\psi}\psi^2\,, \quad \widetilde{\mathcal{V}}(\kappa) \to \frac{4}{3}\pi\left(\frac{\kappa}{2\pi}\right)^3\,, \tag{6.29}$$

in Eq. (6.18). For simplicity, we restrict ourselves to the physically meaningful terms $\sim\bar{\psi}$, i.e. we only calculate the non-equilibrium force F. Thus, integrating Eq. (6.18), we find that the long range fluctuation around $\kappa = 0$ give rise to a term

$$-\frac{\pi^{1-\frac{d}{2}}}{\Gamma\left(\frac{d}{2}\right)\sin\left(\frac{\pi d}{2}\right)}\left(\frac{\mu\psi}{2}\right)^{\frac{d}{2}+1}\,, \tag{6.30}$$

(where Γ denotes the Γ-function and not the average action) which is valid for a real-valued dimension d, as long as it is not an even natural number. We notice that the correction alternates its sign, from a positive contribution in 3 dimensions, to a negative in 5 dimensions, and so on. As d approaches an even number, the result diverges, indicating logarithmic correction term. In four and six dimensions, for instance, we find that a term

$$-\frac{\mu^3\psi^3\ln(\mu\psi)}{8\pi^2}\,, \quad \frac{\mu^4\psi^4\ln(\mu\psi)}{32\pi^3}\,, \tag{6.31}$$

respectively, is added to the force F.

Let us summarize the implications of our findings to the non-equilibrium force $F(\rho)$. The higher the dimensions, the less impact long range fluctuations have on the kinetics. Up to order $n = \frac{d}{2}+1$ the coefficients $g_\kappa^{(1,n)}$ converge to a finite, non-universal value and give a contribution $\frac{1}{n!}g_{\kappa=0}^{(1,n)}\rho^n$. The leading order term, which stems from modes of long wavelengths and slow frequencies, behaves as $(\mu\rho)^{\frac{d}{2}+1}$ and $(\mu\rho)^{\frac{d}{2}+1}\ln(\rho)$, for odd and even dimension d, respectively.

6.3.2 The General Picture

By our analysis we can also study higher order corrections to the effective potential. Again, we confine ourselves to the physically relevant terms $\sim \bar{\psi}$ which determine the non-equilibrium force F. Let us start with the non-universal terms, which give analytic contributions. In the previous subsection, we already mentioned the non-universal terms which come from convergent coefficients $g_{\kappa=0}^{(1,n)}$, $n < d/2+1$. For divergent terms, the non-universal contributions can, at least in principle, be obtained by simply subtracting the divergent part of the flow. For instance, in three dimensions the coupling $g_\kappa^{(1,3)}$ has a divergency $\sim \frac{8\mu^3}{\pi^2\kappa}$, but the difference $g_\kappa^{(1,3)} - \frac{8\mu^3}{\pi^2\kappa}$ goes to a constant, non-universal term. This adds to F a contribution of the order ρ^3, and by the same token, for a general n, the convergent part of $g_\kappa^{(1,n)}$ gives rise to a term of the order ρ^n. The prefactor to these terms are non-universal and can only be obtained by integrating $g_\kappa^{(1,n)}$ over the complete flow.

In addition, there are terms which originate in divergencies that sum up to give finite contributions to the flow. These divergencies are caused by long range fluctuations ($\kappa \to 0$) and are functions of the non-universal coefficients. We have already treated the most relevant of these terms $\sim c(\mu)\rho^{\frac{d+2}{2}}$. It comes from one-loop diagrams with n incoming legs and one outgoing leg which only contain (1,2)- and (2,2)-vertices, and diverge as κ^{d+2-2n}. This infinite sum of diverging terms can be expressed as $\kappa^{d+2} f\left(\frac{\mu\rho}{\kappa^2}\right)$ (see Eq. (6.27)) and implies a contribution of order $\rho^{\frac{d+2}{2}}$ (with logarithmic correction in even dimensions) to F. If in these most divergent diagrams, two vertices connected by a propagator are replaced with a (1,3)- or a (2,3)-vertex, the one-loop diagram only gives rise to divergencies of the order κ^{2d-2n}. In analogy to the previous subsection, the infinite sum of all diagrams can be written as

$$\kappa^{2d}\bar{\psi}^m g\left(\frac{\mu\rho}{\kappa^2}\right) , \tag{6.32}$$

suggesting a contribution of order ρ^d. Indeed, by integrating Eq. (6.18) for three dimensions, we find that these divergent terms add up to a contribution

$$\frac{4\mu^4 \ln(\rho)\rho^3}{3\pi^4} , \tag{6.33}$$

to the non-equilibrium force F. Furthermore, by the same token, also the sums over the diagrams which contain exactly one (1,4)-vertex, or one (1,5), etc. but otherwise only (1,2)- and (2,2)-vertices, imply contributions of order ρ^d.

Let us define the difference $\epsilon = d - d_c = d - 2 > 0$. The lowest order contribution of divergent terms, which comes from diagrams that contain exclusively (1,2)- and (2,2)-vertices behaves as $\rho^{2+\frac{\epsilon}{2}}$, the next contribution, from diagrams with exactly one vertex that has three and more incoming legs, as $\rho^{2+2\frac{\epsilon}{2}}$, and for diagrams with exactly l vertices that have more then two incoming legs, we expect a term that behaves as

$$\rho^{2+l\frac{\epsilon}{2}} . \tag{6.34}$$

As we approach the critical dimension $\epsilon \to 0$, all these terms approach the order of the mass action term $\sim \mu\rho^2$. Together with Ingo Homrighausen and Erwin Frey, we currently analyze

the strong deviations which such terms give rise to. This is done studying the coagulation model with Lévy Flights [149, 178–180], which alter the critical dimension so that a small difference $\epsilon = d - d_c$ can be realized by one- or two-dimensional lattices and our findings can be compared with stochastic simulations.

For concreteness, let us again consider the three-dimensional case for the remainder of this section. The divergent terms treated so far arise from the lowest order terms in κ of the coefficients $g_\kappa^{(m,n)}$. However, we expect that in addition to a term of order κ^{5-2n} there are terms of higher order, κ^{5-2n+1}, κ^{5-2n+2}, and so on. (We remark they do not necessarily have to be divergent, but can also go to zero with κ or to a finite value.) Along the same lines as above this implies contributions of the form $\rho^{\frac{5+l}{2}}$ (up to possible logarithmic corrections) for a natural number l. As an example, consider the renormalized decay rate $\lambda_\kappa = \mu + \kappa\mu'(\kappa = 0) + \ldots$ It is easily verified that the derivative $\mu'(\kappa = 0)$ is a universal function of μ, namely $\mu' = \frac{\mu^2}{12\pi^2}$. Integrating Eq. (6.18) we find that diagrams with only (1,2)- and (2,2)-vertices, where we insert $\kappa\mu'(\kappa)$ for exactly one of the vertices, sum up to a term

$$-\frac{\mu^4\rho^3\ln\rho}{6\pi^4}\,, \tag{6.35}$$

to the non-equilibrium force F.

Similarly, the expansion in the momenta $\mathbf{q}$ and frequencies ω of non-universal terms implies higher order corrections. For instance, let us assume that the dispersion relation can be expanded as $\epsilon(\mathbf{q}) = q^2 + \epsilon^{(4)}\sum_{\nu=1}^3 q_\nu^4 + \ldots$ For the reciprocal volume $\widetilde{\mathcal{V}}_3(\kappa)$ in Eq. (6.18) this gives,

$$\widetilde{\mathcal{V}}_3(\kappa) = \int_{\mathbf{q}} \Theta(\kappa^2 - \epsilon(\mathbf{q})) \sim \frac{4}{3}\pi\left(\frac{\kappa}{2\pi}\right)^3 + c(\epsilon^{(4)})\sum_{\nu=1}^d \kappa^5 + \ldots\,, \tag{6.36}$$

for some function c. In the non-equilibrium force F this implies, in particular, a term $f(\mu, \epsilon^{(4)})\rho^{7/2}$. As a second example, suppose the expansion of the macroscopic decay rate reads $\mu(\mathbf{q}) = \mu(\mathbf{q} = \mathbf{0}) + \mu^{(2)}\sum_{\nu=1}^3 q_\nu^2 + \ldots$, then there arises a term of the form $g(\mu, \mu^{(2)})\rho^{7/2}$.

In summary our analysis suggests an expansion of the form

$$F(\rho) = \sum_{i\geq 2}\frac{1}{i!}c_i\rho^i + \sum_{j\geq 4}\tilde{c}_{\frac{j}{2}}\rho^{\frac{j}{2}}\,. \tag{6.37}$$

The c_i are non-universal coefficients which can only be obtained by integrating over the full renormalization group flow, from $\kappa = \infty$ to $\kappa = 0$. The $\tilde{c}_{j/2}$ are universal functions of a finite number of such non-universal coefficients, and are induced by divergencies around $\kappa = 0$. (Strictly speaking, we must also allow for analytic logarithmic corrections multiples of $\ln(\rho)$ to $\tilde{c}_{j/2}$. Also notice that in addition to the coefficients c_i, there exist further non-universal coefficients which determine the universal factors $\tilde{c}_{j/2}$, as for instance $\mu^{(2)}$ from the above expansions of $\mu(\mathbf{q})$ and $\epsilon(\mathbf{q})$, respectively.) The larger j the more non-universal coefficients enter in the function $\tilde{c}_{j/2}$. While the lowest order term $\tilde{c}_{5/2}$ only depends on $\mu(\mathbf{q} = 0)$ and on the diffusion constant $D = \partial_{q_\nu}^2\epsilon(\mathbf{q} = 0)$ (which for isotropic diffusion is independent of the coordinate ν and which we normally set to one), for higher order terms we require further non-universal coefficients, in particular we must know the momentum dependence macroscopic reaction kernel $\mu(\mathbf{q})$ and of the dispersion relation $\epsilon(\mathbf{q})$ up to a

certain order. Thus, the microscopic details (large q) of the macroscopic reaction kernel $\mu(\mathbf{q})$ and the dispersion relation $\epsilon(\mathbf{q})$ (which determines the lattice structure) have more and more impact as the order in ρ of the terms becomes higher. The first terms in the expansion read

$$\begin{aligned} F(\rho) = \mu\rho^2 + \tilde{c}_{\frac{5}{2}}(D,\mu)\rho^{\frac{5}{2}} + \tilde{c}_3(D,\mu,\ln(\rho))\,\rho^3 + c_3\rho^3 + \\ + \tilde{c}_{\frac{7}{2}}\left(D,\epsilon^{(4)},\mu,\mu^{(2)},\ln(\rho)\right)\rho^{\frac{7}{2}} + \ldots \end{aligned} \tag{6.38}$$

6.4 Conclusion

The central result of the chapter is that the non-equilibrium force is given by (exact up to higher orders in ρ):

$$F(\rho) = \mu\rho^2 + \frac{\mu^{\frac{5}{2}}}{2\sqrt{2}\pi}\rho^{\frac{5}{2}}\,. \tag{6.39}$$

This equation bears a new fundamental insight: Beyond the law of mass action term, quadratic in the density, the non-equilibrium force driving the reaction kinetics contains a non-analytic term violating the law of mass action. Similar as for critical phenomena, long wavelength fluctuations and many-particle interactions are the physical origin of this term. Unlike in critical dynamics, the anomalous power law is not governed by a renormalization group flow close to a fixed point but is a genuine strong coupling result. In contrast to low-dimensional systems the three-dimensional coagulation process is not critical. Nevertheless, we find that the term violating the law of mass action is a *universal* function of the macroscopic decay rate μ. From our theoretical analysis we anticipate this to be a generic feature of reaction-diffusion processes in three dimensions with upper critical dimension $d_c = 2$.

A possible candidate to test our theoretical predictions experimentally is exciton luminescence. These systems have been previously used to investigate low-dimensional reaction kinetics. By accurate measurements of the fusion of excitons, anomalous behavior was observed in an effectively one-dimensional system [71, 72]. We expect that our prediction of a strong violation of the law of mass action could be revealed with similar kinds of experiments for three-dimensional systems. In addition, we believe that our theoretical results will stimulate further experimental activities to explore the fundamental implications of fluctuations and correlations on reaction kinetics, and to map out the range of validity of the law of mass action.

A Smoluchowski Theory for Finite Coagulation Rates in Three Dimensions

In this appendix we calculate the macroscopic decay rate μ of the coagulation process for finite microscopic reaction rates λ, following Smoluchowski's approach, discussed in Section 1.2. Relative to the test particle, the surrounding particles effectively diffuse with diffusion constant $2D$, where D is the actual diffusion constant. Once a particle is within a distance R of the test particle, it is destroyed with rate λ. Thus, the density of the particle field obeys

$$0 \equiv \partial_t \rho(\mathbf{x},t) = \begin{cases} 2D\nabla^2\rho(\mathbf{x},t) - \lambda\rho(\mathbf{x},t) & \text{if } \mathbf{x} < R\,, \\ 2D\nabla^2\rho(\mathbf{x},t) & \text{if } \mathbf{x} > R\,. \end{cases} \tag{A.1}$$

The initial condition is

$$\rho(\mathbf{x}, t=0) = \rho_0\,. \tag{A.2}$$

It is adequate to switch to spherical coordinates. Equation (A.1) then reads,

$$0 \equiv \begin{cases} \frac{2D}{r^2}\partial_r\left(r^2\partial r\rho(r)\right) - \lambda\rho & \text{if } r < R\,, \\ \frac{2D}{r^2}\partial_r\left(r^2\partial r\rho(r)\right) & \text{if } r > R\,. \end{cases} \tag{A.3}$$

Far away from the origin, the density will be the initial density, $\rho(|\mathbf{x}|,t) = \rho_0$. Thus,

$$\rho(r) = \begin{cases} c_{<,1}\frac{\exp\left[-(r-R)\sqrt{\frac{\lambda}{2D}}\right]}{r} + c_{<,2}\frac{\exp\left[(r-R)\sqrt{\frac{\lambda}{2D}}\right]}{r} & \text{if } r < R\,, \\ \rho_0 + \frac{c_>}{r} & \text{if } r > R\,. \end{cases} \tag{A.4}$$

Two of the three unknowns $c_{<,1}, c_{<,2}, c_>$ are determined by the continuity of the density and its flux at the boundary of the test particle $r = R$,

$$\lim_{r\nearrow R}\rho(r) = \lim_{r\searrow R}\rho(r)\,, \quad \lim_{r\nearrow R}\rho'(r) = \lim_{r\searrow R}\rho'(r)\,. \tag{A.5}$$

The third condition is that in the stationary state the incoming flux into the sphere of radius R around test particle must be equal to the mean number of reactions taking place in unit time

$$-8\pi D c_> = \int_{|x|<R} \mathrm{d}^3x\,\lambda\rho(\mathbf{x})\,. \tag{A.6}$$

The result is

$$c_{<,1} = \rho_0 \frac{\tanh\left(R\sqrt{\frac{\lambda}{2D}}\right) - 1}{2\sqrt{\frac{\lambda}{2D}}}\,, \tag{A.7}$$

$$c_{<,2} = \rho_0 \frac{\tanh\left(R\sqrt{\frac{\lambda}{2D}}\right) + 1}{2\sqrt{\frac{\lambda}{2D}}}\,, \tag{A.8}$$

$$c_{>} = \rho_0 \left(\frac{\tanh\left(R\sqrt{\frac{\lambda}{2D}}\right)}{\sqrt{\frac{\lambda}{2D}}} - R \right)\,. \tag{A.9}$$

Therefore, the effective reaction rate is given by

$$\mu = -\frac{1}{2}\frac{8\pi D c_{>}}{\rho_0} = 4\pi D \left[R - \sqrt{\frac{2D}{\lambda}} \tanh\left(R\sqrt{\frac{\lambda}{2D}}\right) \right]\,, \tag{A.10}$$

where the factor 1/2 accounts for fact that for coagulation only one of the two reactants is annihilated.

B Leading Correction to the Interface Density of the RPS model with mutations

This appendix is devoted to the calculation of the leading correction to the interface density, which to lowest order is $n = \sqrt{2\mu_l}$ for pure mutations to the predator, and $n = 2\mu_r$ for pure mutations to prey. The analysis in not absolutely rigorous, but treats the effects which causes deviations of order $\mu_l^{3/4}$ and $\mu_r^{3/2}$ more carefully than in Section 2.3.2. The agreement with the stochastic simulation is excellent.

B.1 Mutations to the Predator

Consider the case $\mu_l \ll 1$ and $\mu_r = 0$. We have seen that to lowest order the stationary state is perfectly uncorrelated, such that, say, an interface R annihilates *ballistically*, that is it collides with an L, with rate $\widetilde{n}$. In this case, the decay rate simply is equal to the interface density, $\widetilde{n} = n = \sqrt{2\mu_l}$. Let us assume that also for the leading correction the system is sufficiently uncorrelated such that we can define a decay rate $\widetilde{n}$ (i.e. the probability that an R collides with an L in the next time step is $\widetilde{n}$, independent of when it has been created). We expect that

$$\widetilde{n} = \sqrt{2\mu_l} + \mathcal{O}(\mu_l)\,, \tag{B.1}$$

with a finte limit $\lim_{\mu_l \to 0} \frac{\mathcal{O}(\mu_l)}{\mu_l}$.

In a first step, we calculate the ratio of Rs that annihilate not ballistically but *diffusively*, i.e. via the reaction $RR \to \varnothing L$. Suppose an R is created x sites to the left of the nearest further R to the right (there may only be empty sites and Ls in between them). For instance, if there are no Ls in between, which is the most important case, this looks like

$$\underbrace{R\varnothing \ldots \varnothing}_{x \text{ sites}} R\,. \tag{B.2}$$

Relative to each other, the two interfaces move diffusively, with diffusion constant 1, and thus the two Rs might collide with each other through this diffusional motion. Their expected lifetime (due to ballistic annihilation) is of the order $\frac{1}{n}$, so that the relevant diffusional distances are of the order $\frac{1}{\sqrt{n}}$. Therefore, we may assume $x \ll \frac{1}{n}$ in the following and neglect the possibility of an L in between the two interfaces.

The probability

$$P_{\text{pair}}(x,t) = P_d(x,t) P_b(t)\,, \tag{B.3}$$

that the pair of R interfaces is intact after a time t equals the probability that they have not yet interacted diffusively (a well-known formula in the theory of first passage problems, see e.g. [96]),

$$P_d(x,t) = \frac{2}{\sqrt{\pi}} \int_0^{x/2\sqrt{t}} \mathrm{d}s \; e^{-s^2} \,, \tag{B.4}$$

times the probability that the right R has not yet crashed into an L by ballistic motion, which is equal to

$$P_b(t) = \exp\left(-\widetilde{n}t\right) \,. \tag{B.5}$$

When $x \ll \frac{1}{n}$ the probability $P_R(x)$ that an R interface is created x sites to the left of the next R is $\frac{n}{2} = \frac{\widetilde{n}}{2} + \mathcal{O}(\mu_l)$, since the density of R is $\frac{n}{2}$. Thus the probability that a particle annihilates diffusively becomes

$$-\int_0^\infty \mathrm{d}x \int_0^\infty \mathrm{d}t \, P_R(x) \left(\frac{\partial}{\partial t} P_d(x,t)\right) P_b(t) = -\int_0^\infty \mathrm{d}x \int_0^\infty \mathrm{d}t \, \frac{\widetilde{n}}{2} \left(\frac{\partial}{\partial t} P_d(x,t)\right) P_b(t) = \frac{\sqrt{\widetilde{n}}}{2} \,. \tag{B.6}$$

This holds up to higher order terms in μ_l. In the first equation $P_R(x)$ can be replaced by $\frac{\widetilde{n}}{2}$ because $P_d(x,t)$ and its derivative in time goes to zero on length scales of the order $\frac{1}{\sqrt{n}}$, whereas $P_R(x) = n = \widetilde{n} + \mathcal{O}(\mu_l)$ is valid up to larger length scales.

We now need to determine the decay rate $\widetilde{n}$. To lowest order it can be calculated from $n = 2\mu_l \frac{1}{n}$, and is equal to the interface density, $\widetilde{n} = n$. Here $2\mu_l$ is the input rate for the interfaces and $\frac{1}{n}$ the average time of survival. Since only the fraction $\left(1 - \frac{\sqrt{\widetilde{n}}}{2}\right)$ annihilates diffusively, the input rate for interfaces that annihilate ballistically is $2\mu_l \left(1 - \frac{\sqrt{\widetilde{n}}}{2}\right)$ and we expect that the decay rate can be obtained from

$$\widetilde{n} = \left[2\mu_l \left(1 - \frac{\sqrt{\widetilde{n}}}{2}\right)\right] \frac{1}{\widetilde{n}} \,, \tag{B.7}$$

or, resolving for the density $\widetilde{n}$ up to the first correction in μ_l,

$$\widetilde{n} = \sqrt{2\mu_l \left(1 - \frac{\sqrt{\widetilde{n}}}{2}\right)} = \sqrt{2\mu_l} \left(1 - \frac{\sqrt{\widetilde{n}}}{4}\right) + \mathcal{O}(\mu_l) = \sqrt{2\mu_l} - \frac{2^{3/4}}{4} \mu_l^{3/4} + \mathcal{O}(\mu_l) \,. \tag{B.8}$$

$\widetilde{n}$ is not yet the interface density n that we are looking for. To calculate n we look at the average time of survival $\tau(x)$ of an R interface that is created x sites to the left of the next R. We also introduce the quantity $\tau_b(x)$, which denotes the average time of survival if the interfaces were truly ballistic, in a system with interface density $\widetilde{n}$. We know the average time of survival of these interface, which will eventually be subject to the reaction $RL \to \varnothing\varnothing$, is $\frac{1}{\widetilde{n}}$, i.e.

$$\langle \tau_b \rangle \equiv \int_0^\infty \mathrm{d}x \, P_R(x) \tau_b(x) = \frac{1}{\widetilde{n}} \,. \tag{B.9}$$

When it is created at a short distance, $x \ll \frac{1}{n}$, to the left of the next R, the average time of survival of such an R is $2 \cdot \frac{1}{\widetilde{n}}$, since the right R must be annihilated before the left one can be

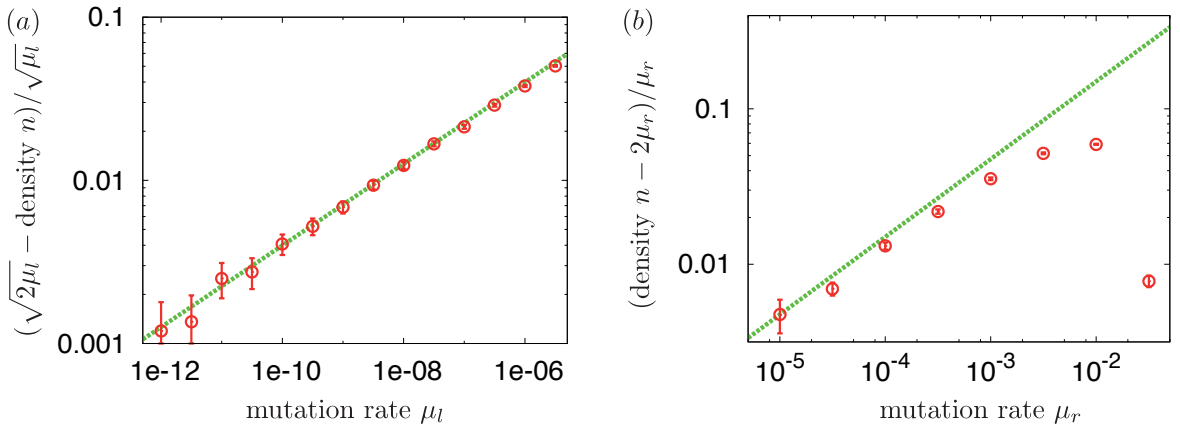

Figure B.1: Double logarithmic plot of the first correction to the interface density versus the mutation rate. In (a) the case of pure mutations to the predator $\mu_l \ll 1, \mu_r = 0$ is shown. According to our analytic result $(\sqrt{2\mu_l} - n)/\sqrt{\mu_l} = \frac{3}{4}2^{3/4}\mu_l^{1/4}$ (dotted green line) up to higher orders in μ_l. This is in excellent agreement with our data (red circles with error bars that are twice the size of the estimated standard deviation). The plot in (b) is for pure mutations to the prey $\mu_l = 0, \mu_r \ll 1$, where our analysis yields $(n - 2\mu_r)/\mu_r = \sqrt{\mu_r}$ (dotted green line). The data (again the red circles with error bars twice the size of the estimated standard deviation) indeed appears to approach the theoretical curve for small μ_r.

destroyed. For a general R, which may also be subject to diffusional annihilation, the average time of survival becomes instead

$$\tau(x) = -\int_0^\infty \mathrm{d}t \left[t \left(\frac{\partial}{\partial t} P_d(x,t) \right) P_b(t) + \left(t + \frac{1}{\widetilde{n}} \right) P_d(x,t) \left(\frac{\partial}{\partial t} P_b(t) \right) \right] . \tag{B.10}$$

(Notice that upon ballistic annihilation of the right R at time t, the left one lives on for $\frac{1}{\widetilde{n}}$ units of time on average, whence the factor $t + \frac{1}{\widetilde{n}}$.) For $x \gg \frac{1}{\sqrt{n}}$, diffusion is negligible, $\tau(x) \equiv \tau_b(x)$, justifying the boundary c in the following integral. Again we remark that when $x \ll \frac{1}{n}$, then $P_R(x) = \frac{n}{2} = \frac{\widetilde{n}}{2} + \mathcal{O}(\mu_l)$. Thus, to lowest order in μ_l, the difference between the average time of survival of an arbitrary interface and one that is going to annihilate ballistically is

$$\langle \tau \rangle - \langle \tau_b \rangle = \int_0^c \mathrm{d}x \, \frac{\widetilde{n}}{2} \left(\tau(x) - \tau_b(x) \right) = \int_0^\infty \mathrm{d}x \, \frac{\widetilde{n}}{2} \left(\tau(x) - \frac{2}{\widetilde{n}} \right) = -\frac{1}{\sqrt{\widetilde{n}}} , \tag{B.11}$$

where $\frac{1}{\sqrt{n}} \ll c \ll \frac{1}{n}$. Therefore, the average time of survival of the particles is

$$\langle \tau \rangle = \frac{1}{\widetilde{n}} - \frac{1}{\sqrt{\widetilde{n}}} . \tag{B.12}$$

Expressing $\widetilde{n}$ in terms of μ_l we finally find for the interface density

$$n = 2\mu_l \langle \tau \rangle = \sqrt{2\mu_l} - \frac{3}{4} 2^{3/4} \mu_l^{3/4} + \mathcal{O}(\mu_l) . \tag{B.13}$$

This is corroborated by the data of our stochastic simulations.

B.2 Mutations to the Prey

Most of the above analysis can also be applied to the case $\mu_l = 0, \mu_r \ll 1$. As discussed in Subsection 2.3.3, a μ_r mutation on an empty stretch of the lattice first gives rise to the pair RL, whose life span is $\frac{1}{2}$. If there is a second mutation at the same site before this pair has decayed, a pair LR is produced. Thus, the effective production rate of this pair is $\frac{\mu_r^2}{2}$ instead of just μ_l for mutations to the predator.

However, for non-zero μ_r, there are two further mechanisms which cannot be neglected, where a pair of R interfaces is created. The first mechanism again concerns the unstable pairs RL, which cover a fraction μ_r of the lattice. In every step that a "free" L moves to the left it can collide with such a pair, $RLL \to RR\varnothing$. Since the density of these Ls is $\frac{\mu_r}{2}$, to lowest order, we effectively have a contribution of $\frac{\mu_r^2}{4}$ to the production of the pair RR. Secondly, we have $\varnothing L \to RR$ with rate μ_r, which gives a contribution of $\frac{\mu_r^2}{2}$ to the effective rate for the production of the pair RR.

For both mechanisms of the production of the pair RR, the two interfaces are initially a distance 1 apart. In most cases they will annihilate with each other after a while, due to their diffusional motion relative to each other. The probability that the right R collides with an L before this happens is

$$-\int_0^\infty \mathrm{d}t \left(\frac{\partial}{\partial t} P_d(1,t)\right) P_b(t) = \frac{\sqrt{\widetilde{n}}}{2} = 1 - \exp\left(-\sqrt{\widetilde{n}}\right) = \sqrt{\widetilde{n}}\,, \tag{B.14}$$

up to higher order terms. Thus, the creation of pairs RR effectively gives rise to the creation of an R with rate $\frac{\mu_r\sqrt{2\mu}}{2}\sqrt{\widetilde{n}}$. Therefore, the analogue of Eq. (B.7) for mutations to the prey reads

$$\widetilde{n} = \left[\mu_r^2\left(1 - \frac{\sqrt{\widetilde{n}}}{2}\right) + \frac{3}{2}\mu_r^2\sqrt{\widetilde{n}}\right]\frac{1}{\widetilde{n}}\,, \tag{B.15}$$

so that

$$\widetilde{n} = \mu_r\sqrt{1+\sqrt{\widetilde{n}}} = \mu_r + \frac{1}{2}\mu_r^{3/2} + \mathcal{O}\big(\mu_r^2\big)\,. \tag{B.16}$$

The time of survival $\langle\tau\rangle$ of an interface created in the "traditional" way, i.e. by a mutation which turns and LR into a pair RL, can be obtained in the same way as for the case of mutations to the predator. Therefore, Eq. (B.12), is valid and yields

$$\langle\tau\rangle = \frac{1}{\mu_r} - \frac{3}{2}\frac{1}{\sqrt{\mu_r}} + \mathcal{O}(1)\,. \tag{B.17}$$

This gives a contribution of

$$\mu_r^2\langle\tau\rangle = \mu_r - \frac{3}{2}\mu_r^{3/2} + \mathcal{O}(\mu_r^2)\,, \tag{B.18}$$

to the interface density n. For interfaces originating in the creation of a pair, say $\varnothing L \to RR$, the life span of the left R, until it either interacts diffusively with the right R or it collides

with an L after the right R (which shields the left R) has annihilated with another L, is given by

$$-\int_0^\infty \mathrm{d}t \left[t \left(\frac{\partial}{\partial t} P_d(1,t) \right) P_b(t) + \left(t + \frac{1}{\widetilde{n}} \right) P_d(1,t) \left(\frac{\partial}{\partial t} P_b(t) \right) \right] = \frac{2}{\sqrt{\widetilde{n}}} + \mathcal{O}(1) = \frac{2}{\sqrt{\mu_r}} + \mathcal{O}(1) \,. \tag{B.19}$$

Since these pairs are produced with a rate $\frac{3}{2}\mu_r^2$ this gives another contribution of $3\mu_r^{3/2}$ to the interface density n.

Finally, the pairs RL contribute a term $\mu_r + \mathcal{O}(\mu_r^2)$: They are created at rate μ_r and destroyed with a rate $2 + \mathcal{O}(\mu_r)$, since $RL \to \varnothing\varnothing$ with rate 2. (With a rate of the order μ_r such an RL it is turned to LR, or gives rise to a pair RR or LL, as described at the beginning of this subsection. For the frequency of the pair RL these transitions only provide corrections of order μ_r^2.) Adding up all the terms for interface density, we obtain

$$n = 2\mu_r + \frac{3}{2}\mu_r^{3/2} \,. \tag{B.20}$$

This is in accordance with the result of the stochastic simulations, see Figure B.1.

Bibliography

[1] S. Sachdev and M. Müller, Quantum criticality and black holes, J. Phys.-Condens. Mat. **21**, 164216 (2009).

[2] A. Einstein, Über die von der molekularkinetischen Theorie der Wärme geforderte Bewegung von in ruhenden Flüssigkeiten suspendierten Teilchen, Ann. Phys. **322**, 549 (1905).

[3] R. Feynman, R. Leighton, and M. Sands, *The Feynman Lectures on Physics*, Addison-Wesley, first edition, 1964.

[4] R. Marro, M. Dickman, *Nonequlibrium Phase Transitions in Lattice Models*, Cambridge University Press, first edition, 1999.

[5] T. M. Liggett, *Interacting Particle Systems*, Springer Verlag, first edition, 1985.

[6] T. M. Liggett, *Stochastic Interacting Systems: Contact, Voter and Exclusion Processes*, Springer Verlag, first edition, 1999.

[7] G. Szabo and G. Fáth, Evolutionary games on graphs, Phys. Rep. **446**, 97 (2007).

[8] V. Torsvik, J. Goksoyr, and F. Daae, High diversity in DNA of soil bacteria., Appl. Environ. Microb. **56**, 782 (1990).

[9] D. Dykhuizen, Santa Rosalia revisited: Why are there so many species of bacteria?, Antonie van Leeuwenhoek **73**, 25 (1998).

[10] M. Loreau, S. Naeem, P. Inchausti, J. Bengtsson, J. Grime, A. Hector, D. Hooper, M. Huston, D. Raffaelli, and B. Schmid, Biodiversity and ecosystem functioning: current knowledge and future challenges, Science **294**, 804 (2001).

[11] G. Hardin, The competitive exclusion principle, Science **131**, 1292 (1960).

[12] G. Gause, *The Struggle for Existence*, Williams & Wilkins, first edition, 1934.

[13] G. Hutchinson, The paradox of the plankton, Am. Nat. **95**, 137 (1961).

[14] M. Kimura, *The Neutral Theory of Molecular Evolution*, Cambridge University Press, first edition, 1983.

[15] T. Miyazaki, K. Tainaka, T. Togashi, T. Suzuki, and J. Yoshimura, Spatial coexistence of phytoplankton species in ecological timescale, Popul. Ecol. **48**, 107 (2006).

[16] J. Hofbauer and K. Sigmund, *Evolutionary Games and Population Dynamics*, Cambridge University Press, first edition, 1998.

[17] M. A. Nowak, *Evolutionary Dynamics*, Belknap Press, first edition, 2006.

[18] E. Frey, Evolutionary game theory: Theoretical concepts and applications to microbial communities, Physica A **389**, 4265 (2010).

[19] L. Frachebourg, P. Krapivsky, and E. Ben-Naim, Segregation in a one-dimensional model of interacting species, Phys. Rev. Lett. **77**, 2125 (1996).

[20] L. Frachebourg, P. Krapivsky, and E. Ben-Naim, Spatial organization in cyclic Lotka-Volterra systems, Phys. Rev. E **54**, 6186 (1996).

[21] A. Provata, G. Nicolis, and F. Baras, Oscillatory dynamics in low-dimensional supports: A lattice Lotka–Volterra model, J. Chem. Phys. **110**, 8361 (1999).

[22] G. Tsekouras and A. Provata, Fractal properties of the lattice lotka-volterra model, Phys. Rev. E **65**, 016204 (2001).

[23] B. Kerr, M. Riley, M. Feldman, and B. Bohannan, Local dispersal promotes biodiversity in a real-life game of rock-paper-scissors, Nature **418**, 171 (2002).

[24] B. C. Kirkup and M. A. Riley, Antibiotic-mediated antagonism leads to a bacterial game of rock-paper-scissors in vivo, Nature **428**, 412 (2004).

[25] T. Reichenbach, M. Mobilia, and E. Frey, Coexistence versus extinction in the stochastic cyclic Lotka-Volterra model, Phys. Rev. E **74**, 051907 (2006).

[26] T. Reichenbach, M. Mobilia, and E. Frey, Mobility promotes and jeopardizes biodiversity in rock-paper-scissors games, Nature **448**, 1046 (2007).

[27] T. Reichenbach, M. Mobilia, and E. Frey, Noise and correlations in a spatial population model with cyclic competition, Phys. Rev. Lett. **99**, 238105 (2007).

[28] J. C. Claussen and A. Traulsen, Cyclic dominance and biodiversity in well-mixed populations, Phys. Rev. Lett. **100**, 058104 (2008).

[29] M. Peltomäki and M. Alava, Three- and four-state rock-paper-scissors games with diffusion, Phys. Rev. E **78**, 031906 (2008).

[30] T. Reichenbach and E. Frey, Instability of spatial patterns and its ambiguous impact on species diversity, Phys. Rev. Lett. **101**, 58102 (2008).

[31] M. Berr, T. Reichenbach, M. Schottenloher, and E. Frey, Zero-one survival behavior of cyclically competing species, Phys. Rev. Lett. **102**, 48102 (2009).

[32] S. Venkat and M. Pleimling, Mobility and asymmetry effects in one-dimensional rock-paper-scissors games, Phys. Rev. E **81**, 021917 (2010).

[33] H. Shi, W.-X. Wang, R. Yang, and Y.-C. Lai, Basins of attraction for species extinction and coexistence in spatial rock-paper-scissors games, Phys. Rev. E **81**, 030901 (2010).

[34] B. Andrae, J. Cremer, T. Reichenbach, and E. Frey, Entropy production of cyclic population dynamics, Phys. Rev. Lett. **104**, 218102 (2010).

[35] S. Rulands, T. Reichenbach, and E. Frey, Threefold way to extinction in populations of cyclically competing species, J. Stat. Mech.-Theory E. , L01003 (2011).

[36] W.-X. Wang, Y.-C. Lai, and C. Grebogi, Effect of epidemic spreading on species coexistence in spatial rock-paper-scissors games, Phys. Rev. E **81**, 046113 (2010).

[37] M. Mobilia, Oscillatory dynamics in rock-paper-scissors games with mutations, J. Theor. Biol. **264**, 1 (2010).

[38] Q. He, M. Mobilia, and U. Täuber, Spatial rock-paper-scissors models with inhomogeneous reaction rates, Phys. Rev. E **82**, 051909 (2010).

[39] A. A. Winkler, T. Reichenbach, and E. Frey, Coexistence in a one-dimensional cyclic dominance process, Phys. Rev. E **81**, 60901 (2010).

[40] A. Dobrinevski and E. Frey, Extinction in neutrally stable stochastic Lotka-Volterra models, Arxiv preprint arXiv:1001.5235 (2010).

[41] L. Jiang, T. Zhou, M. Perc, and B. Wang, Effects of competition on pattern formation in the rock-paper-scissors game, Phys. Rev. E **84**, 021912 (2011).

[42] Y. Li, L. Dong, and G. Yang, The elimination of hierarchy in a completely cyclic competition system, Physica A **391**, 125 (2012).

[43] S. Case, C. Durney, M. Pleimling, and R. Zia, Cyclic competition of four species: Mean-field theory and stochastic evolution, Europhys. Lett. **92**, 58003 (2010).

[44] C. Durney, S. Case, M. Pleimling, and R. Zia, Saddles, arrows, and spirals: Deterministic trajectories in cyclic competition of four species, Phys. Rev. E **83**, 051108 (2011).

[45] C. Johnson and I. Seinen, Selection for restraint in competitive ability in spatial competition systems, P. Roy. Soc. Lond. B Bio. **269**, 655 (2002).

[46] B. Sinervo and C. Lively, The rock-paper-scissors game and the evolution of alternative male strategies, Nature **380**, 240 (1996).

[47] A. Lotka, Contribution to the energetics of evolution, P. Natl. Acad. Sci. U.S.A. **8**, 147 (1922).

[48] V. Volterra, Fluctuations in the abundance of a species considered mathematically, Nature **118**, 558 (1926).

[49] R. May and W. Leonard, Nonlinear aspects of competition between three species, SIAM J. Appl. Math. **29**, 243 (1975).

[50] R. Durrett and S. Levin, Allelopathy in spatially distributed populations, J. Theor. Biol. **185**, 165 (1997).

[51] R. Durrett and S. Levin, Spatial aspects of interspecific competition, Theor. Popul. Biol. **53**, 30 (1998).

[52] T. Czárán, R. Hoekstra, and L. Pagie, Chemical warfare between microbes promotes biodiversity, P. Natl. Acad. Sci. U.S.A. **99**, 786 (2002).

[53] K. Tainaka, Stationary pattern of vortices or strings in biological-systems - lattice version of the Lotka-Volterra model, Phys. Rev. Lett. **63**, 2688 (1989).

[54] M. Smoluchowski, Versuch einer mathematischen Theorie der Koagulationskinetik kolloider lösungen, Z. phys. Chem. **92**, 129 (1917).

[55] R. Zsigmondy, Über Koagulation und Teilchenattraktion, Z. phys. Chem. **92**, 600 (1917).

[56] F. Lai, S. Friedlander, J. Pich, and G. Hidy, The self-preserving particle size distribution for brownian coagulation in the free-molecule regime, J. Colloid interf. Sci. **39**, 395 (1972).

[57] H. Zhou, Rate theories for biologists, Q. Rev. Biophys. **43**, 219 (2010).

[58] T. Waite, Theoretical treatment of the kinetics of diffusion-limited reactions, Phys. Rev. **107**, 463 (1957).

[59] V. Kuzovkov and E. Kotomin, Kinetics of bimolecular reactions in condensed media: critical phenomena and microscopic self-organisation, Rep. Prog. Phys. **51**, 1479 (1988).

[60] R. Kopelman, Fractal reaction kinetics, Science **241**, 1620 (1988).

[61] C. Castelnovo, R. Moessner, and S. L. Sondhi, Thermal quenches in spin ice, Phys. Rev. Lett. **104**, 107201 (2010).

[62] D. Toussaint and F. Wilczek, Particle–antiparticle annihilation in diffusive motion, J. Chem. Phys. **78**, 2642 (1983).

[63] S. Chandrasekhar, Stochastic problems in physics and astronomy, Rev. Mod. Phys. **15**, 1 (1943).

[64] M. Doi, Stochastic theory of diffusion-controlled reaction, J. Phys. A: Math. Gen **9**, 1479 (1976).

[65] D. C. Torney and H. M. Mcconnell, Diffusion-limited reactions in one dimension, J. Phys. Chem. **87**, 1941 (1983).

[66] J. Spouge, Exact solutions for a diffusion-reaction process in one dimension, Phys. Rev. Lett. **60**, 871 (1988).

[67] C. Doering and D. Ben-Avraham, Interparticle distribution functions and rate equations for diffusion-limited reactions, Phys. Rev. A **38**, 3035 (1988).

[68] D. Ben-Avraham, Complete exact solution of diffusion-limited coalescence, A+A to A, Phys. Rev. Lett. **81**, 4756 (1998).

[69] V. Privman, Exact results for diffusion-limited reactions with synchronous dynamics, Phys. Rev. E **50**, 50 (1994).

[70] G. Schütz, Nonequilibrium correlation functions in the A+A to 0 system with driven diffusion, Phys. Rev. E **53**, 1475 (1996).

[71] R. Blakley, C. Martinez, M. Herman, and G. McPherson, Exciton annihilation in one-dimensional inorganic crystals: power dependent luminescence decay curves from (CH3)4NMnCl3 (TMMC), (CH3)4NMnBr3 (TMMB) and CsMnBr3 (CMB), Chem. Phys. **146**, 373 (1990).

[72] R. Kroon, H. Fleurent, and R. Sprik, Diffusion-limited exciton fusion reaction in one-dimensional tetramethylammonium manganese trichloride (TMMC), Phys. Rev. E **47**, 2462 (1993).

[73] A. Srivastava and J. Kono, Diffusion-limited exciton-exciton annihilation in single-walled carbon nanotubes: A time-dependent analysis, Phys. Rev. B **79**, 205407 (2009).

[74] Y. Murakami and J. Kono, Existence of an upper limit on the density of excitons in carbon nanotubes by diffusion-limited exciton-exciton annihilation: Experiment and theory, Phys. Rev. B **80**, 035432 (2009).

[75] Y. Murakami and J. Kono, Nonlinear photoluminescence excitation spectroscopy of carbon nanotubes: exploring the upper density limit of one-dimensional excitons, Phys. Rev. Lett. **102**, 37401 (2009).

[76] L. Peliti, Renormalisation of fluctuation effects in the A+ A to A reaction, J. Phys. A-Math. Gen. **19**, L365 (1986).

[77] B. Lee, Renormalization group calculation for the reaction kA to 0, J. Phys. A-Math. Gen. **27**, 2633 (1994).

[78] E. Melo and J. Martins, Kinetics of bimolecular reactions in model bilayers and biological membranes. a critical review, Biophys. Chem. **123**, 77 (2006).

[79] P. Meakin and H. Stanley, Novel dimension-independent behaviour for diffusive annihilation on percolation fractals, J. Phys. A-Math. Gen. **17**, L173 (1984).

[80] L. Monchick, J. Magee, and A. Samuel, Theory of radiation chemistry. IV. chemical reactions in the general track composed of n particles, J. Chem. Phys. **26**, 935 (1957).

[81] A. Ovchinnikov and Y. Zeldovich, Role of density fluctuations in bimolecular reaction kinetics, Chem. Phys. **28**, 215 (1978).

[82] B. Lee and J. Cardy, Renormalization group study of the A+B to 0 diffusion-limited reaction, J. Stat. Phys. **80**, 971 (1995).

[83] P. Avakian and R. Merrifield, Triplet excitons in anthracene crystals—a review, Mol. Cryst. Liq. Cryst. **5**, 37 (1968).

[84] G. Lipari and A. Szabo, Diffusion-controlled bimolecular reaction rates. the effect of rotational diffusion and orientation constraints, Biophys. J. **36**, 697 (1981).

[85] V. Privman, editor, *Nonequilibrium Statistical Mechanics in One Dimension*, Cambridge University Press, first edition, 1997.

[86] H. Hinrichsen, Nonequilibrium critical phenomena and phase transitions into absorbing states, Adv. Phys. **49**, 815 (2000).

[87] C. Castellano, S. Fortunato, and V. Loreto, Statistical physics of social dynamics, Rev. Mod. Phys. **81**, 591 (2009).

[88] A. Bray, Theory of phase-ordering kinetics, Adv. Phys. **43**, 357 (1994).

[89] R. Blythe, M. Evans, and Y. Kafri, Stochastic ballistic annihilation and coalescence, Phys. Rev. Lett. **85**, 3750 (2000).

[90] A. Winkler, Renormalization arguments on species coexistence far from equilibrium, Diploma thesis, Ludwig-Maximilians-Universität München, 2007.

[91] N. G. van Kampen, editor, *Stochastic Processes in Physics and Chemistry*, North Holland, fourth edition, 2003.

[92] R. Glauber, Time-dependent statistics of the Ising model, J. Math. Phys. **4**, 294 (1963).

[93] G. M. Schütz, *Phase Transitions and Critical Phenomena*, volume 19, Academic Press, first edition, 2001.

[94] D. Ben-Avraham and J. Köhler, Mean-field (n, m)-cluster approximation for lattice models, Phys. Rev. A **45**, 8358 (1992).

[95] K. Tainaka, Vortices and strings in a model ecosystem, Phys. Rev. E (1994).

[96] S. Redner, *A Guide to First-Passage Processes*, Cambridge University Press, first edition, 2001.

[97] C. W. Gardiner, *Stochastic Methods: A Handbook of the Natural and Social Sciences*, Springer Verlag, fourth edition, 2009.

[98] M. Frean and E. Abraham, Rock–scissors–paper and the survival of the weakest, P. Roy. Soc. Lond. B Bio. **268**, 1323 (2001).

[99] B. Drossel and F. Schwabl, Self-organized critical forest-fire model, Phys. Rev. Lett. **69**, 1629 (1992).

[100] W. Mossner, B. Drossel, and F. Schwabl, Computer simulations of the forest-fire model, Physica A **190**, 205 (1992).

[101] B. Drossel, S. Clar, and F. Schwabl, Exact results for the one-dimensional self-organized critical forest-fire model, Phys. Rev. Lett. **71**, 3739 (1993).

[102] B. Drossel, Self-organized criticality and synchronization in a forest-fire model, Phys. Rev. Lett. **76**, 936 (1996).

[103] S. Clar, B. Drossel, and F. Schwabl, Forest fires and other examples of self-organized criticality, J. Phys.-Condens. Mat. **8**, 6803 (1996).

[104] C. Wetterich, Average action and the renormalization group equations, Nucl. Phys. B **352**, 529 (1991).

[105] N. Tetradis and C. Wetterich, Scale dependence of the average potential around the maximum in phi 4 theories, Nucl. Phys. B **383**, 197 (1992).

[106] C. Wetterich, Exact evolution equation for the effective potential, Phys. Lett. B **301**, 90 (1993).

[107] U. Ellwanger, Collective fields and flow equations, Z. Phys. C Part. Fields **58**, 619 (1993).

[108] U. Ellwanger, Flow equations and BRS invariance for Yang-Mills theories, Phys. Lett. B **335**, 364 (1994).

[109] T. Morris, The exact renormalization group and approximate solutions, Int. J. Mod. Phys. A **9**, 2411 (1994).

[110] T. Morris, Derivative expansion of the exact renormalization group, Phys. Lett. B **329**, 241 (1994).

[111] J. Berges, N. Tetradis, and C. Wetterich, Non-perturbative renormalization flow in quantum field theory and statistical physics, Phys. Rep. **363**, 223 (2002).

[112] B. Delamotte, An introduction to the nonperturbative renormalization group, Arxiv preprint cond-mat/0702365 (2007), 56 pages.

[113] F. Wegner and A. Houghton, Renormalization group equation for critical phenomena, Phys. Rev. A **8**, 401 (1973).

[114] K. Wilson and J. Kogut, The renormalization group and the epsilon expansion, Phys. Rep. **12**, 75 (1974).

[115] J. Polchinski, Renormalization and effective lagrangians, Nucl. Phys. B (1984).

[116] G. Golner and E. Riedel, Renormalization-group calculation of critical exponents in three dimensions, Phys. Rev. Lett. **34**, 856 (1975).

[117] A. Hasenfratz and P. Hasenfratz, Renormalization group study of scalar field theories, Nucl. Phys. B **270**, 687 (1986).

[118] N. Tetradis and C. Wetterich, Critical exponents from the effective average action, Nucl. Phys. B **422**, 541 (1994).

[119] H. Ballhausen, J. Berges, and C. Wetterich, Critical phenomena in continuous dimension, Phys. Lett. B **582**, 144 (2004).

[120] B. Delamotte, D. Mouhanna, and M. Tissier, Nonperturbative renormalization-group approach to frustrated magnets, Phys. Rev. B **69**, 134413 (2004).

[121] M. Tissier, B. Delamotte, and D. Mouhanna, Frustrated heisenberg magnets: A nonperturbative approach, Phys. Rev. Lett. **84**, 5208 (2000).

[122] V. L. Berezinskii, Violation of long range order in one-dimensional and two-dimensional systems with a continuous symmetry group., Sov. Phys.-JETP **32**, 493 (1971).

[123] J. Kosterlitz and D. Thouless, Ordering, metastability and phase transitions in two-dimensional systems, J. Phys. C Solid State **6**, 1181 (1973).

[124] J. Kosterlitz, The critical properties of the two-dimensional xy model, J. Phys. C Solid State **7**, 1046 (1974).

[125] L. Canet, Processus de réaction-diffusion et groupe de renormalisation non perturbatif, Ann. Phys. Fr. **29**, 33 (2004).

[126] L. Canet, Reaction–diffusion processes and non-perturbative renormalization group, J. Phys. A-Math. Gen. **39**, 7901 (2006).

[127] L. Canet and H. Chaté, A non-perturbative approach to critical dynamics, J. Phys. A-Math. Theor. **40**, 1937 (2007).

[128] L. Canet, B. Delamotte, O. Deloubrière, and N. Wschebor, Nonperturbative renormalization-group study of reaction-diffusion processes, Phys. Rev. Lett. **92**, 195703 (2004).

[129] L. Canet, H. Chaté, B. Delamotte, I. Dornic, and M. Muñoz, Nonperturbative fixed point in a nonequilibrium phase transition, Phys. Rev. Lett. **95**, 100601 (2005).

[130] L. Canet, H. Chate, B. Delamotte, and N. Wschebor, Nonperturbative renormalization group for the Kardar-Parisi-Zhang equation, Phys. Rev. Lett. **104**, 150601 (2010).

[131] L. Canet, H. Chaté, B. Delamotte, and N. Wschebor, Nonperturbative renormalization group for the Kardar-Parisi-Zhang equation: General framework and first applications, Phys. Rev. E **84**, 061128 (2011).

[132] J. W. Negele and H. Orland, *Quantum Many-Particle Systems*, Westview Press, new edition, 1998.

[133] M. Doi, Second quantization representation for classical many-particle system, J. Phys. A: Math. Gen **9**, 1465 (1976).

[134] Y. B. Zel'dovich and A. A. Ovchinnikov, The mass action law and the kinetics of chemical reactions with allowance for thermodynamic fluctuations of the density, Sov. Phys. JETP **47**, 829 (1978).

[135] P. Grassberger and M. Scheunert, Fockspace methods for identical classical objects, Fortschr. Phys. **28**, 547 (1980).

[136] L. Peliti, Path integral approach to birth-death processes on a lattice, J. Phys.-Paris **46**, 1469 (1985).

[137] U. Täuber, M. Howard, and B. Vollmayr-Lee, Applications of field-theoretic renormalization group methods to reaction–diffusion problems, J. Phys. A-Math. Gen. **38**, R79 (2005).

[138] G. R. Grimmett and D. R. Stirzaker, *Probability and Random Processes*, Oxford University Press, third edition, 2001.

[139] G. Wick, The evaluation of the collision matrix, Phys. Rev. **80**, 268 (1950).

[140] L. Canet, H. Chaté, and B. Delamotte, General framework of the non-perturbative renormalization group for non-equilibrium steady states, J. Phys. A-Math. Theor. **44**, 495001 (2011).

[141] S. Krishnamurthy, R. Rajesh, and O. Zaboronski, Kang-Redner small-mass anomaly in cluster-cluster aggregation, Phys. Rev. E **66**, 066118 (2002).

[142] D. Litim, Optimized renormalization group flows, Phys. Rev. D **64**, 105007 (2001).

[143] F. V. Wijland, K. Oerding, and H. Hilhorst, Wilson renormalization of a reaction-diffusion process, Physica A **251**, 179 (1998).

[144] J. Cardy, *Scaling and Renormalization in Statistical Physics*, Cambridge University Press, first edition, 1996.

[145] S.-K. Ma, *Modern Theory of Critical Phenomena*, Westview Press, first edition, 1976.

[146] K. Kang and S. Redner, Scaling approach for the kinetics of recombination processes, Phys. Rev. Lett. **52**, 955 (1984).

[147] K. Kang and S. Redner, Fluctuation effects in Smoluchowski reaction kinetics, Phys. Rev. A **30**, 2833 (1984).

[148] K. Kang and S. Redner, Fluctuation-dominated kinetics in diffusion-controlled reactions, Phys. Rev. A **32**, 435 (1985).

[149] D. Vernon, Long range hops and the pair annihilation reaction A+A to 0: Renormalization group and simulation, Phys. Rev. E **68**, 041103 (2003).

[150] M. Moshe, Recent developments in Reggeon field theory, Phys. Rep. **37**, 255 (1978).

[151] D. J. Amit, *Field Theory, the Renormalization Group and Critical Phenomena*, World Scientific, third edition, 2005.

[152] J. Zinn-Justin, *Quantum Field Theory and Critical Phenomena*, Oxford University Press, fourth edition, 2002.

[153] M. Le Bellac, *Quantum and Statistical Field Theory*, Clarendon Press, first edition, 1992.

[154] M. Beccaria, B. Allés, and F. Farchioni, Coherent-state path-integral simulation of many-particle systems, Phys. Rev. E **55**, 3870 (1997).

[155] J.-C. Lin, Symmetry between diffusion-limited coagulation and annihilation, Phys. Rev. A **43**, 5714 (1991).

[156] D. Balboni, P.-A. Rey, and M. Droz, Universality of a class of annihilation-coagulation models, Phys. Rev. E **52**, 6220 (1995).

[157] M. Henkel, E. Orlandini, and G. Schutz, Equivalences between stochastic systems, J. Phys. A-Math. Gen. **28**, 6335 (1995).

[158] H. Simon, Concentration for one and two-species one-dimensional reaction-diffusion systems, J. Phys. A-Math. Gen. **28**, 6585 (1995).

[159] F. Family and J. Amar, Diffusion-annihilation and the kinetics of the ising model in one dimension, J. Stat. Phys. (1991).

[160] J. Adams, J. Berges, S. Bornholdt, F. Freire, N. Tetradis, and C. Wetterich, Solving non-perturbative flow equations, Arxiv preprint hep-th/9507093 (1995).

[161] W. H. Press, S. A. Teukolsky, W. T. Vetterling, and B. P. Flannery, *Numerical Recipes in C: The Art of Scientific Computing*, Cambridge University Press, second edition, 1992.

[162] G. Hämmerlin and K.-H. Hoffmann, *Numerische Mathematik*, Springer Verlag, second edition, 1991.

[163] M. Bramson and D. Griffeath, Asymptotics for interacting particle systems on Z d, Z. Wahrscheinlichkeit **53**, 183 (1980).

[164] M. Droz and L. Sasvári, Renormalization-group approach to simple reaction-diffusion phenomena, Phys. Rev. E **48**, 2343 (1993).

[165] B. B. Mandelbrot, *The Fractal Geometry of Nature*, Henry Holt, second edition, 2000.

[166] A. S. Mikhailov and V. Yashin, Quantum field methods in the theory of diffusion-controlled reactions, J. Stat. Phys. **38**, 347 (1985).

[167] A. A. Winkler and E. Frey, Validity of the law of mass action in three-dimensional coagulation processes, Phys. Rev. Lett. **108**, 108301 (2012).

[168] H. Kim and K. Shin, Single species diffusion-influenced reaction A+A to alpha A: Validity of the smoluchowski approach, Phys. Rev. E **61**, 3426 (2000).

[169] C. Kittel, *Introduction to Solid State Physics*, Wiley John & Sons, eighth edition, 2004.

[170] N. Dupuis and K. Sengupta, Non-perturbative renormalization-group approach to lattice models, Eur. Phys. J. B **66**, 271 (2008).

[171] T. Machado and N. Dupuis, From local to critical fluctuations in lattice models: A nonperturbative renormalization-group approach, Phys. Rev. E **82**, 041128 (2010).

[172] F. Höfling, C. Nowak, and C. Wetterich, Phase transition and critical behavior of the d=3 Gross-Neveu model, Phys. Rev. B **66**, 205111 (2002).

[173] L. Canet, B. Delamotte, D. Mouhanna, and J. Vidal, Optimization of the derivative expansion in the nonperturbative renormalization group, Phys. Rev. D **67**, 065004 (2003).

[174] A. S. Mikhailov, Path-integrals in chemical kinetics 1, Phys Lett A **85**, 214 (1981).

[175] A. S. Mikhailov, Path-integrals in chemical-kinetics 2, Phys Lett A **85**, 427 (1981).

[176] A. M. Gutin, A. S. Mikhailov, and V. V. Yashin, Fluctuation phenomena in systems with diffusion-controlled reactions, Sov. Phys. JEPT **65**, 533 (1987).

[177] J. Keizer, Nonequilibrium statistical thermodynamics and the effect of diffusion on chemical reaction rates, The Journal of Physical Chemistry **86**, 5052 (1982).

[178] R. Metzler, A. Chechkin, and J. Klafter, Lévy statistics and anomalous transport: Lévy flights and subdiffusion, Arxiv preprint arXiv:0706.3553 (2007).

[179] H. Hinrichsen and M. Howard, A model for anomalous directed percolation, Eur. Phys. J. B **7**, 635 (1999).

[180] I. Goncharenko and A. Gopinathan, Vicious lévy flights, Phys. Rev. Lett. **105**, 190601 (2010).

Danksagung

Zuerst möchte ich mich bei meinem Betreuer Prof. Erwin Frey bedanken. Er hat mir die Möglichkeit gegeben an seinem Lehrstuhl die Doktorarbeit zu schreiben und mich über den gesamten Zeitraum geduldig unterstützt. Die fachlichen Diskussionen mit ihm waren mir stets Ermutigung und eine Quelle der Inspiration. Mit Rat und Tat stand er mir des Weiteren zur Seite, wenn es darum ging die wissenschaftlichen Erkenntnisse in Artikel für Fachzeitschriften umzusetzen. Großzügig war auch die finanzielle Förderung, insbesondere konnte ich mich auf mehreren Konferenzen im In- und Ausland und einer Summer School in den U.S.A. fortbilden und die wissenschaftliche Gemeinde meines Fachbereiches kennenlernen.

Für zahlreiche Diskussionen möchte ich mich bei Tobias Reichenbach bedanken. Er hat mir wichtige Impulse für die Arbeit am Stein-Schere-Papier Spiel gegeben.

Mein Dank gilt auch meiner Bürokollegin Cristina Pop, die mich in der Bewältigung des Arbeitsalltags begleitet hat.

Allen Kollegen des Lehrstuhls danke ich für eine gute, offene Atmosphäre. Meinen Freunden möchte ich für ihre Gesellschaft und die Unterstützung auch in den schwierigen Phasen meiner Doktorarbeit danken. Insbesondere gilt mein Dank Michael Brunnhuber, Patrick Hillenbrand, Jan-Timm Kuhr, Anna Melbinger und Cristina Pop für die kritische Durchsicht dieser Arbeit. Interessante fachliche Diskussionen hatte ich mit Ingo Homrighausen und mit Christoph Weber, der mich an seinem Expertenwissen zur Optimierung von Computersimulationen teilhaben ließ. Louis Reese bin ich dankbar, dass er mich frühzeitig auf ein für mich wichtiges, neu erschienenes Paper aufmerksam gemacht hat.

Ganz besonders gilt mein Dank meinen Eltern für ihre immerwährende Unterstützung meines beruflichen Werdegangs und insbesondere meinem Vater, der diese Arbeit hinsichtlich Rechtschreibung und Grammatik geprüft hat.